Deformation and melt in natural mantle rocks:

The Hilti Massif (Oman) and the Othris Massif (Greece)

DISSERTATION

Universiteit Utrecht, The Netherlands

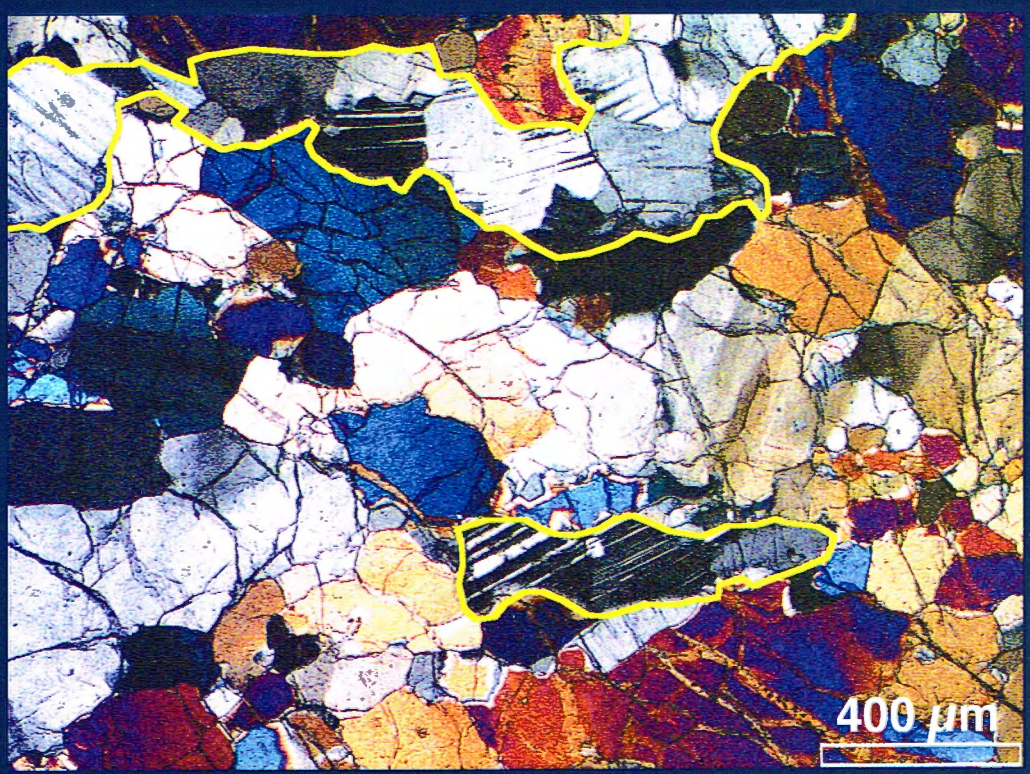

Arjan H. Dijkstra

Deformation and melt in natural mantle rocks:
The Hilti Massif (Oman) and the Othris Massif (Greece)

Deformatie en smelt in natuurlijke mantel gesteenten:
Het Hilti Massief (Oman) en het Othris Massief (Griekenland)

(met een samenvatting in het Nederlands)

PROEFSCHRIFT

ter verkrijging van de graad van Doctor aan de Universiteit Utrecht
op gezag van de Rector Magnificus Prof. Dr. W.H. Gispen
ingevolge het besluit van het College voor
Promoties in het openbaar te verdedigen
op 23 april 2001, des morgens te 10.30 uur

door
Arjan Henry Dijkstra
Geboren op 7 maart 1971 te Rotterdam

Promotores:

Prof. Dr. R.L.M. Vissers

Prof. Dr. S.H. White

Co-promotor:

Dr. M.R. Drury

Dit proefschrift werd mede mogelijk gemaakt met financiële steun van de Nederlandse Organisatie voor Wetenschappelijk Onderzoek (NWO), in de vorm van een PIONIER subsidie aan Dr. Martyn R. Drury, project nummer 030-75-346.

NWO

ISBN 90-393-2707-6

Ik heb een steen verlegd in een rivier op aarde.
Het water gaat er anders dan voorheen.
De stroom van een rivier hou je niet tegen.
Het water vindt er steeds een weg omheen.
(...)
Ik heb een steen verlegd in een rivier op aarde.
Nu weet ik dat ik nooit zal zijn vergeten.
Ik leverde bewijs van mijn bestaan.
Omdat door het verleggen van die ene steen
de stroom nooit meer dezelfde weg zal gaan.

[Bram Vermeulen, 1985]

LOOK ON MY WORKS, YE MIGHTY, AND DESPAIR!

[Percy B. Shelley, 1818]

In dierbare herinnering aan mijn vader

Members of the dissertation committee:

Dr. G.R. Davies
Faculteit Aardwetenschappen,
Vrije Universiteit Amsterdam, The Netherlands

Dr. J.G. Hirth
Woods Hole Oceanographic Institution,
Woods Hole, Massachusetts, United States

Prof. Dr. W.M. Lamb
Department of Geology and Geophysics,
Texas A&M University, College Station, Texas, United States

Prof. Dr. M.A. Menzies
Department of Geology,
Royal Holloway, University of London, United Kingdom

Prof. Dr. A. Nicolas
Laboratoire de Tectonophysique,
Université Montpellier II, France

Content

Samenvatting in het Nederlands

Binnen de Aardwetenschappen neemt de theorie van *Plaattektoniek* een centrale plaats in. Volgens deze theorie is de circa 100 km dikke, relatief koude en rigide buitenste schil van de Aarde (de *lithosfeer*) opgebroken in een tiental grote en enkele kleinere fragmenten (*platen*) die ten opzichte van elkaar verschuiven. Sommige van die platen omvatten continenten, vandaar dat het concept van de plaattektoniek vaak beter bekend is als *continent verschuiving*. Op sommige plaatsen schuiven platen onder elkaar, in zogenaamde subductie zones die worden gemarkeerd door diepzee troggen, zoals aan de randen van de Pacifische Oceaan. Op andere plaatsen, bij de zogenaamde *mid-oceanische ruggen* zoals bijvoorbeeld in het midden van de Atlantische Oceaan, bewegen platen uit elkaar. De hierdoor onstane ruimte wordt daar opgevuld door nieuw gevormde lithosfeer.

De bewegingen van de lithosfeer platen is mogelijk doordat de onderliggende laag in de aarde (de *asthenosfeer*) relatief zwak is en dus werkt als een glijlaag waarover de platen kunnen schuiven. De asthenosfeer is geheel gelegen in het gedeelte van de Aarde dat we de *bovenmantel* noemen en bestaat voor het overgrote deel (>95%) uit vast materiaal en wel voornamelijk uit het gesteente peridotiet. De asthenosfeer dankt zijn zwakte vooral aan de hoge temperatuur (>1300°C) in deze zone. Onder deze condities gedraagt peridotiet zich als een stroperige substantie die aanzienlijke vervorming (*deformatie*) toelaat. Echter, door middel van deformatie experimenten in laboratoria op kunstmatig vervaardigd peridotiet-achtig materiaal, uitgevoerd onder omstandigheden die overeenkomen met die in de asthenosfeer, is recentelijk aangetoond dat dit materiaal aanmerkelijk verzwakt wordt (het vervormt 10-100 keer sneller) door de aanwezigheid van een kleine hoeveelheid gesmolten gesteente (*smelt*). Algemeen wordt aangenomen dat de asthenosfeer gedeeltelijk opgesmolten is, maar de hoeveelheid smelt is waarschijnlijk zeer gering. De vraag is nu of de asthenosfeer genoeg smelt bevat zodat het in het laboratorium gevonden verzwakkingeffect ook inderdaad in de Aardse asthenosfeer kan optreden. Mocht dit wel het geval zijn, dan is de asthenosfeer aanzienlijk zwakker dan tot nu toe wordt gedacht, hetgeen weer implicaties heeft voor de schattingen van de krachten en spanningen die betrokken zijn bij plaattektoniek. Om een idee te geven: indien door het genoemde verzwakkingseffect tengevolge van de aanwezigheid van smelt de asthenosfeer 10-100 keer sneller zou vervormen dan wordt aangenomen (bij spanningen gelijk aan de huidige schattingen), dan zouden Noord-Amerika en Europa 10-100 keer sneller uit elkaar moeten drijven dan het geval is, en zou de Atlantische Oceaan per jaar 20 cm tot 2 m breder worden in plaats van de waargenomen 2 cm/jaar. Derhalve is de conclusie onvermijdelijk dat hetzij de huidige schattingen voor de spanningen betrokken bij plaattektoniek te hoog zijn, of dat het in het laboratorium gevonden verzwakkingseffect niet optreedt in de asthenosfeer, bijvoorbeeld omdat de concentratie smelt te laag is.

Mijn promotieonderzoek was erop gericht om aanwijzingen te zoeken voor verzwakking door de aanwezigheid van smelt in natuurlijke gesteentemonsters die ooit zijn vervormd in de asthenosfeer. De enige plek waar de asthenosfeer relatief dicht aan het aardoppervlak komt is onder mid-oceanische ruggen; aan de randen van de oceanen en onder continenten is de lithosfeer zo dik (circa 100 km) dat we de onderliggende asthenosfeer onmogelijk kunnen bemonsteren (ter illustratie: tot op heden heeft men bij boringen nooit dieptes groter dan zoïn 13 km gehaald). Tijdens de periodes van sluitingen van vroegere oceanen die met enige regelmaat zijn voorgekomen in de geologische geschiedenis van de Aarde, zijn vaak fragmenten van de oceanische lithosfeer op de continenten geschoven. Dit proces noemen we *obductie*. Deze fragmenten, zogenaamde *ofiolieten*, zijn oorspronkelijk gevormd bij mid-oceanische ruggen. Ze omvatten vaak gesteentes uit de aardmantel die ooit deel uitmaakten van de asthenosfeer. Mantelgesteentes in ofiolieten zijn dus bijzonder geschikt om een inzicht te verkrijgen in de deformatieprocessen in de asthenosfeer, en om te onderzoeken of er aanwijzingen zijn voor verzwakking door smelt. Voorwaarde is wel dat er genoeg overblijfselen van de asthenosferische deformatie bewaard zijn gebleven in de structuren in deze gesteentes, met andere woorden, dat deze structuren niet volledig zijn uitgewist door latere deformatie, bijvoorbeeld tijdens de obductie van de ofioliet.

In het kader van mijn promotieonderzoek heb ik de gesteentes uit de aardmantel in twee ofiolieten in detail onderzocht, namelijk in de Othris Ofioliet in

centraal Griekenland en in de Oman Ofioliet in het oosten van Oman. Beide ofiolieten zijn fragmenten van de vroegere Neotethys Oceaan die zoín 100-200 miljoen jaar geleden tussen Europa-AziÎ en Afrika-India lag, en waarvan er zich nog kleine restanten bevinden in de Middellandse Zee. Vóór de aanvang van het onderzoek was relatief weinig bekend over de Othris Ophioliet, en ik heb veel tijd besteed aan het maken van een gedetailleerde geologische kaart door uitgebreid veldonderzoek. Tijdens het veldwerk heb ik vele tientallen gesteentemonsters genomen voor later laboratorium onderzoek. De Oman Ofioliet daarentegen was al goed in kaart gebracht, en een kort veldwerk was voldoende om een inzicht te verkrijgen in de vervormingsgeschiedenis van de mantelgesteenten en om geschikte monsters voor nader laboratorium onderzoek te verzamelen. In het veld heb ik structuren gekaarteerd, zoals zones waarin het gesteente sterker vervormd is dan het omliggende gesteente, zones met verschillende stijlen van vervorming, en breuken. Verder heb ik gelet op verschillen in de samenstellingen van de gesteentes. Tijdens de laboratorium studie van de deformatie geschiedenis van de monsters, de zogenaamde *microstructurele analyse*, heb ik uitgebreid gebruik gemaakt van licht en electronen microscopie. Hierbij heb ik gekeken naar kristalvormen en -groottes van het belangrijkste mineraal in mantelgesteente, olivijn, naar relaties tussen olivijn kristallen, en naar de relaties tussen olivijn en andere mineralen. Verder heb ik een electronen microsonde gebruikt voor chemische analyses van de verschillende aanwezige mineralen.

De resultaten van de microstructurele analyse van de monsters uit Oman laten zien dat aanwijzingen voor deformatie onder condities zoals die heersen in de asthenosfeer over het algemeen goed bewaard zijn gebleven in deze gesteentes. Verder zijn er duidelijke aanwijzingen voor een honderden meters brede zone waarin meer smelt aanwezig was dan in het aangrenzende gesteente, en waarin de deformatie intenser was dan erbuiten. Dit suggereert dat het materiaal in deze smelt-rijke zone zwakker was dan in het smelt-armere materiaal erbuiten, zodat de vervorming zich concentreerde in de smelt-rijke zone. Ik heb geconcludeerd dat verzwakking van het gesteente door de aanwezigheid van smelt, net zoals in eerdergenoemde deformatie experimenten, de oorzaak was voor deze concentratie van deformatie. Met andere woorden, de resultaten van mijn studie wijzen erop dat verzwakking van mantelgesteente door smelt daadwerkelijk in de natuur voor komt. Echter, ik heb ook geconcludeerd dat dit alleen onder relatief zeldzame omstandigheden plaats vindt, als de concentratie gesmolten gesteente groter is dan normaal en als de smelt niet in staat is uit het gesteente te ontsnappen. Een opeenhoping van smelt in mantelgesteente kan bijvoorbeeld worden verwacht vlak onder de grens tussen de aardmantel en de overliggende oceanische korst bij mid-oceanische ruggen. Verder heb ik met behulp van de gesteentemonsters uit Oman geprobeerd een beter inzicht te verkrijgen in het mechanisme dat verantwoordelijk is voor verzwakking door smelt. Het blijkt dat de oorzaak niet gelegen is in processen binnen de kristallen, maar dat de verzwakking waarschijnlijk gerelateerd is aan processen die een rol spelen op de grenzen tussen kristallen, de korrelgrenzen. Het zou kunnen zijn dat diffusie van materiaal langs de korrelgrenzen versneld wordt door de aanwezigheid van smelt, of dat de lokale spanningen op korrelgrenzen verhoogd worden op ĕdrukpuntenî, punten waar aangrenzende kristallen in contact zijn. Tenslotte heb ik geconcludeerd dat de vervorming in de smelt-rijke, zwakke zone in de Oman Ofioliet waarschijnlijk veroorzaakt werd door het begin van de obductie van de ofioliet.

Ook in Othris zijn er veel aanwijzingen dat de mantelgesteenten ooit sterk gedeformeerd werden terwijl er smelt aanwezig was. Echter, microstructurele analyse van deze gesteenten laat zien dat de deformatie niet plaatsvond in de asthenosfeer, zoals in Oman, maar in de koudere lithosfeer. De resultaten suggereren dat bij de mid-oceanische rug waar de Othris Ofioliet zoín 200 miljoen jaar geleden gevormd werd de lithosfeer relatief dik was. Het is waarschijnlijk dat de mantelgesteentes in Othris ooit deel uitmaakten van de wortelzone van een transform breuk, zoals die veel voorkomen bij mid-oceanische ruggen in de huidige oceanen. Gesmolten gesteente, afkomstig uit de onderliggende asthenosfeer, infilteerde deze zone, reageerde met het relatief koude mantelgesteente in de wortelzone, en kristalliseerde uiteindelijk gedeeltelijk uit. Bovendien heb ik aangetoond dat de reacties tussen smelt en mantelgesteente een mix van bijzonder fijnkorrelig materiaal produceerden. Dit was van groot belang tijdens het begin van de latere obductie van de Othris Ophioliet, omdat tijdens het obductie proces de deformatie zich concenteerde in banden van fijnkorellige reactieproducten, dit als gevolg van het feit dat onder bepaalde condities fijnkorrelig materiaal mechanisch zwakker is dan grofkorrelig materiaal.

Mijn studie laat tenslotte zien dat er enorme verschillen bestaan tussen de ofiolieten in Oman en Othris, zowel wat betreft structuur, samenstelling en deformatie geschiedenis. De Oman en Othris ofiolieten zijn waarschijlijk de eindleden van een heel scala van verschillende ofioliet types. Dit werp ook nieuw licht op de recente ondekking dat de lithosfeer in de huidige Mid-Atlantische rug qua structuur en samenstelling sterk verschilt van die van bijvoorbeeld de mid-oceanische ruggen in de Pacifische Oceaan. De Othris Ophioliet lijkt in velerlei opzichten op de Mid-Altantische lithosfeer, terwijl de Oman Ophioliet veel meer gelijkenis vertoont met de ondergrond van de Pacifische oceaan. Naar alle waarschijnlijkheid speelt de snelheid waarmee de lithospherische platen uit elkaar drijven bij de mid-oceanische ruggen een belangrijke rol. Snel spreidende ruggen, zoals in de Pacifische Oceaan, hebben een warme structuur waarbij de lithosfeer dun is en lijkt op de Oman Ofioliet, en waar en de onderliggende asthenosfeer tot dicht, slechts enkele kilometers, aan het oppervlak komt. Langzaam spreidende mid-oceanische ruggen daarentegen, zoals de Mid-Atlantische rug, hebben een veel koudere structuur met een meer dan zes kilometer dikke lithosfeer, die sterk lijkt op de Othris Ofioliet.

Onderzoek naar huidige mid-oceanische ruggen in de diepzee is relatief omslachtig en duur, en laat het bovendien nog niet toe om de diepere delen van de ruggen en de wortelzones van transform breuken te bestuderen. Ofiolieten bieden een aantrekkelijk alternatief. Mijn promotie onderzoek heeft geleid tot nieuwe inzichten in belangrijke aspecten van plaattektoniek, zoals de vervorming van gesteentes uit de aardmantel en de structuur van de oceanische lithosfeer, die niet eenvoudig op een andere wijze dan door ofioliet studies verkregen hadden kunnen worden.

Summary

For a full understanding of plate tectonics, one of the central paradigms in Earth Sciences, it is critical to know the mechanical properties of the material of which the earth's upper mantle consists, *i.e.*, peridotite. The cold outer shell of the Earth, the *lithosphere*, is broken up into strong and almost rigid plates, which can move with relatively little resistance over a weak substratum in the upper mantle, the *asthenosphere*. The weakness of the asthenosphere is primarily caused by the high, near-solidus ambient temperature in this zone. However, questions remain as to the effects of the presence of small fractions of molten material ('melt') on the deformation properties and strength of these asthenospheric peridotites. Recent laboratory experiments have shown that small amounts of melt (4-10%) can have a drastic weakening effect on peridotite-like materials. If this weakening effect of melt plays a role in the earth's upper mantle, then the asthenosphere could be significantly weaker than commonly believed. The current research was therefore initiated, aiming to investigate the factors which govern melt-weakening of peridotites and to determine whether evidence could be found for melt-weakening in natural peridotites deformed under asthenospheric conditions. However, samples from the asthenosphere are generally unavailable, mainly because of the great depth of this zone (generally >100 km). Only at mid-ocean ridges, the asthenosphere reaches relatively shallow levels of only a few kilometres. Ophiolites, fossil fragments of mid-ocean ridges, occasionally emplaced onto continents as a result of the closure and disappearance of oceans during the earth's geological history, are therefore the most suitable source of samples of upper mantle rocks deformed under asthenospheric conditions. Peridotites in ophiolites can thus provide a window into the asthenosphere, provided that the effects of deformation related to emplacement of the ophiolite superimposed on asthenospheric deformation can be distinguished and that relics of the early asthenospheric deformation have been preserved.

This thesis comprises a detailed geological study of peridotites found in two ophiolites, the Oman Ophiolite (Oman) and the Othris Ophiolite (Greece). Both ophiolites represent remnants of an ancient ocean, the Neotethys, which existed in Mesozoic times. Structural geological and lithological maps and sections of selected areas were made, and rock samples were subjected to detailed microstructural and petrographic analysis using light microscopy, electron microscopy, and chemical (electron microprobe) analysis.

It is found that the peridotites in the Hilti Massif in Oman are characterised by widespread preservation of structures and microstructures relating to deformation under asthenospheric conditions. Such peridotites have relatively coarse-grained microstructures with evidence of ductile deformation at low stresses (< 10 MPa) and high temperatures (>1200 °C). Moreover, they contain petrographic evidence that basaltic melt was present during their deformation, suggesting near- to super-solidus deformation conditions. It is argued that the peridotites just below the boundary between the mantle and the overlying oceanic crust not only contained more melt, but were also more strongly deformed than peridotites at deeper levels. This suggests that these melt-rich, shallow peridotites were weaker than the deeper peridotites which contained less melt. It is demonstrated that their weakness was not caused by grain size effects, nor by a change in the mechanism of deformation (*i.e.*, from dislocation to grain-size sensitive creep). It is concluded that the rocks were weakened by melt, probably as a result of enhancement of processes taking place at the grain boundaries between crystals which affect the deformation (*i.e.*, enhancement of grain boundary diffusion or local concentration of stresses). The presence of relatively large melt fractions below the crust-mantle boundary can be explained by local trapping of rising melts produced by decompression

melting of mantle rocks at depth under a mid-ocean ridge. Crystallisation of new minerals (plagioclase, pyroxene) clogging the porosity and forming a melt migration barrier, reduced vertical permeability caused by anisotropy of the crystals in the peridotites, grain size variations, or piezometric pressure effects in the zone of localised deformation could have caused melt accumulation. Based on microstructural and crystal fabric analysis, it is argued that the deformation which was concentrated in the melt-rich zone just below the crust-mantle boundary was not related to forced mantle flow as a result of the upwelling of mantle diapirs at the Oman paleo-ridge, as previously proposed. Instead, the deformation is attributed to the onset of compression close to the paleo-ridge, leading to collapse of the melt-bearing zone followed by melt expulsion and intrusion of a crystal-melt mixture into the overlying oceanic crust, which formed numerous wehrlite bodies.

Despite widespread evidence for the presence of melts, no positive evidence for melt weakening in the peridotites in the Othris Massif in Greece has been found. No zone could be identified which was both more melt-rich and more strongly deformed than adjacent peridotites. Microstructures indicative of deformation under asthenospheric conditions are rare, as most peridotites have a strong imprint of deformation taking place at the base of the lithosphere. Such peridotites have relatively fine-grained microstructures with evidence of ductile deformation at intermediate stresses (5-38 MPa) and temperatures (1000-1200 °C). Using microstructural and petrological arguments, it is shown that the melt relics in the Othris peridotites are the products of a stage of melt impregnation in the base of the oceanic lithosphere. Rising melts cooled below their liquidus temperature in the cold lithospheric layer, which caused fractional crystallisation of new minerals, most importantly plagioclase and pyroxene, from the melt. It is concluded that melt impregnation most likely occurred in the lithospheric root of a transform fault at a slow-spreading Othris paleo-ridge, since only in such an environment the lithosphere is expected to be thick enough to reach well into the mantle during magmatic activity.

There is abundant petrographic evidence in Othris that a stage of melt-rock reaction preceded and accompanied melt impregnation, at conditions close to those at the asthenosphere-lithosphere transition. One of the effects of the reactions between transient melts and peridotites was the production of very fine-grained domains consisting of a mixture of the minerals olivine and orthopyroxene. Later, as a result of deformation of the peridotites during the first stages of emplacement of the Othris Ophiolite in a transpressional setting, these fine-grained domains coalesced to form continuous fine-grained bands. The deformation in these fine-grained bands became controlled by the relatively fast grain-size sensitive creep mechanism, resulting in strong weakening and localisation of deformation in fine-grained mylonite shear zones. The research on Othris peridotites has thus shown the importance of *indirect* melt weakening, involving extreme grain size reduction by melt-rock reaction.

This study has demonstrated that melt weakening such as observed in deformation experiments of mantle-like materials can indeed occur in nature, provided that the melt fractions present exceed those normally found in mantle rocks. A process leading to accumulation of melt is therefore required for peridotite melt weakening. Moreover, since the mechanisms causing the weakening effect of melt in peridotites is probably caused by enhancement of grain boundary processes involving diffusive mass transfer, melt weakening is expected to be most significant in fine-grained rocks. In addition, the distribution of the melt in the host peridotites is probably important; melt concentrated in lenses and veins is less likely to have a significant weakening effect than melt present along grain boundaries and in grain interstices, as it does not provide a well-connected grain-scale network of fast diffusion pathways. Finally, highly siliceous, very viscous melts, such as the first melt fractions produced

by partial melting of peridotites, are less likely to cause melt weakening than silica-poor melt fractions produced by high degrees of partial melting, because of slow diffusion in viscous melts.

Comparison between the structures, microstructures, and petrology of the mantle rocks in Oman and Othris has shown that they represent two very different, end-member types of ophiolites. The first type of ophiolite (the Oman end-member) is probably typical for a fast-spreading ridge with a relatively thin thermal lithosphere and a high magma supply. In such an environment the oceanic crust reaches a full thickness of ~6 km, consisting of a sequence of gabbros, sheeted dolerite dykes, and basaltic pillow lavas; peridotites predominantly preserve evidence for deformation under asthenospheric conditions in their microstructures. In contrast, the Othris-like ophiolite type probably represents a slow-spreading ridge near a transform fault, where magma supply is low, where the oceanic crust is thin or absent, and where rising melts fractionally crystallise minerals in the base of a relatively thick lithospheric layer.

Chapter 1

Introduction

1.1. Melt weakening in experiment and nature

The present study is centred around the rheological significance of the presence of melts in naturally deformed mantle peridotites. The starting point for this research was the recent discovery, in deformation experiments, that the presence of an interstitial melt can have a drastic weakening effect on olivine-bearing rocks. Creep experiments by Hirth and Kohlstedt (1995a,b) and Bai *et al.* (1997) showed that olivine aggregates containing 4-10% interstitial basaltic melt were significantly weaker than 'nominally' melt-free (containing very little or no melt) aggregates (figure 1.1).

Such a weakening effect, observed in experiments, of melts on mantle-like materials may have major implications for the mechanical behaviour of mantle rocks in nature. If these same effects would play a role in the Earth's upper mantle - in particular in the low velocity zone which is generally considered to contain a (small) melt fraction - then the upper mantle may be significantly weaker than currently estimated on the basis of nominally melt-free olivine rheologies (figure 1.2).

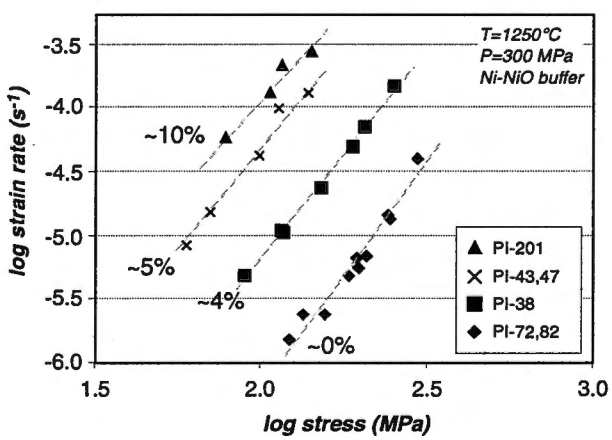

Figure 1.1: Selected results from deformation experiments on olivine aggregates in the dislocation creep regime by Hirth & Kohlstedt (1995b) showing the weakening effect, *i.e.*, de increase of strain rate at constant stress or the decrease of stress at constant strain rate, of the presence of 4-10% interstitial basaltic melt.

The extrapolation of the mechanical effect of melts on olivine aggregates to the rheology of the upper mantle is not straightforward, however. Viscosity estimates for the upper mantle based on melt-bearing olivine rheologies are orders of magnitude weaker than viscosity estimates based on post-glacial rebound studies (10^{20}-10^{21} Pas; *e.g.*, Haskell, 1937; Peltier, 1996), whereas mantle viscosities calculated from melt-free olivine flow laws are in agreement with results of post-glacial rebound studies (*e.g.*, Karato & Wu, 1993; Ranalli, 1991). Melt-weakened rheologies are also lower than most estimates of viscosities in the asthenosphere. This suggests that melt weakening does not play a role in nature, at least not at the scale of the entire upper mantle or the asthenosphere.

There are two caveats that need to be taken into account before the rheology of melt-weakened olivine in experiments can be extrapolated to the Earth's upper mantle. First, melt-weakening is only observed in olivine aggregates deforming under conditions close to the deformation mechanism boundary between dislocation creep and grain size sensitive diffusion creep. It is difficult to assess whether this condition is met (anywhere) in the upper mantle. Ranalli (1991) argued that the grain size in the convecting upper mantle may be close to the grain size at which diffusion creep starts to become important (approximately 1 mm), but no solid constraints exist on grain sizes in the upper mantle. Mantle xenoliths often have grain sizes in the order of 1 mm, but they are generally derived from

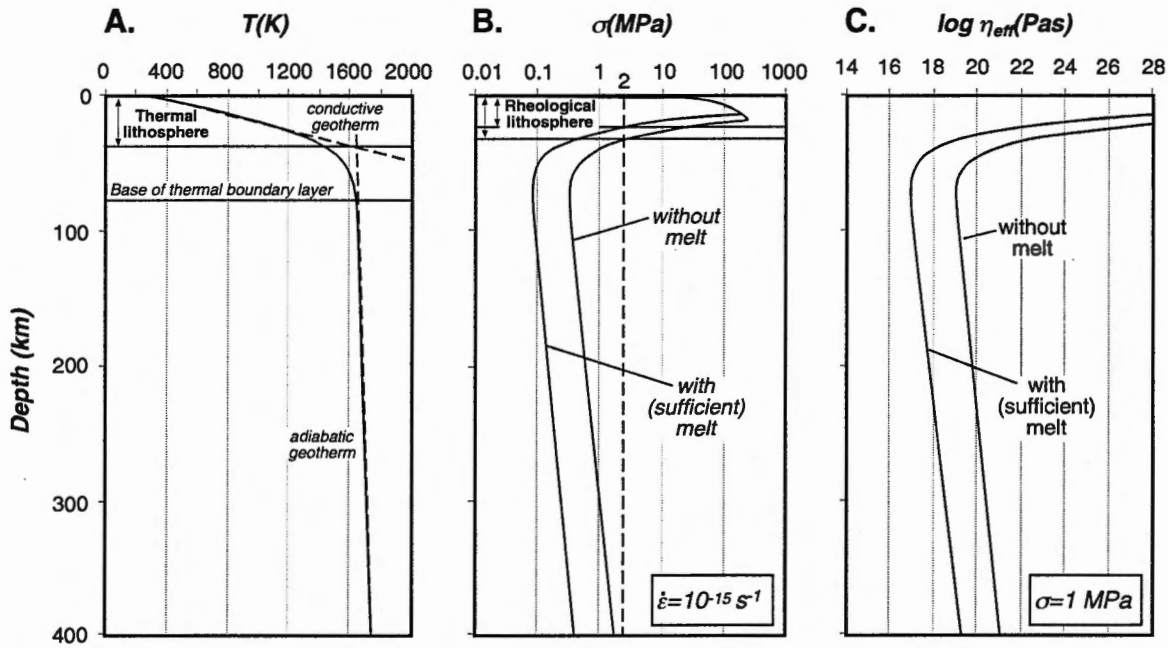

Figure 1.2: Sections through the upper mantle showing the effect of a melt weakened rheology on the strength and effective viscosity of the mantle. Temperature in (A) is defined by a geotherm through 10 Ma old oceanic lithosphere (calculated using an error-function) at the top, and an adiabatic geotherm at depth. The strength profiles in (B) are calculated using power-law creep relations limited by a frictional strength relation at high stresses/low pressures. Melt-free and melt-weakened creep in olivine are represented by the [c]- and [a]-limited creep laws given in Drury & Fitz Gerald (1998). An activation volume of 10 cm^3/mole is used. Effective viscosities at a stress of 1 MPa in (C) are calculated using the same flow laws. Also shown in (A) and (B) are the definitions of the thermal lithosphere, thermal boundary layer, and rheological lithosphere used throughout the thesis. The base of the thermal lithosphere is taken as the transition between the conductive and the adiabatic geotherm. The thermal boundary layer is the layer in which the effect of conduction is significant. The rheological lithosphere is the layer which is too strong to deform at strain rates (taken as 10^{-15} s^{-1}) and stresses associated with convective mantle flow (0.5-10 MPa according to Ranalli, 1991 - here taken as 5 MPa).

the rigid mantle lithosphere and do not provide information about deformation conditions in the convecting upper mantle where melt weakening is most likely to play a role. Secondly, from the experimental data it seems that significant weakening is only found in olivine aggregates in which the melt content exceeds a critical value of approximately 4%. There are questions as to whether such large melt fractions normally occur in the upper mantle. Experiments by Daines and Richter (1988) on melt-bearing peridotites showed that melt fractions as low as 1% already form an interconnected network, and that at fractions of 2% all melt is connected. Due to its buoyancy, basaltic melt present in a connected network will probably be extracted rapidly from the olivine-rich host rock, provided that the host rock can compact and that resistive forces due to the viscous interaction between the solid matrix and the melt do not exceed the buoyancy forces (McKenzie, 1984, 1989; Scott and Stevenson, 1986). Estimates for the melt fraction which may be stable in mantle rocks range from <1% (Von Bargen & Waff, 1986; McKenzie,1989; Kohlstedt, 1992) to 2-3% at most (Faul, 1997). In addition, geochemical studies of mid-ocean ridge basalts (MORBs) suggest that mantle porosities in the mantle below ocean ridges are very small. The preservation of isotopic U-Th disequilibria found in MORBs requires porosities much smaller than 1-2% (*e.g.*, McKenzie, 1985; Spiegelman & Elliott, 1993; Macdougal, 1995; Salters & Longhi, 1997). As yet, geophysical constraints

on melt contents of the upper mantle are limited. The recent seismic study of the upper mantle beneath the East Pacific Rise showed that 1-2% melt is present in a wide, tent-shaped domain (figure 1.3; MELT Seismic Team, 1998), but this estimate is surrounded with uncertainties on the actual distribution of the melt in this domain, and the melt content may be higher in a narrow zone directly underneath the ridge axis. These results of theoretical, geochemical, and geophysical studies on melts in mantle rocks show that melt fractions estimated in the upper mantle generally do not exceed the critical fraction of 4% required for significant melt weakening of olivine rocks in experiments (see also chapter 2). Therefore, questions remain as to the relevance of melt weakening in natural mantle peridotites.

This study aims to establish if, and under what conditions melt weakening occurs in natural mantle rocks. At the onset of the study it was concluded that the best available proof for melt weakening in natural mantle rocks – the geological 'smoking gun' – is the evidence for strain localisation into zones which can be shown to have been melt-rich during some stage of their deformation history. Structures and microstructures in the upper mantle sections of two ophiolites, exposed in Oman and in Greece, are systematically searched for such evidence for melt weakening. The methods employed comprise structural and lithological mapping followed by detailed microstructural and petrologic sample analysis by means of light and scanning electron microscopy, crystal fabric analysis (universal stage and electron backscatter diffraction), and chemical analysis (electron microprobe). The results of these investigations are reported and discussed in this thesis.

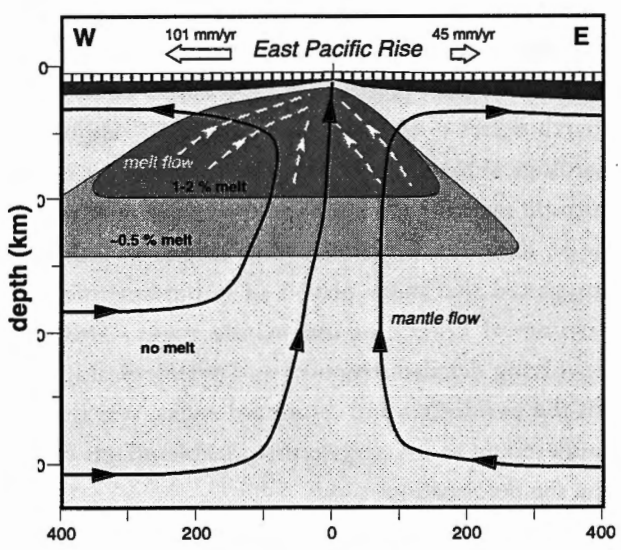

Figure 1.3: Results from the MELT seismic experiment showing the presence of a melt-bearing zone underneath the East Pacific Rise (redrawn from Cann, 1998, after MELT Seismic Team, 1998). Mantle and melt flow patterns as based on measured seismic anisotropies.

1.2. The study areas

The mantle sections of the Oman Ophiolite exposed in the Hilti Massif of Oman, and of the Othris Ophiolite in the western Othris Mountains, central Greece, were selected for a detailed structural, petrological, and microstructural study (see figure 1.4 for locations).

The Oman Ophiolite is widely known for its excellent preservation and exposure. Previous studies (*e.g.*, Nicolas & Prinzhofer, 1983; Gregory, 1984; Smewing *et al.*, 1984; Ceuleneer & Rabinowics, 1992; Boudier and Nicolas, 1995) have shown that evidence for the presence of an interstitial basaltic melt has been preserved in the mantle rocks directly beneath the crust-mantle boundary (in the crust-mantle transition zone). Moreover, it has been proposed that some sort of melt weakening must have occurred in the peridotites of the crust-mantle transition zone to account for the narrowness of the zone in which mantle flow structures turn sharply from subvertical to subhorizontal in some areas (Rabinowicz *et al.*, 1987; see also chapter 2 & 3). Mantle flow models based on structures in the Oman Ophiolite, which comprise mantle flow forced by upwelling diapirs (*e.g.*, Nicolas *et al.*, 1994; see also chapter 3), also require a low viscosity – possibly as the result of melt weakening - in the crust-

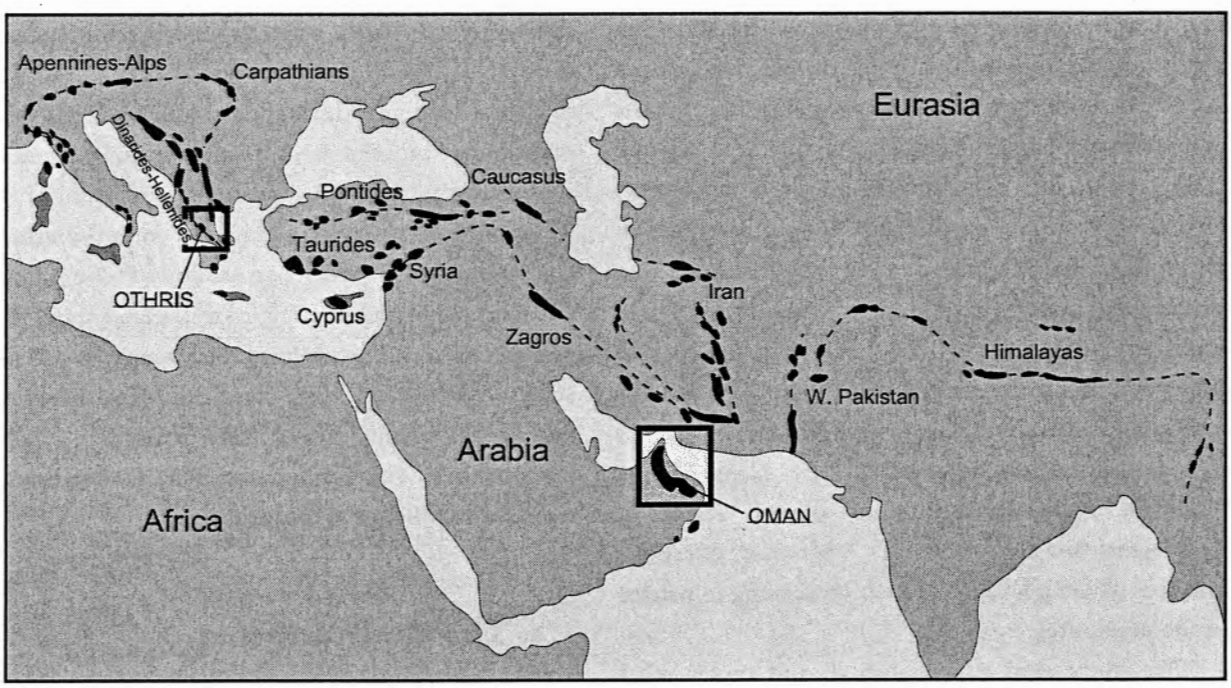

Figure 1.4: Map showing the distribution of Tethyan ophiolites along the Alpine-Himalayan suture zone. Location of Othris and Oman ophiolites indicated by black box. For more detailed maps the reader is referred to the following chapters. Map redrawn from Lippard et al. (1986).

mantle transition zone, to explain the apparent decoupling between the fast-flowing mantle and the overlying lithospheric plate (Ceuleneer & Rabinowics, 1992). The results of these previous studies thus suggested that the mantle section of the Oman Ophiolite could represent an excellent natural laboratory to investigate in detail the effects of possible melt weakening on the deformation of natural peridotites. The Hilti Massif was chosen because of its relatively simple structure (Ceuleneer *et al.*, 1988). The results of the present study are reported in chapters 2 and 3 .

At the onset of this project, the mantle section of the Othris Ophiolite was less well studied. Pioneering petrological work by Menzies (1973; 1974; 1975; 1976a,b; Menzies & Allen, 1974; and Menzies *et al.*, 1977) had shown that plagioclase-lherzolites containing melt relics are relatively abundant in Othris, and it was argued that these plagioclase-lherzolites represented rocks that underwent incipient partial melting (*e.g.*, Menzies, 1973). Later structural work in the area by Rassios (Rassios & Konstantopoulou, 1993; A. Rassios, personal communication, 1995) demonstrated the strongly dismembered character of the ophiolite, but also showed the presence of large dunite bodies within harzburgites (A. Rassios/IGME, unpublished geological map, 1995). Similar dunite bodies in other mantle massifs have been interpreted as melt conduits (*e.g.*, Kelemen, 1990). Previous studies in Othris thus suggested that melts played an important role in the geological history of the mantle rocks. This study, involving detailed structural and petrological mapping of the peridotites and associated rocks, was therefore undertaken to investigate the possible effects of melts on the deformation.

The Oman and Othris Ophiolites are both remnants of the Neotethys ocean which existed between Eurasia and Gondwanaland during the Jurassic and Cretaceous. They represent two different end-member types of ophiolites (Nicolas, 1989). It is generally accepted that

the Oman Ophiolite originated in a relatively fast-spreading environment (*e.g.*, Nicolas *et al.*, 1994), possibly similar to the present-day Pacific Ocean. In contrast, the Othris Ophiolite was probably formed in a relatively slow-spreading environment, near a continental margin at the inception of rifting (Menzies & Allen, 1974) or at a Mid-Atlantic type spreading centre (chapter 4). It is likely that the different thermal structures in such contrasting settings have an effect on mantle deformation and on the possible role of melt weakening. The Oman and Othris ophiolites are thus complementary, and a comparison between the two could potentially elucidate the conditions governing melt weakening of natural mantle rocks.

1.3. Outline of the thesis

- Chapter 2 of this thesis is concerned with a detailed microstructural analysis of peridotites in the Hilti Massif (Oman). The study focuses on the peridotites containing melt-relics from directly beneath the crust-mantle boundary.
- Chapter 3 expands on these results and investigates the causes for the deformation in the Hilti mantle rocks, in particular the deformation in the rocks found directly beneath the crust-mantle boundary. The question whether the deformation can be attributed to forced mantle flow (e.g., Nicolas et al., 1994; Ildefonse et al., 1995) or to some other tectonic process is addressed.
- Chapter 4 is concerned with the plagioclase-peridotites in the Othris Peridotite Massif. Structural, petrological, and microstructural evidence for the presence of a melt during the geological history of these peridotites is studied in detail and it is investigated whether this melt was associated with either incipient partial melting or with an episode of melt impregnation.
- Chapter 5 deals with tectonites and mylonites in Othris. It is investigated whether the development of these structures was related to reactions between the host peridotites and an interstitial melt.
- Chapter 6 summarises the geological evolution of the Othris peridotites and discusses two contrasting views on the paleogeographic origin of the Othris Ophiolite.
- Chapter 7 presents a synthesis of the results of this study on the role of melts on the deformation of mantle rocks in the Hilti and Othris massifs. In addition, a comparison is made between the geometry and deformation history of the Oman and Othris ophiolites, and the implications are explored for the structure and strength of the lithosphere, and for the nature of the Moho at fast- and slow-spreading ridges.
- Chapter 8 summarises the main conclusions of the thesis and presents some suggestions for further research.

Chapter 2

Geological evidence for melt weakening in natural peridotites: The Hilti Massif, Oman Ophiolite

Abstract

Experimental studies have shown that olivine aggregates with >4% melt are significantly weaker than melt-free aggregates. However, questions remain as to the importance of melt weakening in nature. In several studies, melt weakening has been invoked to explain patterns of mantle flow in the Oman Ophiolite. Evidence for melt weakening in the Hilti mantle section is re-investigated in this chapter, by means of structural and microstructural methods. The average olivine grain size increases with depth below the crust-mantle boundary. This is related to a change from dominantly equigranular microstructures at shallow levels to coarse porphyroclastic microstructures at depth. A strong foliation and high degree of recrystallization in the upper part of the mantle section are interpreted as the imprint of localised deformation at stresses of ~4-10 MPa. Grain size sensitive creep can probably be ruled out as the cause for weakening and strain localisation. Since there is petrographic evidence for melt in the high-strain zone, strain localisation may have been caused by a melt-related weakening mechanism. The high melt contents required for melt weakening suggest that melt accumulated just below the crust-mantle boundary. On the basis of experimental data it has been proposed that melt weakening in olivine aggregates is caused by a change from [c]- to [a]-limited slip. The results of the microstructural analysis presented in this chapter do not support this hypothesis. Melt weakening is probably related to enhancement of grain boundary rather than intragranular deformation processes. Effective viscosities $<2 \cdot 10^{16}$ Pas may locally exist in the uppermost mantle beneath ridges if melt weakening occurs.

2.1. Introduction

The effects of small melt fractions on the strength and deformation of mantle rocks has been debated for some years. Early deformation experiments on partially molten olivine aggregates showed that they were only modestly weaker than melt-free peridotites (Kohlstedt, 1992). More recent work has shown that drastic weakening of melt-bearing mantle-like materials in the laboratory only occurs if melt contents exceed a critical melt fraction of ~4% (Hirth & Kohlstedt, 1995a, 1995b; Bai *et al.*, 1997). In addition, weakening has only been found in fine-grained peridotites deforming at conditions close to the transition between the diffusion and dislocation creep deformation mechanisms.

Experimental studies of melt distributions and melt migration by porous flow in partially molten peridotites have shown that permeability is high at low melt fractions, allowing melt to escape easily due to buoyancy forces (Daines & Richter, 1986; Kohlstedt, 1992). Estimates for the melt fraction that can remain within a peridotite without being extracted, range from

<1% (Von Bargen & Waff, 1986; McKenzie, 1989; Kohlstedt, 1992), to 2-3% at most (Faul, 1997). In addition, geochemical studies of mid-ocean ridge basalt (MORB) have confirmed that melt segregates from residual mantle rocks at very low fractions. ^{230}Th excess in MORB for instance indicate that porosities in the mantle below ocean ridges are very small, probably (much) less than 1-2% (*e.g.* McKenzie, 1985; Spiegelman & Elliott, 1993; Macdougall, 1995; Salters & Longhi, 1997). In summary, it seems unlikely that melt contents high enough to cause significant weakening of peridotites normally exist in the mantle. However, melt weakening has been shown to occur in melt-rich *conduits* in the mantle section of the Josephine Ophiolite, leading to a positive feedback between focusing of melt flow and deformation in replacive dunites (Kelemen & Dick, 1995).

The best locations to study the possible effects of melt weakening in natural mantle rocks are ophiolitic peridotite massifs. Most structures and microstructures in the mantle rocks of ophiolites are thought to be produced by high-temperature, near- to super-solidus ('asthenospheric') mantle flow underneath an ocean ridge and the successive accretion of the oceanic lithosphere (*e.g.*, Smewing *et al.*, 1984; Ceuleneer *et al.*, 1988; Nicolas, 1989; Suhr, 1993). Detailed studies of these structures and microstructures can give insight into the kinematics and mechanisms of high-temperature mantle deformation. Such investigations in the mantle section of the Oman Ophiolite have provided kinematic models of mantle flow at ocean ridges. It has been argued that the mantle is upwelling in a 3-dimensional fashion, in 10 km-scale diapirs, and that mantle flow becomes horizontal at shallow levels (Nicolas *et al.*, 1988, 1994). The narrow width of the zone in which mantle flow rotates from vertical to horizontal requires a very low viscosity in rocks just below the crust-mantle boundary. It has been suggested that weakening due to the presence of melt may be the cause for this low viscosity (Rabinowicz *et al.*, 1987). Moreover, several workers have argued that during subhorizontal mantle flow, mantle flow driven by active - possibly diapiric - mantle upwelling at the ridge axis may sometimes be decoupled from the movement of the overlying lithospheric plate (figure 2.1). In several

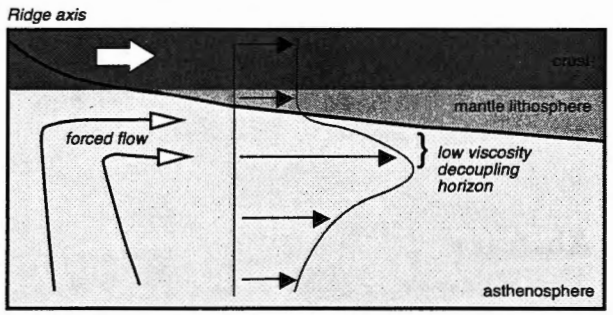

Figure 2.1: Schematic section across a spreading ridge showing forced mantle flow – possibly driven by active mantle diapirism underneath the ridge axis – decoupled from the motion of the overlying lithospheric plate by a low viscosity horizon (after Nicolas et al., 1994; Ildefonse *et al.*, 1995).

areas in the Oman Ophiolite a decoupling horizon has been documented within the most shallow part of the mantle section, just below the crust-mantle boundary (Ceuleneer *et al.*, 1988; Ceuleneer & Rabinowicz, 1992). The high strain in this horizon has been attributed to forced (active) mantle flow (Ceuleneer *et al.*, 1988; Ceuleneer & Rabinowicz, 1992) which may have been channelled (Ildefonse *et al.*, 1995). A horizon recording forced mantle flow has also been described at 1.5 to 4 km below the crust-mantle boundary in the Bay of Islands Ophiolite (Suhr, 1992). Again, melt weakening has been suggested as the cause of the required low viscosity of such horizons (Ceuleneer & Rabinowicz, 1992).

The present study aims to bridge the gap between results from experiments and studies of ophiolitic mantle sections. A detailed structural and microstructural study of the mantle section of the Oman Ophiolite exposed in the Hilti Massif has been made (figure 2.2). In this area, a thin, high strain, low viscosity, possibly melt-weakened decoupling horizon has been reported immediately below the crust-mantle boundary (Ceuleneer *et al.*, 1988; Ildefonse *et al.*, 1995).

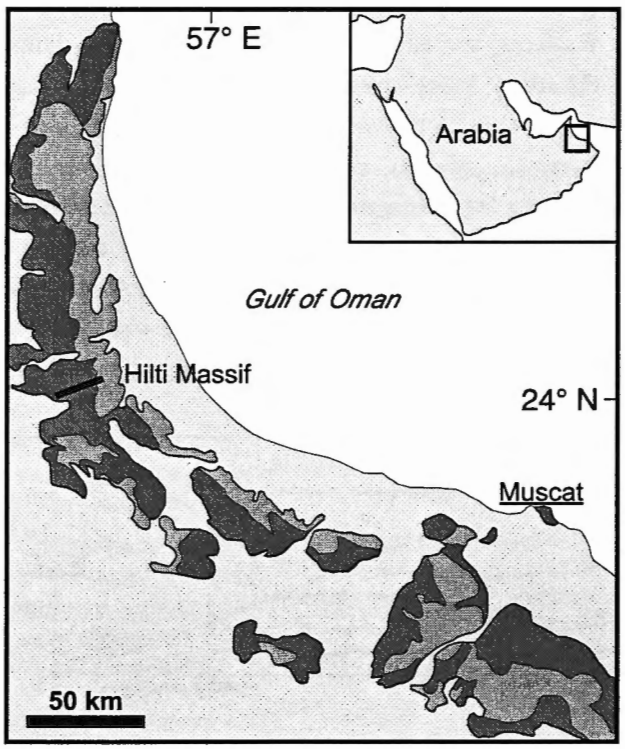

Figure 2.2: Map of Northern Oman, showing the extent of the ophiolite. Oceanic crustal rocks in light grey, mantle rocks in dark grey. Dark line shows location of sampling traverse in the Hilti Massif.

First, the evidence for strain localisation is discussed using structural and microstructural observations. A careful characterisation of microstructures is presented, which allows a comparison between natural and experimentally deformed peridotites, and permits to make inferences about the deformation mechanisms and rheology of mantle rocks at the Oman paleo-ridge. Furthermore, petrographic clues for the presence of melt in the highly strained peridotites are evaluated. It is argued that a weakening mechanism is required to explain strain localisation in nature. Two weakening processes are investigated which could have caused strain localisation, *i.e.*, a change from deformation controlled by dislocation creep to deformation controlled by grain size sensitive creep, and melt weakening. Finally, it is discussed whether the results of the microstructural observations can be reconciled with current ideas about the underlying mechanisms of melt weakening.

The study confirms results of earlier studies which suggested that melt weakening played a role in the mantle section of the Oman Ophiolite. It is argued that melt weakening requires melt accumulation in the uppermost mantle, and that the zone which preserves evidence for melt accumulation is wider than previously reported. Such a melt accumulation zone may, however, be a feature of a dying ridge system and may not be so well developed at active spreading ridges.

2.2. Results

2.2.1. The Hilti Massif

The research has focussed on the mantle section exposed in the Hilti Massif in Northern Oman (Ceuleneer *et al.*, 1988; Ildefonse *et al.*, 1995). The mantle structures in this massif are reported to fit the 'standard' or 'off-axis' flow pattern (Ceuleneer *et al.*, 1988). This pattern comprises foliations subparallel to the crust-mantle boundary and lineations perpendicular to the strike of the sheeted dykes. In the Hilti Massif the entire ophiolitic sequence has been tilted by about 25° to the east (Ildefonse *et al.*, 1995). Thus progressively deeper levels of the ophiolite are encountered towards the west. A structural and sampling traverse across the mantle section following the main Wadi Hilti and a few subsidiary wadis was made. At about one kilometre horizontal intervals orientations of peridotite foliations, lineations, and orientations of modal compositional layering were recorded. In addition, oriented samples for microstructural and petrographic analysis were taken. At a number of locations both harzburgitic and dunitic peridotites were sampled for comparison.

The peridotites in the upper ~575-800 m (based on the crust-mantle boundary geometry - see below) of the mantle section are well foliated. This foliation is defined by a relatively strong orthopyroxene shape fabric. This foliation, which is parallel to the spinel

defined foliation, is roughly parallel to the crust-mantle boundary and the layering in the overlying gabbros. Orthopyroxene and spinel lineations plunge to the east to southeast and are parallel to lineations in the gabbros. The mantle rocks near the crust-mantle boundary locally contain interstitial plagioclase and clinopyroxene crystals (wehrlites), and coarse gabbroic dykes with dunitic margins.

In contrast, peridotites deeper in the mantle section are not clearly foliated. Orthopyroxene crystals are granular and coarser than in the shallow peridotites. Flattened spinel could sometimes be used to define a foliation. More commonly a clear cm- to dm-scale compositional layering (caused by modal variations in pyroxene content) was observed and it was assumed that this layering is roughly parallel to the deformation fabric. The lineation is generally well defined by elongate spinel on top of layering planes. These coarse granular peridotites were found all the way to the base of the studied section. Well foliated or mylonitic

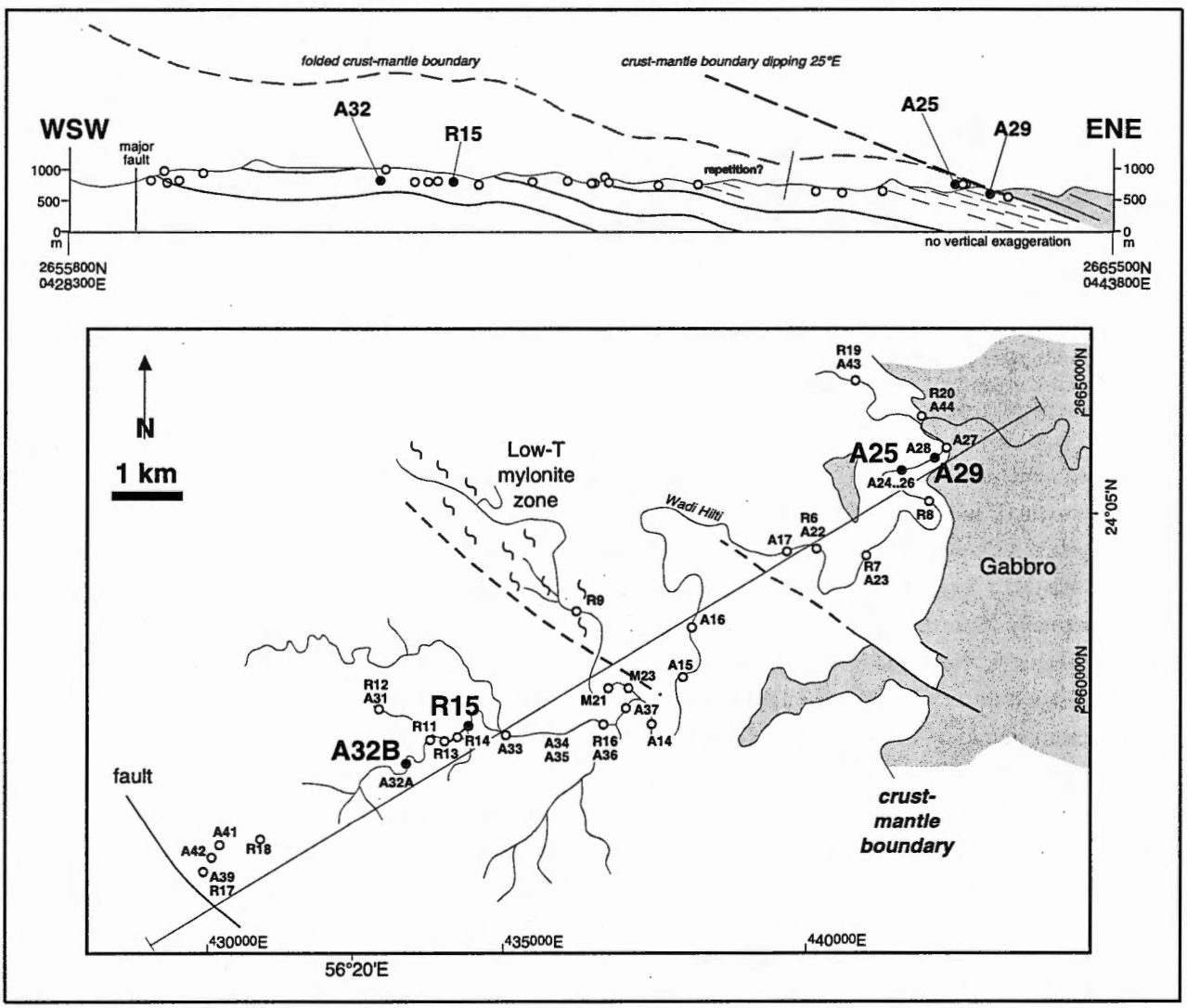

Figure 2.3: Profile across the Hilti Massif, with sample localities projected onto it. The localities of samples discussed in text are shown. Dashes in shallow part of the mantle section indicate foliated peridotites. Gabbros in light grey. The two crust-mantle boundary geometries shown are discussed in the text.

peridotites, common in the basal parts of the Oman mantle sections (*e.g.* Ceuleneer *et al.*, 1988; Boudier *et al.*, 1988) were not found at the base of the studied section. The base is defined by a large brittle fault with unknown displacement. West of this fault a new succession of mantle rocks is exposed.

In order to analyse the (micro)structural and petrological trends with depth in the mantle section, the depth below the crust-mantle boundary was established for every sample. For sample locations relatively close to the crust-mantle boundary the depth below the crust-mantle boundary was determined directly from the available geological map (Ministry of Petroleum and Minerals, 1987) because the crust-mantle boundary is exposed in the ridges surrounding the wadi. For other locations the depth was estimated by assuming a constant dip of the crust-mantle boundary of 25° towards the east. This is the average inclination of the paleo-horizontal in the Hilti Massif, as deduced from the orientation of the sheeted dykes and from the average dip of the uppermost mantle and lowermost gabbro foliations which are subparallel to the crust-mantle boundary (Ildefonse *et al.*, 1995). This yields a total thickness of the studied section of approximately 5.5 km (figure 2.3). This approach does not take into account that the crust-mantle boundary surface may be folded by emplacement or post-emplacement tectonics.

Allowing for a folded crust-mantle boundary, by constructing a geometry in which the crust-mantle boundary surface is parallel to the planar fabrics in the peridotites, yields a thickness of only ~2 km (also shown in figure 2.3). The structure of the Hilti section will be discussed in more detail later.

2.2.2. Petrography

Thin sections, cut perpendicular to the foliation or compositional layering and parallel to the lineation observed in the field, were studied using a polarising light microscope.

An example of a typical near-crust-mantle boundary wehrlite (Nicolas & Prinzhofer, 1983; Boudier & Nicolas, 1995) is shown in figure 2.4a. The interstitial clinopyroxene in figure 2.4a consists of one single poikiloblastic crystal, as shown by the orientation of the cleavage and the interference colours.

The other studied samples comprise spinel-harzburgites with generally less than 5% clinopyroxene, and Cr-spinel-bearing dunites ± clinopyroxene. The harzburgites are frequently compositionally layered; layers consist of dunite, harzburgite, orthopyroxenite and websterite. All samples are serpentinised by at least 10%.

Harzburgite samples from the first few hundred metres below the crust-mantle boundary locally contain interstitial clinopyroxene crystals (figure 2.4c,d), in addition to rounded clinopyroxene porphyroclasts found throughout the entire section. These interstitial clinopyroxenes are found down to a depth of ~800 m and in two samples from ~2000 m (depth obtained from constant dip crust-mantle boundary geometry discussed above). The fact that the irregular shapes of these clinopyroxenes are preserved despite the large strains recorded in these rocks (see next sections), indicates that they must have crystallised from a melt after the deformation, and allows for the possibility that melt has been present *during* deformation (Nicolas & Prinzhofer, 1983; Rabinowicz *et al.*, 1987).

A difference was found in orthopyroxene shape between 'shallow' and 'deep' samples. Orthopyroxenes that are elongate parallel to the foliation or layering were predominantly found in the shallow part of the mantle section. In deeper rocks orthopyroxene occurs as large rounded porphyroclasts, or as irregular crystals intermixed with olivine crystals as part of pyroxene-rich bands (figure 2.4b) that make up the compositional layering. Recrystallisation of large orthopyroxene porphyroclasts to aggregates of smaller crystals occurs throughout the mantle section. The recrystallised aggregates contain small crystals of olivine, commonly

in an interstitial habit (figure 2.4e). The results confirm the observation of Ceuleneer and co-workers (1988) that there is an increase in degree of recrystallisation of orthopyroxene porphyroclasts towards the crust-mantle boundary. In addition, highly stretched, partly recrystallised orthopyroxene crystals (figure 2.4f) and aggregates of recrystallised orthopyroxene that are elongate parallel to the foliation occur in the shallow peridotites. Consequently, orthopyroxene recrystallisation was synchronous with the deformation which produced the orthopyroxene foliation.

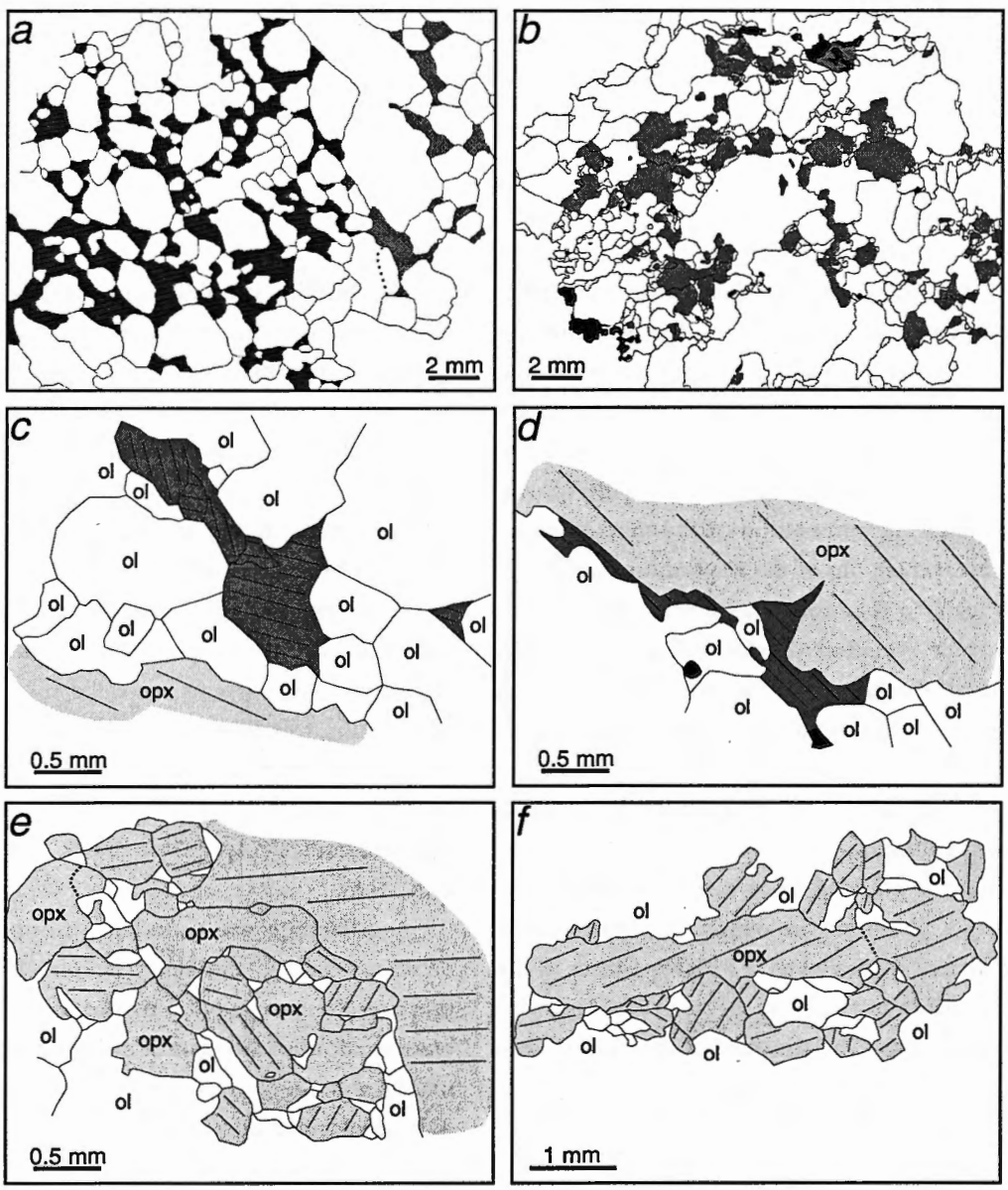

Figure 2.4: Sketches of selected areas of thin-sections. a) Part of wehrlitic sample A29, showing poikiloblastic clinopyroxene and plagioclase; b) harzburgite sample R15, showing effect of orthopyroxene on olivine grain size, compositional layering lies horizontal; c) and d) Interstitial clinopyroxene in shallow harzburgite sample R19; e) and f) recrystallisation of orthopyroxene in shallow harzburgite samples R7 and A26. Olivine crystals in white; orthopyroxene crystals in light grey with hatches parallel to cleavage (in c-f); Clinopyroxene (in a,c,d) in medium grey with hatches parallel to cleavage; Plagioclase (in a) in light grey, stippled; Spinel (in b,d) in darkest grey.

2.2.3. *Olivine grain sizes and microstructures*

The average olivine grain size of 30 collected samples was determined using a linear intercept method. The number of olivine grains intersecting the cross-wire on the eyepiece of the microscope was counted along many random lines in the thin-sections and at different magnifications. The average number of intercepts per unit length, based on several hundreds of intercepts (including double counts because of intersection of lines), was then converted to an average grain diameter. These diameters, not corrected for the sectioning effect, are plotted against depth beneath the crust-mantle boundary in figure 2.5. In addition, the largest grain diameter found in a standard 24x39 mm thin-section is also shown for each sample.

The grain size profile shows a trend of increasing average grain size with depth. Most importantly, the average grain size of the coarsest samples at a given depth interval increases with depth. The coarsest samples are mostly dunites. This compositional control on the grain size is most clearly seen in the harzburgite-dunite pairs sampled at the same outcrop (those points connected by horizontal bars). No coarse (>3 mm) samples were found among the samples from the base of the mantle section in the Hilti Massif, suggesting that the base of the section is finer grained than the middle part. It is also noted that the maximum grain size increases with depth, and the maximum grain diameter in dunites is larger than in harzburgites.

There is a marked microstructural difference between 'shallow' and 'deep' samples. Samples from the first several hundred metres below the crust-mantle boundary have a roughly equigranular microstructure (nomenclature from Mercier & Nicolas, 1975), as seen in sample A25 (figure 2.6a). At depth the microstructure becomes dominantly coarse porphyroclastic. This is illustrated by dunite sample

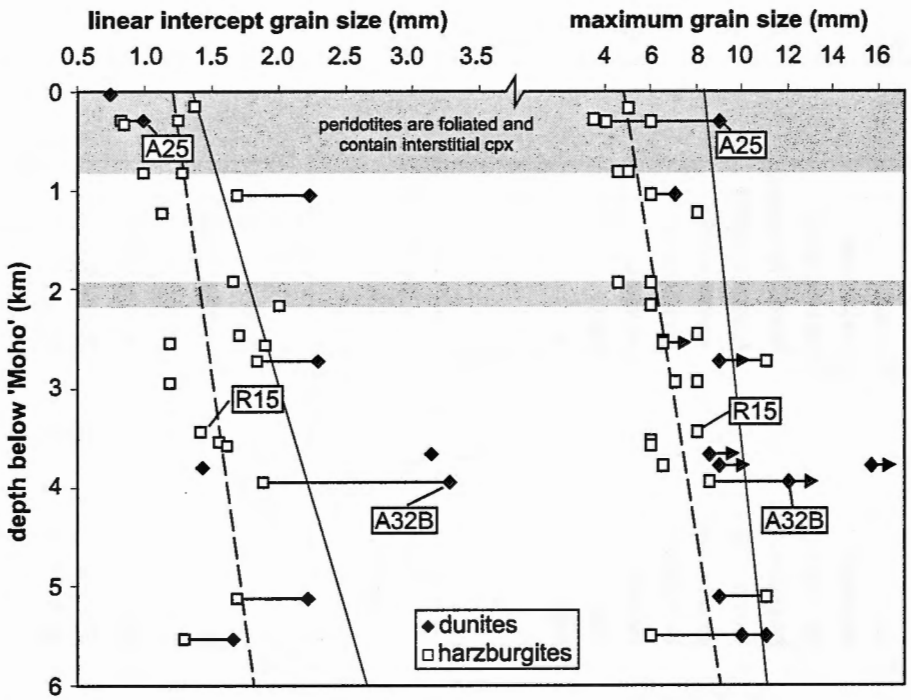

Figure 2.5: Olivine grain diameters measured using a linear intercept method and maximum grain diameter plotted with depth below crust-mantle boundary (using constant dip of crust-mantle boundary of 25°E). Harzburgites are shown as open squares, dunites as closed diamonds. Harzburgite and dunite samples from the same outcrop are connected by horizontal bars. Steep straight lines indicate best linear fit of harzburgite (dashed) and dunite grain size vs. depth. Peridotites from 0-800 m and at ~2 km are foliated and contain interstitial clinopyroxene (shaded part of diagram).

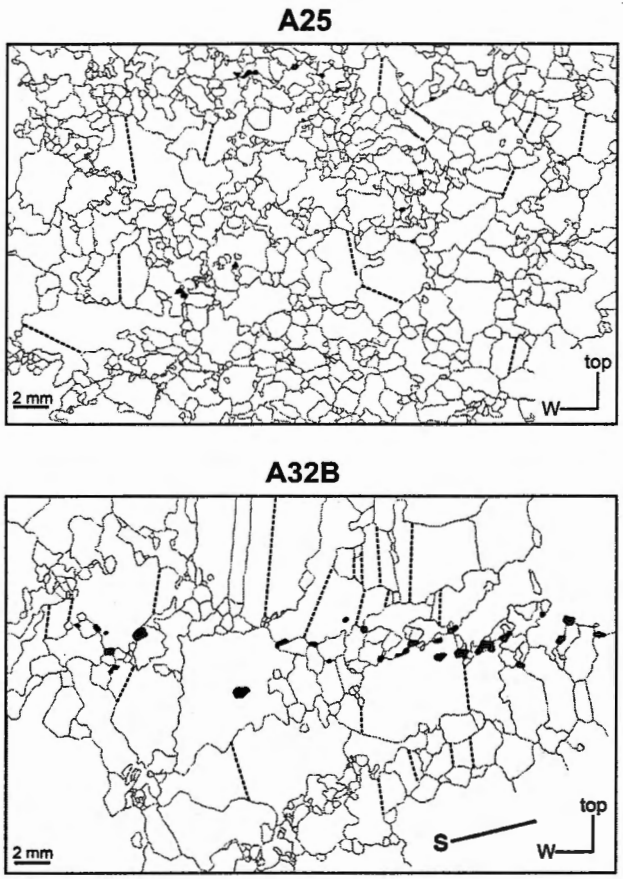

Figure 2.6: Micrographs of representative shallow and deep dunite samples of the mantle section (thin section parallel to lineation) Foliation in A25 was determined in the field and is horizontal in diagram; foliation in A32B is defined by stretched spinel grains and is indicated by thick line (denoted 'S'). Olivine crystals shown in white and spinel in black. Some subgrain wall orientations are indicated by dashed lines.

A32B in figure 2.6b, which contains olivine porphyroclasts of several millimetres in diameter and areas with smaller grains.

The grain size distributions of the equigranular sample A25 and the porphyroclastic sample A32B were determined using image analysis. Both selected samples shown are dunites, in order to exclude the effect of second phases on the distribution. The grain size distributions are presented in the histograms in figure 2.7a and b (see figure caption for details about method). There seems to be surprisingly little difference between the two samples. Both samples have a log-normal distribution, with a mode of ~0.4 mm. The distribution of the porphyroclastic sample A32B is skewed towards the large grain size end of the diagram (the

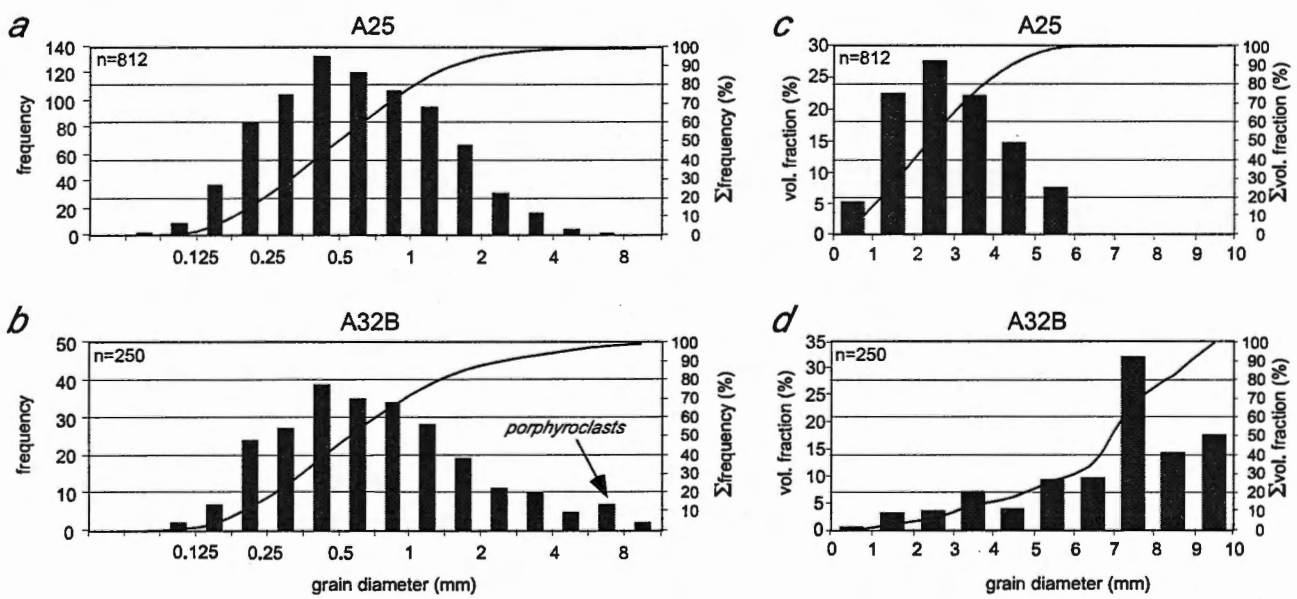

Figure 2.7: Grain diameter distributions by grain number and volume for peridotite samples shown in figure 6. Grain sizes obtained by image analysis, using NIH-Image software (National Institutes of Health, 1996). Diameters shown are average of long and short axis of ellipse fitted to grain area. Approximate volumes of grains are calculated by multiplying measured surface area of grains with short axis of best-fit ellipse.

porphyroclasts), but the number of large grains is very small compared to the number of small grains. To investigate the effect of the large porphyroclasts, the grain size distribution by volume fraction is also shown (figure 2.7c and d - see figure caption for details about method). This yields very different distributions for both samples; the porphyroclasts are volumetrically the most important grains in porphyroclastic sample A32B.

The influence of a second phase, most notably orthopyroxene, on the olivine grain size is visible in figure 2.4b. Olivine grains in orthopyroxene-rich areas are markedly smaller than those in orthopyroxene-poor areas.

Microstructural analysis of thin sections of harzburgites and dunites revealed that the olivines in both equigranular samples and porphyroclastic samples have a well developed substructure. Many grains, especially large olivines, contain subgrain walls. These subgrain walls are commonly oriented at a high angle to the foliation. In porphyroclastic samples lamellar olivine grains with their long axes parallel to these subgrain walls, or small grains along subgrain walls occur frequently (both can be seen in figure 2.6b). Olivine-olivine grain boundaries are mostly irregular. In contrast, only few olivines in the wehrlitic sample A29 contain subgrain boundaries. Most olivine-olivine grain boundaries are straight and ~120° triple junctions are common throughout the sample.

2.2.4. Olivine lattice preferred orientations

Representative samples were chosen for crystal fabric analysis by universal stage. No significant variation with depth or rock composition (*i.e.* dunite or harzburgite) in the nature or strength of these fabrics was found (see also chapter 3). The lattice preferred orientations (LPO) of the near-crust-mantle boundary wehrlitic sample A29, the 'shallow' sample A25, the 'deep' sample A32B, and two composite fabrics of porphyroclasts and small grains are shown in figure 2.8. Samples A25 and A32B are considered representative for the shallow and middle-to-deep part of the mantle section respectively, despite the fact that they are taken from dunitic layers, which are not the dominant rock-type. There is no evidence in the field, nor in the microstructures or lattice fabrics, that strain partitioned into dunitic or harzburgitic layers. Therefore, the use of dunites in the following analysis is not unjustified. Dunites are probably even better suited to study the deformation, recrystallisation, and grain size distribution in the Hilti mantle section, as there is no effect of secondary phases on the microstructures. Furthermore, experimental data on deformation of olivine aggregates can be directly applied to natural dunites.

The wehrlitic sample has virtually no LPO (figure 2.8a). Samples A25 and A32B show LPO's (figure 2.8b and c) with [a]-axes close to the lineations. Olivine [b]-axes form two maxima, one perpendicular to the foliation and one within the foliation plane perpendicular to the lineation. These LPO's are indicative of deformation by dislocation creep, with [a] (010) and [a] (001) as the dominant slip systems (*e.g.* Nicolas & Poirier, 1976; Mainprice & Nicolas, 1989). Olivine [c]-axes in sample A25 have no preferred orientation, whereas the [c]-axes in sample A32B form multiple maxima. These LPO's suggest that the olivine subgrain walls commonly found at a high angle to the foliation are mostly parallel to (100). The obliquity of the maxima of the [a]- and [b]-axes with respect to the foliation indicates non-coaxial deformation and can be used to determine the sense of shear of this deformation (*e.g.* Nicolas & Poirier, 1976). The LPO of sample A25 indicates a top-to-the-west sense of shear, whereas A32B has recorded a top-to-the-east sense of shear. This is part of a general trend: LPO asymmetries with top-to-the-east shear senses are confined to the middle and lower part of the mantle section (chapter 3).

The fabrics of olivine porphyroclasts and small grains are also analysed separately. In figure 2.8d, crystallographic axes of porphyroclasts from 5 different samples, dunites and harzburgites, have been combined.

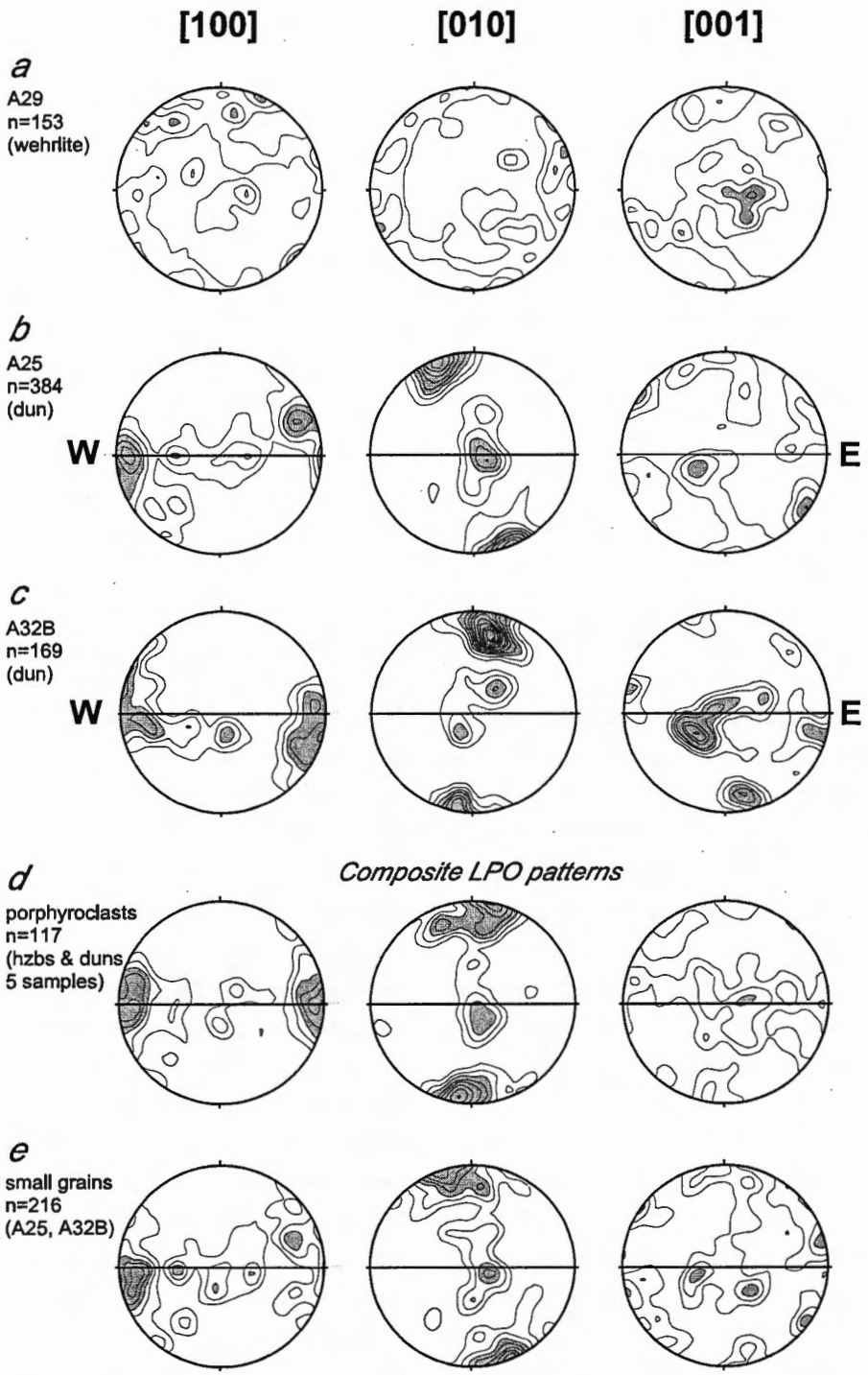

Figure 2.8: Equal area, lower hemisphere projections of olivine crystal axes of selected samples obtained by universal-stage measurements. Shown are fabrics from near-Moho wehrlite (A29), shallow dunite (A25), deep dunite (A32B) and two composite fabrics of porphyroclasts from 5 samples, and recrystallised grains of A25 and A32B. Contour intervals are one time uniform; contours >3 times uniform are shaded. Orientation of foliation or compositional layering shown by horizontal lines, lineations lie on perimeter of stereoplot, and stereoplots are approximately oriented in present-day EW-reference frame.

In figure 2.8e, the fabrics of small grains (<0.5 mm) in samples A25 and A32B are shown. There is no large difference between the crystallographic orientations of porphyroclasts and small grains. Olivine [c]-axes of small grains lie more towards the perimeter of the stereogram, close to the lineation orientation, suggesting a contribution of [c] (010) slip to the deformation of small grains.

Figure 2.9 shows an axial distribution micrograph of sample A25. In this diagram every olivine crystal has been assigned to one of three categories based on the orientation of the [a]-axes. It reveals that the microstructure is domainal. The domains are elongate at an angle of ~30° to the foliation defined by spinel. Analysis of the distribution of crystal axes also revealed the presence of orientation families, *i.e.*, distinct separate grains with similar orientations (Urai *et al.*, 1986).

2.2.5. Misorientation analysis

Three samples, samples A25, R15, and A32B were subjected to a detailed misorientation analysis. In this analysis the crystallographic relations between neighbouring olivine grains, described by a rotation angle and rotation axis of the crystal lattice of one grain with respect to its neighbour, were calculated (see Randle, 1992; Trimby *et al.*, 1998; Fliervoet *et al.*, 1999). The distribution of the rotation angles ('misorientations') and the orientations of the rotation axes of a sample may give information on the recrystallisation and deformation mechanisms. Dynamic recrystallisation involving subgrain rotation can lead to the breakdown of large olivine grains ('porphyroclasts') into smaller 'new' grains (Poirier & Nicolas, 1975; Karato *et al.*, 1982), which largely preserve the crystallographic orientation of the original grain. This is reflected in small rotation angle between the lattices of the porphyroclast and the new recrystallised grain.

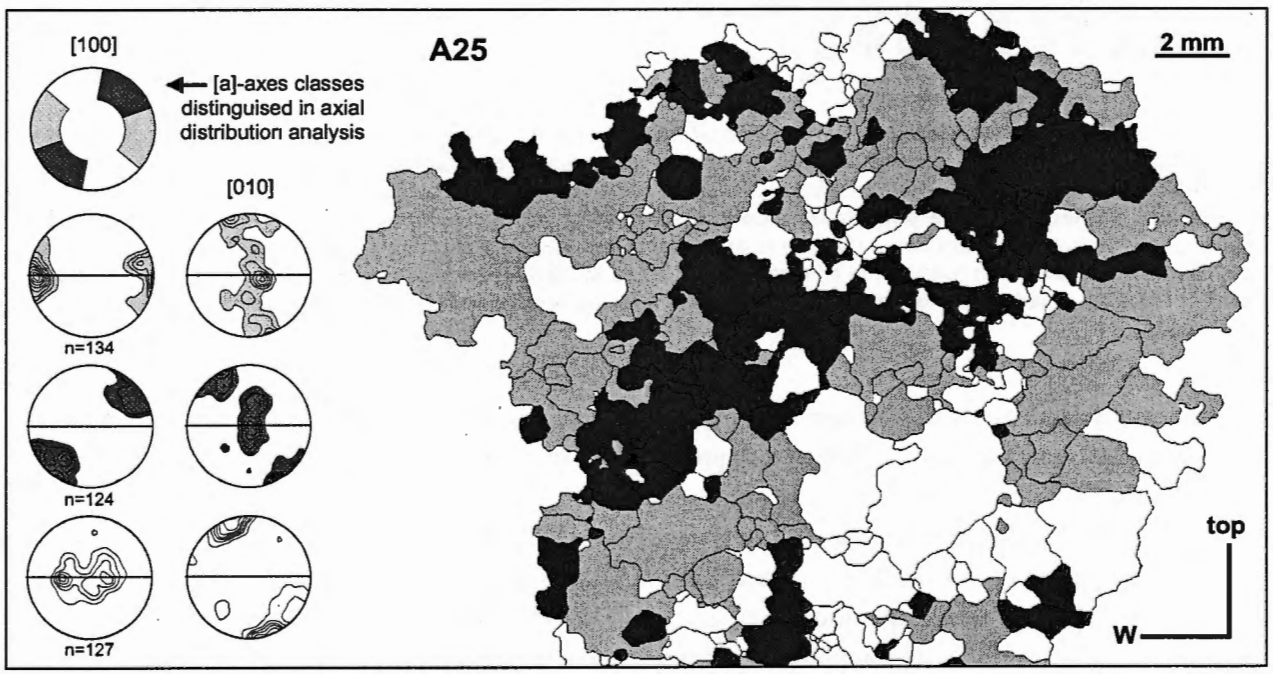

Figure 2.9: Axial distribution micrograph of shallow dunite sample A25. Olivine crystals with [a]-axes approximately parallel to lineation shown in light grey, crystals with [a]-axes at angle of ~45° to lineation in dark grey and [a]-axes perpendicular to lineation in white (see stereograms for [a]- and [b]-axes in inset). Spinels in darkest grey. Diagram shows domainal microstructure.

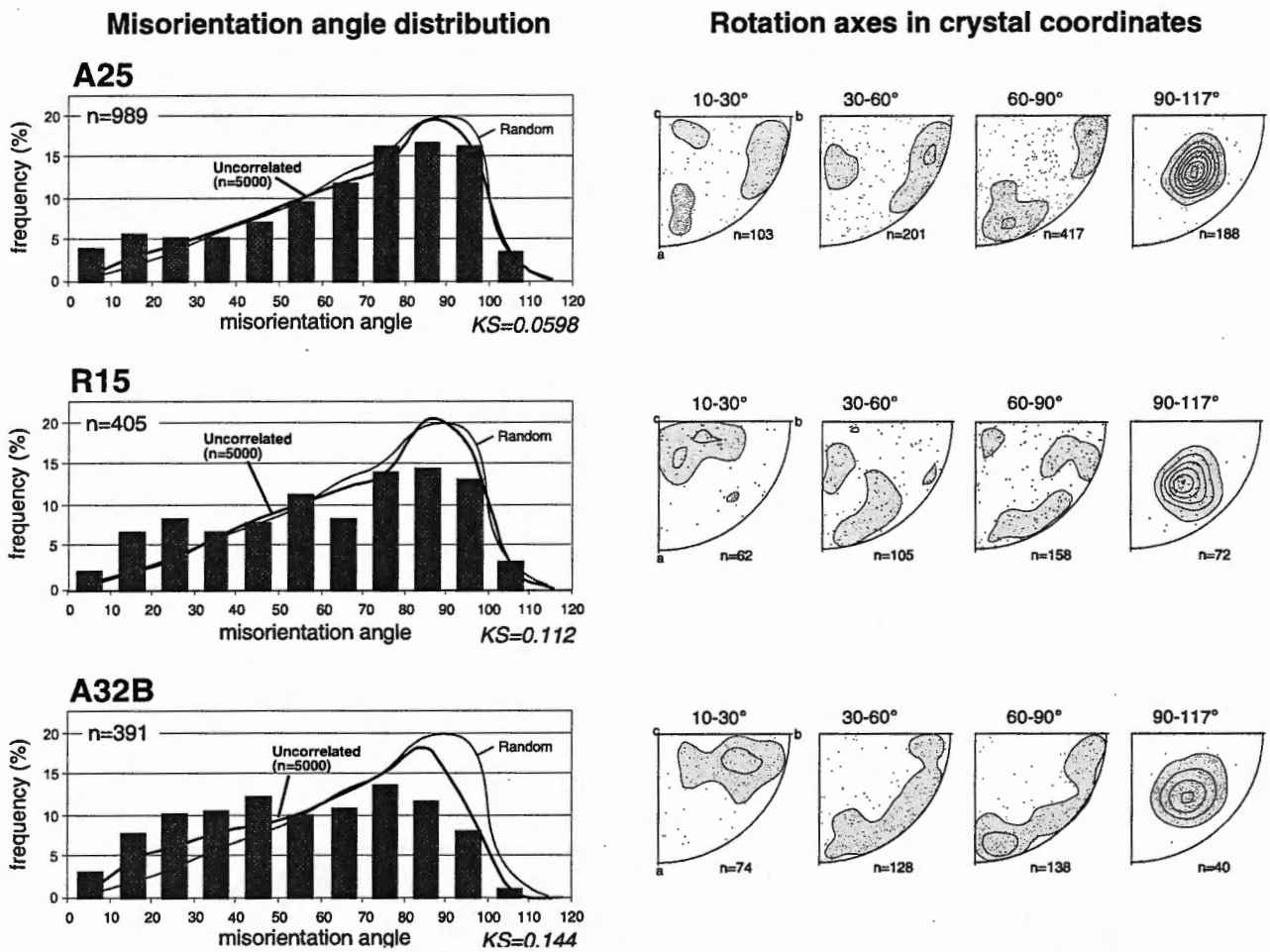

Figure 2.10: Results of misorientation analysis of three selected samples. Histograms show the distribution of misorientation angles in the samples. Also shown are the uncorrelated misorientations (see text) and the misorientations in a theoretical sample with a random fabric. Calculated rotation axes are subdivided into four classes by misorientation angle, and plotted in inverse pole figures. Contoured 1,2,3..... times uniform. Also shown are the values for the Kolmogorov-Smirnov statistic (Davis, 1986) comparing the actual misorientation distribution (MOD) with the uncorrelated misorientation distribution (UMOD). In all three examples the MOD deviates significantly from the UMOD at a confidence level of 5% (two-tailed test) and the largest deviations are found at small misorientation angles. See text for discussion of the results.

For symmetry reasons the relation between two orthorhombic lattices can be described by four possible rotations and the rotation over the smallest angle was taken as the misorientation. Rotation angles of more than 120° can always be described by a smaller rotation around another axis hence all misorientations are smaller than 120°. Outlines of grain boundaries were traced, whereas obvious subgrain boundaries were excluded in the analysis. Yet very small misorientations (<10°) across some of the boundaries were found. This suggests that some subgrain boundaries were included or that the error in the misorientation may be as large as 10°.

The misorientation distributions (MOD's) for the three samples are given in figure 2.10. For comparison, the MOD of a theoretical sample with a random LPO and the distribution of misorientations between pairs of randomly selected grains in the samples, mostly non-neighbours, the so-called uncorrelated MOD (Fliervoet *et al.*, 1999) are also shown. The most prominent

feature in the MOD's is the larger number of small misorientations in all three samples with respect to the uncorrelated and random MOD's. This means that in all three samples significantly more grains have small misorientations (*i.e.* rotation angles smaller than ~30-50°) with respect to their neighbours than would be expected from the fabric alone.

The rotation axes, described in the crystal co-ordinate system, are also given in figure 2.10 (inverse pole figures). They are subdivided into 4 classes of small (<30°), intermediate (30-60°), large (60-90°), and very large misorientations (>90). The error in the measurement of the orientations of crystals by means of the universal stage is ~5°, whereas the error in the orientation of the rotation axis can be much larger (probably up to several tens of degrees), especially in the case of small rotation angles (Prior, 1999; Fliervoet *et al.*, 1999). Therefore, all rotation axes for rotations smaller than 10° have been discarded. For small misorientations (10-30°) there is a weak preference for rotation axis orientations near the olivine [a]-, [b]-, and [c]-axes in sample A25. In R15 small misorientation rotation axes plot in a band near the [c]-axis extending towards the [b]-axis. In A32B the orientations of rotation axes for small misorientations fall within a broad band between the [b]- and [c]-axes. For intermediate and large angles the rotations axes tend to lie close to the [a]- and [b]-axes, or within the (001) plane in all three samples. The strong concentration of rotation axes away from low-symmetry orientations for misorientations >90° is imposed by symmetry related restrictions (Fliervoet *et al.*, 1999).

In the grain boundary hierarchy diagram (Trimby *et al.*, 1998) in figure 2.11, grain boundaries in equigranular sample A25 and porphyroclastic sample A32B have been classified by their misorientations. Clusters of grains can be recognised which have only small or intermediate misorientation with respect to each other. The grain boundary hierarchy diagram of the porphyroclastic sample further shows that most small grains have small misorientations with respect to neighbouring porphyroclasts.

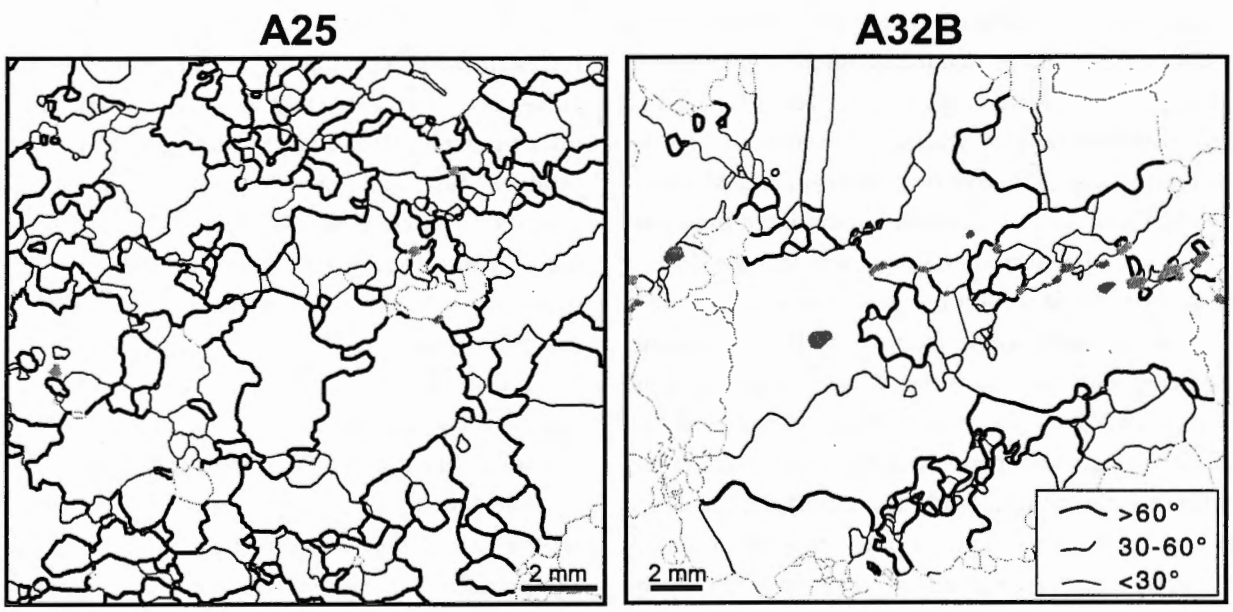

Figure 2.11: Grain boundary hierarchy diagram of near-equigranular shallow sample A25 and porphyroclastic deep sample A32B. Grain boundaries with small misorientations (<30°) are drawn as thin lines, intermediate angle (30-60°) boundaries as thicker lines, and high angle boundaries (>90°) as thick lines. Note different scales.

2.3. Discussion

2.3.1. Crust-mantle boundary geometry

The crust-mantle boundary geometry used in this paper to estimate the depth of the studied samples is probably a simplification of the actual situation. An alternative geometry, based on the assumption that the crust-mantle boundary is curved – possibly as a result of folding – parallel to the planar fabric in the peridotites, yields a much lower estimate (~2 km) for the thickness of the studied mantle section (also shown in figure 2.3). Another factor that should be accounted for is displacements along possible internal faults in the section, which may move the crust-mantle boundary up or down. Indications for such fault activity were found in a few samples from ~2 km depth (in the simple crust-mantle boundary geometry), which are in many respects similar to the peridotites in the first several hundred meters below the crust-mantle boundary. The outcrops from which they were taken were foliated, and a small chromite-pod was found. The samples have a near-equigranular microstructure containing recrystallised and elongate orthopyroxene and at least two samples contain undeformed interstitial clinopyroxene. These samples were collected west of a large serpentinite fault, which is also indicated on the geological map (Ministry of Petroleum and Minerals, 1987). It is likely that this fault has displaced the crust-mantle boundary surface in such a way that the shallow part of the mantle section is repeated west of it.

Folding and possible faulting of the crust-mantle boundary only modestly affects the trends discussed below. The discussion below deals mainly with the foliated equigranular peridotites found in the upper part of the mantle section, while the uncertainty in depth arising from the unknown crust-mantle boundary geometry becomes important away from the crust-mantle boundary, at larger depth.

2.3.2. Deformation and recrystallisation

From the lack of abundant deformation features and crystallographic fabric in the near-crust-mantle boundary wehrlite it can be concluded that it either represents a cumulate rock with some olivine xenocrysts, or a tectonite that underwent recovery and annealing after deformation. The former interpretation has been favoured for similar wehrlites (Nicolas & Prinzhofer, 1983; Boudier & Nicolas, 1995). The lack of an olivine shape and crystallographic fabric does not preclude that this sample was deformed. It is possible that it deformed by grain boundary sliding and/or diffusion creep in the presence of a large melt fraction.

The grain size profile shows that linear intercept grain diameters of olivines in harzburgites and dunites increase with depth. Harzburgites have a smaller average grain size than dunites and orthopyroxene-rich domains in harzburgites are finer grained than mono-minerallic domains. This indicates that there is a compositional control on the average grain size. Secondary phases, in this case mostly orthopyroxene, may locally inhibit olivine grain growth by pinning of grain boundaries, or may act as nucleation sites for recrystallisation, keeping the olivine grain size small in poly-minerallic areas. Furthermore, reactions between orthopyroxene clasts and percolating melts can locally produce fine grained olivine and orthopyroxene (chapter 5). There is also an effect of orthopyroxene on the maximum grain size found in each sample. The interpretation of the maximum grain size is not straightforward since this size is limited by the size of the thin-section. However, the fact that the largest porphyroclasts are commonly found in dunites, suggests that secondary phases limited the initial grain size.

The increase in average grain size with depth is related to a change in microstructure from dominant equigranular to porphyroclastic. The grain size distribution of a deep and a shallow sample obtained from image analysis revealed that the most prominent difference is the volume fraction of large porphyroclasts.

The fabric analysis showed that the studied dunites and harzburgites are tectonites. They have a strong LPO, indicating that they underwent large strains in the dislocation creep regime. The dominant slip systems were [a](010) and [a](001). There is evidence for a minor contribution from the [c](010) slip system, especially in relatively small grains.

The misorientation analysis of an equigranular and two porphyroclastic samples revealed that significantly more grains have small misorientations with respect to their neighbours than would be expected from the LPO's alone. This leads to the suggestion that dynamic recrystallisation by subgrain rotation has been an important process in microstructure development (Fliervoet *et al.*, 1999; Trimby *et al.*, 2000). The weak preference of the orientations of the rotation axes near the crystallographic [b]- and [c]-axes fit with slip in the [a]-direction on {0kl} planes and re-arrangement of [a]-edge dislocations into (100) tiltwalls (figure 2.12 and table 2.1). The presence of rotation axes girdles and the absence of rotation axes coinciding exactly with the [b]- and [c]-axes means that simple subgrain boundaries are rare, and that subgrain boundaries are commonly composites of different types of dislocations (Lloyd *et al.*, 1997). Rotation axes near the [a]-axes, as seen in sample A25, can be produced by lattice rotations across (001) tiltwalls made of [c]-edge dislocations (figure 2.12 and table 2.1). This suggests the presence of [c]-dislocations in sample A25 during deformation and recrystallisation (table 2.1). Alternatively such rotation axes could be the result of lattice rotations across (100) twistwalls made of [b]- and [c]-screw dislocations. However, such twistwalls are unlikely, because of the high energy of [b]-dislocations resulting from their long Burgers vectors.

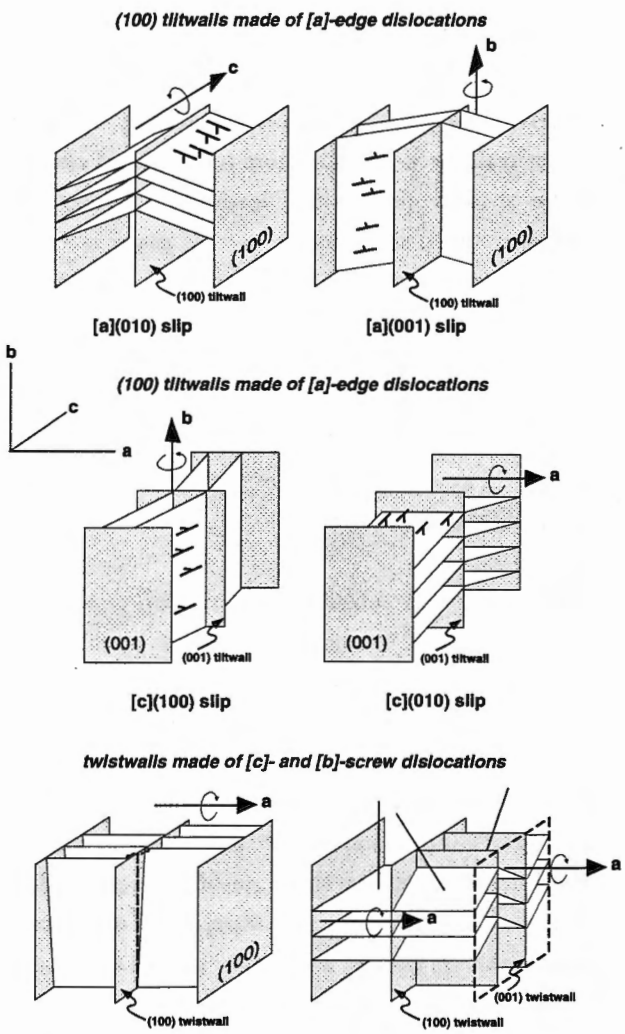

Figure 2.12: Schematic diagram showing lattice rotations across subgrain (tilt-) walls, that can develop into new grains by progressive subgrain rotation. Re-arrangement of [a]-dislocations into (100) subgrain walls can produce rotation axes parallel to the [c]- or [b]-axes. See also table 2.1.

Further support for the subgrain rotation recrystallisation process comes from the grain boundary hierarchy diagrams (figure 2.11). The diagrams show clusters of grains which have only small misorientations with respect to each other, suggesting that they were derived from an original coarser grain by rotational recrystallisation. Small grains in the porphyroclastic sample have small misorientations with respect to the adjacent porphyroclasts and are probably produced by breakdown of the porphyroclasts by subgrain rotation recrystallisation largely preserving the crystallographic orientation of the porphyroclasts. The recrystallisation has led to a net grain size reduction. The domainal microstructure of the equigranular sample A25, as revealed by the axial distribution analysis (figure 2.10),

Table 2.1
Slip systems in olivine crystals and subgrain rotation axes

Slip system[1]	Denoted as[2]	Strength[3]	Tiltwall[4]	Rotation axis[5]
[a] (010)	$[110]_c$	low	//(100)	// [c]
[a] (001) + [c] (100)	$[101]_c$	intermediate	//(100)+(001)	// [b] + [b]
[c] (010)	$[011]_c$	high	//(001)	// [a]

[1] Burgers vector and slip plane
[2] Notation used in single crystal deformation literature
[3] See for instance Mackwell *et al.* (1990)
[4] Expected orientation of tiltwall with respect to crystal lattice (see figure 2.12)
[5] Expected lattice rotation axis with respect to crystal lattice (see figure 2.12)

also suggests that it was formed from a coarse (mm-size) protolith by rotational recrystallisation, with the domains probably representing recrystallised porphyroclasts. Irregular grain boundaries and orientation families in the studied samples indicate that grain boundary migration was also important. In conclusion, recrystallisation has occurred by a general mechanism involving a combination of new boundary formation and grain boundary migration (Drury & Urai, 1990).

The results of the study of the grain size variations with depth can be directly compared to the theoretical analysis of the expected grain size variations in the oceanic mantle lithosphere by Karato (1984). Karato investigated two scenarios of mantle lithosphere moving away sideways from a spreading centre and growing downward as a result of cooling. If the initial grain size in the vertical upwelling underneath the spreading centre is small and if during subsequent horizontal off-axis flow the grain size in the mantle is controlled by grain growth, then deeper rocks will attain larger grain sizes as they have more time to grow before they cool down below the temperature at which grain growth is effectively arrested. In contrast, when the initial grain size is large, the grain size will be controlled by dynamic recrystallisation and the preserved grain size is expected to decrease with depth as the stress at which the rocks are frozen-in increases with distance from the spreading centre (Karato, 1984).

Neither of the two scenarios suggested by Karato (1984) is supported by the results from the Hilti area. The grain size is seen to increase with depth yet there is abundant evidence that dynamic recrystallisation involved grain size reduction rather than grain growth. Importantly, the principal microstructural difference between the peridotites in the first several hundred metres below the crust-mantle boundary and those deeper in the section is the more recrystallised character of the shallow peridotites, leading to equigranular microstructures and smaller *average* grain sizes. No significant differences in the *recrystallised* grain size are found in the studied harzburgites and dunites, suggesting no stress differences at the time of freezing in of the microstructures.

2.3.3. Stress and strain

It is generally found in deformation experiments that the size of recrystallised grains produced by dynamic recrystallisation in the dislocation creep regime is inversely related to the stress (Twiss, 1977; Ross *et al.*, 1980;Van der Wal *et al.*, 1993). The recrystallised grain size may also be temperature dependent (De Bresser *et al.*, 1998), although experiments on olivine show no obvious dependence (Van der Wal *et al.*, 1993). Moreover, deformation experiments on olivine are usually carried out at near- or super-solidus conditions. Therefore, the use of stress-grain size relations to infer stresses in the mantle at ocean ridges does not require temperature extrapolations. In order to determine the size of the recrystallised grains in the studied peridotites and to exclude the effect of relic porphyroclasts, the grain size

distribution of the almost completely recrystallised equigranular sample A25 was analysed. The median of the log-normal grain size distribution of sample A25 (0.56 mm), multiplied by a geometric factor of 1.2 to correct for sectioning, was taken as the typical recrystallised grain size. This grain size of 0.7 mm yielded a stress of 10 MPa using the piezometer of Van der Wal *et al.* (1993). There is, however, some uncertainty as to the relevance of this piezometer as in recent olivine deformation experiments by Zhang *et al.* (2000) smaller recrystallised grains were produced than predicted by the Van der Wal relation. Extrapolating the Zhang *et al.* (2000) data using the slope of the Van der Wal relation gave a stress of 4 MPa for a recrystallised grain size of 0.7 mm. It is noted again that the *qualitative* microstructural study of all collected samples showed no significant differences in microstructure, fabric strength, or size of the recrystallised grains between dunites and harzburgites. Therefore, the use of a dunite sample for the *quantitative* grain size analysis to obtain a stress estimate is justified.

The more recrystallised character of the shallow harzburgites and dunites can most easily be interpreted as the result of a stronger imprint (*i.e.* more accumulated strain) of a deformation 'episode' at a stress of 4-10 MPa. Ceuleneer and co-workers (1988) also concluded that the plastic shear strain recorded in the mantle sections of the Fizh and Salahi (Hilti) massifs of the Oman Ophiolite increases rapidly towards the crust-mantle boundary. This conclusion was based on a systematic crystallographic study of the average angle between flow planes and foliations. The strong foliation in the shallowmost ~800 m of the mantle section, caused by elongation of orthopyroxene porphyroclasts, is in full agreement with higher finite strain. It also follows that the higher degree of recrystallisation of orthopyroxene and olivine – and thus the smaller average grain size - is the effect of more strain during the relatively high stress deformation episode. Consequently, the strain rate in the shallow part must have been higher and/or deformation must have ceased later, compared to the deeper part. In either case, it follows that at some stage the deformation was localised in the shallow part (the first several hundred meters) of the mantle section.

2.3.4. Shear localisation, melt weakening, and rheology

Shear localisation can occur in materials under various conditions. In materials exhibiting elastic, elastic-brittle, or pressure sensitive elastic-plastic deformation, a shear localisation instability can be initiated during strain softening, steady-state deformation, or strain hardening (Hobbs *et al.*, 1990). However, for deformation to remain localised in a shear zone the material inside the shear zone has to be significantly weaker than the surrounding material, otherwise the zone of localised deformation would widen and the shear zone would become a self-arresting instability (*e.g.*, White *et al.*, 1980; Hobbs *et al.*, 1990; Rutter, 1999). A weakening mechanism is thus required to explain the inferred shear localisation in the upper part of the mantle section in Hilti.

The principal differences between the shallow and deeper samples studied are the smaller average grain size (most notably by volume%) of the shallow peridotites, and the petrographic indications, *i.e.* undeformed interstitial clinopyroxene, that melt may have been present during deformation at relatively high stress. There are no significant differences in the recrystallised grain size between the studied shallow and deep sample, which implies no significant variations of stress with depth. As a result, the weakening mechanism is either melt or grain size related.

A possible weakening mechanism is a change of dominant deformation mechanism, from dislocation to grain size sensitive creep (*e.g.*, Rutter & Brodie, 1988; see also chapter 5). In order to analyse the role of grain size sensitive diffusion creep, it is necessary to take the grain size distribution into account. It is shown in

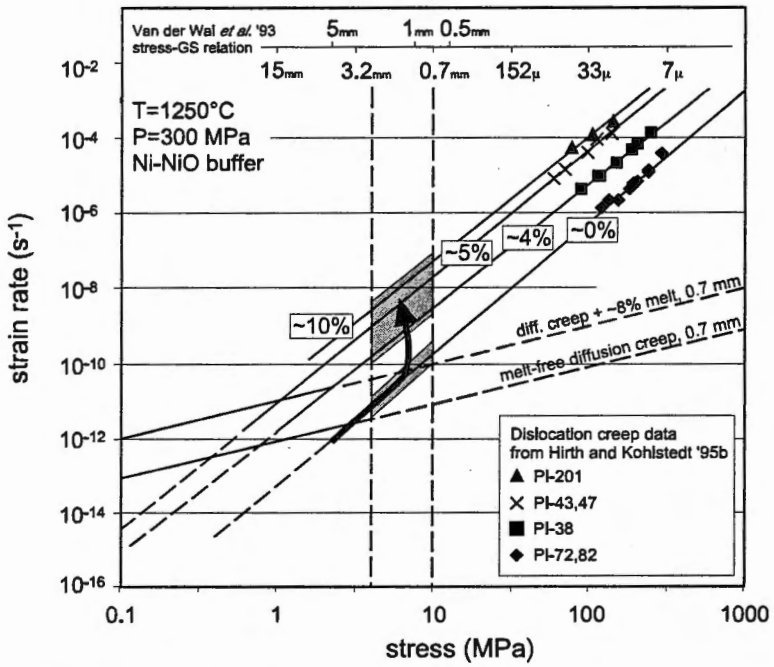

Figure 2.13: Rheological data on experimental olivine deformation at temperature of 1250°C and pressure of 300 MPa extrapolated to natural stresses and strain rates. Diagram shows selected data of Hirth and Kohlstedt (1995b) of deformation of olivine aggregates containing variable amounts of melt (0%, ~4%, ~5% and ~10%) in the *dislocation* creep regime (steep set of lines). Line labelled '~10%' is best-fit line to data of Hirth and Kohlstedt (1995b) of sample PI-201 containing ~10% melt, with an imposed stress exponent of 3.1. Also shown in same diagram are lines describing results of Hirth and Kohlstedt (1995a) of olivine deformation in the *grain size sensitive diffusion* creep regime of nominally melt-free and melt-bearing olivine aggregates, recalculated to a grain size of 0.7 mm using a grain size exponent in the fitted olivine flow law of 3. Grey boxes indicate deformation conditions of studied samples at inferred stress of 4-10 MPa; lower grey box indicates deformation of melt-free peridotite, whereas upper grey box indicates deformation of peridotite with >4% melt at same conditions. It can be seen that the presence of >4% melt can lead to a significant increase of the strain rate.

figure 2.13 that diffusion creep at a grain size of 0.7 mm at 1250°C is subordinate to dislocation creep. This is consistent with the widespread evidence for dislocation creep in the studied samples. However, even the so-called 'equigranular' sample A25 has a distributed grain size. The effect of a distributed grain size on the bulk deformation of an aggregate may be large due to a contribution of diffusion creep in small grains (Freeman & Ferguson, 1986; Ter Heege *et al.*, 1999). The grain size at which diffusion creep and dislocation creep contribute equally to the deformation of an olivine crystal at 10 MPa and 1250°C in a melt-free rock is 0.25 mm (based on the flow laws given in caption of figure 2.13). The grain size distribution of sample A25 (figure 2.7a and c) shows that only 25% of the grains (less than 1 volume%) in this sample are smaller than this transition grain size (divided by 1.2 to account for sectioning effect), hence may have deformed (partly) by diffusion creep. At a stress of 4 MPa the transition grain size is 0.54 mm. In A25 approximately 50% of the grains are smaller than this grain size (again divided by 1.2), but these grains still account for less than 10% of the total volume. It is unlikely that a contribution of diffusion creep to the deformation of these small grains led to significant weakening of the aggregate as a whole, since such a small volume fraction of grains will not form an interconnected network to accommodate the deformation, unless the small grains are organised in bands. Another indication that a small grain size alone cannot explain the inferred weakening lies in the

observation that olivine grains in orthopyroxene-rich areas throughout the mantle section are generally fine grained, yet there is no evidence for localisation of deformation in orthopyroxene-rich bands.

As grain size effects can be ruled out as the cause of weakening and shear localisation, the processes were most likely related to the presence of melt. It has been found in experiments that mantle rocks deforming by dislocation creep in the presence of a critical amount (~4%) of melt are significantly weaker than melt-free mantle rocks (Hirth & Kohlstedt, 1995a,b; Bai *et al.*, 1997). Melt weakening could therefore have been responsible for the localisation observed in the study area. Figure 2.13 shows the deformation data of Hirth & Kohlstedt (1995a,b) at super-solidus temperature (1250°C), extrapolated to natural stresses and strain rates (see figure caption for details). The temperature at the top of the mantle section of the Oman Ophiolite, albeit above a mantle diapir, has been estimated to have been ~1240°C during plagioclase crystallisation (Kelemen & Aharonov, 1998). Therefore, these experimental data can be used directly - without the need for a temperature correction - to constrain the deformation of the studied section. A stress of 4-10 MPa yields a strain rate of $\sim 10^{-11}$-10^{-10} s^{-1} (*i.e.* an 'effective' viscosity of $\sim 5 \cdot 10^{16}$ -$2 \cdot 10^{17}$ Pas) by melt-free dislocation creep. The Hirth & Kohlstedt data suggest that deformation at the same stress in the presence of 4-10% melt may be at least 1 order of magnitude faster (a viscosity drop of at least 1 order).

It is impossible to estimate the amount of interstitial melt that may have been present in the peridotites from directly beneath the crust-mantle boundary during deformation using petrographic observations alone. The wehrlites locally contain at least 20% of interstitial minerals, but it is crucial to note that these minerals are cumulates, the products of fractional crystallisation. If they were derived by fractional crystallisation of one pulse of magma that was subsequently extracted, the melt volume was larger than the volume of cumulate minerals. On the other hand, if they crystallised during a prolonged period of magma percolation, their volume may be larger than the melt fraction present in the rocks *at one time* (the instantaneous melt fraction).

It has been argued that melt in peridotites forms a permeable network at melt fractions of <1% (Kohlstedt, 1992;Von Bargen & Waff, 1986; McKenzie, 1989), or 2-3% at most (Faul, 1997). Therefore, melt fractions in excess of 4%, required to explain the inferred weakening, can only be expected below melt migration 'barriers'. Kelemen & Aharonov (1998) concluded that the crust-mantle boundary can indeed act as such a barrier, due to crystallisation of plagioclase clogging the porosity. In addition, anisotropic melt distributions could also lead to melt accumulation. It has been found that during low stress deformation basaltic melts preferentially wet (010) faces of olivine (Waff & Faul, 1992; Daines & Kohlstedt, 1997), which will become orientated subparallel to the flow plane during dislocation creep (e.g. Zhang & Karato, 1995 and results presented above). It is therefore expected that peridotites in vertical upwellings will be more permeable vertically than horizontally (Daines & Kohlstedt, 1997). As soon as mantle flow rotates to become subhorizontal at shallow levels, vertical permeability will be reduced and melt may become trapped in the shallow mantle. Moreover, grain size variations can affect melt distributions: melts tend to become concentrated in fine-grained domains (Wark & Watson, 2000). Finally, 'piezometric' pressure gradient effects in zones undergoing shear deformation could cause melt accumulation leading to a positive feedback between deformation, melt concentration, and melt weakening (e.g. Rabinowics et al., 1987; Ribe, 1987; Kelemen & Dick, 1995).

One proposed explanation for the melt weakening found in olivine deformation experiments is a change from creep of olivine limited by the [c]-slip system to [a]-slip limited creep through relaxation of the Von Mises criterion (Hirth & Kohlstedt, 1995b; Drury & Fitz Gerald, 1998). Normally, some contribution of the strong [c]-slip system is required during dislocation

creep deformation of olivine poly-crystals in order to preserve strain compatibility. Under these conditions, the deformation rate and the strength of an olivine rock are controlled by the strong [c]-slip system, even though most of the strain - and thus the LPO - is produced by the weaker [a]-slip system. It has been argued that, in the presence of melt, alternative mechanisms such as grain boundary sliding or a diffusion-related deformation process can take over the role of [c]-slip, leading to deformation whose rate is controlled by [a]-slip rather than [c]-slip (Hirth & Kohlstedt, 1995b; Drury & Fitz Gerald, 1998). Single [a]-slip, in combination with grain boundary sliding or a diffusion related deformation process, is more than two orders of magnitude faster than [c]-slip at near-solidus conditions (Mackwell *et al.*, 1990; Hirth & Kohlstedt, 1995b; Drury & Fitz Gerald, 1998). If deformation in the apparently melt-weakened shallow peridotites in Hilti was accommodated only by [a]-slip plus grain boundary sliding or a diffusion process, then no activation of [c]-slip would be expected. The LPO and misorientation analysis show that [a]-slip was responsible for the bulk strain (and the development of the LPO), but that [c]-dislocations contributed significantly to subgrain rotation, and perhaps as well to creep to some extent, in the shallow highly recrystallised, apparently melt-bearing, sample A25. Therefore, the data does not support the underlying mechanism causing melt weakening of olivine rocks proposed by Hirth & Kohlstedt (1995b).

The melt weakening observed in experiments is only found in peridotite samples with a grain size close to the transition from dislocation to diffusion creep. In consequence, a fine-grained melt-bearing olivine aggregate is weaker than a coarse-grained aggregate. It is possible that the weakening of melt-bearing samples takes place through an indirect grain size effect. Hirth & Kohlstedt (1995b) found that the recrystallised grain size of a melt-bearing sample was about four times smaller than predicted by the piezometer of Van der Wal and co-workers (1993). They explain this grain size difference by inhibition of grain growth due to pinning of grain boundaries by melt. In this study it is found that the recrystallised grain sizes of the apparently melt-bearing shallow samples are not significantly different from the apparently melt-free deep samples. It is however possible that the stress in the zone of localised deformation was relaxed as a consequence of weakening, but that melt prevented the grains to grow and attain their equilibrium grain size. Moreover, small fractions of melt may have been present throughout the mantle section, in enough quantity to lead to pinning of grain boundaries but in insufficient amounts to cause weakening.

In summary, the results of this study suggest that melt weakening is not related to an *intra-granular* deformation process such as a change of the limiting slip system. The observation that melt weakening occurs at a small grain size, and that the effect of weakening is proportional to the melt content (Hirth & Kohlstedt, 1995a, 1995b; Bai *et al.*, 1997) can most easily be explained by enhancement of *grain boundary* deformation processes such as grain boundary sliding and/or grain boundary diffusion promoting Coble creep. Mechanisms that may be responsible for enhancement of grain boundary processes in a porous melt-bearing olivine aggregates are enhancement of diffusion along melt-wetted grain interfaces, a decrease in load-bearing area causing a stress concentration at solid-solid grain contacts, and/or a shortening of the grain boundary diffusion distance (Hirth & Kohlstedt, 1995b; De Kloe, 2001).

This study shows that melt weakening of mantle rocks, as found in experiments, can indeed occur in natural mantle rocks, provided that melt concentrations are large, for instance in a sub-crust-mantle boundary zone of melt accumulation at an oceanic ridge. Melt accumulation is most likely to occur at the base of the thermal lithosphere, just below the level at which plagioclase and clinopyroxene start to crystallise from upward migrating melts. The relatively wide zone of melt accumulation inferred in this study may be,

however, a feature of a dying, compressive ridge system, where magma transport in the mechanical boundary layer through melt veins and dykes is less effective than in an actively spreading system.

2.4. Conclusions

(I) Peridotites in the first few hundred metres (~800 m in a constant dip crust-mantle boundary geometry, ~575 m in the alternative, folded crust-mantle boundary geometry discussed) of the mantle section exposed in Wadi Hilti exhibit a strong spinel and orthopyroxene foliation whereas in deeper peridotites only a spinel foliation and a compositional layering was observed.

(II) The average olivine grain size of the mantle increases with depth below the crust-mantle boundary. This increase is related to a change of microstructure from dominantly equigranular in the first several hundreds of metres, to porphyroclastic at depth. Both equigranular and porphyroclastic samples have a distributed grain size.

(III) Olivines and orthopyroxenes in peridotites of the upper part of the mantle section are more strongly recrystallised than those deeper in the section. In addition, shallow peridotites contain interstitial clinopyroxene to a depth of ~800 m (~575 m in alternative crust-mantle boundary geometry discussed), which is interpreted as a cumulate phase from a melt which was present during deformation. The zone which preserves evidence for melt accumulation is wider than previously reported (*e.g.* Boudier & Nicolas, 1995).

(IV) All samples studied, except for one near-crust-mantle boundary wehrlite, contain evidence for deformation by dislocation creep. Fabric studies of representative samples show that they were deformed by [a](010), [a](001) and minor [c](010) slip.

Misorientation analysis showed that in the three studied samples significantly more crystals have small misorientations with respect to their neighbours than expected from the fabric alone. This means that subgrain rotation was an important process in making the microstructure. Subgrain rotation recrystallisation has led to a reduction of the original olivine grain size of several mm's to a final size of ~0.7 mm.

(V) The grain size reduction is most likely associated with strain localisation into the top part (~575-800 m) of the mantle section. The strain localisation is attributed to a melt-related weakening mechanism. This requires high melt contents, suggesting that melt accumulated below the crust-mantle boundary.

(VI) LPO and misorientation analysis showed that the hard [c]-slip system was active in the 'melt-weakened' sample. This cannot be reconciled with the hypothesis that melt weakening is caused by a change from [c]-limited slip to [a]-limited slip (Hirth & Kohlstedt, 1995b; Drury & Fitz Gerald, 1998). Based on this observation, and on the published experimental data which show that melt weakening occurs in fine-grained aggregates and that the weakening effect is proportional to melt content, it is inferred that melt weakening was produced by enhancement of grain boundary processes.

(VII) Extrapolation of experimental data to the stress (4-10 MPa) estimated from the recrystallised grain size yields a strain rate of $\sim 10^{-11}$-10^{-10} s^{-1} for melt-free peridotites and $>10^{-10}$-10^{-9} s^{-1} for peridotites containing more than 4% melt. This converts to an effective viscosity of $2 \cdot 10^{17}$-$5 \cdot 10^{16}$ Pas for melt-free, and a viscosity of $2 \cdot 10^{16}$-$5 \cdot 10^{15}$ Pas for melt-bearing peridotites. This viscosity drop of at least one order agrees well with the viscosity drop required by the modelling of the pattern of mantle flow at diapiric upwellings based on observations on the mantle section of the Oman Ophiolite by Rabinowicz and co-workers (1987).

Chapter 3

Deformation in the shallow peridotites in the Hilti Massif (Oman Ophiolite): Active mantle flow or collapse of the crust-mantle transition zone in a dying ridge system?

Abstract

In previous studies it has been proposed that deformation structures and microstructures in peridotites from the Oman Ophiolite record 'active', buoyancy-driven flow in the asthenosphere beneath the Oman paleo-ridge. This chapter presents a new analysis of (micro)structures and lattice fabrics in samples from the mantle section of the Hilti Massif in Oman, one of the type-areas for structures attributed to active mantle flow. The analysis has revealed that two high-temperature and one lower-temperature ductile deformation stages can be recognised. The first stage (D1) comprised low stress (a few MPa) deformation at temperatures >1250°C. The coarse microstructures associated with D1 were overprinted during a second, non-coaxial deformation stage (D2), which occurred at stresses of ~4-10 MPa and at temperatures of 1200-1250°C, and which was localised in the upper part of the mantle section. Olivine lattice preferred orientations show that D2 deformation had a top-to-the-west vergence. Subsequent D3 deformation at temperatures of 1000-1100°C or less led to the development of peridotite mylonites which record left-lateral strike-slip deformation. D2 deformation is attributed to the onset of compression slightly off-axis from the Oman paleo-ridge, rather than to active mantle flow associated with asthenospheric upwelling at the ridge-axis. D2 deformation caused the expulsion of melts from the crust-mantle transition zone, leading to intrusion of wehrlites into the just consolidated oceanic crust. It is demonstrated that two existing geotectonic scenarios for the formation and emplacement of the Oman Ophiolite can provide an adequate kinematic framework for the D1 to D3 deformation history of the mantle section of the Hilti massif.

3.1. Introduction

3.1.1. Scope and outline

Mantle sections of ophiolites often preserve microstructures produced by high strains at temperatures near the peridotite solidus and at very low deviatoric stresses (Nicolas & Poirier, 1976; Nicolas, 1986b; Ceuleneer et al., 1988; Suhr, 1993; Ildefonse et al., 1998a). This suggests that ophiolitic mantle rocks

have recorded deformation taking place within the asthenosphere. It has therefore been argued that structural studies of ophiolitic mantle sections can provide crucial information about the geometry and driving forces of flow in the asthenosphere beneath ocean ridges (Nicolas & Violette, 1982; Nicolas et al., 1988a; Nicolas, 1989; Suhr, 1993). Based on such studies in the mantle section of the Oman Ophiolite it has been concluded that the shallow asthenosphere beneath the Oman spreading ridge was undergoing buoyancy-driven convection and that the flow in the asthenosphere was faster than the motion of the lithosphere above (the active flow model; e.g., Ceuleneer et al., 1988; Ceuleneer & Rabinowicz, 1992; Nicolas et al., 1994).

This conclusion is at variance with the current views on the nature of flow in the asthenosphere. Despite some indications for along-axis variations in the sub-crustal gravity structure of ocean ridges, which are interpreted as the result of active mantle flow focussed into diapiric upwellings (Wang *et al.*, 1996), most geophysical observations have been interpreted in terms of *passive* upwelling as a response to the movement of the lithospheric plates (Davies & Richards, 1992; Dunn & Toomey, 1997; The MELT Seismic Team, 1998). It appears that the asthenosphere simply acts as a decoupling horizon which accommodates differential movements between the lithospheric plates and the deeper convecting mantle (e.g., Phipps Morgan et al., 1995).

This study re-investigates the mantle section in the Hilti Massif, which is one of the type areas in the Oman Ophiolite for the active asthenospheric mantle flow model (Ceuleneer et al., 1988; Ceuleneer & Rabinowicz, 1992; Ildefonse et al., 1995; Michibayashi et al., submitted, 2000). In this chapter the results of a structural, microstructural, and petrofabric study of collected samples are presented. A new interpretation regarding the time sequence of deformation in the mantle section of the Hilti Massif is put forward. It is argued that the peridotites just below the crust-mantle boundary in the Hilti Massif have recorded a late stage of deformation taking place off-axis. The kinematic data are interpreted within a framework of compressional tectonics close to the Oman paleo-ridge axis. The compression caused deformation which was localised in a melt-rich zone just below the crust-mantle boundary. In the proposed model a crystal-melt mixture was squeezed out of the peridotites in this zone, forming the wehrlitic intrusions which are found in the plutonic section of the Hilti Massif. This event probably represents the onset of compressional tectonics resulting from intra-oceanic subduction (e.g., Searle & Cox, 1999), or from intra-oceanic thrusting in a microplate setting (e.g., Boudier et al., 1997).

3.1.2. The standard model of accretion of oceanic mantle lithosphere

In this chapter the terms (oceanic) lithosphere and asthenosphere are used in their rheological meaning. The lithosphere is defined as the outer layer of the Earth which only deforms at geological strain rates at relatively high deviatoric stresses. This means that the lithosphere only behaves as a rigid plate in low-stress settings, such as during mantle convection or spreading at oceanic ridges. When stresses are high enough the oceanic lithosphere is a high viscosity layer which can undergo internal deformation. The term asthenosphere is used for the weak zone directly beneath the lithosphere, which already yields at stresses of only a few mega-pascals (MPa).

It is generally thought that beneath ocean ridges, asthenospheric mantle material rises up from depth meanwhile undergoing decompression melting (McKenzie, 1984; Nicolas, 1986a; Niu, 1997). Near the surface the asthenospheric mantle flow plane rotates and becomes subhorizontal (Ceuleneer *et al.*, 1988; Nicolas, 1989; Suhr, 1993). During this stage the mantle cools by conductive heat-loss to the surface. As a result of cooling, the strength of the peridotites increases until

ductile deformation ceases and the material has become part of the 'rigid' lithosphere (Schubert *et al.*, 1976; Karato, 1984). In this way the lithosphere grows downward during drift away from the ridge axis (Parker & Oldenburg, 1973), a process often referred to as 'plate thickening' or 'plate accretion' (figure 3.1). Note that in plate thickening models the lithosphere is defined by its basal temperature, often 0.9 times the peridotite melting temperature. It is assumed that the peridotites which build the lithosphere are essentially rigid at lower temperatures.

Over 20 years of mapping in the Oman Ophiolite has led to detailed maps of structures in the mantle section of the ophiolite (*e.g.*, Lippard *et al.*, 1986; Nicolas & Boudier, 1995). It has been found that most mantle rocks have preserved microstructures produced by low stress (typically <5 MPa) and high-temperature (near- to super-solidus, *i.e.*, >1250°C) deformation (Nicolas, 1986b; Ceuleneer *et al.*, 1988; Nicolas, 1989; Ildefonse *et al.*, 1998a). Only locally, shear zones are found which are formed by higher stress (few tens to a hundred mega-pascals) and lower temperature (<1000°C) deformation, possibly associated with the earliest stages of emplacement of the Oman Ophiolite (Boudier *et al.*, 1988; Ceuleneer *et al.*, 1988; Ildefonse *et al.*, 1998b). It is often concluded that the low stress, high-temperature deformation reflects mantle flow in the asthenosphere. This is a reasonable conjecture: dry, melt-free peridotite at a stress of 2 MPa and a temperature of 1250°C will deform at a strain rate of $\sim 7 \cdot 10^{-13}$ s^{-1} (according to the experimental flow law for dry, melt-free peridotite determined by Hirth & Kohlstedt, 1995b). This corresponds to an effective viscosity of $\sim 1.4 \cdot 10^{18}$ Pas, which is a typical value for the viscosity of the oceanic asthenosphere (*e.g.*, Phipps Morgan *et al.*, 1995). If ophiolitic peridotites have indeed recorded deformation in the asthenosphere, then patterns of foliations and lineations of the peridotites deformed under such conditions can give information about the geometry and kinematics of mantle flow in the asthenosphere.

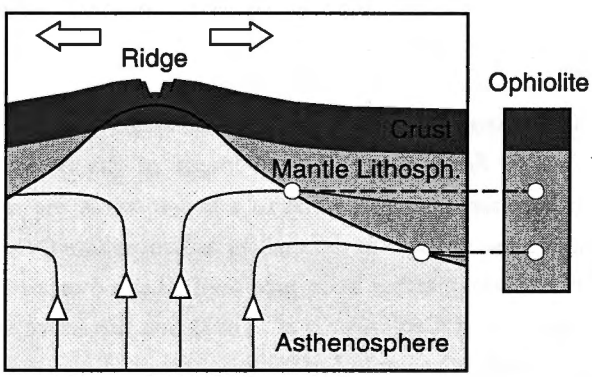

Figure 3.1: Schematic diagram of spreading centre (across ridge axis section) showing the downward thickening of oceanic lithosphere with drift away from the ridge axis. Points deeper in the mantle are frozen in later, at greater distance from the ridge. Consequently, fragments of oceanic lithosphere preserved as ophiolites should theoretically be 'read' from bottom to top: the shallowmost peridotites were chilled first, closest to the ridge axis while deeper peridotites were frozen in later, further away from the ridge. Oceanic crust is created almost instantaneously at the ridge.

Structural mapping in the Oman Ophiolite mantle section has revealed two types of high-temperature mantle flow patterns. The first type has been found in a few areas in Oman: it is the 'upwelling' or 'diapiric' flow pattern (Nicolas & Violette, 1982; Ceuleneer et al., 1988; Nicolas et al., 1988a; Ceuleneer & Rabinowicz, 1992; Jousselin et al., 1998). It comprises circular domains, 5-10 km in diameter, of steep foliations with lineations radially plunging away from the centre of the circular feature. At the centre of the upwelling the foliation dies out at shallow levels. In the uppermost 50 m of the mantle section and away from the axial zone the steep foliations become flat-lying, parallel to the crust-mantle boundary (Ceuleneer & Rabinowicz, 1992). The diapiric pattern may represent upwelling mantle flow directly underneath a ridge axis (Nicolas, 1989; Ceuleneer & Rabinowicz, 1992).

Information about the subhorizontal high-temperature mantle flow away from the ridge axis may be obtained from the more regular and more common 'standard' or 'off-axis' flow pattern

(Ceuleneer et al., 1988; Ceuleneer & Rabinowicz, 1992). This pattern features foliations parallel to the crust-mantle boundary and lineations (i.e., approximately flow directions) roughly perpendicular to the strike of the sheeted dykes (Nicolas, 1989; Ceuleneer & Rabinowicz, 1992). It is assumed that this pattern represents the mantle flow at some distance from a ridge axis. In theory, mantle sections exhibiting such patterns may have recorded a history of asthenospheric mantle flow frozen-in as a result of downward lithospheric accretion (Nicolas, 1989; Nicolas et al., 1994) or alternatively, a snapshot of off-axis mantle flow preserved as a result of whole-scale freezing during intra-oceanic thrusting (Ceuleneer & Rabinowicz, 1992). The Hilti Massif, the subject of this study, is an example of such an 'off-axis' section.

3.1.3. Shear senses and the active flow model

Studies of shear senses as recorded in asymmetric crystallographic fabrics in peridotites from the mantle section of the Oman Ophiolite have revealed systematic trends (Ceuleneer & Rabinowics, 1992; Nicolas *et al.*, 1994; Ildefonse *et al.*, 1995). In areas exhibiting a diapiric flow pattern the shear sense in the peridotites surrounding the diapir is generally top-away from the upwelling. However, sometimes a shear sense inversion is observed in the shallowmost peridotites or in the lower gabbros. In the rocks above this inversion the shear sense is top-towards the centre of the upwelling (Nicolas *et al.*, 1994; Jousselin *et al.*, 1998). In areas exhibiting an off-axis flow pattern a shear sense reversal is found at shallow but variable depth beneath the crust-mantle boundary (Ceuleneer *et al.*, 1988; Ildefonse *et al.*, 1995). To correctly understand this shear sense reversal it is necessary to establish on which side of a spreading ridge such off-axis mantle sections were formed. Such criteria are often lacking. One possible criterion, the dip of the layering in the gabbro section, is debated since it depends on the choice of a lower-crustal accretion model. Proposed models for the formation of the oceanic lower crust comprise magma-chambers with an onion- (*e.g.*, Pallister & Hopson, 1981) or tent- (*e.g.*, Nicolas *et al.*, 1988b; Boudier *et al.*, 1996) shape, 'sheeted' gabbro sills (*e.g.*, Boudier *et al.*, 1996; Kelemen & Aharonov, 1998), or transport from an upper crustal melt lens by 'gabbro glaciers' (*e.g.*, Phipps Morgan & Chen, 1993; Quick & Denlinger, 1993). In the absence of reliable criteria it is generally assumed that the shallowmost peridotites have recorded a top-towards the ridge axis sense of shear, by analogy to the shear senses in the shallowmost rocks in diapiric areas. Conversely, the peridotites occurring at deeper levels in ophiolitic mantle sections have recorded a top-away from the ridge axis sense of shear.

The shear sense reversal in the Oman Ophiolite has been interpreted in terms of 'active' mantle flow close to a spreading ridge (Rabinowicz *et al.*, 1984, 1987; Ceuleneer *et al.*, 1988; Ceuleneer & Rabinowics, 1992; Nicolas *et al.*, 1994; Ildefonse *et al.*, 1995; Jousselin *et al.*, 1998). The active flow model comprises active upwelling of the mantle beneath the ridge axis, possibly due to small-scale convection driven by the buoyancy of excessively hot, partially molten, or depleted peridotites. Active mantle flow (figure 3.2a) induces forced subhorizontal flow away from the ridge axis. Forced flow is faster than the movement of the overlying lithospheric plate, leading to a top-towards the ridge axis sense of shear in the shallow asthenosphere (Nicolas *et al.*, 1994). It has been proposed (Rabinowicz *et al.*, 1984, 1987; Ceuleneer *et al.*, 1988) that the active flow component becomes less important with distance from the ridge axis until it is superseded by the flow component caused by the drag of the overlying lithospheric plate ('passive' or 'plate-driven' flow). As a result of the downward growth of the oceanic lithosphere, flow structures produced by on-axis active flow verging towards the ridge axis are preserved in the top of the mantle section, while top-away from the ridge axis shear senses associated with off-axis passive

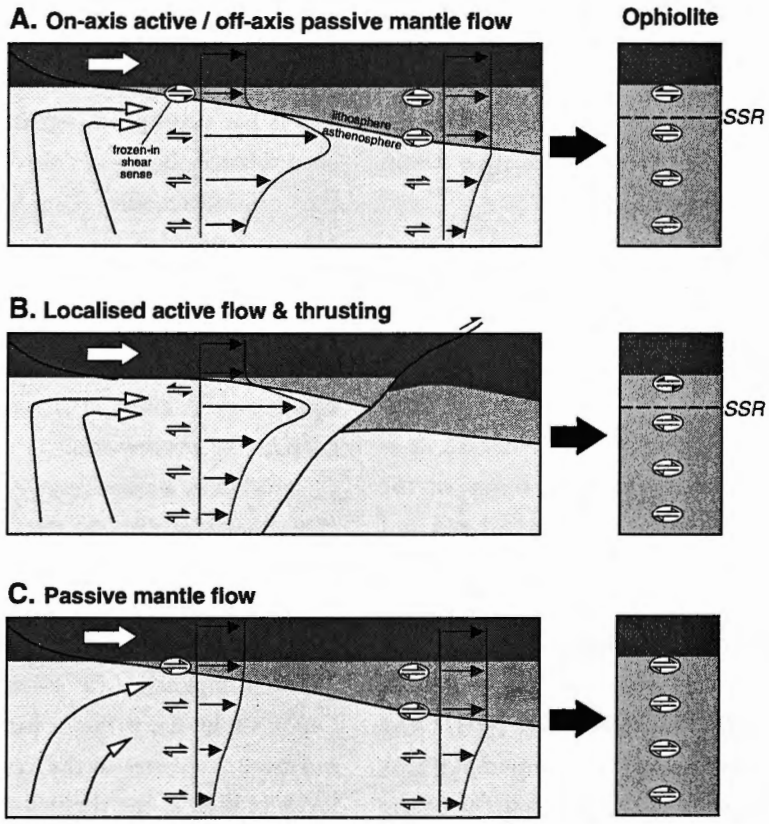

Figure 3.2: Mantle flow patterns, velocity profiles, and shear senses underneath and at some distance from an active spreading centre and predicted pattern of shear senses frozen-in in ophiolitic mantle sections. Dark grey upper layer is oceanic crust, middle grey represents the oceanic lithosphere which thickens off-axis. A) Active mantle flow associated with mantle diapirism near the ridge axis giving way to passive, plate driven flow off axis. Top-towards the ridge axis shear senses (associated with active flow) will be recorded in the uppermost peridotites of ophiolite, while rocks at greater depth preserve top-away from the ridge axis (passive) shear senses, leading to a shear sense reversal (SSR) in the ophiolitic mantle section. B) Whole-scale freezing of an active flow profile as a result of intra-oceanic thrusting at the ridge could also lead to a shear sense reversal in the ophiolitic mantle section. C) Passive flow both on- and off-axis would lead to a constant shear sense. Because of the discovery of a shear sense reversal in the mantle section of the Oman Ophiolite it has previously been concluded that mantle flow had been active at the Oman paleo-ridge.

flow (figure 3.2b) are preserved in the deeper parts (Rabinowicz *et al.*, 1984, 1987; Ceuleneer *et al.*, 1988; Ildefonse *et al.*, 1995). Alternatively, the shear sense pattern can also be interpreted as a snapshot of a mantle flow profile comprising strongly localised active flow at the top giving way to passive flow at depth preserved due to whole-scale freezing of the mantle section during intra-oceanic emplacement (Ceuleneer & Rabinowicz, 1992). An important aspect of either model is that the flow recorded in the shallowmost mantle rocks occurred *before* (closer to the ridge axis) or at least *at the same time* as the deformation recorded in the deeper parts of the mantle section of the ophiolite.

In summary, evidence for diapiric upwellings and shear sense reversals in the mantle section of the Oman Ophiolite have led to the hypothesis that high-temperature flow was *active* in the shallow mantle underneath the Oman paleo-ridge, giving way to *passive* flow off-axis or at depth. As outlined above, this conclusion seems to be at odds with current ideas about flow in the asthenospheric mantle at modern ocean ridges. The scope of this chapter is therefore to re-

investigate the evidence for active flow in the Oman Ophiolite. Emphasis lies on the shear senses recorded in the mantle section of the ophiolite exposed in the Hilti Massif. In addition, an attempt is made to establish the time relation between the different deformation events which are recognised in the study area.

3.1.4. The Oman Ophiolite – the northern versus the southern massifs

The Oman Ophiolite (figure 3.3), also referred to as Samail, Semail, or Sumail Ophiolite, is one of the largest (~500 km in length and ~50 km wide) and best exposed ophiolites in the world. Moreover, it is unique in the way that it has escaped tectonic disruption associated with continent-continent collision after obduction onto the Arabian continent (Lippard et al., 1986; Nicolas, 1989; Nicolas & Boudier, 1995). The age of the ophiolite crust is well constrained at 97-94 Ma, and it has been shown that emplacement of the ophiolite started when the oceanic crust was only a few million years old (e.g., Hacker & Gnos, 1997). The emplacement mechanism of the Oman Ophiolite is a point of contention. One theory is that emplacement occurred by intra-oceanic thrusting close to the Oman paleo-ridge (Boudier et al., 1988; Nicolas, 1989). Another view is that the ophiolite was emplaced onto the Arabian Peninsula due to subduction of the leading edge of the Arabian Plate underneath the supra-subduction zone basin in which the Oman Ophiolite formed (Searle & Malpas, 1982; Lippard et al., 1986; Searle & Cox, 1999).

Previous studies in the Oman Ophiolite have revealed along-strike tectonic and compositional segmentation (Juteau et al., 1988a; Reuber et al., 1988; MacLeod & Rothery, 1992; Nicolas & Boudier, 1995; Boudier et al., 1997). One of the most prominent discontinuities is the Haylayn Massif, which has been noted for its complexity, particularly with regard to its plutonic sequence and sheeted dyke complex (e.g., Juteau et al., 1988a; MacLeod & Rothery, 1992; Boudier et al., 1997). This area has been interpreted as the tip of a fossil propagating ridge system (figure 3.3) and it has been proposed that the propagating ridge encompassed the greater part of the southern massifs of the ophiolite belt (Boudier et al., 1997). This propagating ridge, associated with a NW-SE striking sheeted dyke complex, opened up and propagated northwestwards in older oceanic lithosphere with N-S to NE-SW striking dykes (MacLeod & Rothery, 1988; Boudier et al., 1997; all directions are in the present day geometrical framework).

Studies by Reuber (1988) and MacLeod & Rothery (1992) have focussed on the northern part of the Oman Ophiolite. In the Northern and Southern Fizh Massif the sheeted dyke complex is locally tilted and intruded by a second generation of ESE-WNW striking dykes. Another characteristic of the northern part of the Oman Ophiolite is the occurrence of large volumes of intrusive wehrlites in the crustal section which reach levels as high as the sheeted dykes and the lavas (Benn et al., 1988; Juteau et al., 1988b; Reuber, 1988). Moreover, late-stage gabbro-norite intrusions are found in the Fizh Massif (Reuber, 1988; MacLeod & Rothery, 1992). The presence of numerous mylonitic shear zones in the crustal and mantle sections of the northern massifs, coeval with magmatism, and evidence for tilting of the ophiolite sequence, locally putting the sequence on-edge with a vertical crust-mantle boundary, suggests that the northern part of the Oman Ophiolite has recorded a history of intra-oceanic tectonics close to the paleo-ridge (Reuber, 1988; MacLeod & Rothery, 1992). Such ridge tectonics have been attributed to a southward propagating ridge system whose tip was located in the Fizh Massif (Reuber, 1988; MacLeod & Rothery, 1992). The northern massifs are further characterised by a basaltic andesite lava series (V2), which overlies the 'normal' tholeiitic basalts of the V1 series. These andesitic V2 lavas are generated by hydrous melting of previously depleted underlying mantle (Pearce et al., 1981) and are

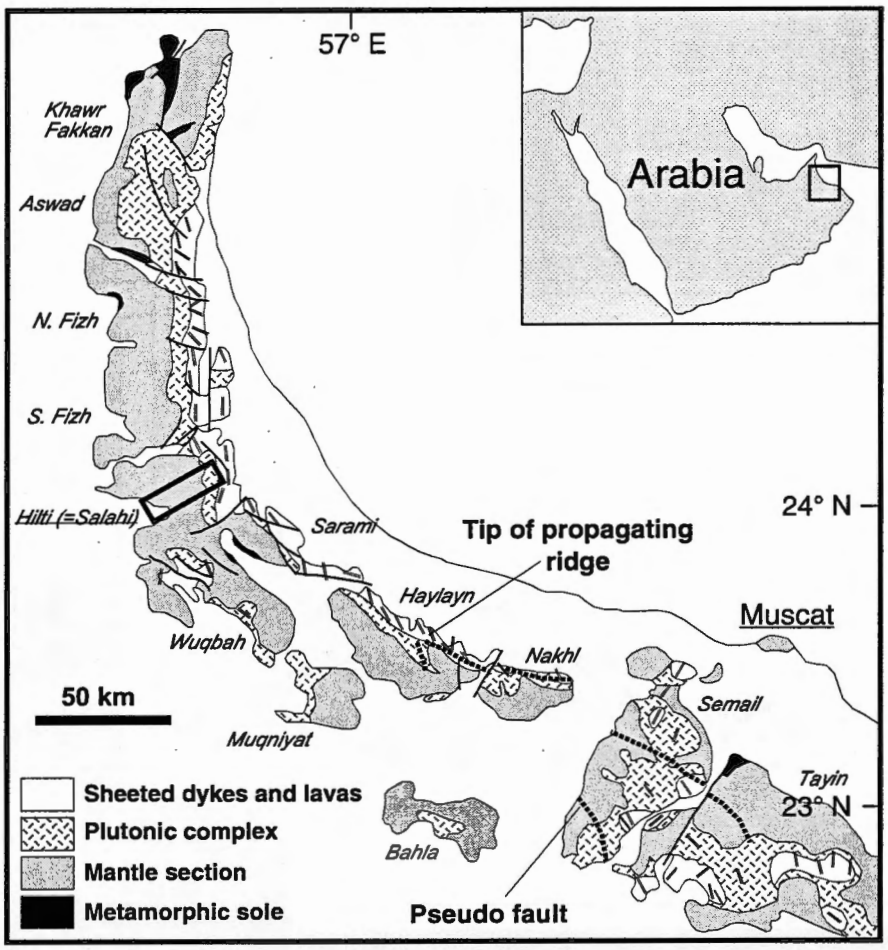

Figure 3.3: Geological map of the Oman Ophiolite. General orientations of sheeted dyke complex indicated by small symbols consisting of double lines (taken from MacLeod & Rothery, 1992). Also shown is the extent of the fossil propagating ridge system including its pseudo faults proposed by Boudier *et al.* (1997). The area in the Hilti Massif which is the subject of this study is shown by rectangle.

assumed to be related to arc magmatism in a supra-subduction zone setting (Pearce et al., 1981; Searle & Cox, 1999) or to magmatism coeval with intra-oceanic thrusting (Boudier et al., 1988; Boudier et al., 1997).

3.2. Results

3.2.1. The Hilti Massif

This study has focussed on the mantle section exposed in the Hilti Massif (figure 3.3). The mantle structures in this massif fit the off-axis flow pattern (Ceuleneer *et al.*, 1988). Because the entire ophiolitic sequence has been tilted by about 25° towards the east (Ildefonse *et al.*, 1995), progressively deeper levels of the ophiolite are encountered towards the west. A structural and sampling traverse across the mantle section of the massif was made, following the main Wadi Hilti and a few subsidiary wadis (figure 3.4). At *c.* 1 km horizontal intervals orientations of peridotite foliations, lineations, and modal compositional layering were recorded. In addition, oriented samples for microstructural and petrofabric analysis were taken.

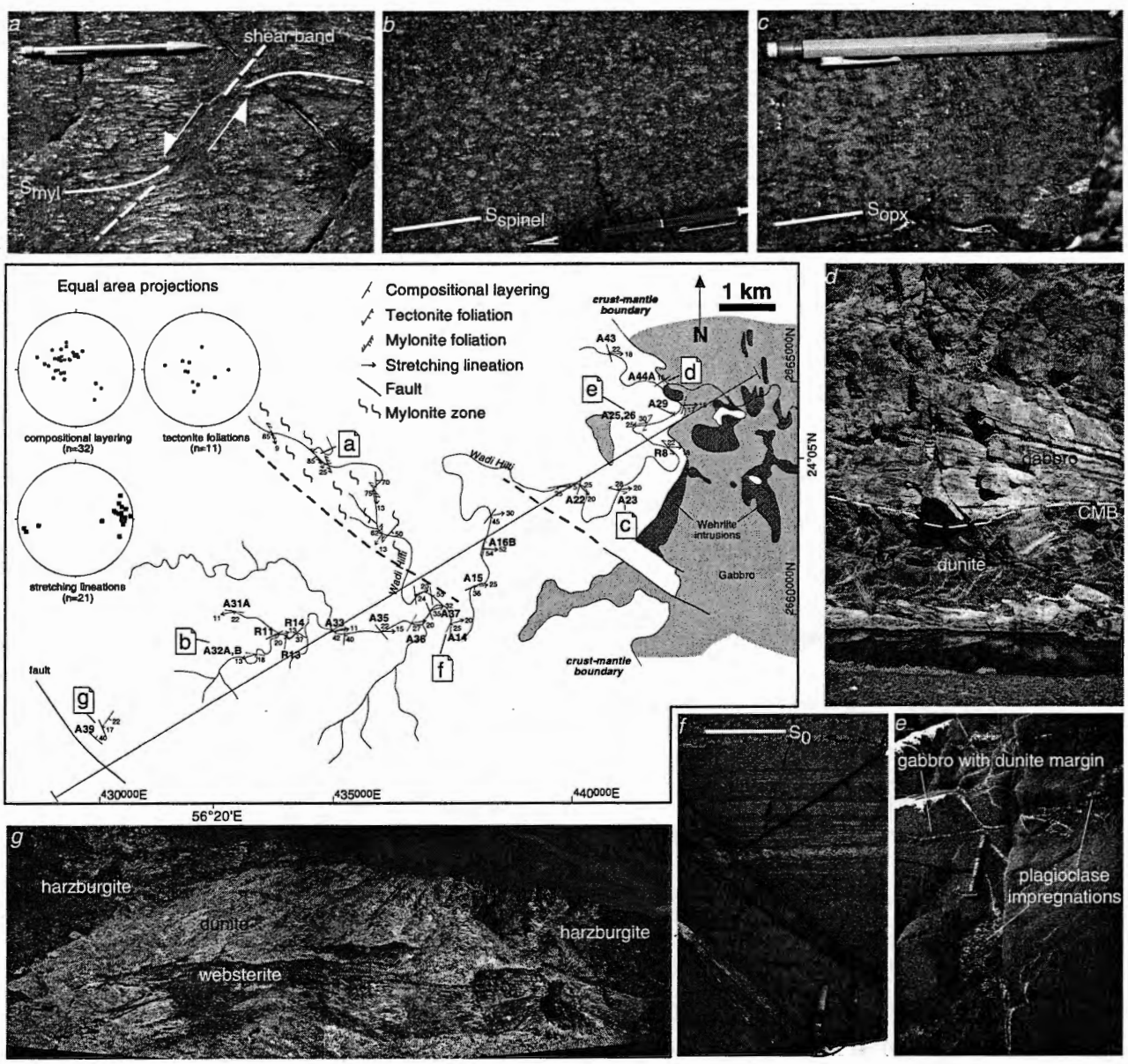

Figure 3.4: Map of the Wadi Hilti area showing structural data and sample localities. Lower crustal rocks shown in grey and mantle rocks in white. Crust-mantle boundary is drawn after geological map (Ministry of Petroleum and Minerals, 1987) and Juteau *et al.* (1988). Wehrlites in dark grey (after Juteau *et al.*, 1988). ENE-WSW running line indicates cross-section of figure 3.6. Also shown are lower hemisphere, equal area projections of poles to compositional layering and tectonite foliations, and spinel and orthopyroxene stretching lineations in peridotites. Photographs a-g (locations shown on map) shown typical geological features of the area. a) Mylonitic fabric with shear band indicating left lateral sense of shear; b) Typical aspect of harzburgites in middle and lower part of the section. Note the absence of a clear orthopyroxene shape fabric; c) Orthopyroxene crystals in the harzburgites from the first several hundreds of meters below the crust-mantle boundary are flattened and elongate, defining a clear foliation and lineation; d) Shallowly east dipping crust-mantle boundary in Wadi Hilti; e) Dunites and harzburgites containing impregnations of plagioclase and clinopyroxene occurring at shallow levels in the mantle section; f) Outcrop of harzburgites containing modal orthopyroxene layering, typical for the middle and deeper part of the section; g) Large dunite body associated with websterite occurring in the western part of the section. Height of the rock section shown is approximately 20-30 m.

3.2.2. Field observations

In this study the following field observations in the Wadi Hilti and two subsidiary wadis are reported:

(I) The crust-mantle boundary in Wadi Hilti is a relatively sharp transition across a few metres, in which dunites and gabbros occur together (figure 3.4d). The contact is parallel to the layering in the gabbros directly above the crust-mantle boundary, dipping ~20-25° towards the east. The gabbros show a plagioclase and pyroxene mineral lineation with an azimuth towards the E, parallel to the lineations in the underlying peridotites.

(II) The dunites and harzburgites directly below the crust-mantle boundary contain interstitial impregnations of clinopyroxene and plagioclase (figure 3.4e). Locally, plagioclase-wehrlites are found. Within the harzburgites diffuse coarse gabbroic dykes with dunitic margins occur. Some heavily impregnated harzburgites are coarse granular, with remnants of a compositional layering (modal variations in orthopyroxene).

(III) The harzburgites within the first several hundreds of meters below the crust-mantle boundary generally exhibit a clear orthopyroxene shape fabric, defining a good foliation and lineation (figure 3.4c). The estimated average orthopyroxene grain size is generally 4-5 mm, with aspect ratios up to 4. At several locations it could be confirmed that the orthopyroxene lineation is parallel to the spinel lineation. In addition, a compositional layering is present, which is parallel to the orthopyroxene foliation.

(IV) Deeper in the mantle section orthopyroxene does not define an obvious foliation and lineation but has a granular shape (figure 3.4b). Moreover, orthopyroxene is coarser than in the uppermost peridotites (>5 mm). At a few locations flattened spinel could be used to define a foliation. More commonly only a clear cm- to dm-scale compositional layering (caused by modal variations in orthopyroxene content) was observed (figure 3.4f), which was assumed to be parallel to the deformation fabric (this was later confirmed by the study of thin sections). Spinel generally defines a relatively good lineation on top of layering planes.

(V) The orientations of the foliations and layering planes in the entire mantle section in the study area (except for the mylonite zone described below) are on average relatively flat or east dipping (figure 3.4 - stereoplots). The azimuths of the lineations observed are consistently east-west.

(VI) Towards the west, following a subsidiary wadi of the main Wadi Hilti, dunites become more abundant and thicker. In the east dunitic bands are part of the cm- to dm-scale compositional layering, while in the west, towards the end of Wadi Hilti, m-scale dunites occur. Moreover, several outcrops contain cross-cutting orthopyroxenite dykes.

(VII) A km-wide zone comprising *mylonitic* harzburgites and dunites (figure 3.4a) was encountered in the more central part of the Hilti Massif, north of the section (figure 3.4 - map). In this zone orthopyroxene (aspect ratios up to 6) and spinel define a clear subvertical foliation, striking N to NNW, with a subhorizontal lineation. At a few locations a clear left-lateral sense of shear was established from asymmetric orthopyroxene clasts and small, cm-scale shear bands. Some of the mylonitic peridotites have a vitreous appearance caused by a very small grain size. A few cross-cutting gabbros and pyroxenites were observed, while at an other location a strongly sheared amphibole-bearing gabbro was found. The continuation of this km-scale mylonite zone is highly problematic: no mylonitic peridotites were encountered in the subsidiary wadi south of the main Wadi Hilti.

(VIII) In the western end of the studied section many thick (metres to tens of metres) irregular dunite bodies were observed. These dunites locally contain a compositional layering defined by varying modal chromite content. From a distance it was clear that this part of the section contains abundant dunite lenses forming an irregular network. At several locations these

dunitic lenses occur in close association with large (also metre to tens of metres-scale) coarse dark websterite (orthopyroxene + clinopyroxene + minor olivine) bodies (figure 3.4g) with a coarse (cm-size) grain size. The harzburgites in this part of the section also have a granular appearance, without an orthopyroxene fabric but with a local compositional layering. It is emphasised that at the base of the studied section no peridotite mylonites have been found. In other areas in Oman basal mylonites often occur and are thought to be associated with the emplacement of the ophiolite (Boudier *et al.*, 1988).

3.2.3. Microstructures

A petrographic and microstructural description and interpretation of the coarse, non-mylonitic peridotites from the Hilti Massif is presented in chapter 2. Only the main conclusions are repeated here.

There is a rough trend of increasing linear intercept olivine grain size with depth below the crust-mantle boundary. The grain size increase with depth is related to a change in microstructure from dominantly fine-grained porphyroclastic to equigranular (figure 3.5a,b) in the first several hundred metres of the mantle section to coarse porphyroclastic (figure 3.5c,d) at depth. Both types of microstructures preserve evidence for grain size reduction by dynamic recrystallisation with subgrain rotation as the dominant recrystallisation mechanism. It is estimated that the original olivine grain size was as large as several millimetres, and that recrystallisation produced new grains with a (median) size of ~0.7 mm. The coarse porphyroclastic peridotites exhibit typical core-and-mantle textures. The porphyroclastic microstructure is interpreted as an incompletely recrystallised microstructure, in which remnants of the original coarse grains are preserved as porphyroclasts. In contrast, the recrystallisation was probably nearly complete in the peridotites close to the crust-mantle boundary, leading to the observed equigranular microstructures. Since a relation between the fine-grained, highly recrystallised equigranular olivine microstructure and orthopyroxene elongation and recrystallisation was found, it is argued that the shallow peridotites have a strong imprint of a deformation event which was localised just below the crust-mantle boundary. Moreover, the highly recrystallised shallow peridotites contain interstitial clinopyroxene, which is probably derived from an interstitial melt by fractional crystallisation. It is, therefore, proposed that the deformation was localised in the upper 575-800 m of the mantle section as a consequence of melt-weakening of peridotite (chapter 2). Melt weakening has been shown to occur in deformation experiments on olivine aggregates (Hirth & Kohlstedt, 1995a,b; Bai *et al.*, 1997).

Mylonitic peridotites from the study area consist of bands of very fine-grained (<10 μm) olivine and orthopyroxene with a fluidal microstructure, enclosing bands or lenses of coarser (50-200 μm) grained olivine (figure 3.5f). Fine and coarse bands contain some porphyroclasts of olivine, orthopyroxene, and spinel, which are up to 5 mm in size. Olivine porphyroclasts often contain strong undulose extinction and numerous irregular, closely spaced subgrain walls. Orthopyroxene porphyroclasts are often strongly stretched or broken up in fragments. The coarser bands consist of polygonal olivine crystals with straight grain boundaries and many 120° triple-junctions. Olivine crystals in such bands are free of substructure. The large variation in birefringence colours suggests that there is only a weak olivine lattice preferred orientation in the olivine bands.

3.2.4. Olivine lattice preferred orientations and shear senses

Olivine crystal orientations of 16 non-mylonitic peridotite samples, including two dunites with large fractions of interstitial clinopyroxene and plagioclase

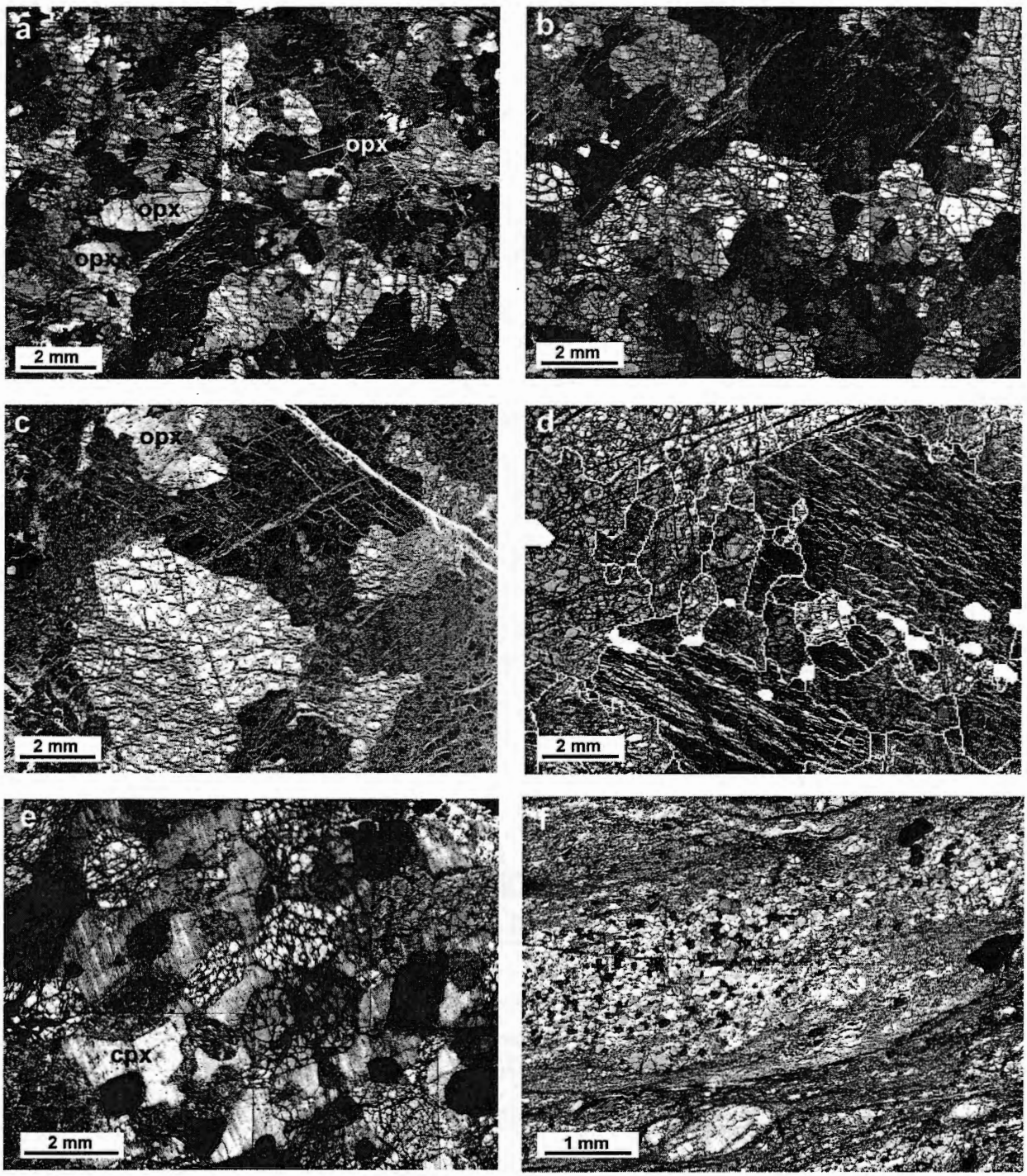

Figure 3.5: Photomosaics of representative microstructures in cross-polarised light. Top two photographs show strongly recrystallised harzburgite (a – sample A23) and dunite (b – sample A25) from the foliated shallow part of the mantle section. Middle two photographs show porphyroclastic harzburgite (c – sample A32A) and dunite (d – sample A32B) typical for the middle and lower part of the section. Photo e) shows a wehrlite (sample A29) from the zone just beneath the crust-mantle boundary containing poikiloblastic clinopyroxene (other areas in same sample contain poikiloblastic plagioclase). Photo f) shows mylonitic microstructure of fine grained band enclosing coarser olivine lenses with a granular (annealed) appearance. Fine-grained bands contain porphyroclasts of orthopyroxene, olivine, and spinel.

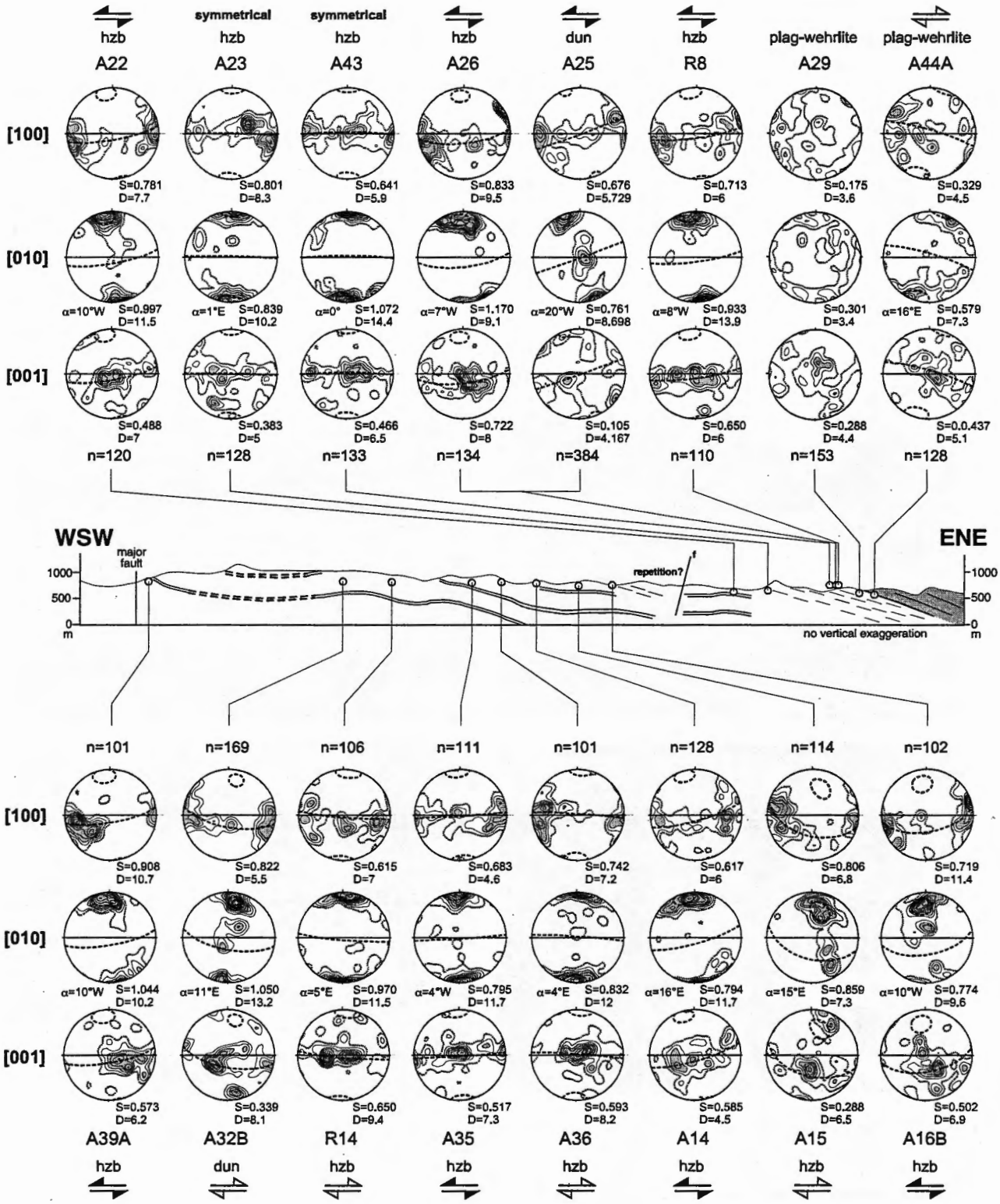
hzb
A22
symmetrical
hzb
A23
symmetrical
hzb
A43
hzb
A26
dun
A25
hzb
R8
plag-wehrlite
A29
plag-wehrlite
A44A
[100]
[010]
[001]
S=0.781 D=7.7
S=0.801 D=8.3
S=0.641 D=5.9
S=0.833 D=9.5
S=0.676 D=5.729
S=0.713 D=6
S=0.175 D=3.6
S=0.329 D=4.5
α=10°W S=0.997 D=11.5
α=1°E S=0.839 D=10.2
α=0° S=1.072 D=14.4
α=7°W S=1.170 D=9.1
α=20°W S=0.761 D=8.698
α=8°W S=0.933 D=13.9
S=0.301 D=3.4
α=16°E S=0.579 D=7.3
S=0.488 D=7
S=0.383 D=5
S=0.466 D=6.5
S=0.722 D=8
S=0.105 D=4.167
S=0.650 D=6
S=0.288 D=4.4
S=0.0.437 D=5.1
n=120
n=128
n=133
n=134
n=384
n=110
n=153
n=128
WSW
major fault
ENE
repetition?
1000
500
0
m
no vertical exaggeration
n=101
n=169
n=106
n=111
n=101
n=128
n=114
n=102
S=0.908 D=10.7
S=0.822 D=5.5
S=0.615 D=7
S=0.683 D=4.6
S=0.742 D=7.2
S=0.617 D=6
S=0.806 D=6.8
S=0.719 D=11.4
α=10°W S=1.044 D=10.2
α=11°E S=1.050 D=13.2
α=5°E S=0.970 D=11.5
α=4°W S=0.795 D=11.7
α=4°E S=0.832 D=12
α=16°E S=0.794 D=11.7
α=15°E S=0.859 D=7.3
α=10°W S=0.774 D=9.6
S=0.573 D=6.2
S=0.339 D=8.1
S=0.650 D=9.4
S=0.517 D=7.3
S=0.593 D=8.2
S=0.585 D=4.5
S=0.288 D=6.5
S=0.502 D=6.9
A39A
hzb
A32B
dun
R14
hzb
A35
hzb
A36
hzb
A14
hzb
A15
hzb
A16B
hzb

(figure 3.5e - referred to as plagioclase-wehrlites below) from the crust-mantle transition zone (figure 3.6) were determined by means of a universal stage. The samples were cut parallel to the stretching or mineral lineation, perpendicular to the foliation or compositional layering. The sense of shear recorded in the samples was determined from the angular relation between the shape fabric (spinel foliation) and the crystallographic fabric (e.g., Den Tex, 1969; Nicolas & Poirier, 1976). In the case of 5 other samples it was possible to determine the sense of shear with some confidence using the relatively fast method used by Ildefonse et al. (1995) and Michibayashi et al. (submitted, 2000). The orientation of the bulk crystallographic fabric of these 5 samples was estimated by rotating an oriented sample under a low-magnification microscope until maximum extinction was attained. The shear sense was then determined from the angular relation between the orientation of the foliation and the maximum extinction direction (Nicolas & Poirier, 1976).

With the exception of one of the plagioclase-wehrlite samples, all peridotite samples have a moderately strong to strong lattice preferred orientation (LPO). The LPO of the olivine in one of the plagioclase-wehrlites (A29) is significantly weaker than in the other peridotite samples. No systematic relation of the strength of the LPO with depth, nor with rock-type (dunite or harzburgite) was found. The olivine [a]-axes have preferred orientations close to the orientations of the lineations. The [b]-axes are oriented close to the poles of the foliations. This indicates that the dominant slip-plane of olivine was the (010)-plane, with [a] as the slip-direction (i.e., [100] (010) slip). Many samples, in particular those with a weakly asymmetrical LPO, exhibit [a]- and [c]-axes girdles around the foliation pole, suggesting a component of flattening.

The plane perpendicular to the [b]-axis maximum was taken as an approximation of the flow plane of the deformation. The flow plane orientations in most samples are 5-20° oblique to the foliation or layering plane, indicating dominant non-coaxial deformation. The LPO of one of the plagioclase-wehrlites gave a top-to-the-east sense of shear. The majority of the samples deeper in the mantle section gave a top-to-the-west sense of shear (8 out of 14 samples measured with the U-stage, 12 out of 19 if samples measured using the quick method are also included). It is also noted that the samples which yielded a top-to-the-east sense of shear are all located in the middle part of the section.

Figure 3.6 (previous page): Schematic cross-section through the mantle section in the Wadi Hilti area (location of section shown in figure 3.4), showing foliated peridotites just below the crust-mantle boundary and peridotites with a compositional layering (and sometimes a spinel foliation) at depth. Above and below the section lower hemisphere, equal area projections of olivine [100], [010], and [001] crystal axes in selected samples are given (contoured 1,2,3,.... times uniform distribution). Orientations of compositional layering and/or spinel or orthopyroxene foliations are represented by horizontal lines with the orientation of the spinel lineation lying on the perimeter of the circle. Flow planes (planes perpendicular to [010] maxima) are shown as dashed great circles and the shear sense is determined from the asymmetry between the foliation and the flow plane. Filled shear sense symbols indicate west-vergent flow, and open shear sense symbols indicate east-vergent flow. Values for the angle of asymmetry (α), and LPO strength parameter S and maximum density D (see Stereoplot™, N. Mancktelow, 1989 for details) are given.

3.3. Discussion

3.3.1. Deformation history

The microstructures of the non-mylonitic peridotites show that the mantle rocks in the Hilti Massif have recorded a deformation history which was concurrent with grain size reduction by dynamic recrystallisation (chapter 2). The well-developed foliation and the high degree of recrystallisation of the peridotites in the first several hundred metres below the crust-mantle boundary suggest that the deformation which led to the recrystallisation was localised in the shallow part of the

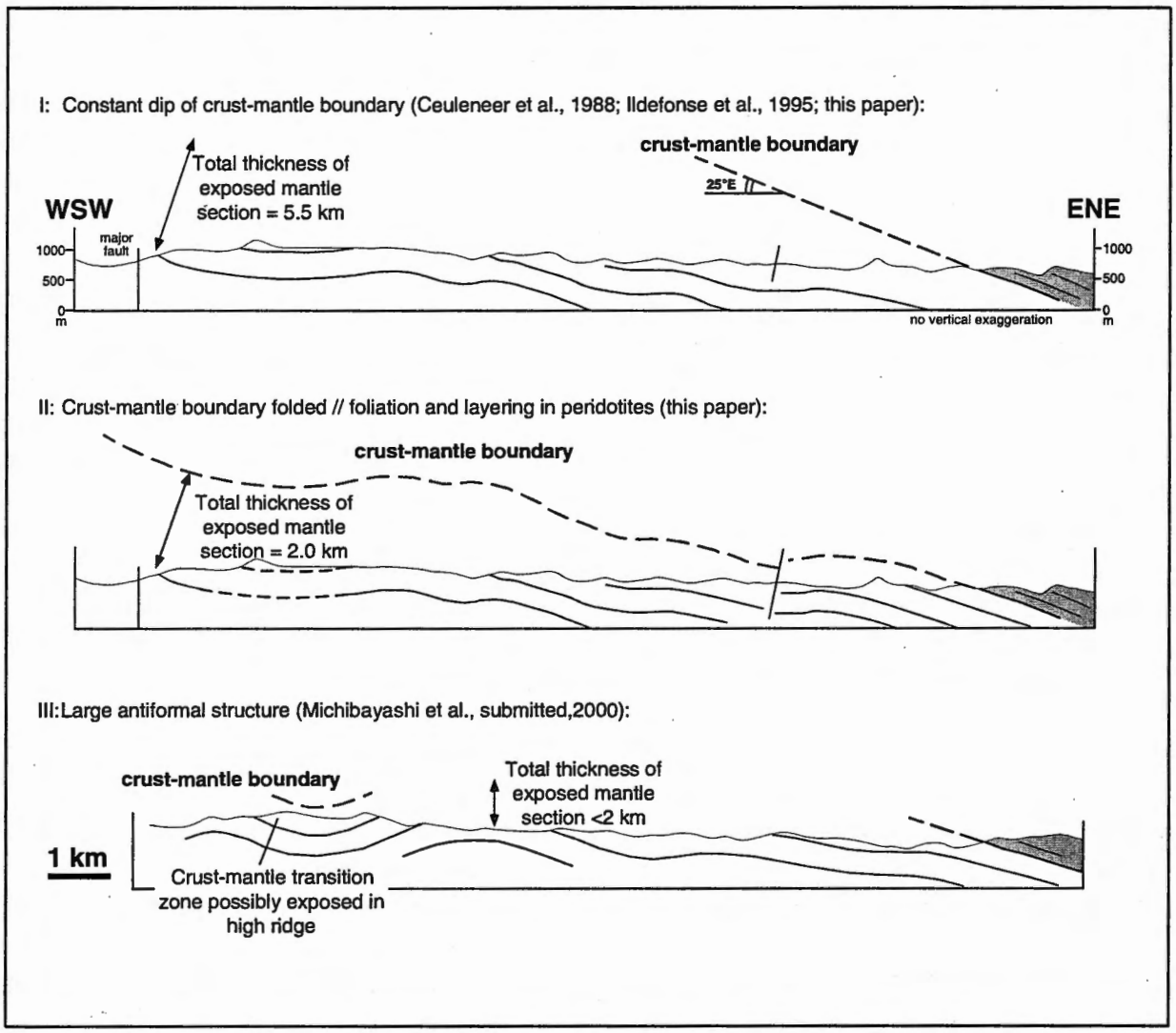

Figure 3.7: Difficulties in estimating the depth of the sample localities and the total thickness of the exposed section arise from the uncertainty with regard to extrapolation of the geometry of the crust-mantle boundary 'into the sky'. Geometry I comprises a crust-mantle boundary with a constant dip of 25° towards the east. Geometry II allows for a folded crust-mantle boundary: it is assumed that the crust-mantle boundary is parallel to the compositional layering and/or foliation in the mantle section. Geometry III is taken from Michibayashi et al. (submitted, 2000) and is based on the interpretation that peridotites in the west represent rocks from the crust-mantle transition zone on the western flank of a large antiform.

mantle section. The base of the zone of well foliated, highly recrystallised peridotites lies at a depth of ~575-800 m below the crust-mantle boundary. The uncertainty in this depth estimate arises from uncertainties with respect to the attitude of the crust-mantle boundary when extrapolated 'into the sky' (figure 3.7). Using a flat crust-mantle boundary with a constant dip is probably an oversimplification as it is likely that the actual boundary is folded (see for instance Reuber, 1991). The peridotites deeper in the mantle section were only partly recrystallised and remnants of an original coarse microstructure have been preserved as porphyroclasts of several mm's in size. The recrystallised grain size is relatively constant (~

Table 3.1
a) Average grain sizes and shear senses of studied samples

sample	rock[1]	S_{Odx}[2]	depth[3] (m)		grain size[4] (mm)	shear sense[5]	
			from map	calculated		u-stage	bulk
A44A	plag-wehrl		20		±1	**E**	
A29	plag-wehrl		150		<1	no LPO	
R8	hzb	+	280		1.3	W	
A25	dun	+	290		1.0	W	
A26	hzb	+	290		0.9	W	
A43	hzb	+	300		0.8	symm	
A23	hzb	+		808	1.0	symm	
A22	hzb			1031	1.5	W	
A16B	hzb	+		1921	1.7	W	
A15	hzb			2163	2.0	**E**	
A14	hzb			2467	1.7	W	
A37	hzb			2537	1.2		W
A36	hzb			2729	1.8	**E**	
A35	hzb			2942	1.2	W	
R14	dun			3538	1.5	**E**	
R13	hzb			3589	1.6		W
R11	dun			3670	3.1		**E**
A32A	hzb			3952	1.9		W
A32B	dun			3952	3.3	**E**	
A31A	hzb			4443	1.1		W
A39A	hzb			5527	1.3	W	

b) Trends (correlation coefficients)[6]

n=14	g.s.	$S_{[100]}$	$D_{[100]}$	$S_{[010]}$	$D_{[010]}$	$S_{[001]}$	$D_{[001]}$	α
depth	**0.52**	0.28	0.15	0.04	0.01	0.15	0.35	α0.27
g.s.		0.21	-0.18	0.00	0.17	-0.17	0.32	**α0.50**

[1] Rock-type (plag-wehrl=plagioclase-wehrlites; dun=dunite; hzb=harzburgite).
[2] Presence of foliation defined by flattened orthopyroxene (+=present).
[3] Depth below the crust-mantle boundary (determined directly from geological map for shallow samples, estimated assuming constant dip of crust-mantle boundary for deeper samples – see figure 3.7).
[4] Grain size determined by linear intercept method (chapter 2).
[5] Shear sense from lattice preferred orientation determined using U-stage or bulk maximum extinction method described in text (**E**=top towards east, W=top towards west, symm=symmetrical LPO).
[6] Calculated coefficients for correlations between depth, grain size (g.s.), LPO strength parameters (see figure 3.6), and asymmetry of LPO ($\alpha<0$ for top towards east, $\alpha>0$ for top towards west) of 14 peridotite samples. Significant correlations shown in bold type-face (determined by Student's t-test for 12 degrees of freedom and confidence level of 5%).

0.7 mm) throughout the entire mantle section. According to the stress-grain size relationship of Van der Wal *et al.* (1993) this recrystallised grain size corresponds to a stress of approximately 10 MPa. In recent deformation experiments by Zhang *et al.* (2000) smaller recrystallised grains were produced than predicted by the relationship of Van der Wal *et al.* (1993). Extrapolation of the Zhang *et al.* (2000) data using the slope of the Van der Wal relation yields a stress of 4 MPa for a grain size of 0.7 mm. The presence of largely undeformed interstitial clinopyroxene crystals, which probably crystallised from a melt during or after deformation (chapter 2), within completely recrystallised peridotites from the shallow part of the mantle section indicates that the peridotites were still relatively hot, at temperatures near the liquidus of basaltic melt (1200-1250° C), during this deformation episode.

The LPO's of 3 out of 4 completely recrystallised, foliated peridotites from the top of the mantle section record a top-to-the-west sense of shear. Another highly recrystallised sample (A16B) from a foliated outcrop further west, which is probably part of a down-faulted block of shallow peridotites, also gave a top-to-the-west sense of shear. It is, therefore, concluded that the deformation which caused the strong foliation and extensive olivine recrystallisation and which was concentrated in the top of the mantle section was non-coaxial with a top-to-the-west sense of shear. Partial olivine recrystallisation and top-to-the-west shear senses in the more westerly samples indicate that the deeper peridotites were also affected by this deformation event.

Reversed, top-to-the-east shear senses were found in 5 samples from the middle part of the mantle section of the Hilti Massif. This shear sense is restricted to samples with the coarsest average grain sizes (table 3.1). These are the least recrystallised peridotites, *i.e.*, the peridotites which have the weakest imprint of the relatively high stress (4-10 MPa) deformation episode. These peridotites have probably partly preserved the microstructures associated with an earlier deformation history. The LPO's indicating top-to-the-east shear senses, found in these least recrystallised peridotites, are attributed to an earlier deformation episode (D1) during which the original coarse microstructure with a grain size of several mm's was produced. The observation that all the studied samples have some imprint of the second, relatively high stress deformation episode (D2) leads to difficulties interpreting the sense of shear of the D1 deformation. It cannot be established with certainty that the LPO's in the least recrystallised rocks were deformed during non-coaxial top-to-the-east deformation, since the shape fabric that is used as a reference frame to interpret the sense of shear may have been produced during D2 deformation. Combining the LPO produced during one deformation event with the shape fabric (foliation and lineation) produced during another deformation event can give erroneous results with regard to the sense of shear. It is, therefore, concluded that the sense of shear of the D1 deformation, despite indications for a top-to-the-east asymmetry in the LPO's, remains uncertain. The coarse grain size suggests that the D1 deformation which produced the original coarse microstructure took place at a low stress (<4.5 MPa for an olivine grain size >2 mm, using the piezometer of Van der Wal *et al.*, 1993). High, near- to super-solidus temperature conditions (>1250° C) are required for olivine deformation at such low stresses.

Mylonites cut through coarse grained peridotites in a wadi north of the studied section. These mylonites are probably related to the last significant ductile deformation episode (D3) in the peridotites. The lack of evidence for an LPO in either the very fine-grained fluidal bands or the coarser olivine lenses in mylonitic peridotites allows for the possibility that the dominant deformation mechanism in the mylonites was grain-size sensitive creep (possibly involving diffusion creep and/or grain boundary sliding) instead of dislocation creep. Moreover, the polygonal shapes of olivine crystals in the olivine lenses suggest that the crystals were formed by static rather than dynamic recrystallisation. The use of recrystallised grain size-stress relations to

estimate the stress during D3 deformation is therefore not warranted. However, strong undulose extinction and numerous irregular, closely spaced subgrain walls in olivine porphyroclasts within fine-grained bands indicates that during D3 deformation stresses where higher (probably in the order of tens of MPa's), and temperatures lower, than during D1 and D2 deformation. The presence of a both sheared and cross-cutting gabbros suggest that D3 mylonite deformation started at temperatures around the gabbro solidus. These temperatures are in the order of 1000-1100°C (Sinton & Detrick, 1992), but could be lower if these gabbros crystallised from Fe-rich and/or wet melts.

3.3.2. Comparison with previous studies

Previous studies in the Hilti Massif also reported top-to-the-west sense of shear for peridotites close to the crust-mantle-boundary, giving way to top-to-the-east shear senses at depth (Ceuleneer *et al.*, 1988; Ildefonse *et al.*, 1995; Michibayashi *et al.*, submitted, 2000). Michibayashi *et al.* (submitted, 2000) also report top-to-the-west shear senses in the westernmost, basal part of the Hilti Massif. As a consequence, Michibayashi and co-workers interpreted the geometry of the mantle section in the Hilti Massif as a large open antiform, in which peridotites from the crust-mantle transition zone are repeated at the westernmost end (figure 3.7). The olivine grain size data (chapter 2), which suggest that the peridotites in the western end of the section are again finer grained than those of the middle part, seem to support this view. However, the peridotites in the western end of the studied section do not resemble the peridotites near the crust-mantle boundary: they were not found to contain plagioclase or interstitial clinopyroxene and they are poorly foliated. Moreover, the large-scale websterite bodies (which are also plagioclase free) at the western end of the studied section are not known to be typical for the crust-mantle transition zone.

The results of the present study show the presence of a zone of foliated, highly recrystallised peridotites with interstitial clinopyroxene which have recorded a top-to-the-west sense of shear just beneath the crust-mantle boundary. This conclusion is in agreement with the conclusions of Ildefonse *et al.* (1995) and Michibayashi *et al.* (submitted, 2000). However, the existence of an alternation of domains of top-to-the-east and top-to-the-west beneath the crust-mantle boundary, interpreted as a channel-like flow geometry by Ildefonse *et al.* (1995), is not supported by the results of this thesis. Top-to-the-west shear senses were found in two samples which are located in a zone of inferred top-to-the-east shear in the study of Ildefonse *et al.* (1995).

By analogy to the shear sense reversal found in areas exhibiting a diapiric flow pattern, Ceuleneer *et al.* (1988), Ildefonse *et al.* (1995), and Michibayashi *et al.* (submitted, 2000) interpreted the top-to-the-west shear sense at shallow level in the mantle section in the Hilti Massif as top-towards the ridge axis. In this interpretation the Hilti massif represents the eastern half of a spreading ridge (in the present-day geographic reference frame). Furthermore, Ceuleneer *et al.* (1988), Ildefonse *et al.* (1995), and Michibayashi *et al.* (submitted, 2000) interpreted the top-to-the-west sense of shear as the result of active flow close to the ridge axis. The peridotites with an LPO with a top-to-the-east asymmetry found at depth are thought to represent rocks that were frozen-in later, at some distance from the ridge axis, recording passive, top-away from the ridge axis mantle flow. However, the conclusions of the present study with respect to the time sequence of deformation are inconsistent with the interpretations of previous workers in the Hilti Massif. On the basis of the microstructural analysis it is suggested that the top-to-the-west sense of shear is associated with a relatively late deformation episode, which overprints microstructures at depth. The implications of this alternative interpretation are further discussed below.

Mylonites, such as the mylonites produced during D3 deformation described in this study, are commonly

found in the mantle section of the Oman Ophiolite. They occur predominantly in the basal parts of the ophiolite section. Such basal mylonites generally have sub-horizontal N-S (ridge-parallel) oriented stretching lineations (Boudier *et al.*, 1988; Nicolas, 1989). Stretching and mineral lineations in the emplacement-related metamorphic sole of the ophiolite also have N-S orientations in all but the southernmost massifs (Boudier *et al.*, 1988; Hacker & Gnos, 1997). This kinematic similarity has led to the widely accepted view that that the peridotite mylonites are linked to the metamorphic sole thrust and, therefore, to the emplacement of the ophiolite (Boudier *et al.*, 1988; Nicolas, 1989). Peak metamorphic temperatures of ~800-875°C for the mineral assemblages in the metamorphic sole (Ghent & Stout, 1981; Hacker & Gnos, 1997; Searle & Cox, 1999) indicate that the mantle section was still relatively hot during activity of the sole thrust. This constraint is in agreement with the temperature estimate of 800-1000°C for the deformation in peridotite mylonite zones in the base of the mantle section of the Oman Ophiolite (Boudier *et al.*, 1988). The temperature estimate based on the solidus temperature of gabbro intrusions is higher (1000-1100°C) but depends on the compositions of the gabbros. Boudier *et al.* (1988) estimated that stresses up to 100 MPa where attained within some peridotites mylonites. Mylonites are also found in the crustal and mantle sections of the Fizh Massif, where they are associated with synkinematic intrusions of gabbros, gabbro-norites, and plagiogranites (Reuber, 1988; MacLeod & Rothery, 1992).

3.3.3. The active flow model and alternative hypotheses

As outlined above, the results of this study with regard to the kinematics of the deformation recorded in the Hilti peridotites are in first order agreement with the results of previous studies by Ceuleneer *et al.* (1988), Ildefonse *et al.* (1995), and Michibayashi *et al.* (submitted, 2000). However, the conclusions concerning the *time-sequence* of deformation differ from those of earlier studies. It is concluded that the peridotites at relatively deep levels in the mantle section preserve evidence for an *early* deformation stage (D1), which pre-dated the deformation recorded in the peridotites just below the crust-mantle boundary (D2). D2 deformation took place at higher stresses and possibly somewhat lower temperatures compared to D1 deformation. It is unlikely that the early D1 microstructures were produced during vertical upwelling underneath the ridge axis. The LPO's of the samples which have largely preserved D1 microstructures show that the olivine shear planes are flat-lying, subparallel to the crust-mantle boundary. The D1 deformation must therefore have been associated with an early stage of subhorizontal mantle flow which pre-dated the deformation recorded in the shallowmost peridotites. These conclusions are at variance with those of earlier studies in the Hilti Massif, in which it is assumed that the peridotites just below the crust-mantle boundary have recorded the earliest deformation taking place very close to the ridge axis and that the deeper peridotites have recorded *later* passive flow at some distance from the ridge. The two-stage high-temperature deformation history presented in this chapter is also inconsistent with models in which the mantle section is interpreted as a frozen-in snapshot of localised active flow just beneath the crust-mantle boundary taking place *at the same time* as passive flow at depth (*e.g.* Ceuleneer and Rabinowicz, 1992).

It cannot be ruled out that asthenospheric mantle flow at the Oman paleo-ridge was active, *i.e.*, faster than the motion of the overlying lithospheric plate. Since neither the shear sense of the early low stress D1 deformation nor the origin of the Hilti Massif with respect to the paleo-ridge can be constrained with certainty at this stage, D1 deformation may have been associated with either non-coaxial top-towards the ridge active mantle flow or with non-coaxial top-away

from the ridge passive flow. If the tent-shaped magma chamber model (Nicolas *et al.*, 1988b; Boudier *et al.*, 1996) is correct, then the dip of the gabbros in the Hilti Massif indicate that the massif originated on the eastern side of a ridge (Ildefonse *et al.*, 1995). In that case west-vergent D2 deformation in the shallowmost peridotites could indeed have been the result of active mantle flow. If, however, alternative magma chamber models are correct then the Hilti Massif may have originated on the western side of a ridge and the D2 deformation is in agreement with passive flow.

However, the deformation history can also be interpreted in terms of ridge tectonics. Since D2 microstructures overprint D1 microstructures, D2 deformation probably took place off-axis. The question then remains: how far off-axis? In this light it is important to point out the significance of wehrlite bodies, which have been found in large numbers in the

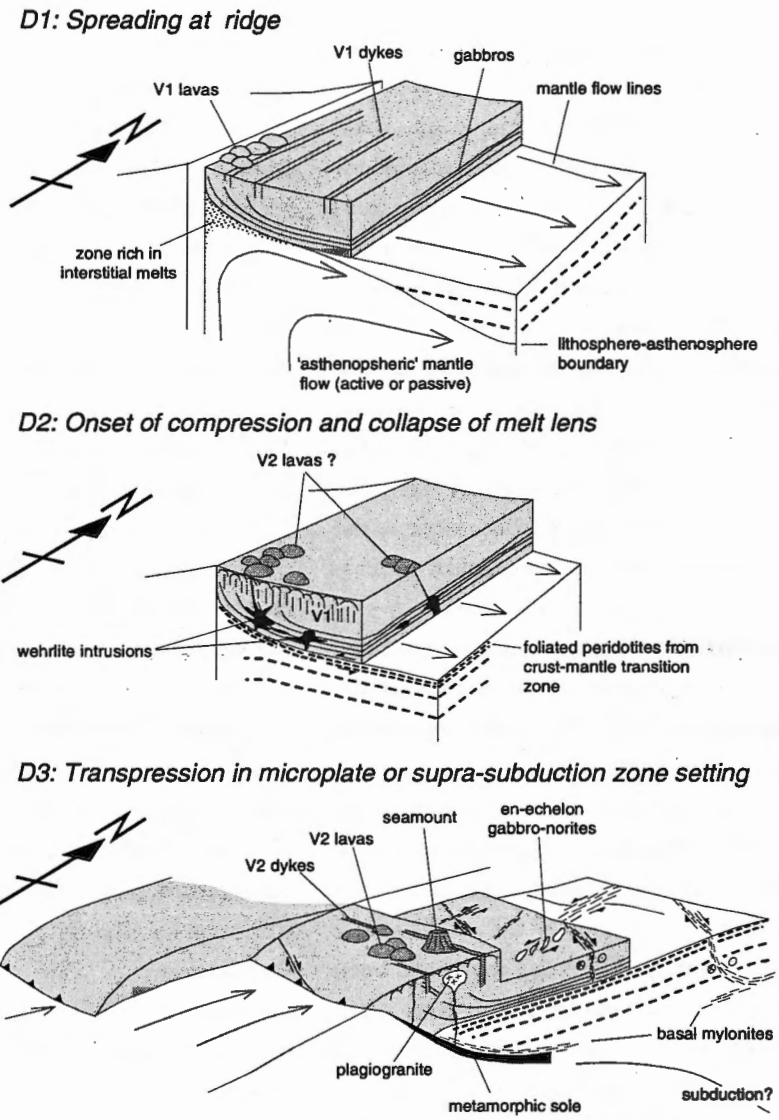

Figure 3.8: Schematic representation of the proposed three-phase deformation history based on the structural analysis of this study. This history comprises spreading, the onset of compression at a dying ridge system, and emplacement of the ophiolite in a transpressional setting (see text for discussion).

plutonic section of the Hilti Massif (Juteau *et al.*, 1988b). These wehrlites and associated picritic extrusives may be co-magmatic with the secondary basaltic andesites of the V2 lava series (Nicolas, 1989, p. 58 & 87). Magmatic relationships between wehrlite bodies and enclosing gabbros in the Hilti Massif, as well as in other massifs in the northern part of the Oman Ophiolite, show that the gabbros were just consolidated when the wehrlites intruded (Benn *et al.*, 1988; Juteau *et al.*, 1988b; Reuber, 1988). Moreover, these studies have shown that the wehrlites are rooted in the peridotites from the crust-mantle transition zone; wehrlites are never found in the mantle rocks below the crust-mantle transition zone (Benn *et al.*, 1988; Juteau *et al.*, 1988b; Reuber, 1988). Juteau and co-workers (1988b) concluded that the parent magmas of the wehrlites were squeezed out of the crust-mantle transition zone as a consequence of deformation in this zone, analogous to the action of a filter press. On the basis of the microstructural analysis reported in this chapter, it is proposed that it is this deformation whose effect is recorded in the peridotites from just below the crust-mantle boundary. This is consistent with the hypothesis that D2 deformation did not occur *at* the ridge-axis, but somewhat off-axis, when most gabbros of the plutonic section were just consolidated.

It is proposed that D2 deformation was associated with the onset of compression in the mantle at the Oman paleo-ridge (figure 3.8b). The high temperatures during D2 deformation imply that the mantle section was still hot, *i.e.*, that compression started not far to the ridge-axis. In this scenario, compression led to deformation which was focussed in the weakest rocks, *i.e.*, the melt-bearing peridotites of the crust-mantle transition zone (chapter 2). This zone may have been particularly melt-rich as melt pooled in this zone when the spreading rate fell at the transition between extension and compression. As a result, melts or crystal-melt mushes were expelled from the crust-mantle transition zone, leading to intrusions of wehrlites bodies and picritic dykes into the overlying oceanic crust. Interestingly, this scenario of collapse of the melt-rich crust-mantle transition zone and associated intrusions of wehrlites at higher levels provides an alternative explanation for the observation that the thickest crustal sections are found in areas which exhibit the thinnest crust-mantle transition zones, and vice versa, in the Oman Ophiolite (Nicolas *et al.*, 1996).

In the Hilti massif D2 deformation was followed by D3 deformation comprising sinistral strike-slip movements along N-S to NNW-SSE striking mylonite zones (figure 3.8c). Studies by Reuber (1988), Boudier *et al.* (1988), and MacLeod & Rothery (1992) showed numerous mylonite zones in the mantle and crustal sections of the Fizh Massif, just north of the Hilti Massif. In the Fizh Massif N-S striking mylonites recording sinistral strike-slip occur together with WNW-ESE striking mylonites recording predominantly dextral strike slip (Reuber, 1988; Boudier *et al.*, 1988; MacLeod & Rothery, 1992). In addition, it is found in these studies that shearing along the mylonites was coeval with intrusions of gabbro dykes, gabbro-norites, plagiogranites, and WNW-ESE striking sheeted dykes.

It was considered whether two previously published geotectonic models for the formation and emplacement of the Oman Ophiolite can account for the deformation history of the Hilti and Fizh mantle sections (figure 3.9). These two models were (a) the subduction zone model of Searle & Malpas (1982), Pearce *et al.* (1981), Lippard *et al.* (1986), and Searle & Cox (1999), and (b) the microplate model of Nicolas *et al.* (1997). Both models provide a framework for 'hot' compression perpendicular to a N-S striking ridge axis followed by slightly cooler oblique (transpressional) thrusting.

Searle & Cox (1999) noted that a supra-subduction zone model adequately explains the andesitic character of the V2 lava series and the high pressures (up to 9 kbar) conditions during formation of the metamorphic sole of the ophiolite. It also accounts for the possibility that the overridden and metamorphosed basaltic and

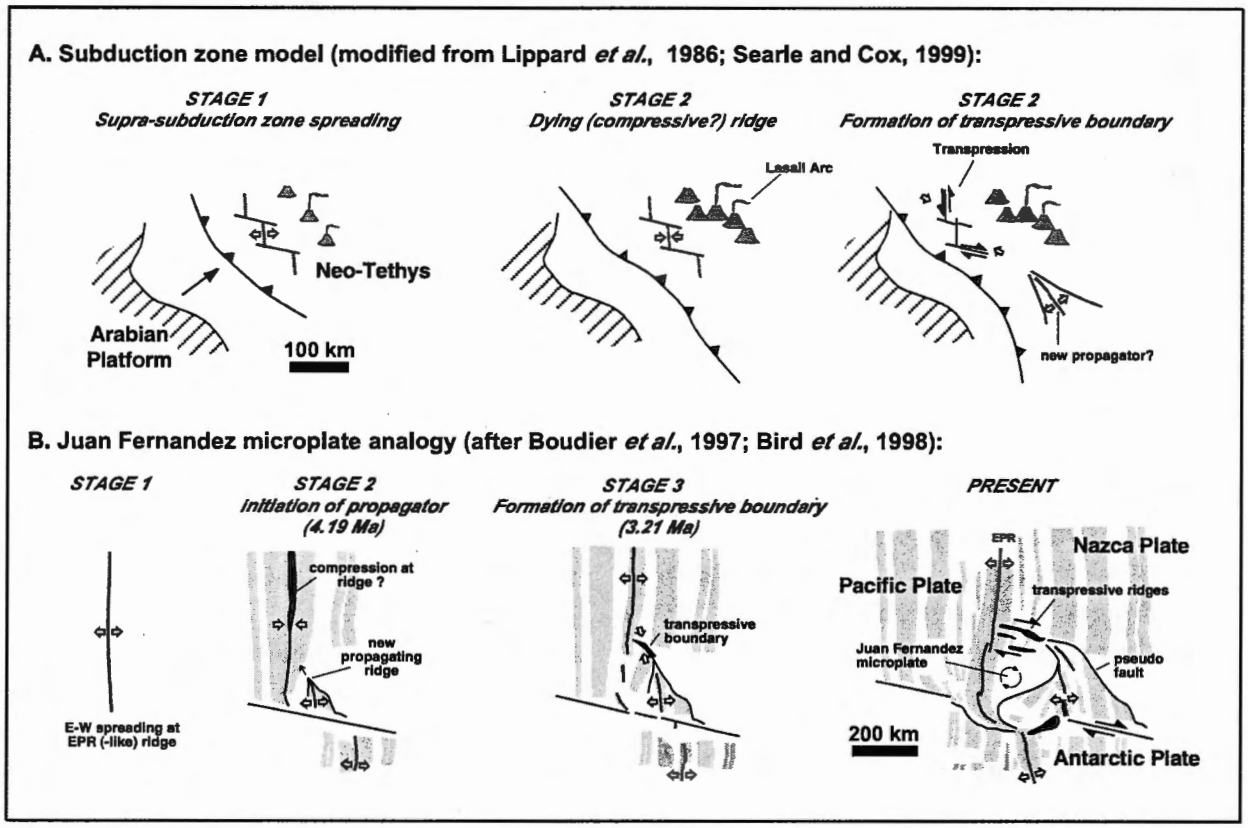

Figure 3.9: Two existing geotectonic models which can account for the proposed structural history of the mantle rocks in the Hilti Massif and other areas of the Oman Ophiolite. A) supra-subduction zone model; and B) Juan Fernandez microplate analogy.

alkalic volcanic rocks are significantly older - of Triassic and Jurassic age - than the 97-94 Ma old overriding ophiolite (Searle & Cox, 1999). In the version of the subduction zone model shown in figure 3.9a, spreading at a N-S oriented fore-arc ridge system ceased as the result of the Arabian passive margin approaching the subduction zone. This caused compression, localised deformation in the crust-mantle transition zone, and expulsion of melts. Finally, when the subduction zone became locked in the north, continued convergence led to transpressional tectonics in the northern part of the Oman Ophiolite. It is possible that a new propagating fore-arc spreading centre was initiated at this stage in the southern part.

The second model, the microplate model of Nicolas *et al.* (1997) is largely based on, and therefore in agreement with, the conclusions of studies in the southern massifs of the Oman Ophiolite. In this model an analogy is drawn to the tectonic situation at the Juan Fernandez and Easter microplates in the Pacific Ocean (figure 3.9b). At the northern margin of each of these microplates young oceanic lithosphere is presently undergoing transpressional deformation as a result of the action of a new propagating ridge and associated rotation of the microplate (Naar & Hey, 1991; Larson *et al.*, 1992; Rusby & Searle, 1993; Bird *et al.*, 1998). Moreover, reconstructions of the development of the Juan Fernandez and Easter microplates have shown that the ridge segments involved may have been undergoing compressive deformation during the early stages of microplate development (Naar & Hey, 1991; Bird *et al.*, 1998 – figure 3.9b, 4.19 Ma time-slice).

It is concluded that the previously published active flow model does not follow necessarily from the reconstructed kinematic history of the Hilti and other northern ophiolite massifs in Oman. It is argued that structures previously attributed to active flow could have been the result of collapse of a melt-rich crust-mantle transition zone as the result of the onset of compression close to the (dying) Oman paleo-ridge, at a distance from the ridge at which the gabbros were just consolidated but the mantle section was still hot. Moreover, it is possible to reconcile the kinematic history of the Hilti and other northern massifs with two existing end-member geotectonic models. In our interpretation, the high strain in the peridotites immediately below the crust-mantle boundary and the presence of cross-cutting wehrlites in the overlying crust are features of a dying, rather than a normal, actively spreading ridge system.

3.4. Conclusions

(I) The microstructures of the peridotites in the Hilti Massif have recorded a poly-phase deformation history. An early, low stress (<4.5 MPa), near- to super-solidus (>1250°C) deformation stage (D1) is recognised, which produced coarse microstructures. These microstructures were later overprinted by higher stress (~4-10 MPa) deformation (D2) taking place at temperatures near the liquidus of basaltic melt (1200-1250°C). D2 deformation led to development of a well-defined foliation and to grain size reduction by dynamic recrystallisation. The imprint of D2 deformation is strongest in the peridotites from the first 575-800 m below the crust-mantle boundary, implying that the deformation was localised. The D1-D2 structures were later cut by N-S to NNW-SSE striking mylonite zones, which were produced by high stress (in the order of tens of MPa) deformation (D3) at temperatures of 1100-1000°C or lower. Field observations showed that D3 mylonites have recorded sinistral strike-slip movements.

(II) Olivine crystal orientation measurements indicated that D2 deformation was non-coaxial, with a top-to-the-west sense of shear. LPO asymmetries in accordance with reversed, top-to-the-east shear senses were only found in the least recrystallised peridotites from the middle part of the mantle section, and are attributed to D1 deformation. Due to uncertainties with regard to the foliation and lineation reference frame required to interpret the LPO asymmetry, the sense of shear of D1 deformation cannot be constrained with certainty. The results of this study do not support the model of channels of westward directed (active flow) of Ildefonse *et al.* (1995). Instead, it is proposed that there is a more simple structure with mainly top-to-the-west shear senses just beneath the crust-mantle-boundary.

(III) In the proposed kinematic model, evidence for the earliest deformation (D1) is preserved in peridotites from deep levels in the Hilti mantle section, not in peridotites from shallow levels. This is at variance with the paradigm of ophiolite studies that the deepest levels of ophiolitic mantle have recorded the latest high temperature deformation, furthest away from the ridge axis.

(IV) The D2 deformation episode may have been associated with collapse of the melt-bearing crust-mantle transition zone as a result of onset of compression. Melt expulsion occurred at some distance from the ridge axis, as shown by the intrusions of wehrlite bodies in just consolidated gabbros of the Hilti plutonic section. Earlier studies have shown that these wehrlites are rooted in the crust-mantle transition zone.

(V) The new interpretation of the D1 to D3 deformation history in the Hilti Massif proposed in this study is consistent with two existing geotectonic models for the formation and emplacement of the Oman Ophiolite, *i.e.*, the subduction zone model and the microplate model.

Chapter 4

Structural petrology of plagioclase-peridotites in the West Othris Mountains (Greece): Melt impregnation in oceanic mantle lithosphere

Abstract

In this chapter the results of a structural and petrological study of mantle rocks from the strongly dismembered Othris Ophiolite are presented. The top of the mantle section shows ubiquitous evidence for impregnation with a melt, from which plagioclase and clinopyroxene crystallised as cumulate phases thus refertilising previously depleted peridotites. Olivine microstructures indicate that melt impregnation occurred late in the deformation history of the host peridotites. The deformation took place at stresses of 13-26 MPa and at temperatures around 1000-1200°C, i.e., at the base of the thermal lithosphere. The melt therefore impregnated relatively cold mantle rocks, implying that the thermal lithosphere reached into the mantle during magmatic activity. It is concluded that the Othris Ophiolite represents a spreading environment with a relatively thick lithosphere, such as that near an axial discontinuity/transform fault of a slow-spreading ridge. The proposed magmatic and deformation history of the peridotites is in agreement with episodic magmatism at slow-spreading ridges. The heterogeneous character of the mantle section of the Othris Ophiolite probably resulted from melt impregnation processes. It is further suggested that the presence of lherzolitic ophiolite types among harzburgitic ophiolite types in the Hellenic-Dinaric chain reflects variable degrees of melt impregnation and refertilisation rather than partial melting and melt extraction.

4.1. Introduction

4.1.1. Background

Studies of ophiolites worldwide have revealed a great structural and petrological diversity. This diversity is commonly attributed to a variety of extensional geodynamic environments in which ophiolites may form. It has been proposed that these environments span the entire Wilson Cycle, from rift basins through ocean ridges to back-arc basins (*e.g.*, Coleman, 1984; Boudier & Nicolas, 1985; Nicolas, 1989; Bonatti & Michael, 1989). The composition of ophiolitic mantle sections, which are believed to be the residues of partial melting, can give information about the tectono-magmatic environment in which the ophiolites formed. It is generally assumed that harzburgitic mantle sections are formed by a high degree of depletion by melt extraction, corresponding to fast-spreading environments. Ophiolites with lherzolitic mantle sections, often referred to as the lherzolite ophiolite type, are thought to correspond to low degrees of

depletion in slow-spreading or rift settings (Boudier & Nicolas, 1985; Nicolas, 1986a; Nicolas, 1989).

A special kind of lherzolite ophiolite are those with voluminous plagioclase-lherzolites, such as the Trinity Ophiolite (Quick, 1981a,b; Jacobsen *et al.*, 1984; Boudier *et al.*, 1989; Cannat and Lécuyer, 1991), the Lanzo Peridotite Massif (Boudier & Nicolas, 1972; Boudier, 1978; Pognante *et al.*, 1985; Bodinier, 1988; Wogelius & Bishop, 1989), and the Othris Ophiolite (Menzies, 1973; 1974; 1975; 1976a,b; Menzies & Allen, 1974; Hynes, 1974a; Menzies *et al.*, 1977; Rassios & Konstantopoulou, 1993). The presence of plagioclase in the mantle rocks of these massifs indicates that the lherzolites equilibrated at low pressures (<8 kbar), in the metamorphic plagioclase stability field. If lherzolitic compositions indeed reflect low degrees of melt depletion, then these massifs must have ascended through the mantle without undergoing extensive pressure release melting. In the Voltri Massif it has been shown that lherzolitic mantle rocks were tectonically exhumed from deep mantle levels corresponding to the spinel-lherzolite stability field by extensional shear zones (Vissers *et al.*, 1991). The Voltri peridotites followed a largely sub-solidus PT-path and the plagioclase in the Voltri peridotites was formed as a result of a sub-solidus metamorphic reaction (Vissers *et al.*, 1991; Hoogerduijn Strating *et al.*, 1993).

The mantle section of the Othris Ophiolite (Central Greece), however, is compositionally very heterogeneous, comprising mostly harzburgites and minor lherzolites and dunites. In addition, significant volumes of plagioclase-lherzolites containing abundant melt relics occur (*e.g.*, Menzies, 1973). These first order observations cannot easily be reconciled with a scenario of subsolidus exhumation.

In this chapter the results of a structural, microstructural and petrological study of the mantle section of the Othris Ophiolite is presented. It is concluded that the plagioclase-lherzolites in Othris are not simply the residue after limited melt extraction, but that they are the product of melt impregnation and refertilisation of harzburgitic peridotites. Secondly, the structure and petrology of the mantle section are interpreted in terms of its tectono-magmatic environment of origin.

4.1.2. The Othris Ophiolite

The dismembered Othris Ophiolite represents a remnant of the Mesozoic Tethyan ocean basin. The ophiolite forms the uppermost tectonic unit of a series of thrust sheets, showing the characteristics of a Upper Triassic-Jurassic passive margin sequence overlying Triassic volcanics associated with rifting (Smith *et al.*, 1975; Hynes, 1974b). The sheets were emplaced onto the Palaeozoic basement of the Pelagonian Zone in the Late Jurassic-Early Cretaceous and are unconformably overlain by an Upper Cretaceous (Cenomanian to Coniacian) transgressive cover (Hynes *et al.*, 1972; Smith *et al.*, 1975). The entire sequence has later been thrust westward over flysch of Late Cretaceous-Tertiary age (Faupl *et al.*, 1996).

The mantle rocks of the Othris Ophiolite were first studied in detail by Menzies (1973; 1974; 1975; 1976a, b), Menzies and Allen, (1974) and Menzies *et al.* (1977), who concluded that the ophiolite formed in a marginal environment at the inception of rifting (Menzies & Allen, 1974). In contrast, Rassios and co-workers concluded that the Othris Ophiolite originated at an ocean ridge, in the vicinity of a northeast trending transform fault (Rassios & Konstantopoulou, 1993; A. Rassios, personal communication, 1995).

4.2. Results

4.2.1. Crustal rocks

This study has focussed on the Fournos Kaïtsa and Katáchloron areas of the Othris Ophiolite (figure

4.1). Detailed structural mapping has confirmed the strongly dismembered character of the ophiolite. The westernmost peridotites of the Katáchloron area are in tectonic contact with an ophiolitic tectonic mélange, which tectonically overlies turbidites ('Late Cretaceous-Tertiary flysch unit'). The mélange unit consists of basalts, red cherts, and serpentinised peridotite blocks, as well as fragments of amphibolitic meta-gabbros. The amphibolites in the mélange strongly resemble amphibolites that occur elsewhere in the Othris Mountains, near the city of Lamia. The Lamia amphibolites have been interpreted as remnants of a sub-ophiolitic metamorphic sole (Spray *et al.*, 1984; A.G. Smith, personal communication) and their age has been established by $^{40}Ar/^{39}Ar$ dating as 169±4 Ma (Spray *et al.*, 1984).

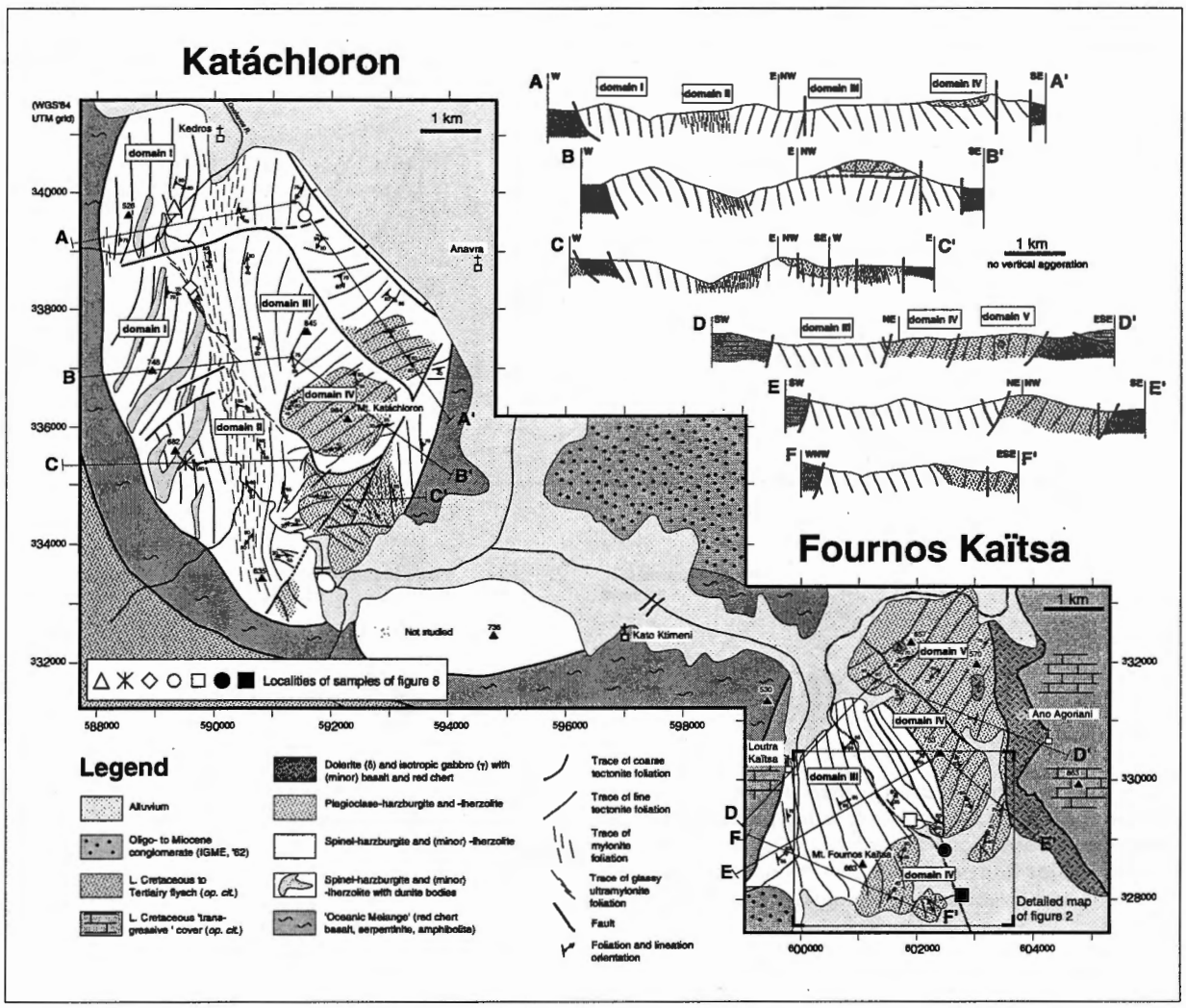

Figure 4.1: Map and cross-sections of the Katáchloron and Fournos Kaïtsa areas. Foliation traces are based on several hundreds of structural measurements. Representative foliation and lineation orientations are shown. Plagioclase-peridotites are stippled. The plagioclase-in boundary is indicated by a drawn line where mapped in the field. Also shown are localities of samples used for chemical analysis shown in figure 4.8. Outlines of dunite bodies in domain I based on personal observations and unpublished (photo-) geological map of Rassios (A. Rassios, personal communication, 1995). Ages of non-ophiolitic rocks based on IGME (1962). Box shows area covered by detailed map of figure 4.2.

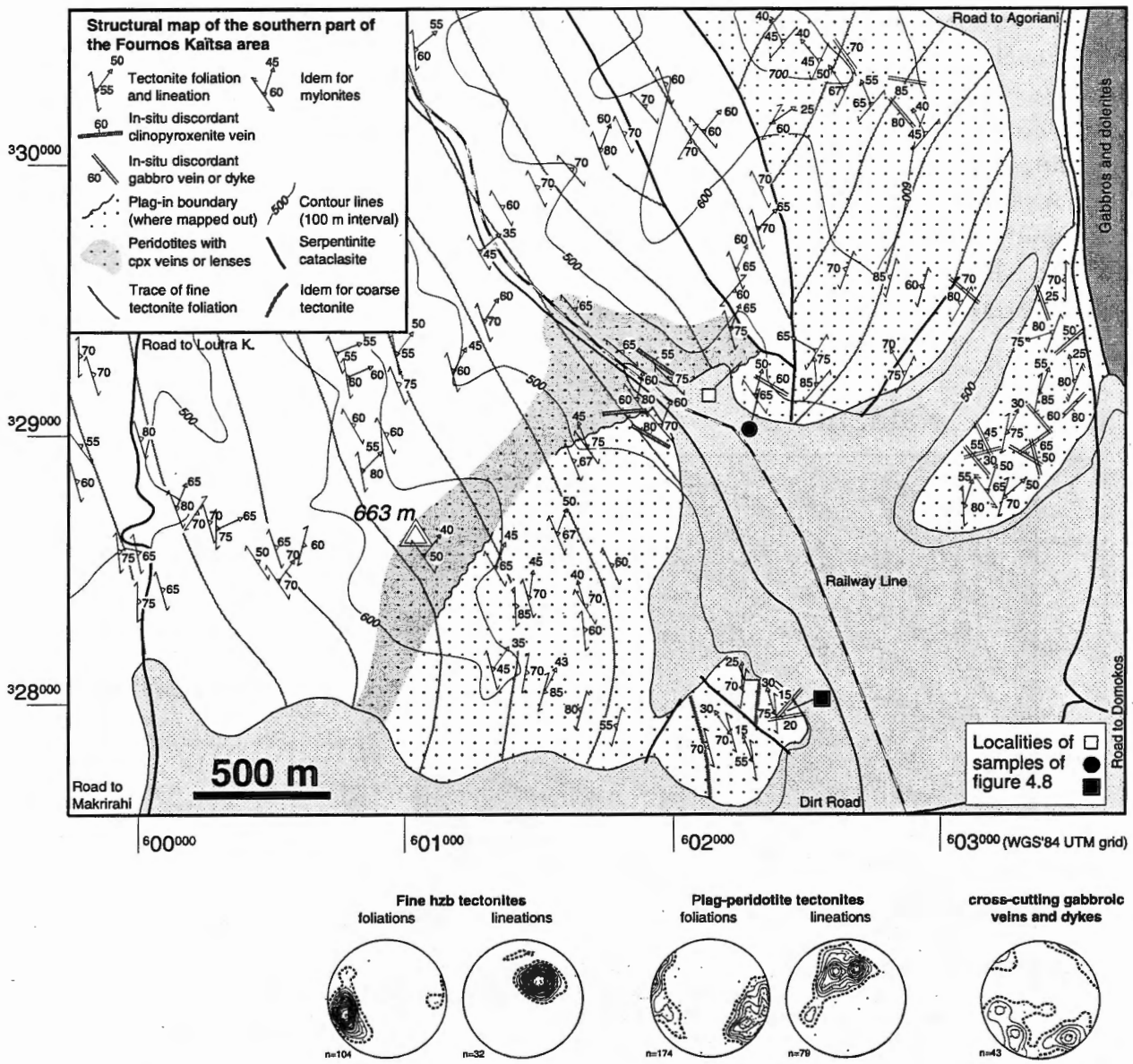

Figure 4.2: Detailed structural map of the southern part of the Fournos Kaïtsa area, showing the transition from plagioclase-free to plagioclase-bearing peridotites. Indicated are orientations of tectonite and mylonite foliations and lineations, orientations of discordant gabbroic and clinopyroxenitic dykes, locations of samples taken for chemical analysis, major fault contacts, and main roads. Also shown are lower hemisphere, equal area projections of poles to foliations and lineations in tectonites, and poles to discordant gabbroic veins and dykes (contoured 1,2,3,.... times uniform).

The easternmost peridotites of the Fournos Kaïtsa area are in tectonic contact with a unit largely made up of isotropic gabbros, basalts, and minor red cherts. This unit is overlain by a limestone/marble unit ('Late Cretaceous transgressive cover unit').

4.2.2. Mantle rocks

The peridotites of the study area are cut by steep NE-SW and moderately to gently inclined NW-SE striking serpentinite cataclasites (figure 4.1, see also figure 4.2).

Rassios & Konstantopoulou (1993) argued that the fault geometry is that of a stack of NE-vergent imbricate thrusts. The domains between the faults shown in figure 4.1 are more or less coherent. The most striking feature of the peridotites exposed in the study area is their compositional, structural and microstructural variability. An east-west section through the area comprises plagioclase-lherzolites and plagioclase-harzburgites, spinel-lherzolites, harzburgites, and amphibole-bearing harzburgites with large dunite bodies. Microstructures range from coarse porphyroclastic to ultramylonitic (nomenclature after Mercier & Nicolas, 1975). In general, foliations are moderately to steeply inclined. On the basis of structure and composition, five lithotectonic domains have been recognised within the studied mantle section (figure 4.1). From west to east, the domains have the following structural, mineralogical, and microstructural characteristics:

Domain I

The westernmost domain, found in the Katáchloron area only, consists of coarse-grained harzburgite tectonites (figure 4.3a) with N-S striking foliations. Large lenses and bodies of dunite (up to 400 m wide) are observed cross-cutting the foliation. Orthopyroxene porphyroclasts in the harzburgites are typically 5-15 mm in diameter. The microstructure of the harzburgites is coarse porphyroclastic; olivine grain sizes range from 0.5 to 3 mm. The harzburgites contain pargasitic hornblende, occurring together with orthopyroxene, clinopyroxene and spinel in recrystallised rims around orthopyroxene, and post-kinematic tremolitic amphibole replacing orthopyroxene or overgrowing the tectonite foliation.

Domain II

Towards the east, the harzburgites become mylonitic (figure 4.3b) and locally ultramylonitic. Ultramylonitic bands have a vitreous appearance due to extremely fine grain sizes (5-50 μm). Dunite lenses are transposed into the plane of mylonitic foliation and are strongly reduced in width to ~0.1-1 m. The mylonitic peridotites are part of a km-wide N-S trending shear zone.

Domain III

East of the mylonite zone, relatively fine-grained amphibole-free harzburgite tectonites occur in the Katáchloron area (figure 4.3c). Such harzburgites also occur in the Fournos Kaïtsa area (see also figure 4.2). The fine-grained harzburgites often show a clear compositional layering caused by modal variations in orthopyroxene and spinel content. The compositional layering is consistently subparallel to the deformation fabric defined by flattened and stretched orthopyroxene and spinel grains. Foliations and layering generally strike NW-SE. The fine-grained harzburgites contain a few relatively thin (cm to m scale) dunite layers, which are locally oblique to the foliation. Remarkably, the rocks of this domain are often almost completely unserpentinised. Orthopyroxene porphyroclasts are generally <5 mm and are surrounded by rims of fine grained polyphase material (mainly orthopyroxene and olivine). These fine-grained rims are often flattened parallel to the foliation. The orthopyroxene clasts surrounded by fine-grained polyphase rims are embedded into coarser domains of predominantly olivine and minor interstitial orthopyroxene. The microstructure of the harzburgites is fine-grained porphyroclastic (see below).

Domain IV

Both in the Katáchloron and Fournos Kaïtsa (figure 4.2) areas the harzburgites grade into peridotites with more fertile bulk compositions (figure 4.3d-g). Up- and eastward the peridotites first become rich in clinopyroxenite lenses and mm-thick veins; eventually they become plagioclase-bearing. Locally, clinopyroxene-poor plagioclase-peridotites occur. However, no attempt was made to distinguish between plagioclase-lherzolites and plagioclase-

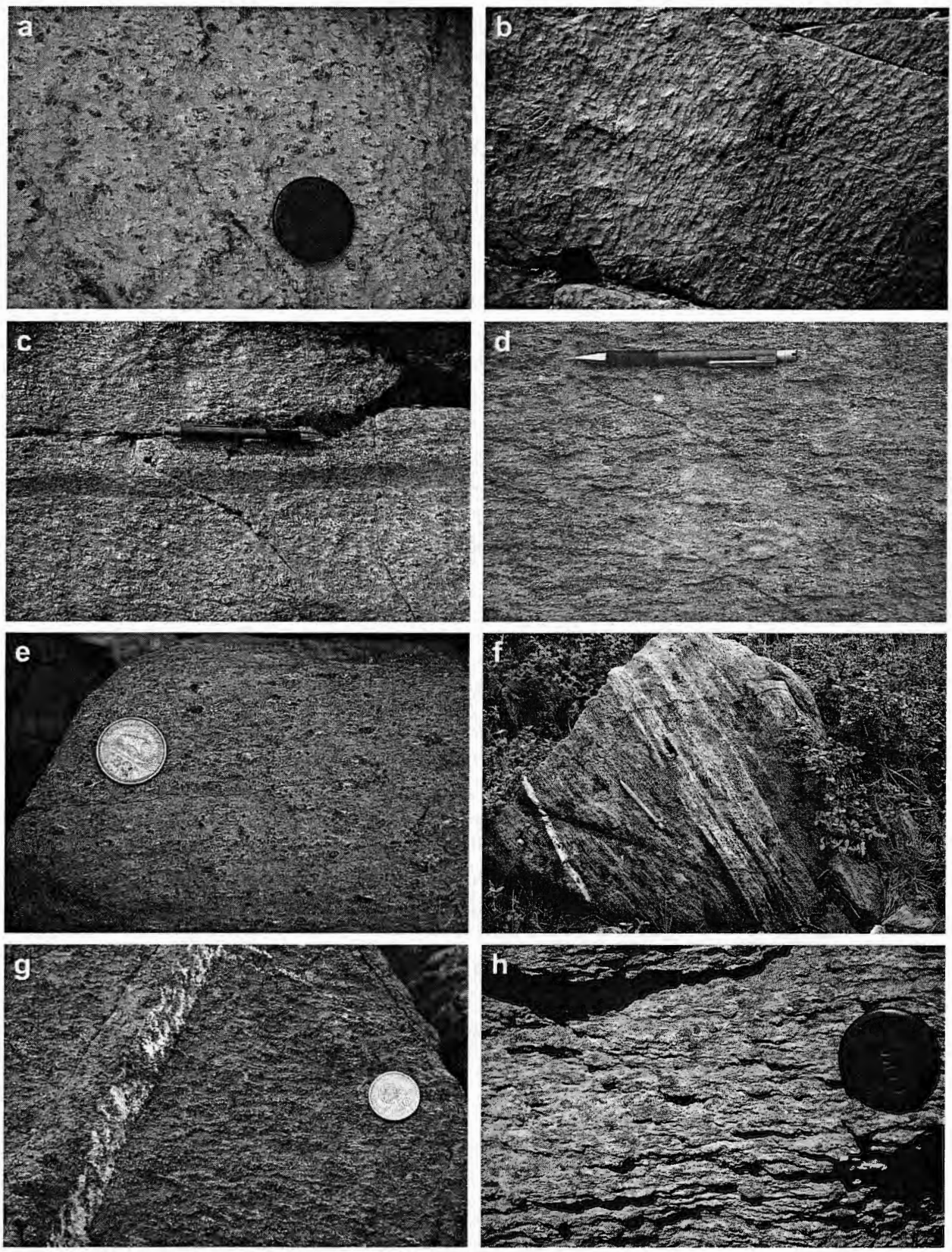
a
b
c
d
e
f
g
h

harzburgites. Plagioclase-peridotites are often serpentinised and plagioclase is sometimes altered to an assemblage of hydrogrossular and zoisite. Plagioclase-peridotites are predominantly fine-grained tectonites, containing orthopyroxene porphyroclasts <5 mm in diameter (figure 4.3d). Within the fine-grained tectonites, however, metre- to 100 m-scale domains of coarse-grained tectonites with orthopyroxene porphyroclasts of 5-15 mm (figure 4.3e) were locally found. In the plagioclase-bearing peridotites plagioclase occurs in mm-scale veins and lenses, which are parallel to the lineation defined by stretched orthopyroxene and spinel grains. Plagioclase is commonly associated with clinopyroxene and/or orthopyroxene. Sometimes pargasitic hornblende also occurs in the plagioclase-bearing clusters. Within the coarse-grained plagioclase-peridotites plagioclase was often found in tapering aggregates flanking orthopyroxene porphyroclasts (figure 4.3e).

Figure 4.3 (previous page): Photographs of representative outcrops. (a) Coarse-grained harzburgite tectonite of domain I, showing large orthopyroxene porphyroclasts surrounded by partially recrystallised rims. Diameter of lens cap is 55 mm; (b) Stretching lineation in mylonitic harzburgite of domain II, defined by stretched orthopyroxenes surrounded by fine-grained rims of orthopyroxene and olivine; (c) Compositional layering (dunite) in fine-grained harzburgite tectonite of domain III. Orthopyroxene porphyroclasts are surrounded by rims of fine-grained olivine and orthopyroxene, which are generally not strongly stretched. Foliation and compositional layering are parallel to pencil; (d) Fine-grained tectonite of domain IV, containing plagioclase and clinopyroxene clusters (whitish specs) which define the foliation (parallel to pencil); (e) Coarse-grained tectonite of domain IV, containing plagioclase in tapering aggregates flanking relatively large orthopyroxene porphyroclasts. Diameter of coin is 27 mm; (f) Fine-grained olivine gabbro at a low angle to the foliation in plagioclase-bearing peridotite (parallel to pencil). Outcrop also contains a thin coarse-grained pegmatitic olivine gabbro, which in 3-D is strongly discordant to the foliation; (g) Detail of discordant coarse-grained pegmatitic olivine-gabbro to gabbro-norite with oblique comb texture, feeding into or tapping from host rock. Diameter coin is 29 mm; (h) Strongly serpentinised coarse-grained plagioclase-bearing tectonite of domain V.

Plagioclase-peridotites contain a compositional layering caused by modal variations in orthopyroxene or plagioclase content (locally layers have a troctolitic composition). The layering is parallel to a foliation defined by flattened orthopyroxene and spinel. Locally concordant clinopyroxenites and websterites occur, some of which contain plagioclase. Much more common are gabbroic dykes, comprising concordant and discordant olivine-gabbros (figure 4.3f) and predominantly discordant coarse-grained pegmatitic olivine-gabbros to gabbro-norites (figure 4.3g). Locally, it was observed that discordant gabbro dykes are contiguous with small plagioclase lenses (*e.g.*, figure 4.3g). The change from harzburgites to plagioclase-peridotites is associated with a change in orientation of the strikes of foliations from NW-SE to N-S or NE-SW. Microstructures in the plagioclase-bearing peridotites range from fine- to coarse-grained porphyroclastic (see below).

Domain V

In the Fournos Kaïtsa area, plagioclase-peridotites with a pervasive serpentine network (figure 4.3h) occur as the most north-easterly mantle domain. They are separated from the less serpentinised plagioclase-peridotites of domain IV by a cataclastic fault. The serpentinised peridotites of this domain are coarse-grained tectonites with orthopyroxene porphyroclasts commonly >5mm. Plagioclase in these rocks is completely altered. In this domain dolerite dykes and bodies have intruded, in which plagioclase is largely unaltered (unrodingitised). A 100 m-scale isotropic gabbro body was found in this domain and the published geological map (IGME, 1962) shows the presence of a 100 m-scale dolerite body which has been entirely removed due to copper mining activities. The microstructures of the tectonites of this domain are often difficult to determine due to serpentinisation, but both coarse- and fine-grained porphyroclastic microstructures have been observed.

4.2.3. Microstructures in plagioclase-peridotites

The following analyses is mainly based on the relatively fresh plagioclase-peridotites of domain IV. As outlined above most of the studied plagioclase-bearing peridotites studied are fine-grained tectonites with a fine porphyroclastic microstructure. Their microstructure is characterised by domains of fine-grained olivine (20-200 μm) and orthopyroxene around orthopyroxene porphyroclasts (figure 4.4a-b, figure 4.5a), and coarser domains (100 μm to 1 mm) consisting of olivine and minor spinel (figure 4.4a, figure 4.5b). Very locally the coarser domains contain orthopyroxene with typical interstitial crystal shapes. The larger olivine grains contain irregular, closely spaced subgrain walls at a high angle to the foliation. Regions between these subgrain walls often show undulose extinction. Orthopyroxene occurs as large round porphyroclasts and as smaller interstitial grains predominantly in the fine-grained domains (figure 4.5a).

Crystal orientation (universal stage) measurements on olivine in relatively coarse olivine bands in a fine-grained tectonite revealed a strong crystallographic preferred orientation (figure 4.6). Olivine [a]-axes coincide with lineation directions. Olivine [b]-axes cluster at a high angle to the foliation, with a secondary maximum within the foliation-plane. The crystallographic preferred orientation indicates that the dominant deformation mechanism in the tectonites was dislocation creep with [100](010) and minor [100](001) as the active slip-system of olivine.

The fine-grained tectonites enclose areas of coarser-grained tectonites. These have a coarser porphyroclastic microstructure, with olivine porphyroclasts of 0.5 to 3 mm surrounded by recrystallised grains of 50-200 μm (figure 4.5c-d). The porphyroclasts contain straight subgrain walls; these are more widely spaced than subgrain walls in fine-grained tectonites.

Clinopyroxenitic and websteritic veins and lenses in the plagioclase-peridotites are generally parallel to the foliation. They often show evidence for boudinage, indicating that they were present during the deformation recorded in the peridotites.

Plagioclase occurs as single crystals or in polycrystalline clusters. Plagioclase clusters are often

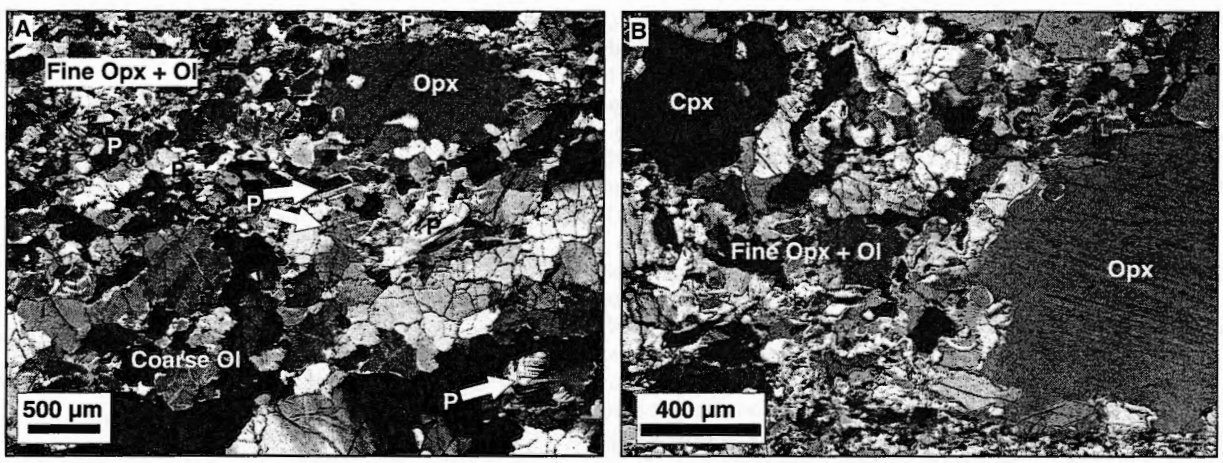

Figure 4.4: Thin section photographs of plagioclase-bearing fine-grained tectonites of domain IV (in cross-polarised light). Sections cut parallel to lineation and perpendicular to foliation. Foliation is horizontal in photographs. (a) Coarse-grained dunitic band (lower half of photograph) and fine-grained band of olivine and orthopyroxene adjacent to small orthopyroxene porphyroclast (upper half). Olivine porphyroclasts contain subgrain walls at high angle to foliation. Plagioclase crystals and aggregates are denoted with 'P'; (b) Detail of fine-grained orthopyroxene and olivine adjacent to orthopyroxene porphyroclasts. Clinopyroxene in upper left corner exhibits simple twinning.

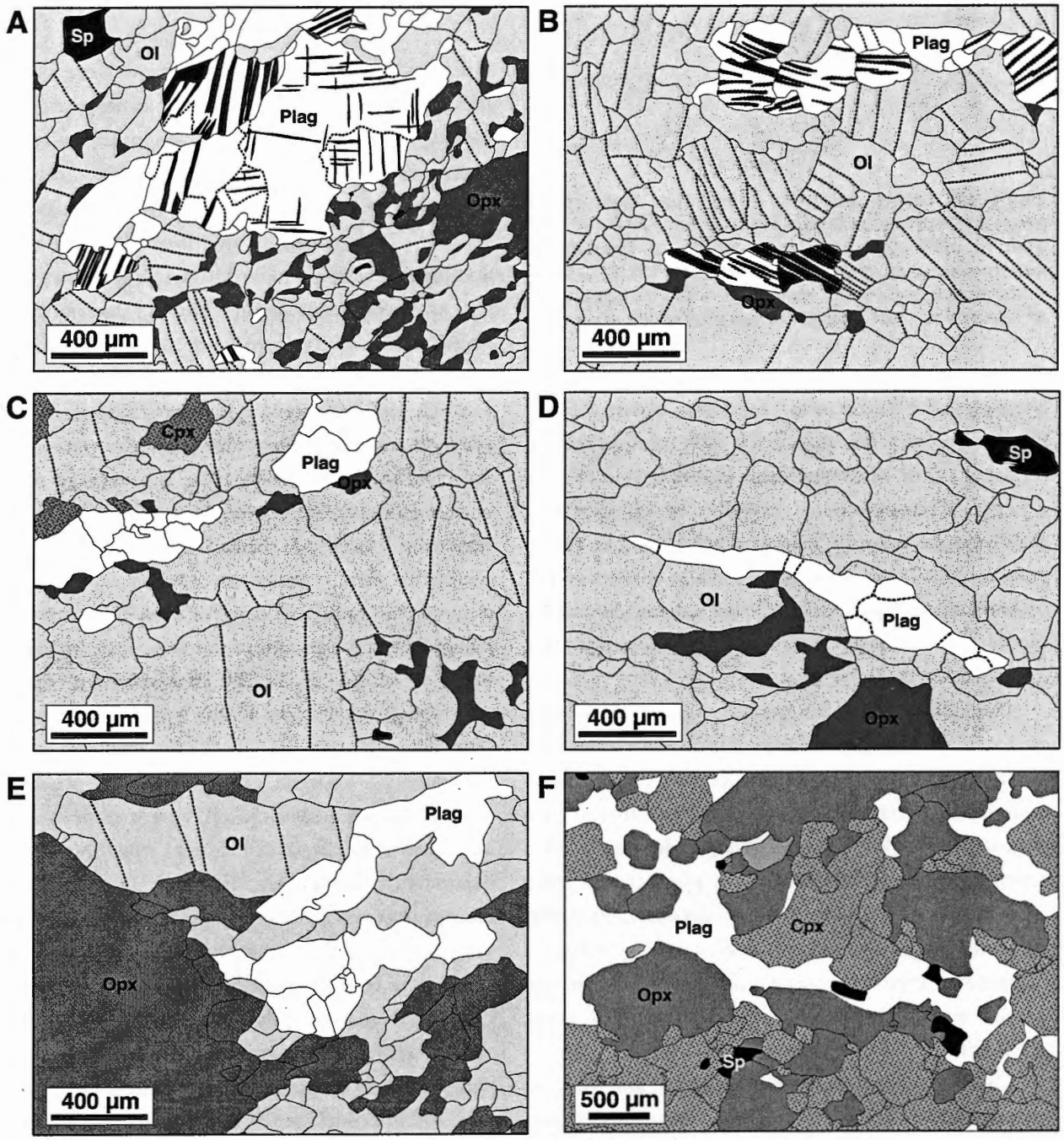

Figure 4.5: Microstructures in plagioclase-bearing rocks of domain IV. Plagioclase in white, with twins in black when indicated. Olivine in lightest grey, containing subgrain walls (dashed lines). Clinopyroxene in medium grey, stippled. Orthopyroxene in plain medium grey. Spinel in black. (a) Plagioclase cluster in fine-grained olivine-orthopyroxene domain in fine-grained tectonite. Foliation oblique, running from upper right to lower left corner of diagram; (b) Plagioclase clusters in coarse-grained olivine domain in fine-grained tectonite; (c) Plagioclase clusters associated with clinopyroxene and orthopyroxene in coarse-grained tectonite; (d) Plagioclase cluster associated with orthopyroxene in coarse-grained tectonite, parallel to foliation defined by stretched spinel; (e) Plagioclase clusters adjacent to orthopyroxene porphyroclast in coarse-grained tectonite; (f) Irregular plagioclase-bearing vein cross-cutting spinel-bearing websterite layer in coarse grained tectonite.

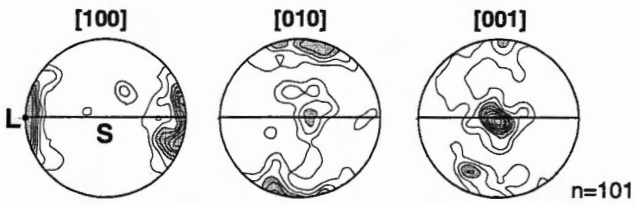

Figure 4.6: Lattice preferred orientations (equal area, lower hemisphere projection) of olivine crystals in fine-grained plagioclase-bearing tectonite of domain IV, determined by universal stage. Contours at 1, 2, 3,.... times uniform distribution. Horizontal line indicates orientation of foliation (S) , dot indicates orientation of lineation (L).

elongate parallel to the spinel and orthopyroxene lineation and foliation in the peridotites (figure 4.5a-e). Plagioclase may be associated with clinopyroxene (figure 4.5c) or orthopyroxene (figure 4.5b-d, figure 4.7a,c). Clinopyroxene crystals in plagioclase-peridotites occasionally exhibit simple {100} or {001} growth twins. Plagioclase also occurs in clusters with a poikilitic shape in rare cm-thick spinel-websterite layers (figure 4.5f) and in the more common cm- to dm-scale troctolitic layers (figure 4.7a).

Plagioclase crystals contain considerably less evidence for intracrystalline deformation than the olivines of the host peridotite. Generally, a magmatic texture is preserved in plagioclase clusters and plagioclase crystals contain relatively wide straight twin lamellae (figure 4.7b,c). Only rarely plagioclase crystals show evidence for crystal plastic deformation; plastically deformed plagioclase crystals exhibit strong undulose extinction, crystal bending, narrow and tapering lamellar twins, and abundant recrystallisation to small grains with irregular grain boundaries (figure 4.7d,e).

Locally the plagioclase-peridotites are cut by mylonite zones. In these zones plagioclase crystals occur as clasts in the fine-grained matrix (figure 4.7f), indicating that they formed prior to the mylonitic deformation. Plagioclase clasts in the mylonites also contain abundant deformation features such as undulose extinction and narrow tapering twins.

4.2.4. Mineral chemistry

Chemical analyses of mineral grains were obtained using a Cameca SX-50 electron microprobe at the Geology and Geophysics Department of Texas A&M University (USA) with wavelength dispersive spectrometers equipped with LiF, PET and TAP crystals. Operating conditions comprised an acceleration voltage of 15 kV, a 10 nA beam current, ~10 μm beam diameter and counting times of 20-60 s. Sodium was always measured first with a counting time of 20 s. As the primary aim of the chemical analyses was pyroxene geothermometry, relatively clinopyroxene-rich (lherzolitic) samples were selected for chemical analysis. In table 4.1 average mineral compositions are presented for a plagioclase-bearing peridotite from the Fournos Kaïtsa area (GOF1) and a plagioclase-free peridotite with a lherzolitic composition (96FK14) sampled close (<100 m) to the plagioclase-in boundary in the same area (figure 4.2). Sample GOF1 is mildly serpentinised (20-30% serpentine), whereas 96FK14 is largely unserpentinised (less than 5% serpentine). GOF1 contains about 5 volume% Ca-rich (An80-88) plagioclase. Clinopyroxene analyses in GOF1 are all from crystals associated with plagioclase clusters. Notably, they have significantly higher Na, Fe- and Ti-contents than clinopyroxenes in the plagioclase-free peridotite sample (table 4.1). Amphiboles associated with plagioclase have pargasitic hornblende compositions. Orthopyroxene porphyroclasts in both samples are zoned, with Al-contents decreasing from core to rim. Orthopyroxene cores sometimes contain oriented grains of spinel, suggesting exsolution from an originally Al-rich orthopyroxene. Orthopyroxenes do not show any obvious Ca-zoning. However, cores of orthopyroxene crystals often contain exsolution lamellae of Ca-rich pyroxene. Orthopyroxene crystals in the matrix have compositions overlapping with those of the rims of porphyroclasts.

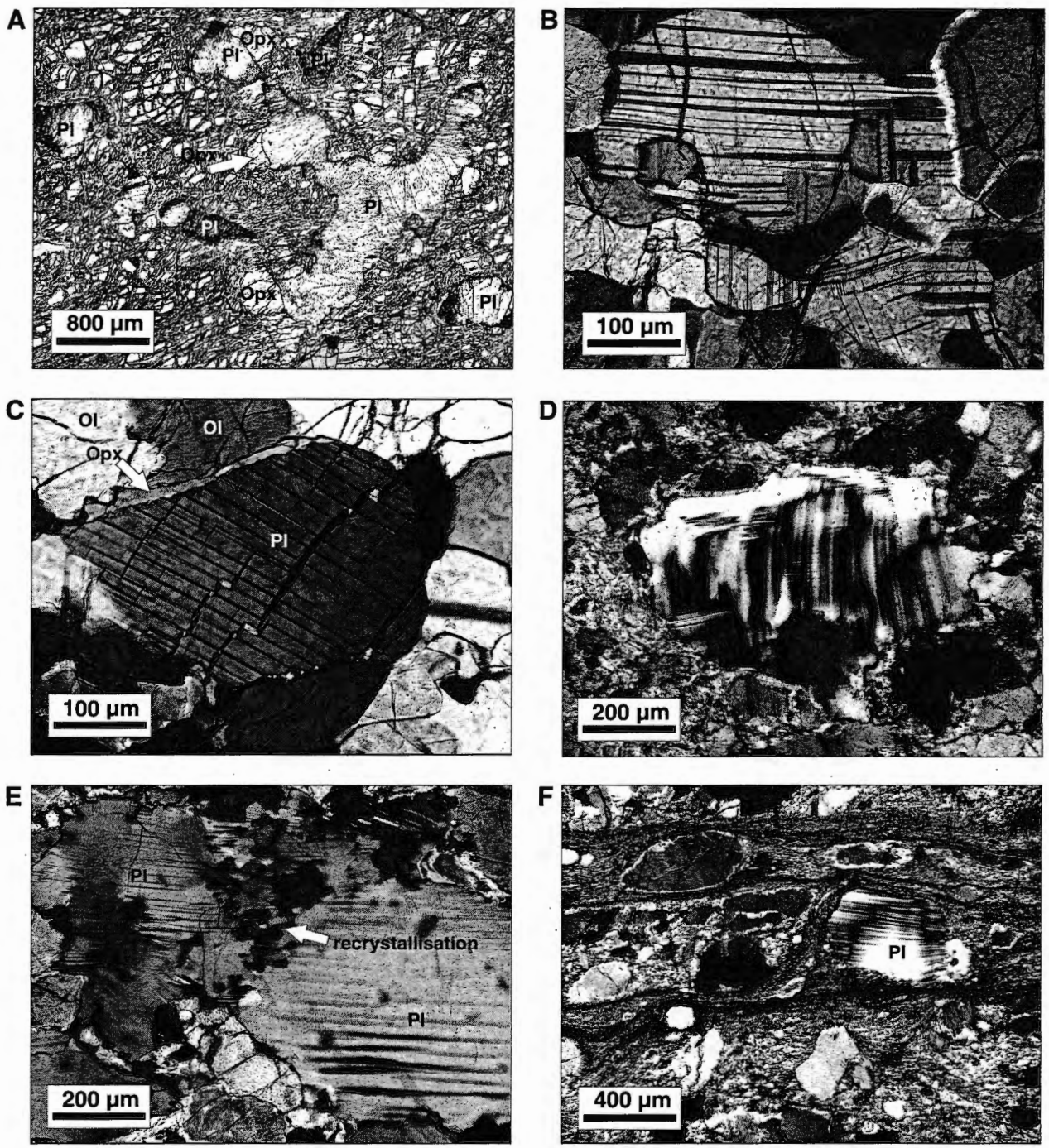

Figure 4.7: Details of plagioclase crystals in plagioclase-bearing peridotites of domain IV. Opx=orthopyroxene, Ol=olivine, Pl=plagioclase. (a) Poikiloblastic plagioclase associated with orthopyroxene in layer with troctolitic composition (in plane polarised light); (b) Magmatic twinning in plagioclase crystals in cluster in fine-grained tectonite (cross-polarised light – XPL); (c) Thin orthopyroxene rim between olivine and plagioclase crystal in fine-grained tectonite (XPL); (d) Thin lamellar twins and crystal bending induced by crystal plastic deformation of plagioclase crystal in fine-grained tectonite (XPL); (e) Partly recrystallised plagioclase crystal in coarse-grained tectonite (XPL); (f) Plagioclase clast in mylonite zone cross-cutting plagioclase-bearing tectonites (XPL).

Table 4.1: Average mineral compositions in plagioclase-bearing and adjacent plagioclase-free tectonite

	GOF1 (plagioclase-bearing coarse-grained tectonite)								*96FK14 (plagioclase-free fine-grained tectonite)*							
	Ol	*Opx*			*Cpx*	*Pl*	*Sp*	*Amph*	*Ol*	*Opx*			*Cpx*			*Sp*
		matrix	*rims*	*cores*	*in clusters*			*(Prg)*		*matrix*	*rims*	*cores*	*matrix*	*rims*	*cores*	
	n=10	n=12	n=6	n=34	n=18	n=6	n=12	n=3	n=9	n=9	n=1	n=32	n=13	n=2	n=7	n=9
oxide wt%:																
SiO_2	40.57	55.79	56.16	55.46	51.94	45.30	0.03	43.23	40.93	57.01	55.78	55.35	52.91	52.66	52.20	0.02
TiO_2		0.13	0.10	0.14	0.40		0.16	2.09		0.04	0.03	0.05	0.12	0.20	0.14	0.05
Al_2O_3	0.01	2.37	2.21	3.21	3.41	34.89	39.77	13.35	0.00	1.71	2.84	3.87	2.64	2.68	3.48	49.26
Cr_2O_3		0.40	0.38	0.66	0.77		25.76	2.01		0.19	0.30	0.61	0.50	0.53	0.82	18.84
FeO	9.71	6.95	7.18	7.07	2.56	0.12	18.92	4.04	9.06	6.80	6.89	6.68	2.25	2.16	2.41	14.33
MnO	0.14	0.16	0.15	0.16	0.08		0.52	0.06	0.12	0.15	0.11	0.14	0.07	0.04	0.07	0.25
MgO	48.87	33.66	33.89	33.39	16.65		14.37	17.42	49.28	34.46	33.90	33.30	17.17	16.97	16.76	17.11
CaO	0.03	0.60	0.58	0.60	23.16	17.82	0.03	12.41	0.02	0.36	0.46	0.54	24.43	24.90	24.24	0.02
BaO						0.05										
NiO	0.39						0.17		0.40							0.27
Na_2O	0.01	0.02	0.01	0.01	0.40	1.41		2.79	0.01	0.01	0.02	0.01	0.13	0.12	0.15	
K_2O						0.01		0.03								
Σ	99.71	100.08	100.67	100.70	99.38	99.60	99.73	97.44	99.83	100.73	100.33	100.55	100.23	100.25	100.27	100.15
Mg#	89.8	89.4	89.2	89.2	91.8				90.0	89.8	89.6	89.7	93.0	93.2	92.3	
%An						86.9										
Cr#							30.3									20.6
activities†	0.80-0.81	0.73-0.77	0.73-0.77	0.72-0.75	0.75-0.80	0.85-0.89	0.25-0.31		0.80-0.81	0.75-0.79	0.76	0.72-0.74	0.79-0.91	0.86-0.87	0.80-0.83	0.32-0.48

† End-member activities defined as: $a^{Fo}_{Ol}=(X_{Mg})^2$; $a^{En}_{Opx}=(X_{Mg}{}^{M2})(X_{Mg}{}^{M1})$; $a^{Di}_{Cpx}=(X_{Ca}{}^{M2})(X_{Mg}{}^{M1})$; $a^{An}_{Pl}=X_{Ca}$; $a^{Sp}_{Sp}=(X_{Mg})(X_{Al})^2$. Distribution of Fe^{2+} and Mg^{2+} over M1- and M2-sites in pyroxenes according to Wood and Banno (1973).

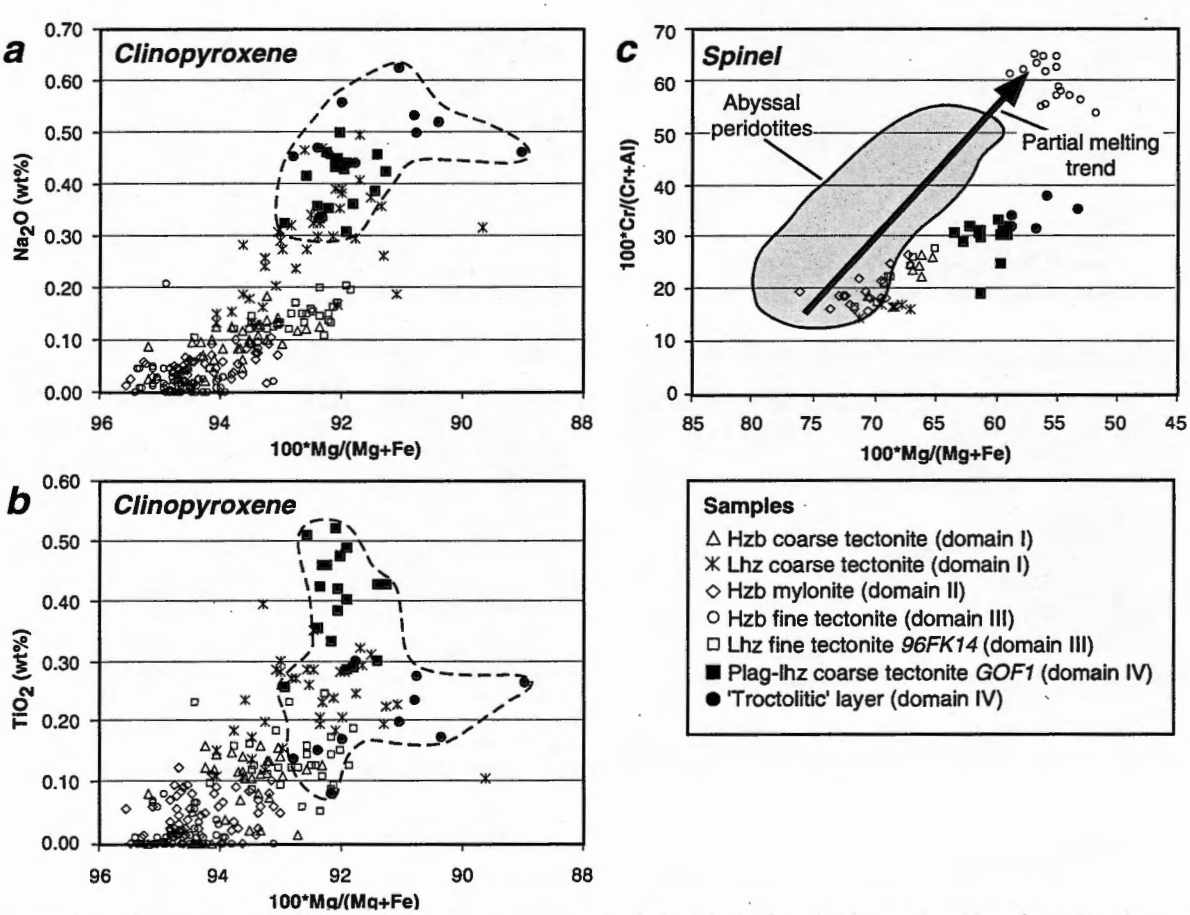

Figure 4.8: Chemical variability in clinopyroxenes and spinels in selected rocks determined by electron microprobe. (a) Na_2O weight% versus Mg-number in clinopyroxene; (b) TiO_2 weight% versus Mg-number in clinopyroxene; (c) Cr-number versus Mg-number in spinel. 'Abyssal peridotites' field and partial melting trend taken from Dick and Bullen (1984). Dashed lines in (a) and (b) outline fields of Othris cumulate clinopyroxenes used in figure 4.9.

The observed variations in Na-, Ti-, and Fe-content of clinopyroxenes are also shown in the diagrams of figure 4.8a-b, in which analyses of samples from different domains are plotted (see figure 4.1 and 2 for sample localities). Clinopyroxenes associated with plagioclase-clusters are chemically distinct, with higher Ti-, Na-, and Fe-contents compared to clinopyroxenes from plagioclase-free peridotites. The Ti-, Na-, and Fe-contents of clinopyroxenes from one plagioclase-free but lherzolitic coarse tectonite from the Katáchloron area (domain I) partly overlap with those of clinopyroxenes associated with plagioclase.

Cr-numbers (Cr/(Cr+Al)) of spinels from the study area are very variable between samples, ranging from 15-65 (figure 4.8d). Spinels from plagioclase-bearing samples are more Fe-rich than spinels from plagioclase-free rocks with similar Cr-numbers. It should be noted however that the two plagioclase-bearing peridotites analysed are also significantly more serpentinised than the plagioclase-free peridotites.

4.3. Discussion

4.3.1. Original geometry of the mantle section

The dismembered nature of the ophiolite and the lack of an unambiguous paleo-crust-mantle boundary, commonly used as a paleo-horizon in ophiolites, pose a major problem to the reconstruction of the original geometry. Yet the following evidence suggests that the easternmost peridotites of domain V represent shallow, near-seafloor peridotites, whereas the westernmost peridotites of domain I represent deeper levels, possibly the base of the mantle section.

(I) The serpentinisation seen in the most north-easterly (plagioclase) peridotites in the Fournos Kaïtsa area (domain V) is pervasive, whereas serpentinisation in the other peridotite domains is limited to shear zones and major tectonic contacts. In addition, the plagioclase-peridotites of domain V are cross-cut by unaltered (unrodingitised) dolerites. These observations suggest that serpentinisation affecting the domain occurred as a result of seafloor metasomatism, pre-dating the cessation of magmatic activity, rather than of emplacement-related serpentinisation (Coulton *et al.*, 1995). Such an imprint of seafloor hydrothermal processes implies that hydrothermal circulation penetrated into the mantle and strongly suggests that domain V represents the uppermost part of the mantle section exposed in the area. This interpretation seems fully consistent with the fact that the rocks of this domain are in tectonic contact with magmatic crustal rocks.

(II) The westernmost peridotites of the Katáchloron area (domain I) contain late, post-kinematic tremolite. They are in contact with a mélange unit containing tremolite-bearing amphibolites. It is, therefore, concluded that this domain was part of the base of the ophiolite, which was infiltrated with fluids during intra-oceanic emplacement and formation of the metamorphic sole.

It should be noted that in the present-day geometry the peridotites are probably part of a relatively thin thrust sheet which overlies a mélange unit (Smith *et al.*, 1975; Ferrière, 1985). Ferrière (1985) argued that the dismemberment of the entire ophiolitic section already occurred during or even before the obduction of the Othris Ophiolite. Indeed, Rassios & Konstantopoulou (1993) found that the serpentinite faults which cut the Othris mantle section and which often separate different mantle domains recognised in this study are locally lined with amphibolite facies metamorphic rocks. This observation suggests that the dismemberment took place early in the history of the Othris Ophiolite, when the peridotites were still relatively hot (Rassios & Konstantopoulou, 1993). It is therefore possible that peridotites which originated at different levels in the oceanic mantle were already juxtaposed well before final emplacement of the stack of thrust sheets now forming the Othris Mountains.

4.3.2. Plagioclase-peridotites: Products of melt impregnation

The occurrence of plagioclase in small lenses and dykes, often in association with clinopyroxene, suggests a melt origin (Menzies, 1973; Nicolas, 1986b; Suhr & Robinson, 1994; Rampone *et al.*, 1997). Menzies (1973) interpreted these melt features as melt-segregations, *i.e.*, the products of in-situ partial melting of the host-rock and incomplete extraction. Plagioclase lenses in the Trinity Ophiolite, which are very similar to those in Othris, were also interpreted as melt-segregations by Quick (1981a). Based on the following considerations an alternative interpretation is favoured in which plagioclase and clinopyroxene represent the cumulate phases of a basaltic melt which impregnated harzburgites, locally turning them into lherzolites:

(I) In the plagioclase-peridotites the compositional layering and lineation, defined by elongate plagioclase-bearing lenses, is always parallel to the olivine and orthopyroxene foliation and spinel lineation. This is confirmed by the measurements of crystallographic fabrics which show that olivine slip-planes and slip-directions are subparallel to the plagioclase layering and lineation (figure 4.6). However, plagioclase crystals are generally much less deformed than the other minerals in the host peridotite. Moreover, gabbro dykes which are contiguous with plagioclase lenses cross-cut foliations. It is, therefore, concluded that plagioclase crystallised late in the deformation history recorded in the plagioclase-peridotites. The following microstructural features indicate that this deformation, and thus plagioclase crystallisation, occurred at relatively cold *(sub- peridotite solidus)* conditions. Most of the plagioclase-peridotites are relatively fine-grained tectonites with typical 'lithospheric' microstructures (Ceuleneer *et al.*, 1988; Nicolas, 1989; Ildefonse *et al.*, 1998). The fine grain size of the tectonites and the substructure of olivine grains indicate deformation conditions at relatively high stresses, and at temperatures at which recovery is not very efficient. The dynamically recrystallised olivine grain size in the plagioclase-bearing tectonites in Othris is smaller than 0.5 mm, probably as small as 0.2 mm. According to the olivine piezometer of Van der Wal *et al.* (1993), this recrystallised grain size corresponds to deviatoric stresses of 13-26 MPa. These stresses give minimum deformation temperatures of 970-1030°C to maintain geological strain rates $>10^{-13}$ s^{-1}, using the dry peridotite dislocation creep flow law of Chopra and Patterson (1984). It should be noted that this flow law determined by Chopra and Patterson corresponds to that of relatively strong peridotites; the temperatures of deformation may be lower if wet or melt-weakened rheologies apply. Estimates for deformation temperatures for similar 'lithospheric' tectonites range typically from 1200-800°C (*e.g.*, Ceuleneer *et al.*, 1988; Suhr, 1993; Ildefonse *et al.*, 1998). It is concluded therefore that during the last stages of deformation the ambient temperature of the host mantle rocks was below 1200°C - possibly as low as 1000°C - *i.e.*, well below the dry peridotite solidus, when plagioclase and clinopyroxene crystallised. If the melt had been produced in-situ and had not been extracted from the host peridotite then the melt should have become saturated in plagioclase when the temperature of the host peridotite fell below 1200-1250°C (Bender *et al.*, 1978; Elthon & Scarfe, 1984; Kelemen & Aharonov, 1998). In that case plagioclase should have been deformed during subsequent subsolidus deformation. The microstructural observation that plagioclase is generally undeformed shows that plagioclase simply could not have been present during most of the lithospheric deformation recorded in the Othris peridotites. It is therefore unlikely that the plagioclase clusters represent the products of in-situ generated melts.

(II) Magmatic segregations formed by in-situ partial melting often show depletion halos, *i.e.*, zones depleted in pyroxenes surrounding plagioclase clusters (Nicolas, 1986b). Nicolas (1986b,1989) cites

the presence of depletion halos is one of the key criteria to distinguish in-situ partial melting. In the Othris peridotites depletion halos are extremely rare. In fact, the opposite is often observed, *i.e.*, plagioclase clusters are often surrounded by ortho- and clinopyroxenes.

(III) The plagioclase-peridotites contain up to ~10 volume% plagioclase. Estimates for the amount of melt that may be stable in partially molten peridotites before permeability is attained range from less than 1% (*e.g.*, Von Bargen & Waff, 1986; McKenzie, 1989) to 3% at most (Faul, 1997). It is therefore unlikely that the peridotites could have partially melted to produce melt volumes of ~10% or more without the melt being extracted. It seems more plausible that plagioclase represents a cumulate phase of a fractionating melt impregnating the peridotites.

4.3.3. Melt composition

Based on the above the plagioclase in the plagioclase-peridotites is interpreted as the product of low-pressure crystallisation from a melt that impregnated the uppermost peridotites of the Othris mantle section. Clinopyroxenes associated with the plagioclase clusters are chemically and texturally distinct and were probably derived from the same melt. The high Mg-numbers, *i.e.*, Mg/(Mg+Fe), of these clinopyroxenes show that the aggregates of melt-derived minerals do not represent frozen-in melt fractions, but rather cumulates deposited during fractional crystallisation. The high anorthite-contents of the plagioclase suggest that the melt had a high CaO/Na_2O-ratio. The presence of orthopyroxene rims at the contact between olivine and melt-derived plagioclase clusters and the frequent occurrence of interstitial orthopyroxene in the Othris peridotites suggests that the melt may also have been relatively silica-rich. Compositions of cumulate plagioclase and clinopyroxene plot at the most depleted end of the field of mid-ocean ridge cumulate minerals (figure 4.9). They partly overlap with compositions of cumulate minerals from ODP site 334 at the Mid-Atlantic ridge, albeit at higher clinopyroxene Mg-numbers (Ross & Elthon, 1993). It is, therefore, most likely that the impregnating melt had a depleted to ultra-depleted melt composition, *i.e.*, the composition of a melt which is produced by low pressure partial melting of a refractory source peridotite (Bloomer *et al.*, 1989; Natland, 1989; Ross & Elthon, 1993; Sobolev & Shimizu, 1993). However, the possibility that the melt composition was that of a magnesian andesite (boninite) cannot be excluded.

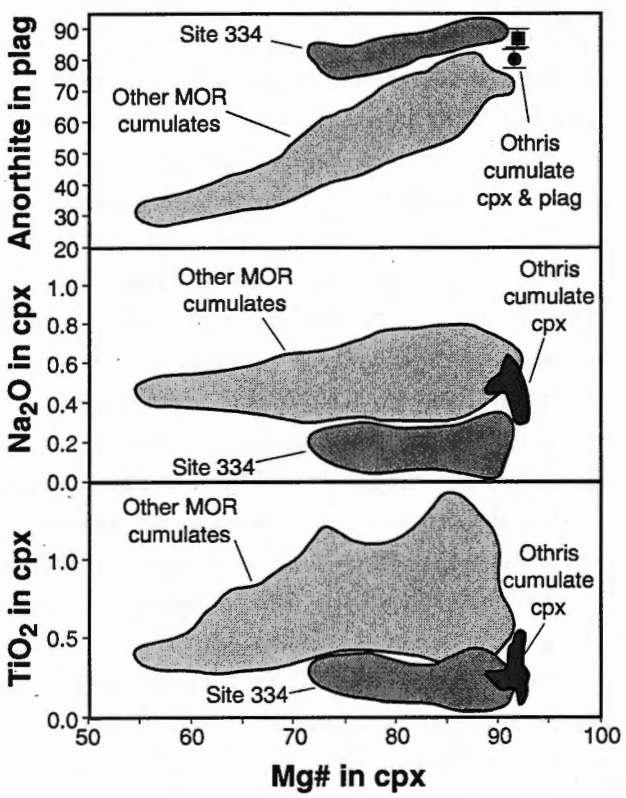

Figure 4.9: Mineral compositions of Othris cumulate minerals compared to compositions of cumulate minerals in oceanic rocks. Othris fields correspond to those in figure 4.8a-b. The Othris cumulate minerals probably crystallised from a depleted melt similar in composition to the melt from which ODP site 334 cumulates were derived. Diagram modified from figure 1 of Ross & Elthon (1993).

4.3.4. Plagioclase-out or plagioclase-in?

The boundary between plagioclase-free and plagioclase-bearing peridotites is everywhere oriented at a high angle to the foliation in the tectonites (figure 4.1 and figure 4.2). Quick (1981b) argued that the boundary between plagioclase-free and plagioclase-bearing peridotites in the Trinity Ophiolite is a plagioclase-out boundary. The Trinity peridotites contain large dunite bodies which were probably melt conduits. Plagioclase was removed from the peridotite margins of these dunites by a reaction with transient melts (Quick, 1981b). However, in Trinity the transition from dunite, via harzburgite, to plagioclase-lherzolite occurs over a distance ranging from 15 cm to a few meters at most (Quick, 1981b), hence at a much smaller scale than the transition in Othris. In Othris, the transition from harzburgites to plagioclase-lherzolites occurs over a distance of a few hundred metres at least. It seems unlikely that the harzburgite domain could represent a melt conduit, which must have been colossal in size (km-scale), and that plagioclase was removed from the conduit margins by melt-wall rock reaction over a distance of hundreds of metres wide. The plagioclase-free harzburgites contain some small dunite bands, but these are generally deformed and transposed into the foliation. Therefore, these dunites *pre*-date the deformation recorded in the harzburgites and cannot have been associated with a melt flow responsible for plagioclase removal taking place *after or during* the last stages of deformation.

Instead, it is more likely that the plagioclase-peridotites represent a zone of melt accumulation and impregnation and that the boundary between plagioclase-free and plagioclase-bearing peridotites is in fact a plagioclase-in boundary. The zone of melt impregnation was probably not restricted to the plagioclase-peridotites alone. Plagioclase-free peridotites adjacent to the plagioclase-peridotites are enriched in clinopyroxene, which sometime occurs in veins. Furthermore, most harzburgites contain interstitial orthopyroxene, which may also have been derived from an impregnating melt. From figure 4.2 it seems that there may even be a layered structure with an upward transition from peridotites with interstitial orthopyroxene (harzburgites of domain III) to peridotites with interstitial clinopyroxene to peridotites with interstitial plagioclase + clinopyroxene (plagioclase-peridotites of domain IV and V). This implies that the boundaries have some petrological significance, *i.e.*, that they represent the boundaries in P/T-space at which the impregnating melt became saturated in orthopyroxene, clinopyroxene, and plagioclase.

Interstitial orthopyroxene and clinopyroxene in websterite and clinopyroxenite veins and lenses generally show evidence for plastic deformation whereas aggregates of plagioclase ± clinopyroxene ± orthopyroxene are generally undeformed. This implies that plagioclase occurred last at the liquidus of the impregnating melt, after orthopyroxene and clinopyroxene. This is not in agreement with crystallisation experiments on basaltic melts, which show that plagioclase crystallises before pyroxene (Bender *et al.*, 1978; Elthon & Scarfe, 1984; Grove *et al.*, 1992; Kinzler & Grove, 1992). This 'delay' of the crystallisation of plagioclase might be explained by the fact that the Othris peridotites had refractory compositions before impregnation and were therefore undersaturated with respect to plagioclase. Harzburgites can potentially 'resorb' some plagioclase components precipitating early from the impregnating melt in the available mineral structures, mainly spinel and clinopyroxene (Suhr & Robinson, 1994). In that case, plagioclase only starts to crystallise if the host-peridotite is sufficiently refertilised. Secondly, melt percolating through a harzburgite by porous flow will re-equilibrate with the host rock. Due to the reaction of the melt with the host harzburgite plagioclase may disappear from the liquidus (Kelemen, 1990; Suhr & Robinson, 1994). In such a scenario plagioclase crystallises as soon the melt ceases to equilibrate with

the host-peridotite, for instance if the melt fraction becomes very large or if the melt stops to percolate. This means that plagioclase will only crystallise from a melt in a zone of melt accumulation.

It should be emphasised that the vertical thickness of the zone of plagioclase-peridotites in Othris cannot be determined. The mapping shows that the plagioclase-peridotites form the highest levels of the Othris peridotite massif and that the zone of plagioclase-peridotites may only be a few hundred metres in thickness. It does therefore not need to be invoked that the impregnating melts travelled over large distances in relatively cold (<1200°C) rocks. The Othris plagioclase-peridotites probably represent the level in the mantle where the host-peridotites became too cold for further porous flow and where the melts started to 'freeze-out', crystallising orthopyroxene, clinopyroxene, and finally plagioclase. From the mineral analyses it is clear that these minerals represent cumulate phase, implying that the remaining melt must have escaped. The remaining melt may have escaped by hydro-fracturing through dykes for which the discordant gabbro-norite dykes are likely candidates.

4.3.5. Depth at which impregnation occurred

An attempt was made to constrain the ambient pressure and temperature conditions during melt impregnation by applying geothermo-barometry. Unfortunately, it was found that all minerals have (partially) re-equilibrated during cooling (chapter 5). Model temperatures obtained on the rims of mineral grains all lie in the range 700-900°C. Some cores of orthopyroxene porphyroclasts gave model temperature plateaus of 1000-1100°C. Lack of equilibrium between pyroxenes precludes the use of geobarometers. However, the complete absence of metamorphic plagioclase, even in very fine-grained domains and small mylonite zones in clinopyroxene-rich peridotites adjacent to plagioclase-peridotites in the Fournos Kaïtsa area, suggests that the plagioclase-free peridotites equilibrated in the metamorphic spinel-peridotite facies. The transition of the spinel- to plagioclase-peridotite facies, the univariant equilibrium 2Forsterite + Anorthite = Spinel + Diopside + Enstatite, is not only dependent on pressure and temperature, but also on the composition of the host-peridotite. The most 'depleted' end-member activities for olivine (a^{Fo}_{Ol}=0.81), orthopyroxene (a^{En}_{Opx}=0.75), clinopyroxene (a^{Di}_{Cpx}=0.79) and spinel (a^{Sp}_{Sp}=0.31) in the plagioclase-free sample 96FK14 (table 4.1) collected very close to the plagioclase-in boundary (figure 4.2) were taken to determine the univariant equilibrium using the 'Thermocalc v.2.4' program (Powell & Holland, 1988; Holland & Powell, 1990). This yields a pressure of 3 Kbar at 1000 °C to 4 Kbar at 1200 °C for the metamorphic spinel-plagioclase boundary. It follows that plagioclase-free peridotites in the Fournos Kaïtsa area equilibrated at pressures exceeding these values. Since these peridotites are in structural continuity with plagioclase-peridotites, the plagioclase-peridotites cannot have been equilibrated at (much) lower pressures. A minimum pressure of 3-4 Kbar is thus inferred for the magmatic plagioclase-in boundary in the Fournos Kaïtsa area. Note that more 'fertile' end-member activities move the phase equilibrium to higher pressures.

4.3.6. Rift, slow- or fast-spreading ridge?

Since plagioclase and at least some clinopyroxene in the plagioclase-peridotites have crystallised from an impregnating melt, the original host rocks were probably much more depleted in composition. It is estimated that before melt impregnation the host rocks must have had harzburgitic, yet clinopyroxene-bearing modal compositions, comparable to the compositions of adjacent plagioclase-free harzburgites. This indicates that the plagioclase-peridotites had been subject to significant melting and melt extraction prior to melt

impregnation. The overall harzburgitic composition of the mantle section, as well as the presence in the Othris Mountains of all the lithologic elements of a true ophiolite sequence (Menzies, 1973; Hynes, 1974b), *i.e.*, oceanic sediments, pillow lavas, dolerites, gabbros, mantle rocks, and fragments of a metamorphic sole thrust, suggests that the Othris Ophiolite formed at an ocean ridge rather than in a rift setting.

Most of the studied harzburgites contain clinopyroxene porphyroclasts, whose formation clearly pre-dates deformation and melt impregnation. Moreover, peridotites occur which have more lherzolitic compositions, containing >5 volume% clinopyroxene porphyroclasts. Their preservation indicates that early melt extraction in the Othris peridotites was limited and that clinopyroxene was left in the residue. Menzies (1975) reported lherzolites from Othris with near-chondritic rare earth element abundances, also compatible with low degrees of melt extraction. The bulk compositions of the peridotites are probably similar to those of peridotites from the slow-spreading Mid-Atlantic Ridge (MAR). MAR peridotites are generally clinopyroxene-rich harzburgites or lherzolites, in contrast to peridotites from the fast-spreading East Pacific Rise (EPR) which have only low modal clinopyroxene contents (*e.g.*, Michael & Bonatti, 1985; Constantin *et al.*, 1995).

Based on the study of the plagioclase-peridotites in Othris, a three-stage scenario for their formation is inferred: (a) partial melting and melt extraction leaving a predominantly cpx-harzburgite residue, (b) deformation at 'lithospheric' mantle temperatures (~1000-1200°C) and stresses of 13-26 MPa, and (c) impregnation with magmas with a depleted composition during and after the last stages of deformation. Such a scenario is in good agreement with the episodic nature of spreading and magmatism postulated for slow-spreading ridges (Karson *et al.*, 1987; Cannat, 1993; Cannat & Casey, 1995; Tartarotti *et al.*, 1995). Stage (a) probably represents a (waning) magmatic stage, followed by an a-magmatic stage (stage b) during which extension (spreading) is accommodated by deformation of the lithosphere at the ridge axis, followed by the start of a new stage of magmatism (stage c).

The extensive hydrothermal alteration and the presence of dolerite dykes in the uppermost plagioclase-peridotites, as well as the absence of large volumes of oceanic crustal rocks in the area (Menzies & Allen, 1974) point to a thin magmatic crust. This is also in accordance with limited magmatism and possibly tectonic denudation of mantle rocks during a-magmatic spreading at slow-spreading ridges (Karson *et al.*, 1987; Cannat, 1993; 1996; Cannat & Casey, 1995).

4.3.7. Segment centre or transform environment?

As discussed above, melt impregnation of the Othris peridotites probably occurred at temperatures below 1200°C, possibly as low as 1000°C. These conditions correspond to the base of the *thermal* lithosphere. In this chapter the lower boundary of the thermal lithosphere is taken as the transition between the adiabatic interior and the conductively cooled boundary layer of the Earth. In this definition, the base of the thermal lithosphere should have a temperature of 1250-1300°C. The observations suggest that the thermal lithosphere may have been relatively thick during magmatic activity at the Othris ridge, reaching well into the mantle. The lower boundary of the impregnated horizon was possibly located at depths equivalent to pressures of at least 3-4 Kbar, implying that the thermal lithosphere at or close to the ridge axis was at least 9-12 km thick.

A relatively cold mantle structure with a thick thermal lithosphere is expected at slow-spreading ridges, where cooling by conductive heat-loss to the surface plays an important role (Cannat, 1993; 1996). Transform fault environments may have a particularly thick thermal lithosphere due to the 'cold-wall effect' (Nicolas & Dupuy, 1984; Nicolas, 1986b, 1989; Cannat, 1996).

Magmatic impregnation is not uncommon in peridotites from transform regions of modern slow-spreading oceans such as the Mid-Atlantic (*e.g.*, Dick, 1989; Bonatti *et al.*, 1992; Cannat *et al.*, 1992; Cannat & Casey, 1995; Tartarotti *et al.*, 1995). However, melt-impregnated peridotites have also been recovered from transform regions of fast-spreading ridges such as the EPR (*e.g.*, Cannat *et al.*, 1990; Constantin *et al.*, 1995; Constantin, 1999). Ghose and co-workers (1996) argued that trapping of magma in a cold lithospheric mantle root may be required to fully explain variations in crustal thickness in the Kane transform area (MAR). Melt impregnated, plagioclase-bearing, peridotites have also been found in an inferred ophiolitic transform fault in New Caledonia (Prinzhofer & Nicolas, 1980; Nicolas & Dupuy, 1984). It is concluded here that the Othris Ophiolite most likely originated in a (near-) transform environment of a slow-spreading ridge (figure 4.10).

4.3.8. Compositional variability among the Hellenic-Dinaric ophiolites

Several authors have emphasised the compositional variation amongst the mantle sections of ophiolites along the Hellenic-Dinaric chain between central Greece and northern Bosnia (*e.g.*, Nicolas & Jackson, 1972; Pamic', 1983; Smith & Spray, 1984; Smith, 1993). For instance, the Vourinos Ophiolite in Greece (Jackson *et al.*, 1975; Ross *et al.*, 1980; Smith, 1993) and the ophiolites of the Inner Dinaric belt such as the Kukës Ophiolite in Albania (Hoxha & Boullier, 1995) have strongly depleted mantle sections and well developed lower crustal sequences. In contrast, ophiolites of the Central Dinaric ophiolite bear resemblance to the Othris Ophiolite, comprising mixed mantle sections in which harzburgites, lherzolites, and plagioclase-bearing peridotites are exposed (Pamic',

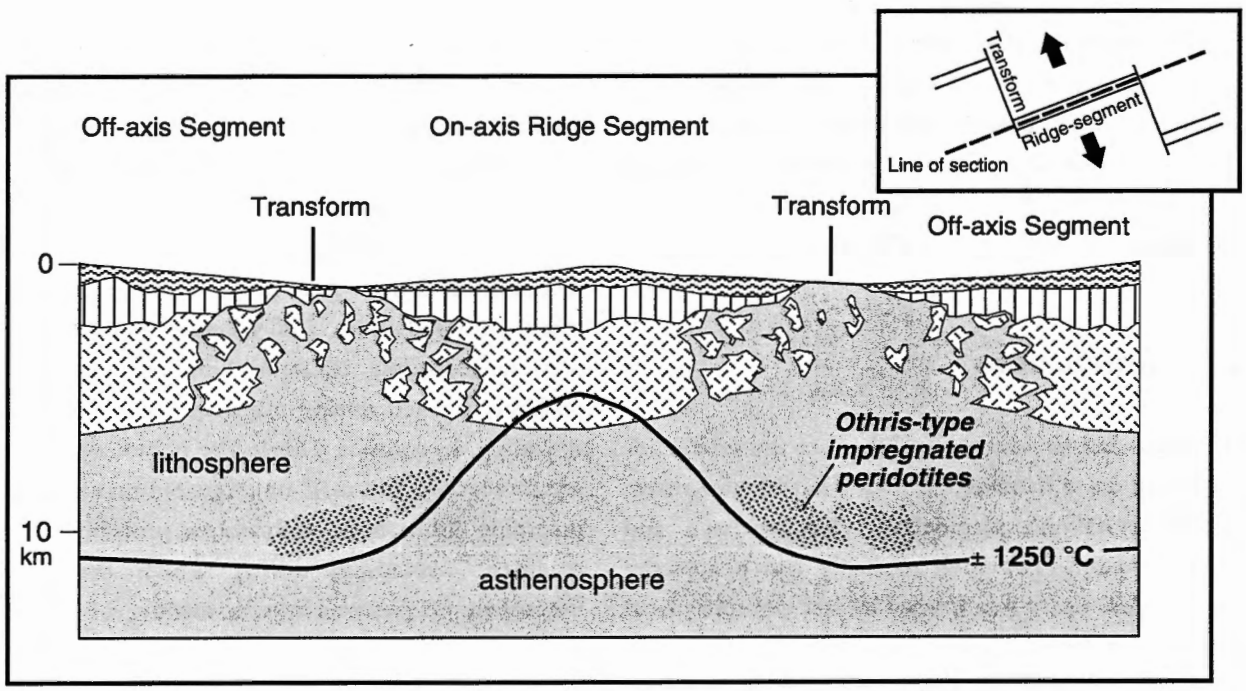

Figure 4.10: Schematic along-axis section through (slow-spreading) ridge-segment into adjacent off-axis segments (vertical and horizontal scale not equal). Crustal rocks are shown in white (lavas indicated with wavy lines, dykes with vertical lines; gabbros with hatches) and mantle rocks in light grey. Thick line represents base of thermal lithosphere. Stippled domains indicate impregnated mantle rocks such as found in Othris. Melt may become trapped in cold lithospheric roots present in transform regions. It is argued in the text that the Othris peridotites represent mantle rocks from a segment-end/transform region. Modified from figure 4 of Ghose *et al.* (1996).

1983). Notably, Boudier, Nicolas and co-workers (Boudier *et al.*, 1999; Nicolas *et al.*, 1999) have also concluded that the heterogeneous character of the Dinaric Mirdita Ophiolite in Albania results from melt impregnation of the uppermost part of the mantle section.

The compositional variability among the Hellenic-Dinaric ophiolites does not require that the pertinent realm of the eastern Tethys ocean consisted of numerous small oceanic basins (Nicolas & Jackson, 1972), nor does it require a large Jurassic left-lateral strike-slip fault juxtaposing ophiolites from different oceanic domains (Smith & Spray, 1984). The episodic nature of the magmatism associated with slow seafloor-spreading inferred in this study renders an alternative explanation. It is hypothesised that the Vourinos and Kukës massifs were formed during magmatic stages of slow seafloor spreading, during which the thickness of the thermal lithosphere at the ridge axis did not exceed the thickness of the magmatic crust. Consequently, the mantle sections of these ophiolites principally record melt extraction and near- to hypersolidus ('asthenospheric') deformation conditions. In contrast, the Othris mantle section has recorded a history of episodic magmatism and lithospheric deformation in a near-transform environment of a slow-spreading ridge.

4.4. Conclusions

(I) Plagioclase-peridotites in Othris are the product of impregnation of harzburgites with a fractionating melt, which crystallised plagioclase, clinopyroxene and orthopyroxene. The melt probably had a depleted composition, *i.e.*, it was formed by low pressure partial melting of a depleted source peridotite. The first order compositional variability of the peridotites of the Othris mantle section is thus the result of melt impregnation, rather than of variable degrees of depletion by melt extraction.

(II) The dominant rock type in the Othris mantle section is clinopyroxene-bearing harzburgite. The plagioclase-peridotites probably had clinopyroxene-bearing harzburgitic modal compositions before melt impregnation as well. Relatively clinopyroxene-rich harzburgite is the dominant peridotite type recovered from the slow-spreading MAR, whereas clinopyroxene-poor harzburgites are typical for the fast-spreading EPR. It is, therefore, concluded that the Othris Ophiolite formed at a slow-spreading ocean ridge.

(III) Plagioclase-peridotites have recorded a multi-stage history of melt depletion, deformation, and melt impregnation. This scenario is in good agreement with the episodic nature of magmatism and spreading at slow-spreading ridges.

(IV) The melt has impregnated mantle rocks deforming at temperatures of 1000-1200°C and stresses of 13-26 MPa. These conditions correspond to those at the base of the (thermal) lithosphere. This means that during magmatic activity the lithosphere at the Othris ridge axis reached into the mantle. Such a cold mantle structure points to a segment end, near-transform, environment of an ocean ridge.

(V) The compositional variability amongst the mantle sections of the Hellenic-Dinaric ophiolites may be a reflection of the episodic nature of magmatism and deformation at slow-spreading ridges. Ophiolites with thick crustal sections and strongly depleted mantle sections recording 'asthenospheric' deformation are probably formed during magmatic stages of seafloor spreading. In contrast, Othris-like ophiolites with thin crustal sections and melt-impregnated mantle sections recording 'lithospheric' deformation probably reflect a-magmatic spreading, during which the thermal lithosphere reaches well into the mantle.

Chapter 5

Peridotite tectonites and mylonites in the Othris Massif (Greece): Melt-rock reaction and shear zone formation

Abstract

A one kilometre wide peridotite mylonite shear zone is exposed in the Othris peridotite massif in central Greece. The mylonites contain lenses of relatively coarse olivine crystals which are interpreted as remnants of the tectonite microstructure seen in the adjacent wall rocks. Microstructure and texture analysis using light and SEM microscopy suggests that the dominant deformation mechanism in the tectonites was dislocation creep, whereas the deformation in the mylonites was probably controlled by grain-size sensitive (GSS) creep in fine-grained (<50 μm) bands consisting of a mixture of olivine and orthopyroxene. The development of the fine-grained material in the mylonites can be explained by a melt-present reaction taking place in the tectonite protolith. This reaction led to the replacement of orthopyroxene porphyroclasts by fine-grained olivine and orthopyroxene. Tectonites adjacent to the mylonite zone preserve evidence for this reaction in the form of rims of fine-grained olivine and orthopyroxene around orthopyroxene porphyroclasts. The deformation recorded in the peridotite mylonites and adjacent fine-grained tectonites is attributed to transpression during the onset of emplacement of the Othris Ophiolite in a near-ridge, transform-fault environment. This study illustrates the significance of rheological weakening of oceanic mantle lithosphere as a result of a change from dislocation to GSS creep.

5.1. Introduction

5.1.1. Peridotite mylonite shear zones

Mylonite shear zones are commonly found in peridotite massifs (*e.g.*, Boudier *et al.*, 1988; Ceuleneer *et al.*, 1988; Vissers *et al.*, 1991; Hoogerduijn Strating *et al.*, 1993; Newman *et al.*, 1999; Furusho & Kanagawa, 1999) and in peridotites recovered from the ocean floor (*e.g.*, Jaroslow *et al.*, 1996). Peridotite mylonites may control the strength of the mantle lithosphere (*e.g.*, Vissers *et al.*, 1995), and therefore play a crucial role in lithosphere-scale deformation processes such as continental rifting or mountain building. Peridotite mylonites in the oceanic lithosphere are responsible for exhumation of mantle rocks to the ocean floor at mid-ocean ridges, in particular in slow-spreading oceans (*e.g.*, Cannat, 1993; Jaroslow *et al.*, 1996). Moreover, peridotite mylonites are commonly involved in the detachment of ophiolite massifs from their oceanic environment and their subsequent emplacement onto the continents (*e.g.*, Boudier *et al.*, 1988). Despite their

important role in tectonics, the formation of peridotite mylonites is still poorly understood. Questions remain as to the processes that lead to strain localisation and to the development of peridotite mylonite shear zones. This chapter presents a case of a well-developed and excellently exposed peridotite mylonite zone in the Othris peridotite massif in Greece. Microstructures suggest that grain-size sensitive creep was an important deformation mechanism in this mylonite zone. It is therefore concluded that a change from dislocation to GSS creep brought about weakening and strain localisation. Based on petrographic and microstructural evidence, it is hypothesised that melt-rock reactions caused grain size reduction and extensive mixing of mineral phases in the protolith and that the small grain size thus achieved, stabilised by secondary phases (i.e., phases other than olivine, most importantly orthopyroxene in this case), led to the later development of the large mylonite zone.

5.1.2. Strain localisation and weakening

Shear localisation, *i.e.*, the formation of shear zones, can occur in materials under various conditions. In materials exhibiting elastic, elastic-brittle, or pressure sensitive elastic-plastic deformation a shear localisation instability can be initiated during strain softening, steady-state deformation, or strain hardening (Hobbs *et al.*, 1990). In materials deforming by largely pressure-insensitive crystal plastic creep or diffusion creep, shear localisation usually requires some strain softening process (Poirier, 1980; White *et al.*, 1980; Drury *et al.*, 1991). The only pressure sensitivity in the crystal plastic flow behaviour of minerals derives from the pressure dependence of the activation enthalpy. This pressure dependence, expressed as the activation volume, is small for minerals such as olivine (Ross *et al.*, 1979; Green & Borch, 1987; Karato & Wu, 1993). More importantly, for deformation to remain localised in a shear zone, the material inside the shear zone has to be significantly weaker than the surrounding material, otherwise the zone of localised deformation would widen and the shear zone would become a self-arresting instability (*e.g.*, Poirier, 1980; White *et al.*, 1980; Hobbs *et al.*, 1990; Rutter, 1999). Therefore, rheological weakening of the material inside a shear zone with respect to the material outside the shear zone is required to explain the occurrence of large shear zones in natural rocks, even if such shear zones have been formed in a system which was hardening with time. The processes that could cause significant weakening in natural rocks (White & Knipe, 1974; White *et al.*, 1980; Poirier, 1980), and peridotites in particular (Drury *et al.*, 1991), are thermal weakening, geometric weakening, reaction weakening, chemical weakening, melt weakening, and a change of the dominant deformation mechanism. Thermal and geometric weakening in peridotites are not likely to cause sufficient long-term weakening leading to stable large-scale shear zones in peridotites (Drury *et al.*, 1991). The other weakening processes are re-summarised here:

(I) *Reaction weakening.* Metamorphic or metasomatic reactions in rocks can lead to the production of relatively soft phases at the expense of hard phases. Olivine is by far the most abundant and probably also the weakest phase in peridotites and controls the deformation of peridotite mylonites. Reactions that can occur under the temperature conditions at which peridotite mylonites are active do not produce phases which are softer than olivine and which can reduce the strength of the bulk rock. However, reactions between peridotites and migrating basaltic melts can remove pyroxenes (*e.g.*, Kelemen *et al.*, 1992), *i.e.*, relatively hard phases, from the host peridotite and crystallise olivine, thus producing a reduction in the bulk strength. Moreover, metamorphic reactions in peridotites can lead to grain size reduction, which in turn can lead to weakening due to a change in deformation mechanism (see below; see also Newman *et al.*, 1999; Furusho & Kanagawa, 1999). At

temperatures below ~500°C under hydrous conditions, the weak mineral serpentine can form at the expense of olivine. Serpentine can then control the strength of serpentinised peridotites leading to the formation of serpentinite shear zones often observed in the upper part of oceanic mantle (Escartin *et al.*, 1997) as well as in peridotite massifs (Hoogerduijn Strating *et al.*, 1993; Coulton *et al.*, 1995).

(II) *Chemical weakening.* A well-established significant chemical weakening effect in peridotites is due to the presence of trace amounts of water in olivine (Mackwell *et al.*, 1985; Hirth & Kohlstedt, 1996; Mei & Kohlstedt, 2000a,b). Water content, and thus the role of water weakening, during deformation of natural peridotites is generally difficult to assess. It is possible that shear zones act as fluid conduits, leading to enhanced water weakening in the shear zone. Secondly, impurity atoms may affect the strength of peridotites. Impurities in olivine may act as nucleation sites for dislocations in olivine but they can also hamper dislocation mobility. Impurities may thus lead not only to a decrease but equally to an increase of the strength of peridotites deforming by dislocation creep.

(III) *Melt weakening* is found to occur in deformation experiments on partially molten olivine aggregates (Hirth & Kohlstedt, 1995a,b; Bai *et al.*, 1997). Hirth and Kohlstedt (1995b) proposed that melt weakening of olivine involves a change from dislocation creep deformation controlled by the hard [c] (010) slip system to deformation controlled by the weaker [a] (010) slip system due to the relaxation of the Von Mises criterion. Alternatively, melt weakening may be caused by enhancement of grain boundary processes in porous melt-bearing olivine aggregates due to fast diffusion along melt-wetted grain boundaries, a decrease in load-bearing area causing a stress concentration at solid-solid grain contacts, or a shortening of the grain boundary diffusion distance (Hirth & Kohlstedt, 1995b; De Kloe, 2001). Melt weakening may therefore be a process leading to strain localisation in partially molten mantle rocks (Kelemen & Dick, 1995; see also chapter 2).

(IV) An important process potentially capable of inducing weakening in ductily deforming crystalline materials is a *deformation mechanism switch*, from dominant dislocation creep to grain-size sensitive (GSS) creep. GSS creep, which comprises a combination of diffusion creep and grain boundary sliding, is favoured at low deviatoric stresses in fine-grained rocks. Extrapolations of experimentally derived flow laws for olivine show that for given values of the flow stress, strain rates attained by GSS creep in fine-grained peridotites may be orders of magnitudes faster than dislocation creep or GSS creep in coarse-grained peridotites.

In summary, the processes discussed above may cause significant weakening in deforming peridotites. The most drastic weakening effect at sub-solidus conditions is produced by a change from dislocation to GSS creep, and most microstructural studies of natural peridotite mylonites indeed conclude that it is this process which leads to shear localisation (Boullier & Gueguen, 1975; Drury *et al.*, 1990; Vissers *et al.*, 1995; Jaroslow *et al.*, 1996; Jin *et al.*, 1998; Newman *et al.*, 1999; Furusho & Kanagawa, 1999). Questions remain, however, as to the processes that can cause the transition from dislocation to GSS creep in peridotites. Clearly, GSS creep is favoured at small grain sizes. Deformation under dislocation creep conditions leads to dynamic recrystallisation and it has been found in experiments that the recrystallised grain size is inversely proportional to the flow stress (Nicolas & Poirier, 1976; Twiss, 1977; Ross *et al.*, 1980; Drury *et al.*, 1985; Van der Wal *et al.*, 1993). It has been proposed that dynamic recrystallisation can lead to grain size reduction, which in turn promotes GSS creep (figure 5.1) leading to weakening and strain localisation (White, 1976; Twiss, 1977; White *et al.*, 1980; Rutter & Brodie, 1988; Karato & Wu, 1993; Jaroslow *et al.*, 1996). It has, however, often been questioned whether simple grain size reduction by dynamic recrystallisation can bring rocks into the GSS creep

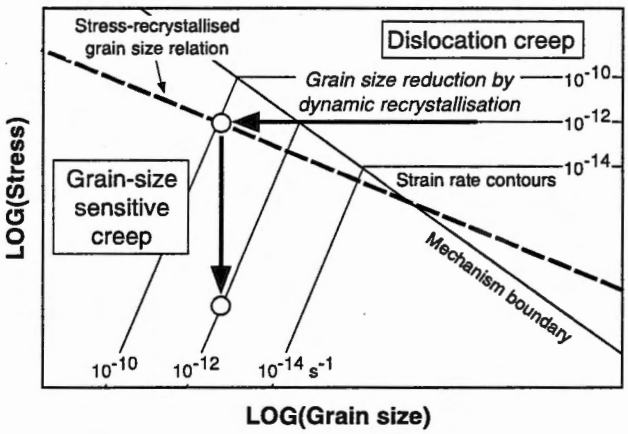

Figure 5.1: Schematic deformation mechanism map for olivine (based on figure 9 of Rutter & Brodie, 1988). Thick line is the mechanism boundary between the dislocation and grain-size sensitive (GSS) creep fields. Thick dashed line shows the empirical relation between the stress and the recrystallised grain size. Thick arrows show weakening effect of grain size reduction by dynamic recrystallisation: the weakening effect can be an increase of the strain rate at constant stress (horizontal arrow), a decrease of stress at constant strain rate (vertical arrow), or a combination of both. It is, however, questionable whether dynamic recrystallisation can bring a rock into the GSS creep field (see text for discussion).

field (*e.g.*, Etheridge & Wilkie, 1979; De Bresser *et al.*, 1998). It is often argued that once in the GSS field, dynamic recrystallisation of grains is strongly reduced or is arrested altogether and grain growth leading to reduction of the total grain boundary area is expected to be the dominant process controlling grain sizes within the GSS field. It has therefore been proposed that the grain size developed during recrystallisation reflects a dynamic balance between grain size reduction and grain growth (Derby & Ashby; 1987; De Bresser *et al.*, 1998) and will tend to organise itself in the boundary region between dislocation and GSS creep (De Bresser *et al.*, 1998). If this concept is correct, then simple dynamic recrystallisation cannot bring a rock into the GSS creep field, hence it cannot explain the weakening leading to strain localisation observed in nature. It is therefore important to investigate alternative mechanisms by which the grain size in a rock can be reduced. Detailed studies by Newman *et al.* (1999) and Furusho and Kanagawa (1999) have shown that the nucleation of new small grains by a metamorphic reaction in peridotites could account for extreme grain size reduction and formation of peridotite mylonites. In this chapter it is argued that melt-rock reaction can have a similar effect.

5.2. Results - The Othris mylonites and tectonites

5.2.1. *The Othris Ophiolite*

The Othris Peridotite Massif constitutes the mantle section of the dismembered Tethyan Othris Ophiolite. Through the work of Menzies and co-workers in the early 70's the Othris peridotites have played a prominent role in the development of the commonly accepted view that ultramafic rocks in ophiolite massifs are the residue of partial melting of more or less primary mantle material (Menzies, 1973; 1974; 1975; 1976a, b; Menzies & Allen, 1974; Menzies *et al.* 1977). Menzies (1973) argued that the plagioclase-lherzolites which occur in addition to the more common harzburgites in Othris represent such primary mantle material. In chapter 4 an alternative view is proposed, namely that the Othris plagioclase-peridotites represent previously depleted mantle rocks with a harzburgitic composition which were refertilised by an impregnating melt (see also Dijkstra *et al.*, 2001). It is argued that impregnation occurred in a near-transform fault environment at a slow-spreading, Atlantic-type ridge. Based on a study of mostly semi-brittle to brittle structures in the Othris massif, Rassios and Konstantopoulou (1993) have reached a similar conclusion regarding the ocean ridge environment.

5.2.2. *The peridotite mylonites*

Mapping of the Othris Peridotite Massif has revealed the presence of a km-wide, vertical to steeply east-dipping N-S striking peridotite mylonite zone exposed along the Onohonos River in the Katáchloron area (figure 5.2). The harzburgites in the Onohonos River mylonite zone exhibit a strong foliation and lineation caused by flattened and stretched pyroxenes and bands or augen-shaped domains of fine-grained material around pyroxenes. Lineations have subhorizontal to moderately steep south-plunging orientations. Mylonitic harzburgites are interleaved by metre to ten-metre scale dunite bands and lenses, which can enclose pyroxene-bearing enclaves. The dunites locally contain bands or clusters of black (chrome-rich) spinel. Within the mylonites thin, cm to dm wide dunite bands are often boudinaged or sometimes broken up into small, relatively angular fragments.

At several locations, the N-S striking mylonites are cross-cut by oblique mylonite to ultramylonite zones, which are generally a few cm wide but which are occasionally as wide as >50 m (figure 5.2). Note that in this study, the term ultramylonite is used for mylonites which have a vitreous appearance in the field due to a high proportion of very fine-grained material. These cross-cutting mylonites and ultramylonites are not restricted to the km-wide domain of the Onohonos River mylonite zone as they are occasionally found within the adjacent harzburgite and plagioclase-peridotite domains. They are generally steeply NE-dipping, striking NW-SE; some are subvertical striking NE-SW. Trails of small spinel grains define shallowly to steeply south-plunging lineations. A reverse, sinistral plus E-up sense of movement could consistently be established from the progressive rotation of older foliations into the thin NW-SE striking mylonite to ultramylonite zones.

A large fault-bound block of plagioclase-bearing mylonites is found on the southern slope of Mt. Katáchloron (figure 5.2). At this location, N-S striking mylonites are cross-cut by numerous 330° striking thinner mylonites to ultramylonites whilst some narrow 040° striking mylonites occur as well. Plagioclase is also present in adjacent tectonites and its crystallisation from an impregnating melt pre-dates the formation of the mylonites (chapter 4)

5.2.3. *The peridotites of the (western) footwall block*

The peridotites occurring west of the Onohonos River mylonite zone (further referred to as the footwall block) are coarse-grained harzburgite tectonites. The coarse-grained appearance is mainly caused by the presence of numerous large orthopyroxene porphyroclasts which are typically 5-15 mm in diameter. The orthopyroxene clasts do generally not produce a strong foliation or lineation. Occasionally flattened and elongated spinel defines a foliation and lineation. More commonly, a well-defined compositional layering defined by variations in the modal orthopyroxene content is observed. At locations where both a foliation and lineation can be discerned, the layering and the foliation are subparallel, striking N-S to NE-SW with a steep down-dip lineation.

Large, ten to hundred metre scale dunite bodies occur within the tectonites of the footwall block. They generally strike NE-SW and cross-cut the harzburgitic tectonite fabric. These dunites consist almost entirely of serpentinised olivine; so little olivine remains in the dunites as a result of serpentinisation, that the original microstructure remains unclear. Occasional spinel forms cm-scale clusters, sometimes with a core of strongly altered orthopyroxene.

The transition from the coarse tectonites to the mylonites is well-defined. One coarse tectonite-mylonite transition exposed in the banks of the Onohonos River has been mapped in detail (figure 5.2). In the transition zone, numerous relatively thin mylonite zones cross-cut the coarse tectonite

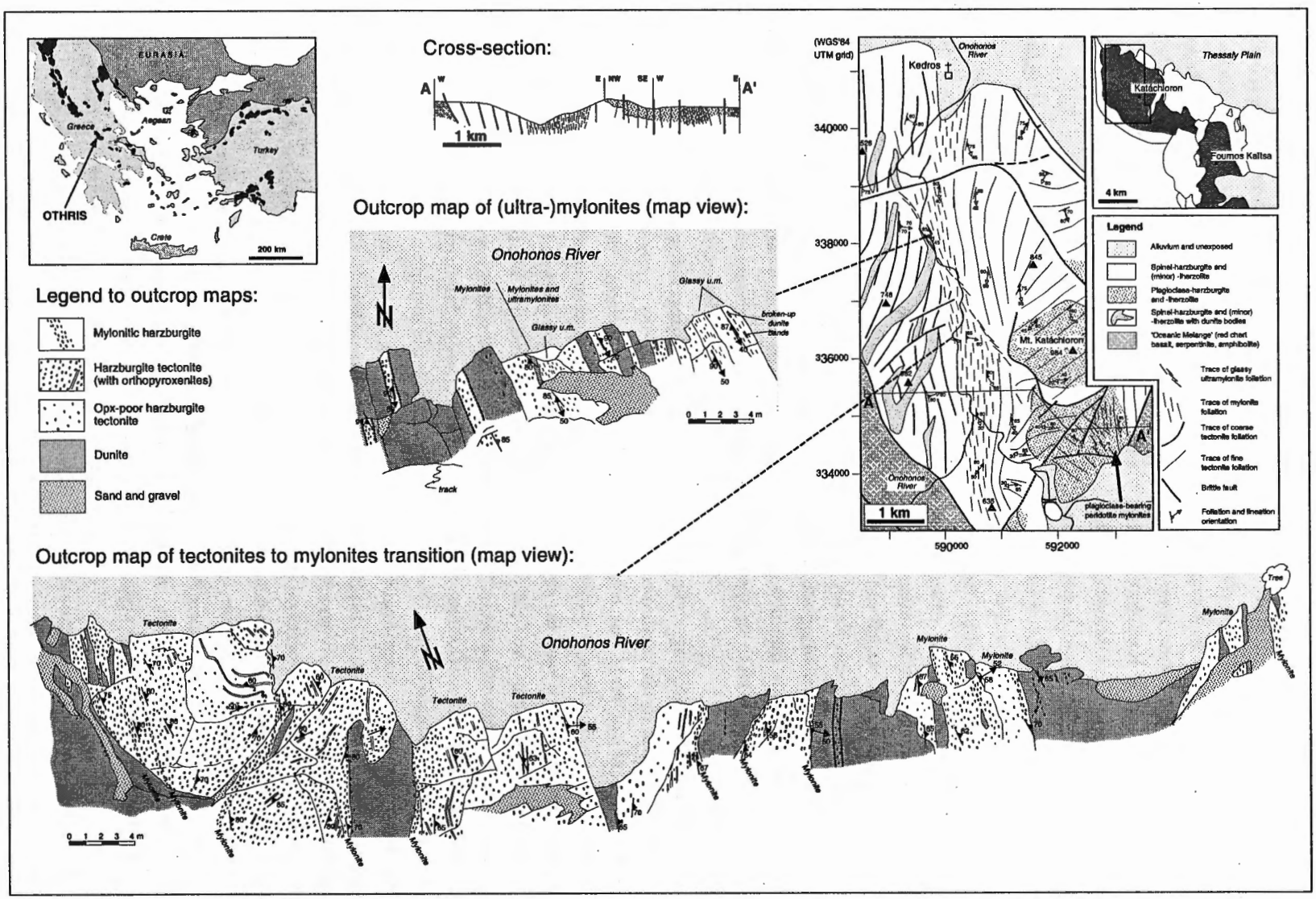

Figure 5.2: Geological maps, cross-sections, and outcrop maps showing location of Othris peridotite massif in Greece (inset at upper left), structure of the Katáchloron area with location of cross-section A-A' (inset at upper right); section across the Onohonos mylonites zone (middle top). Also shown are two detailed outcrop maps showing the transition of coarse-grained tectonites to mylonites (lower part of page) and a band of vitreous ultramylonites within the mylonite zone (middle).

foliation. They are mostly found at the margins of large dunites. In these mylonite zones the orthopyroxene crystals are elongate and their size is reduced as compared to the orthopyroxenes in the tectonite protolith. Towards the east, the mylonitic zones become wider until no more coarse tectonites are found. The width of the dunite bodies within the mylonites is strongly reduced to several tens of metres or even to a few centimetres.

5.2.4. The peridotites of the (eastern) hanging wall block

The peridotites east of the Onohonos River mylonite zone, referred to here as the hanging wall block, are predominantly fine-grained harzburgite tectonites with few, small dunites. Orthopyroxene crystals are mostly small, less than 6 mm in diameter, and they are surrounded by light-coloured rims of fine-grained polyphase material described below, which have a tendency to weather out. The fine-grained tectonites are moderately well foliated; typically, however, they are quite strongly lineated. Lineations and foliations are defined by flattened and stretched orthopyroxene, olivine, spinel, and fine-grained polyphase rims around orthopyroxene porphyroclasts. Locally, the fine-grained tectonites contain ‚orthopyroxene-, spinel-, and olivine-rich layers. This compositional layering is generally parallel to the tectonite foliation, whilst at few locations isoclinally folded layers were found with axial planes parallel to the foliation. Moreover, some strongly boudinaged websterite bands occur. At two locations, small 10-50 cm size, irregular dunites have been found which cross-cut the tectonite foliation and compositional layering. The harzburgite tectonites adjacent to the Onohonos River mylonite zone are structurally continuous with plagioclase-harzburgites and –lherzolites which occur on the top and the southern and northeastern slopes of Mt. Katáchloron. From the foliation pattern it is evident that the deformation in the fine-grained harzburgite tectonites flanking the mylonite zone overprints the deformation in the plagioclase-peridotites towards the east, since NE-SW to E-W striking foliations in the plagioclase-peridotites bend into the N-S striking foliations of the harzburgite tectonites directly adjacent to the mylonite zone.

In contrast to the relatively sharp transition from the footwall coarse tectonites to the mylonites, the transition from hanging wall fine-grained tectonites to mylonites is gradual. Close to the main mylonite shear zone, orthopyroxene crystals and the fine-grained rims around orthopyroxene in particular are increasingly stretched and flattened, and they eventually coalesce and form continuous fine-grained bands within the mylonite zone.

5.3. Microstructures and lattice fabrics

5.3.1. Microstructures in mylonites and ultramylonites

All microstructural observations presented below have been made on thin sections prepared parallel to the lineation and perpendicular to the foliation as determined in outcrop.

Typical peridotite mylonites consist of polyphase bands of fine-grained olivine, orthopyroxene, and minor clinopyroxene and spinel. Within the fine-grained bands porphyroclasts of orthopyroxene and clinopyroxene occur. The fine-grained polyphase bands enclose markedly coarser bands and lenses consisting almost entirely of olivine (figure 5.3a). The mylonites and ultramylonites cross-cutting the main mylonite zone have broadly similar microstructures, but with higher proportions of fine-grained polyphase material. Some ultramylonites display a fluidal texture (figure 5.3b). In general it was found that peridotites described as mylonites in the field were characterised

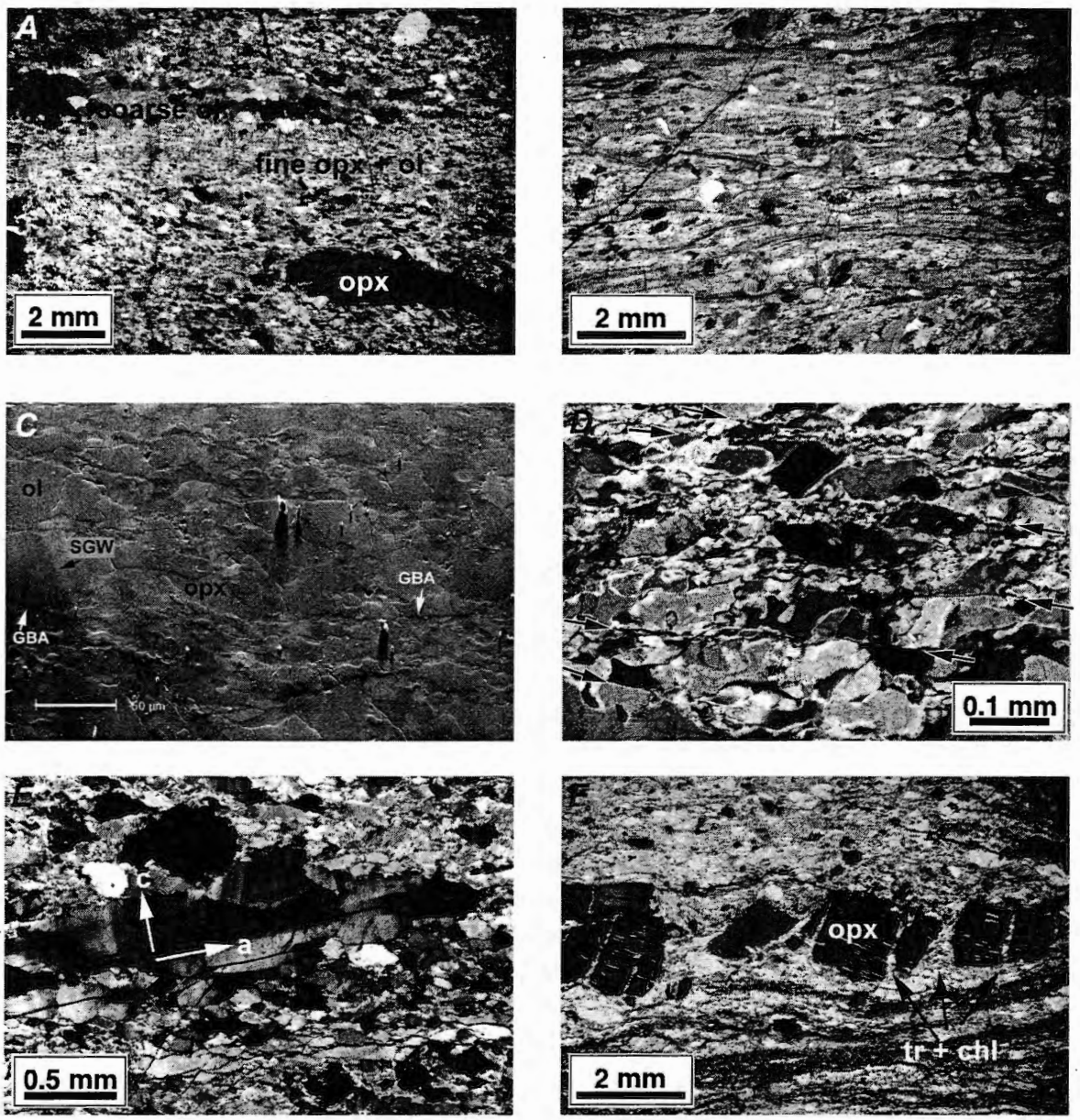

Figure 5.3: Micrographs of mylonitic microstructures. A) photomicrograph in cross-polarised light (XPL) of typical mylonite, showing fine-grained bands made up of a mixture of olivine and orthopyroxene, and lenses of relatively coarse-grained olivine. Note strongly stretched orthopyroxene porphyroclast in lower right corner; B) Photomicrograph (XPL) of very fine-grained, fluidal ultramylonite containing porphyroclasts of olivine, orthopyroxene, and spinel; C) Forescatter SEM image of ultramylonite. Olivine grains have positive relief, orthopyroxene grains show negative relief. Variations in crystallographic orientation cause contrast variations within and among grains (see for instance the subgrain wall (SGW) in relatively large olivine grain in middle left). Note distinct grain boundary alignment (GBA) – interpreted as a sliding surface - between relatively coarse and fine bands in lower half of image; D) Photomicrograph (XPL) of grain boundary alignments (indicated by black arrows) in a fine-grained olivine-orthopyroxene band in a mylonite; E) Ribbon olivine porphyroclast in relatively coarse-grained olivine lens in a mylonite (XPL). The crystal contains two sets of subgrain boundaries, one parallel to (100) and one parallel to (001). Olivine [a]- and [c]-axes indicated by white arrows; F) Broken-up orthopyroxene porphyroclast in ultramylonite (XPL), with fibrous tremolite and chlorite grown in spaces between the orthopyroxene fragments.

Table 5.1
a) Grain sizes of coarse- and fine-grained domains in Othris mylonites

	Geometric mean linear intercept		Corrected for sectioning (*1.2)
	LOG (D(μm)) ±1σ	D(μm)	D' (μm)
Coarse-grained olivine lenses	2.134 ± 0.133[1]	121	145
Fine-grained polyphase bands	1.020 ± 0.186[2]	10.5	12.6

[1]Determined from light microscopy photographs
[2]Determined from SEM orientation contrast images

b) Olivine flow laws used to construct deformation mechanism maps in figure 5.14

	A ($s^{-1}MPa^{-n}m^{p}$)	$Q^{\#}$ (J/mol)	n	m	p	Reference
Dry dislocation creep [c]-slip	$2.88 \cdot 10^{4}$	$5.35 \cdot 10^{5}$	3.6	0	0	Chopra & Patterson (1984); Drury & FitzGerald (1998)
Dry dislocation creep [a]-slip	2.48	$3.85 \cdot 10^{5}$	3.5	≥0	0.33	Drury & Fitz Gerald (1998) and references therein
Dry GSS creep	$2.46 \cdot 10^{-10}$	$3.47 \cdot 10^{5}$	1.0	3	0.15	Hirth & Kohlstedt (1995a)

Strain rate is calculated as $d\varepsilon/dt(s^{-1})=A \cdot (fO_2/fO_2^{ref})^{p} \cdot \sigma^{n} \cdot d(m)^{m} \cdot \exp[-Q^{\#}/RT(K)]$; fO_2 is the relevant oxygen fugacity (FMQ-1 in this study), whereas fO_2^{ref} is the oxygen fugacity of the buffer used during the deformation experiment (Fe-FeO buffer for dislocation creep experiments, and Ni-NiO for GSS creep experiment). In figure 5.14c&d, olivine [a]-slip is assumed to take over from [c]-slip if GSS creep contributes more than 10% to the total deformation rate (corresponding to a relaxed Von Mises criterion), leading to a 'composite creep' regime ([a]-slip + GSS creep) in which the strain rate is grain size dependent (*i.e.*, m≥0 for [a]-slip). See also Drury & Fitz Gerald (1998).

by high (>50%) volume fractions of (very) fine-grained matrix material, such that the use of the term mylonite here is in accordance with the definition of Sibson (1977, see also Vissers *et al.*, 1997). Peridotites described as ultramylonites in the field only occasionally had >90% (very) fine-grained matrix, and, following the classification of Sibson (1977), these should generally be referred to as mylonites as well.

The olivine crystals in the fine-grained polyphase bands have grain sizes which range from a few microns to approximately 50 μm. The grains are generally slightly elongate (aspect ratios < 3) parallel to the mylonite foliation. A mean linear intercept grain size of 11 μm (table 5.1a) was determined from scanning electron microscope (SEM) images. SEM images (*e.g.*, figure 5.3c) of a mechanically and chemically polished mylonite specimen tilted by 70° were obtained using a backscatter detector in a forescatter position; individual grains can be recognised by their orientation contrast in such images (Prior *et al.*, 1996; Fliervoet *et al.*, 1999). It is difficult, however, to distinguish subgrains from grains by this technique since the orientation contrast between two areas in the image is not a measure of the angular difference in lattice orientation. The determined linear intercept grain size of 11 μm may therefore be an underestimation of the actual grain size. Olivine and pyroxene grains can be distinguished by their relief as a result of the polishing technique: olivine crystals show a positive relief whereas pyroxenes show negative relief.

It was found that the fine-grained bands contain numerous grain boundary alignments parallel or at a small angle (<30°) to the mylonite foliation . These grain boundary alignments can be seen by light microscopy (figure 5.3d) as well as by SEM (figure 5.3c). They often separate bands of different grain sizes, and can be traced over distances of about a millimetre at most before they die out within domains of fine-grained matrix material.

The coarse olivine bands have a porphyroclastic microstructure with relatively few olivine porphyroclasts. The mean linear intercept grain size of the coarse bands is 121 μm (table 5.1a), determined from polarised light microscope photo-mosaics. Olivine porphyroclasts can be a few mm's in size; they often have a substructure of subgrain walls oriented at a high angle to the mylonite foliation. Crystal orientation measurements using a universal stage show that these subgrain walls are mostly parallel to the (100) plane. Some porphyroclasts contain a mesh consisting of two sets of closely spaced irregular subgrain walls or deformation bands (figure 5.3e), one subparallel to the foliation (parallel to (001)) and one at high angles to the foliation (parallel to (100)). The smaller grains usually show little or no substructure. They are often elongate and oblique to the mylonite foliation, thus defining a typical oblique fabric (Van der Wal *et al.*, 1992).

The mylonites contain orthopyroxene porphyroclasts, mainly within fine-grained bands. Some of the porphyroclasts are strongly stretched. In one ultramylonitic sample, stretched orthopyroxene porphyroclasts are broken up into smaller fragments, and an assemblage of fibrous tremolite and chlorite occurs in the spaces between the fragments (figure 5.3f).

Although the coarse bands are mainly mono-mineralic, they do contain small grains of orthopyroxene. Such grains were observed to occur in interstices or as narrow tapering crystals along olivine grain boundaries. Similar crystals also occur frequently in the tectonites adjacent to the mylonites, in particular in the fine-grained tectonites. These microstructures are further discussed below.

5.3.2. Microstructures of the coarse tectonites from the footwall block

The microstructures of the coarse tectonites are characterised by coarse, 1-3 mm olivine porphyroclasts surrounded by smaller (0.1-0.7 mm) olivine grains (figure 5.4a). The olivine porphyroclasts have highly irregular grain outlines, in contrast to the smaller grains which have more regular to polygonal, equant shapes (figure 5.4b). The olivine porphyroclasts can be elongate (aspect ratios generally less than 2), but the elongation direction is variable and can be at a high angle to the tectonite foliation. The foliation is defined by stretched spinel grains, by trails of spinel grains, and by bands of olivine neoblasts. The olivine porphyroclasts have a substructure of (100) subgrain walls at a high angle to the foliation, whereas the smaller grains do not seem to have a well-developed substructure.

Finally, the coarse tectonites contain syn-kinematic pargasitic hornblende which is stable with respect to orthopyroxene and clinopyroxene, and post-kinematic tremolitic amphibole which overgrows the tectonite foliation and partially replaces large orthopyroxene crystals.

5.3.3. Microstructures of the fine tectonites from the hanging wall block

The tectonites of the hanging wall block contain two types of domains, *i.e.*, relatively coarse-grained domains of predominantly olivine and trace amounts of orthopyroxene and spinel, and much finer-grained domains consisting of a mixture of roughly equal modal proportions of olivine and orthopyroxene with minor clinopyroxene and spinel.

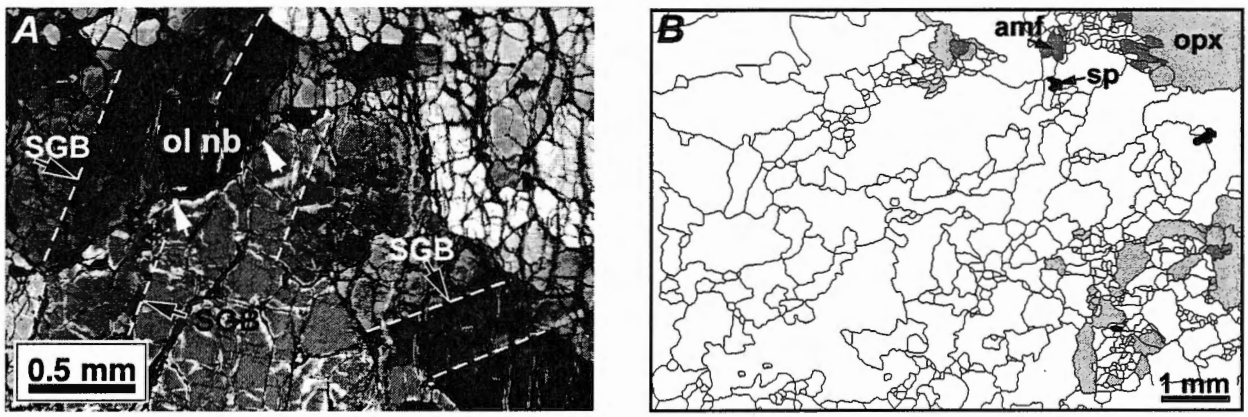

Figure 5.4: Micrographs of coarse tectonites from the footwall block. A) Close-up of coarse tectonite microstructure (XPL), showing polygonal olivine neoblast ('ol nb') surrounded by olivine porphyroclasts. White arrows indicate ~120° triple grain junctions. Black arrows indicate subgrain boundaries (SGB) in olivine porphyroclasts; B) Tracing of photomosaic showing coarse tectonite microstructure.

The coarse-grained, olivine-rich domains have porphyroclastic microstructures, with fewer and smaller olivine porphyroclasts as compared to the coarse porphyroclastic tectonites in the footwall (figure 5.5a). Neoblasts have similar to slightly smaller sizes than the neoblasts in the footwall coarse tectonites, *i.e.*, 0.1–0.5 mm. A striking aspect of the microstructures of the fine tectonites of the hanging wall block is the strong elongation of the olivine porphyroclasts (*e.g.*, figure 5.5a); aspect ratios are generally larger than 2, and some ribbon olivines occur with aspect ratios as high as 15. Olivine porphyroclasts often have a well-developed substructure consisting of (100) subgrain walls generally at a high angle to the foliation. Like in the mylonites, many of the olivine porphyroclasts with [c]-axes approximately in the plane of section show a second set of (001) subgrain walls sub-parallel to the foliation (figure 5.5b). The (001) subgrain walls may actually be quite common, but since the (001) planes are often oriented approximately parallel to the plane of section (see discussion of lattice preferred orientations or LPO's below), such subgrain walls are generally invisible. No strong substructure in the newly recrystallised grains has been observed in the light microscope.

The fine-grained domains occur as rounded or augen-shaped rims around orthopyroxene porphyroclasts (figure 5.5c). The fine-grained domains consist mainly of intimately intermixed olivine and orthopyroxene with minor amounts of clinopyroxene and spinel (figure 5.5d), with grain sizes of 0.2 mm to ~5 μm. Within the fine-grained domains, orthopyroxenes typically exhibit interstitial textures described below. Olivine grains in the fine-grained domains do not show a well-developed substructure but it is noted that, due to the small grain sizes, the internal structure of most of the grains could not be resolved optically.

5.3.4. Olivine lattice preferred orientations

Olivine lattice preferred orientations (LPO) in several mylonites and tectonites were determined using a universal stage (U-stage) mounted on a polarising light microscope. These were supplemented by LPO measurements of fine-grained olivine in two samples using the SEM electron backscatter diffraction (EBSD) technique (Randle, 1992; Fliervoet *et al.*, 1999).

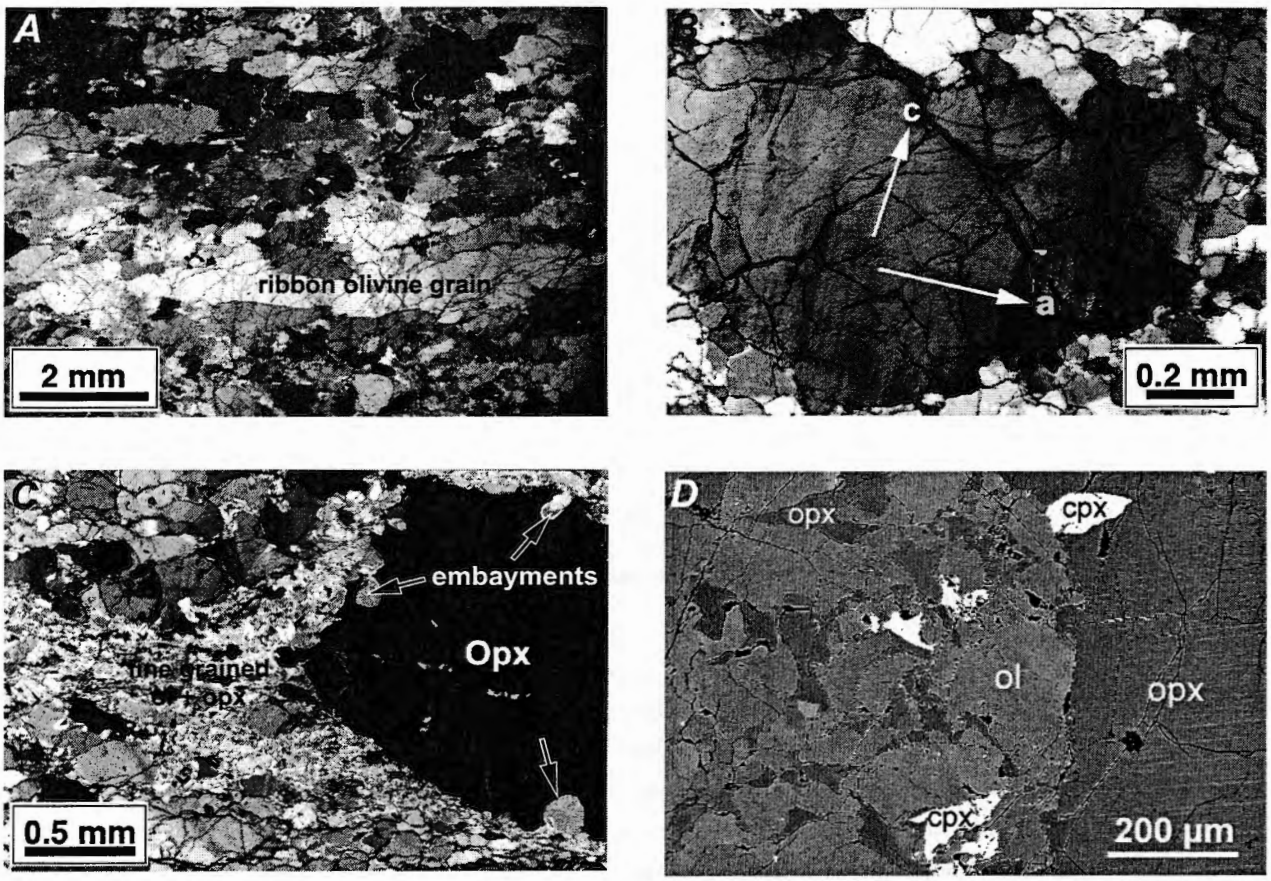

Figure 5.5: Micrographs of fine tectonite microstructures from the hanging wall block. A) Photomicrograph (XPL) of a typical microstructure containing elongate, ribbon-like olivine grains. Lower part of micrograph contains part of relatively fine-grained olivine-orthopyroxene domain; B) Olivine porphyroclasts containing mesh of (100) and (001) subgrain boundaries (XPL); C) Photomicrograph (XPL) showing fine-grained olivine-orthopyroxene in an augen-shaped domain around orthopyroxene porphyroclast (at extinction), interpreted as product of melt-present breakdown reaction of orthopyroxene; D) Backscatter SEM image showing mineralogy and texture of a fine-grained domain adjacent to an orthopyroxene porphyroclast.

Olivine crystals in two coarse tectonites of the footwall block have asymmetric LPO's (figure 5.6a). Olivine [a]-axes cluster at a small angle to the foliation, [b]-axes form a girdle at a high angle to the foliation, and [c]-axes lie within the foliation plane at a high angle to the lineation. These patterns suggest again that the dominant slip system in olivine was [a] (010), with minor slip on the [a] (001) system. The LPO asymmetries of both samples indicate an east-up sense of shear.

Olivine crystal orientations in coarse olivine-rich domains in two mylonites were measured with the U-stage; three to four individual coarse bands were measured in each sample. The crystals in the coarse bands exhibit an LPO (figure 5.6b) with [a]-axes clustering around the lineation orientation and with [b]-axes at a high angle to the mylonite foliation, in accordance with slip on the [a] (010) slip system. Some [c]-axes are oriented at a high angle to the foliation as well, indicating a contribution from the [a] (001) slip system to the deformation. The LPO's of the two investigated samples are both asymmetric, suggesting dominant non-coaxial deformation. The asymmetry of the [b]-maximum with respect to the foliation in one

of the mylonitic samples shown (97GOKAT57) suggests a dextral sense of shear, whereas that of the other mylonitic sample (96KAT42) points to an oblique sinistral plus east-up sense of shear. Note that the [a]-axes show double maxima on either side of the lineation orientation. It was found that the LPO asymmetries of individual bands within samples varies, and that some bands yield opposite senses of shear.

The orientations of the olivine crystals in several fine-grained bands in one mylonite sample were determined using the EBSD technique. The investigated grains exhibit a weak LPO only (Figure 5.6b). Moreover, the weak LPO maxima found do not seem to relate to any clearly defined slip-system in

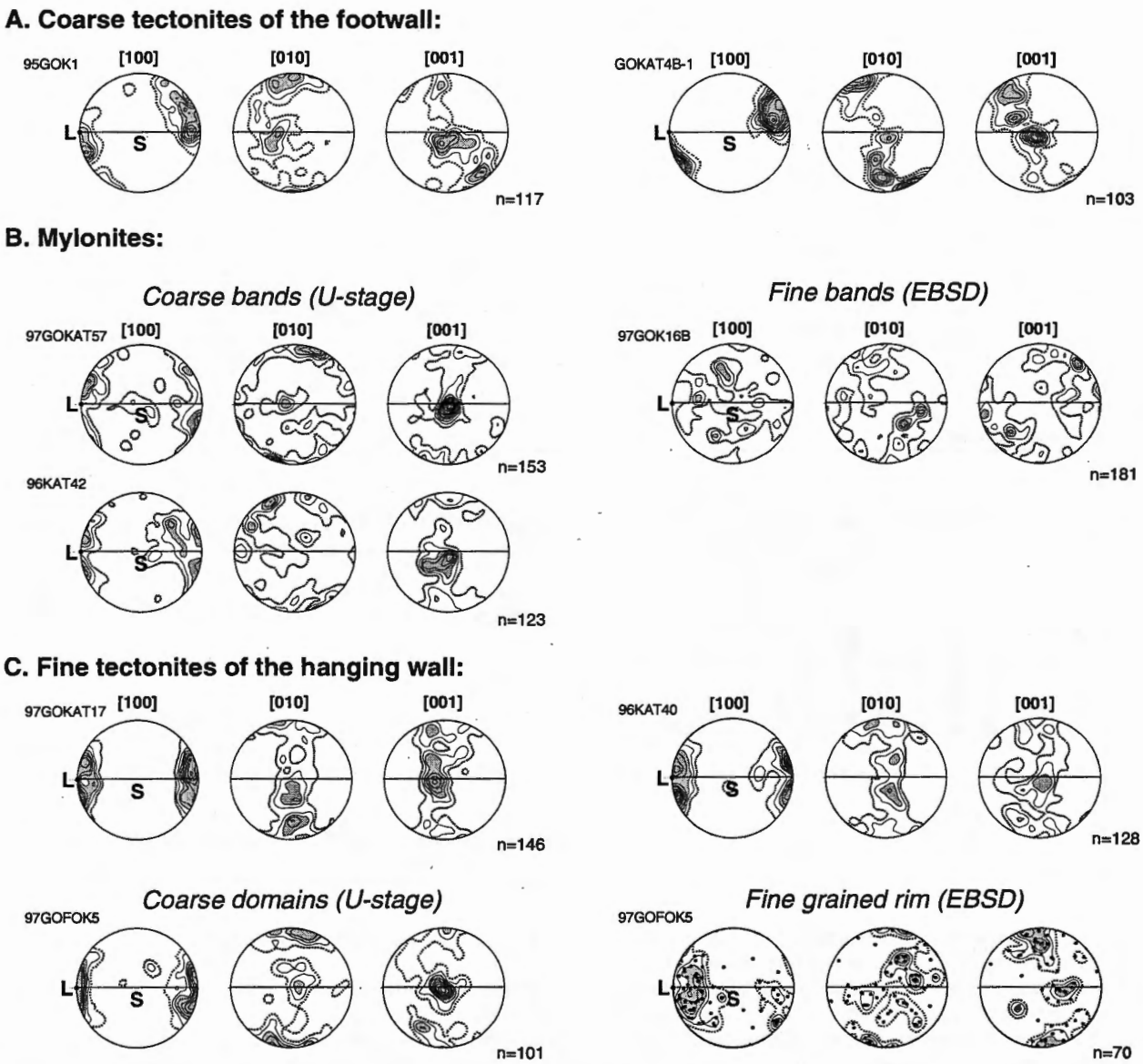

Figure 5.6: Lattice preferred orientation (LPO) patterns of olivine from Othris tectonites and mylonites determined by U-stage and SEM-EBSD; lower hemisphere, equal area projections. Horizontal lines in stereoplots denote orientations of tectonite or mylonite foliation (S) in each sample; lineation (L) oriented on the perimeter of each plot. Data contoured at 1,2,3,... times uniform. See text for discussion.

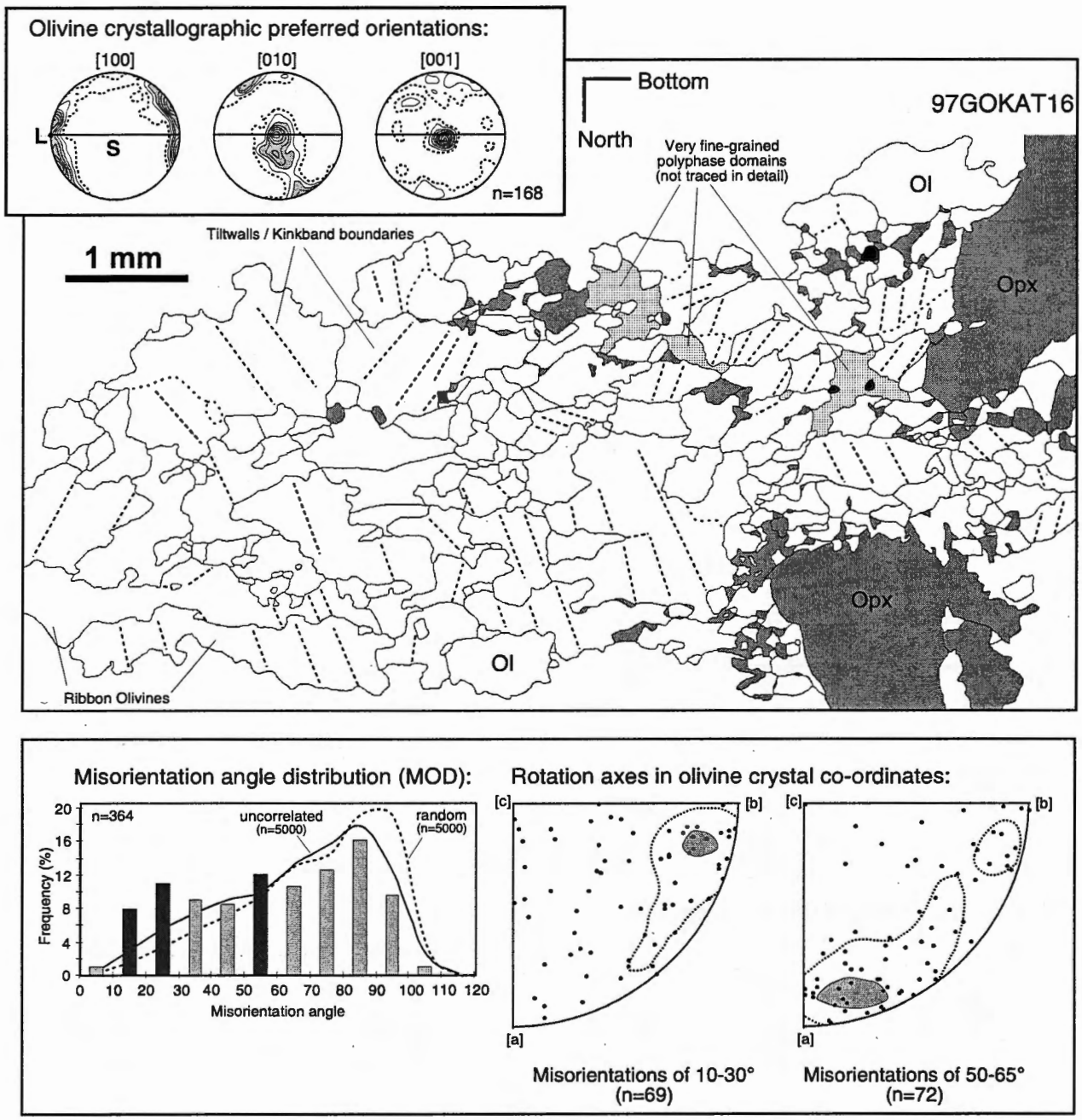

Figure 5.7: Detailed microstructural analysis of selected domain of a fine-grained tectonite from the hanging wall block (sample 97GOKAT16). Inset at top left shows lattice preferred orientation of olivine grains in the domain, determined by U-stage. Main panel shows tracing of a photomosaic of the domain, with orientations of visible subgrain walls in olivine grains indicated by dashed lines. Lower panel shows results of a misorientation analysis (see Randle, 1992 and Fliervoet *et al.*, 1999 for methodology). The distribution of misorientation angles between neighbouring grains is compared with the distribution of misorientation angles between non-neighbouring grains from the sample ('uncorrelated'), and with the distribution of misorientation angles between grains from a hypothetical sample with a random fabric ('random'). Significantly more misorientations between 10 and 30° and between 50 and 60° occur than expected from the fabric alone. Olivine inverse pole figures in right hand side of lower panel show orientations of rotation axes of grain-pairs with 10-30° and 50-65° misorientations, contoured at 1 and 2 times uniform distribution.

olivine. It is therefore inferred that dislocation creep did not play a prominent role in the deformation of the fine-grained bands in the mylonites.

In figure 5.6c, the LPO's are shown of three fine-grained tectonites from the hanging wall block, whilst one more LPO pattern of a fine tectonite is shown in figure 5.7. In general, [a]-axes have a preferred orientation near the lineation. Olivine [b]- and [c]-axes form girdles at a high angle to the lineation. These LPO patterns indicate that slip occurred on the [a] {okl} slip system. In most samples, the LPO's are symmetric or only slightly asymmetric, indicating either dominantly co-axial, or a large non-coaxial deformation. The few asymmetric fabrics suggest a sinistral plus (south)east-up sense of shear.

Orientations of some olivine crystals in a fine-grained domain next to an orthopyroxene porphyroclast were measured by EBSD (figure 5.6c). Despite the relatively small number of grains analysed it is clear that there is an LPO which is roughly similar to the bulk LPO of olivines from coarse bands in the same sample indicating [a] {okl} slip.

In order to study the olivine microstructure of the fine-grained tectonites, in particular the role of recrystallisation in the development of the microstructure, a detailed misorientation analysis was carried out on a coarse olivine domain from a fine tectonite (figure 5.7). Angles between the crystal lattices of adjacent grains ('misorientations') as well as rotation axes were calculated from the measured crystal orientations (according to the method outlined in Randle, 1992). If neighbouring grains are derived from a larger olivine crystal by subgrain rotation recrystallisation, relatively small misorientations are expected. If this is the case then the orientations of the rotation axes give additional information about the types of dislocations involved in the recrystallisation process. The misorientation angle distribution in figure 5.7 shows that in the studied domain grain boundaries with small misorientations are found significantly more frequently then expected from the LPO alone (see figure caption for details), indicating that subgrain rotation recrystallisation has been an important process in the development of the microstructure. Rotation angles of low angle boundaries have a preferred orientation close to the olivine [b]-axes. In addition, slightly more boundaries with misorientations between 50-60° are found then expected from the LPO alone. The rotation axes of such boundaries have a small preference for orientations near the [a]-axis. Rotations of ~60° around the olivine [a]-axis are in accordance with a twinning system in olivine ('t Hart, 1978a).

5.3.5. *Paleopiezometry*

The olivine lattice preferred orientations, the substructures of olivine porphyroclasts, and the evidence for dynamic recrystallisation involving subgrain rotation in the tectonites on either side of the Onohonos mylonite zone all suggest that dislocation creep has been the main mechanism in the tectonites controlling deformation and microstructure development. This allows the use of empirically derived stress-grain size relations for olivine to estimate the differential stress during deformation (Nicolas & Poirier, 1976; Twiss, 1977; Ross *et al.*, 1980). One of most widely used calibrated stress-grain size relationships for olivine is that of Van der Wal *et al.* (1993) based on a data set comprising both the experimental data of Karato *et al.* (1980) and the data of Van der Wal *et al.* (1993). Recently, simple shear deformation experiments on olivine by Zhang and co-workers (2000) have produced markedly smaller grain sizes than those predicted by the Van der Wal *et al.* (1993) paleopiezometer (figure 5.8). The reported recrystallised grain sizes in an experiment by Hirth and Kohlstedt (1995b) also deviates from the Van der Wal *et al.* (1993) relationship and is in agreement with the limited data set of Zhang *et al.* (2000). A regression through the data of Zhang *et al.* (2000) was

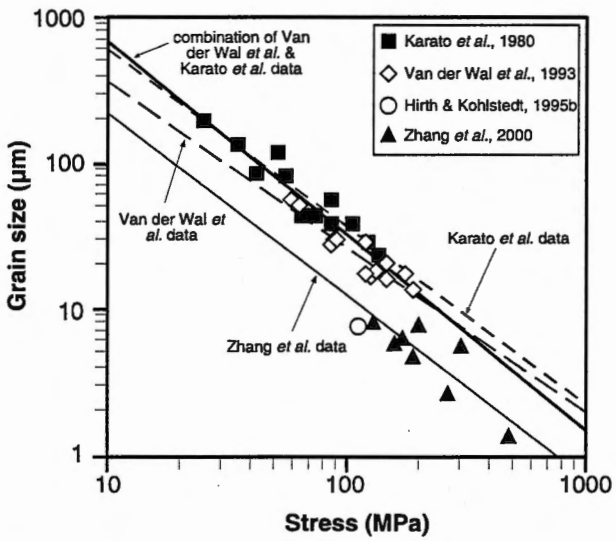

Figure 5.8: Summary of available stress-recrystallised grain size data for olivine. Note that data of Zhang *et al.* (2000) and of Hirth and Kohlstedt (1995b) are at variance with the data from Karato *et al.* (1980) and Van der Wal *et al.* (1993). Upper and lower stress estimates derived from the recrystallised grain sizes in Othris tectonites are based on the regressions through the data-sets shown in this diagram.

therefore used to obtain a minimum stress estimate, and the Van der Wal *et al.* (1993) paleopiezometer was applied to obtain a maximum stress estimate from recrystallised grain sizes in the Othris peridotites (figure 5.8). As the data set on which the Van der Wal *et al.* (1993) relationship is based extends to the relatively low stresses relevant for the Othris peridotites (see below), the Van der Wal *et al.* (1993) paleopiezometer is considered most appropriate. A correction factor of 1.2 was used to convert the mean linear intercept recrystallised grain size in thin section to a three-dimensional grain diameter. The recrystallised grain sizes of 0.1-0.7 mm in the coarse tectonites correspond to stresses of the order of 3-38 MPa. Similarly, the recrystallised grain sizes of 0.1-0.5 mm in the olivine bands in the fine tectonites yield stresses of 5-38 MPa.

5.3.6. Orthopyroxene textures and microstructures

In the peridotites studied from the Othris massif, four morphologically different types of orthopyroxene crystals have been recognised (figure 5.9, see also figure 5.13).

(I) Large (>0.5 mm) porphyroclasts, generally with exsolution lamellae of clinopyroxene along the cleavage, and sometimes with spinel exsolutions, are found in all tectonites and mylonites. In the tectonites, orthopyroxene porphyroclasts tend to be equidimensional or slightly elongate at a high angle to the foliation, whereas in the mylonites orthopyroxene porphyroclasts are rounded or elongate parallel to the foliation, incidentally developing aspect ratios as high as 20. In the mylonites, and in the tectonites directly adjacent to the mylonites, orthopyroxene porphyroclasts are occasionally bent or kinked. Orthopyroxene porphyroclasts in the coarse tectonites of the footwall block are often recrystallised to clusters of equant crystals. Most strikingly, orthopyroxene porphyroclasts often have irregular grain outlines (figure 5.9a), in particular in the coarse tectonites of the footwall block, but also in domains of coarse plagioclase-bearing tectonites of the hanging wall block (described in chapter 4). The irregular grain shape is caused by numerous embayments consisting of olivine and sometimes spinel crystals bulging into orthopyroxene porphyroclasts, which in cases leads to orthopyroxenes with skeletal shapes. Orthopyroxene clasts of this type are referred to as type-I clasts below.

(II) Patches of intermixed olivine and orthopyroxene are found in which the orthopyroxene grains have an interstitial texture. In many cases the orthopyroxene grains seem not to be connected in thin section, yet the individual grains shown simultaneous extinction (figure 5.9b). Such clusters of crystals sharing a common orientation ('orientation family' clusters, referred to as type-II orthopyroxene below) are predominantly found in the coarse-grained tectonites of the footwall block.

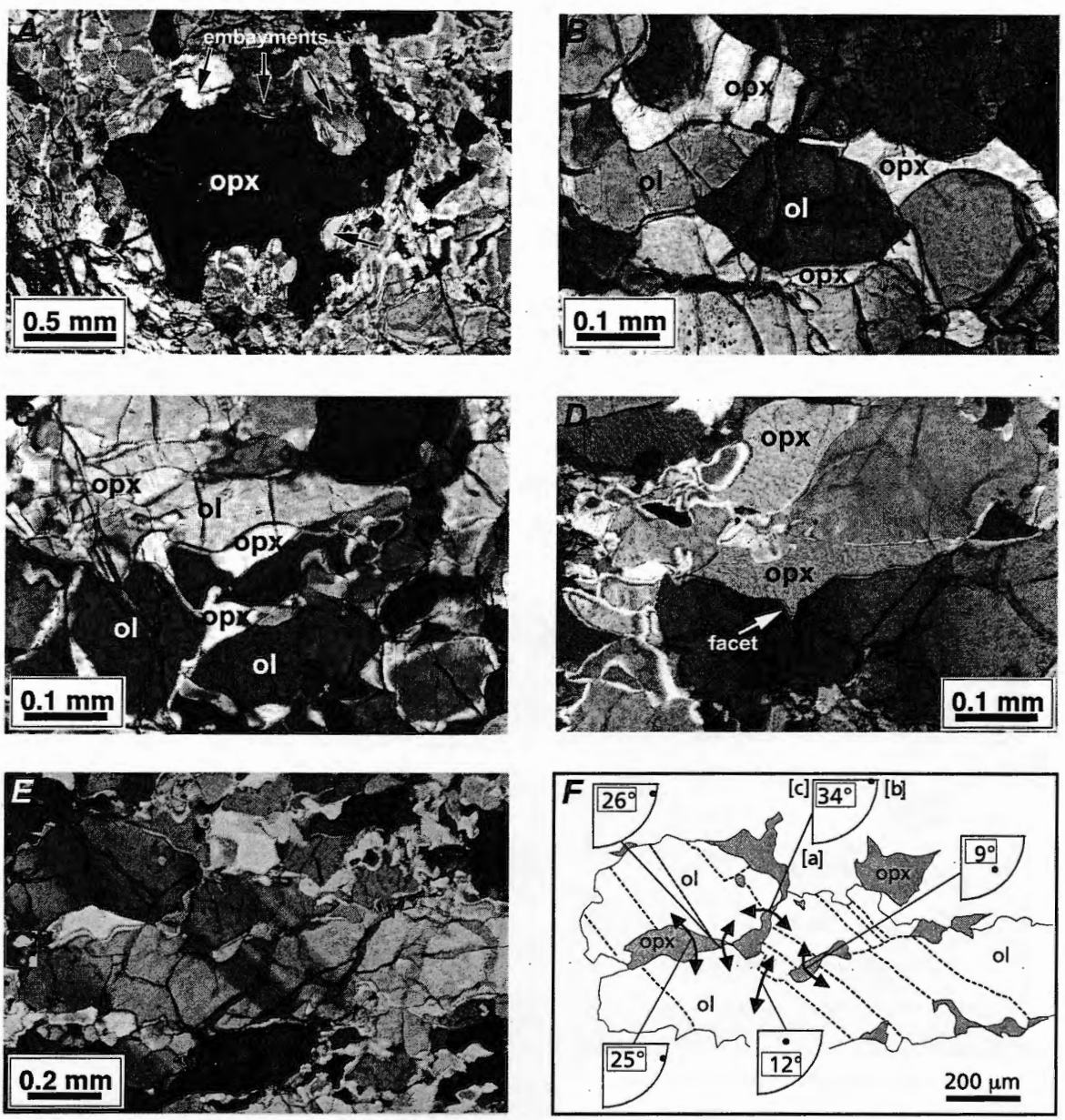

Figure 5.9: Micrographs of typical orthopyroxene morphologies. A) Orthopyroxene porphyroclasts with irregular outline caused by olivine embayments (XPL); B) Cluster of interstitial orthopyroxene grains, all with the same crystallographic orientations, interpreted as relics of one single orthopyroxene porphyroclast (XPL); C) Close-up of fine-grained olivine-orthopyroxene domain in fine-grained tectonite (XPL); D) Typical interstitial orthopyroxene grain in a relatively coarse, olivine-rich domain of a fine-grained tectonite (XPL). Note that lower olivine grain has developed a straight crystal face at the interphase boundary with the interstitial orthopyroxene grain. Note also sharp, wedge-shaped protrusion of the orthopyroxene grain following orientation of a prominent set of subgrain walls in lower olivine grain; E) Photomicrograph (XPL) showing several orthopyroxene grains distributed along low-angle grain and subgrain boundaries in olivine cluster within a relatively coarse olivine-rich domain of a fine-grained tectonite. See adjacent sketch on right for details; F) sketch of photomicrograph on left, showing the misorientation angles between neighbouring olivine (sub)grains separated by interstitial orthopyroxene grains. Inserted inverse pole figures show rotation angles between adjacent (sub)grain pairs. Orthopyroxene is interpreted to be derived by local precipitation from a melt or by replacement of olivine (see text).

(III) In the fine-grained tectonites of the hanging wall block, orthopyroxene occurs together with olivine in the fine-grained domains surrounding orthopyroxene porphyroclasts as well as in the fine-grained bands in the mylonites (figure 5.9c – see also figure 5.5d). In these cases orthopyroxene often shows an interstitial or flaser-like shape (type-III orthopyroxene). One fine-grained domain was studied in detail using SEM, and the orientations of small individual olivine and orthopyroxene crystals were determined by EBSD. In the image shown in figure 5.10 the olivine and orthopyroxene lattice orientations are indicated by short lines. As noted above, olivine crystals have orientations which are in agreement with the bulk fabric of the sample, suggesting the activity of the [a]{okl} slip system. The small orthopyroxene crystals also have a lattice preferred orientation, but this preferred orientation bears no relationship with the known [c](100) or [c](010) slip systems in orthopyroxene. The crystal orientations of the small orthopyroxene crystals are, however, similar to the orientation of the adjacent orthopyroxene porphyroclast.

(IV) Finally, small amounts of orthopyroxene are found in the relatively coarse olivine-rich domains of the fine-grained tectonites and in the mylonites (type-IV orthopyroxene). Orthopyroxene in these domains occurs as elongate, tapering, flaser-like crystals along olivine grain boundaries aligned subparallel to the foliation. Such orthopyroxene crystals are sometimes seen to bulge into adjacent olivines, often following

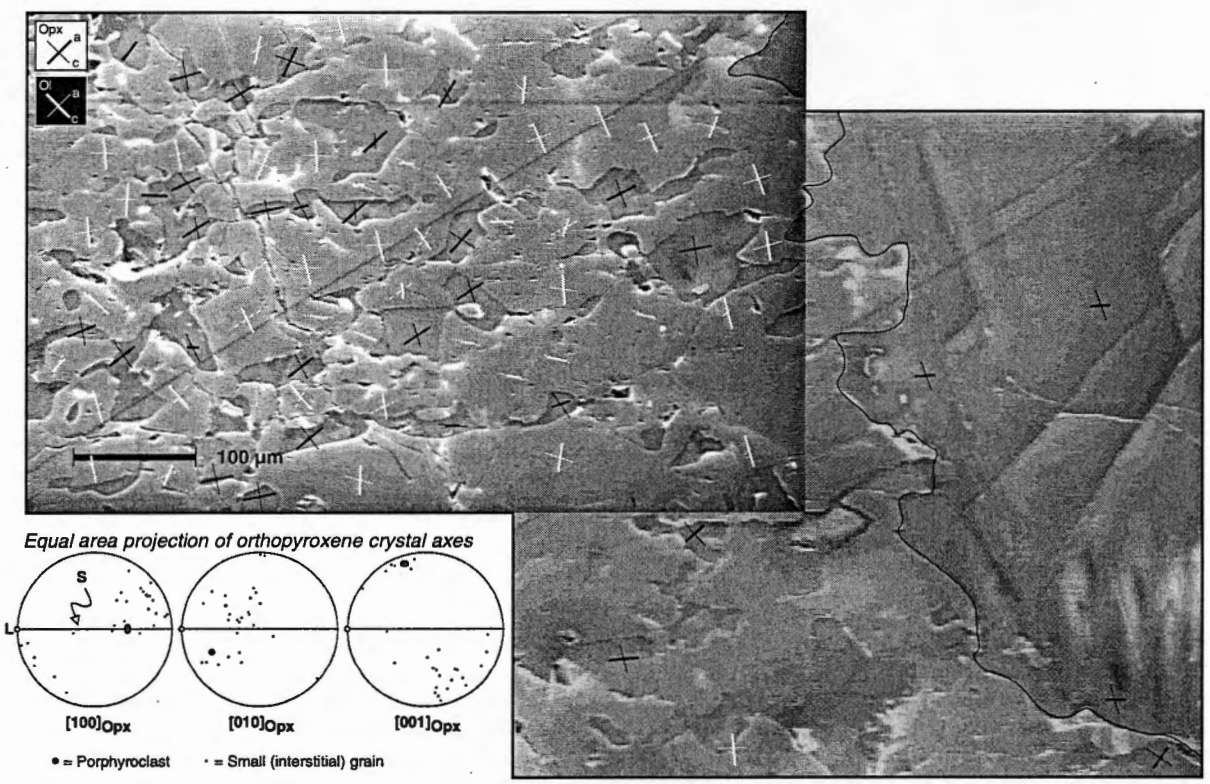

Figure 5.10: Secondary electron SEM image of fine-grained olivine-orthopyroxene domain next to an orthopyroxene porphyroclast (sample 97GOFOK5). Crystal orientations of olivine and orthopyroxene grains determined by EBSD. Orientations of [a]- and [c]-axes are shown by projected short lines of uniform length (black for orthopyroxene, white for olivine). Stereoplots (equal area) of orthopyroxene crystal orientations shown in lower left. Orthopyroxene grains have lattice preferred orientations unrelated to any known slip system in orthopyroxene but probably inherited from adjacent orthopyroxene porphyroclast. For olivine orientations see set of stereoplots in lower right of figure 5.6.

subgrain walls in the olivine crystal. In addition, orthopyroxene crystals occur along low-angle olivine grain boundaries, *i.e.*, grain boundaries between olivine crystals whose lattices are only rotated over small angles (mostly < 30°) with respect to each other (figure 5.9e&f). Interestingly, whereas most olivine-orthopyroxene interphase boundaries are curved, olivine crystals next to typical interstitial orthopyroxene crystals occasionally have straight crystal faces ('facets'- figure 5.9d). Facets were found to be oriented at high angles to the (001) plane of the host olivine (figure 5.11 – see figure caption for details about method of determination). There is a weak preference for orientations near the olivine (111), (121), (110) and possibly the (021) planes. In addition, several facets were found whose poles make a small angle - but never exactly coincided - with the [b]-axis of the host crystal.

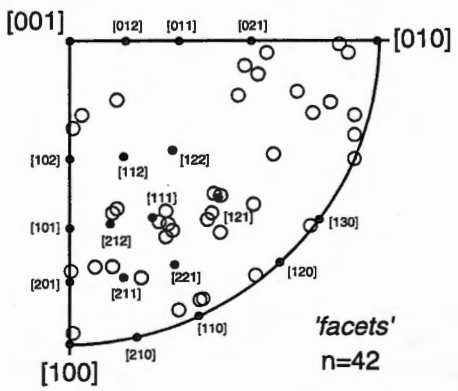

Figure 5.11: Inverse pole figure for olivine showing measured orientations (open circles) of the poles to straight olivine faces ('facets') next to interstitial orthopyroxene grains. Orientations were determined in a U-stage by measuring the orientation of the host crystal, followed by tilting the facet to a vertical position and measuring the orientation of the pole to the facet plane. Black dots indicate (calculated) orientations of poles to low-index olivine crystal planes.

5.4. Mineral chemistry

Chemical analyses of mineral grains were obtained principally for the purpose of pyroxene geothermometry. Major and trace elements were measured using a Cameca SX-50 electron microprobe at the Geology and Geophysics Department of Texas A&M University (USA) with wavelength dispersive spectrometers equipped with LiF, PET and TAP crystals. Operating conditions comprised an acceleration voltage of 15 kV, a 10 nA beam current, and counting times of 20-60 s. Chemical analyses were taken on transects across porphyroclasts, carefully avoiding cracks, inclusions, and exsolutions, using a relatively large 15-20 µm spotsize. Analyses on fine-grained mineral phases were obtained using a smaller spotsize of 5-10 µm.

The pyroxene porphyroclasts studied are chemically zoned. In figure 5.12a profiles are presented of Al and Ca, two of the most important elements for pyroxene thermometry, expressed as the concentrations in the pyroxene M1- and M2-sites respectively. The profiles shown were measured across orthopyroxene and clinopyroxene porphyroclasts in one mylonite and one fine-tectonite sample. The Al concentrations in orthopyroxene decrease from core to rim, whereas Ca concentrations are relatively constant throughout the orthopyroxene grains, and decrease only slightly towards the rim. As a result, the calculated enstatite activity in orthopyroxene increases towards the rim. In clinopyroxene, Al concentrations generally decrease towards the rim, although the Al concentration in the clinopyroxene porphyroclast from a mylonite sample, shown in figure 5.12a, shows a slight increase from core to rim. Ca concentrations in clinopyroxene are seen to decrease towards the rim. Consequently, calculated enstatite activities in clinopyroxene decrease from core to rim.

Fine-grained orthopyroxene and clinopyroxene crystals are also chemically zoned. This is not only observed in multiple analyses within individual crystals, but also when element concentrations are plotted against distance of the centre of the analysis spot from the grain rim. When the chemical data from both the orthopyroxene porphyroclasts and the fine-grained orthopyroxenes are plotted in one diagram against the logarithm of the distance to the rim (figure 5.12b), they form a linear array of decreasing Al and Ca

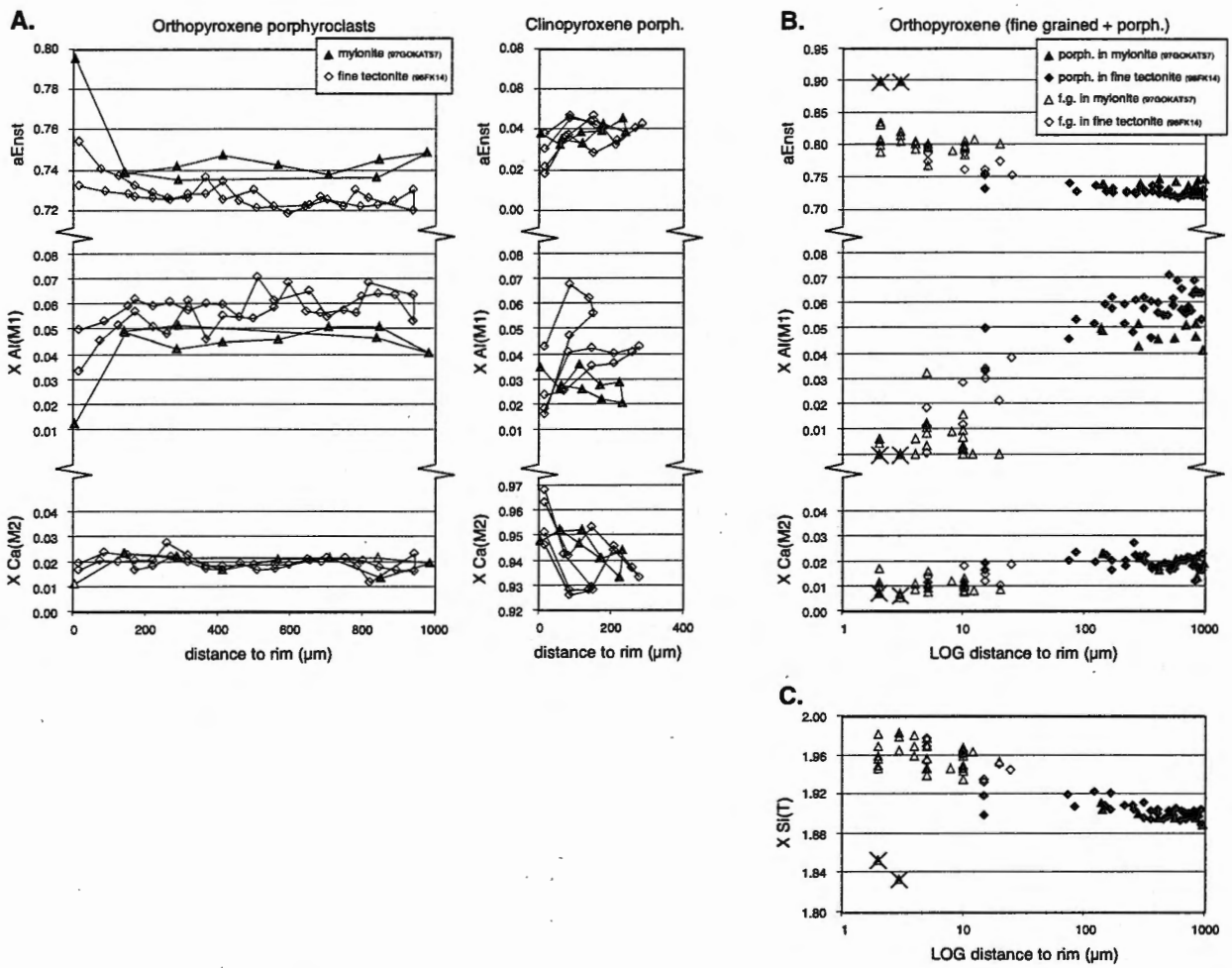

Figure 5.12: Chemical data from pyroxene crystals. A) Chemical profiles of enstatite activity, Al mole fraction in the M1-site and Ca mole fraction in the M2-site as a function of distance between the grain perimeter and the analysis spot, in orthopyroxene and clinopyroxene porphyroclasts from a mylonite- and a fine-grained tectonite; B) Same data for orthopyroxene, with additional chemical data from fine-grained orthopyroxene plotted as a function of the logarithm of the distance to the rim. Crossed points discarded, because the analyses probably included neighbouring olivine grains; C) Si mole fraction in orthopyroxene T-site. For further discussion see text.

concentrations from core to rim. The observed decreasing Al and Ca concentrations towards grain rims might in part be the result of an unwanted 'mixing in' of olivine, because analyses close to the rim are subject to an increased chance that the electron beam partially overlaps with grains - most likely of olivine - adjacent to or underneath the target grain. A test using Si concentrations was performed to investigate this effect. Since Si concentrations in olivine are lower than in orthopyroxene, the effect of a possible contribution of adjacent olivine grains to the analytical results would be to *decrease* the Si concentration. A plot of Si concentrations versus the logarithm of the distance to the rim (figure 5.12c) shows that both the data from the porphyroclasts and the fine-grained orthopyroxenes form again a linear array of *increasing* Si towards the rim. The observed chemical trends are, therefore, not the result of unwanted mixing effects, but likely represent true chemical zonations in the grains. Only two analyses plot at markedly lower Si concentrations, presumably as a result of the discussed mixing effect and have, therefore, been discarded.

5.5. Discussion – Micro-scale processes

In the following sections the deformation conditions and micro-scale processes are discussed which eventually led to the formation of the mylonite zone in Othris. This is followed by a discussion concerning the tectonic implications of shear localisation for the emplacement history of the Othris Ophiolite and for the strength of oceanic lithosphere in general.

5.5.1. Deformation and recrystallisation in the tectonites

An important aspect of the microstructure is the presence of subgrain boundaries parallel to (001) in addition to the more common (100) subgrain boundaries in olivine porphyroclasts. This suggests that dislocations with a [c]-Burgers vector have played a role during subgrain development and have contributed to the deformation. Subgrain rotation involving (001) boundaries would have produced new grain boundaries perpendicular to the foliation and parallel to the lineation in tectonites with [c]-axes maxima such as in figure 5.7, or parallel to the lineation in samples with [c]-axes girdles such as in figure 5.6c. Recrystallisation involving (001) subgrain boundaries can thus (partly) explain the strongly linear character of many fine-grained tectonites.

The misorientation analysis of one fine tectonite sample illustrated in figure 5.7 shows that many of the grain boundaries, which possibly developed from subgrain boundaries by subgrain rotation, are characterised by lattice rotations with rotation axes close to [b]. Such rotations can be produced by the transformation of (100) or (001) subgrain walls into grain boundaries by subgrain rotation. The olivine slip systems that could produce such subgrain walls are [a] (001) and [c] (100), respectively. Both systems are in agreement with the observed (100) and (001) subgrain walls in olivine porphyroclasts. The bulk LPO of the olivine grains indicate that [a] (010) was the slip system which contributed most to the deformation of the fine-grained tectonites. Combined slip on all three systems may thus have led to dominant elongation of olivine grains in the lineation direction plus some flattening of the grains.

The LPO of the olivine crystals in a fine-grained olivine-orthopyroxene rim around an orthopyroxene porphyroclast in a fine-grained tectonite (figures 5.6c, 5.10) may indicate that the olivine grains in the rims also deformed by dislocation creep and that this olivine may thus have undergone dynamic recrystallisation. Alternatively, the preferred orientation may have been inherited from old, precursor olivine grains adjacent to the orthopyroxene porphyroclast. Most importantly, the grain size of olivine in the fine-grained domains is probably not related to the stress through the stress-grain size relations discussed above. As the development of the fine-grained domains was coeval with the deformation and recrystallisation in the coarse olivine bands (as shown by their augen-shapes), the stresses obtained from the recrystallised grain size in the coarse olivine bands must also be a measure of the stress in the fine-grained domains. The small grain sizes in the fine-grained domains as compared to the coarser recrystallised grain sizes in the olivine bands suggests that the olivine in the fine-grained domains is not simply produced by dynamic stress-controlled recrystallisation or that grain growth was inhibited.

5.5.2. Orthopyroxene textures and the origin of the fine-grained polyphase domains

Irregular orthopyroxene porphyroclast outlines (type-I orthopyroxene) – with textures suggesting replacement of orthopyroxene by olivine - are not uncommon in harzburgitic mantle sections of ophiolites (see for instance Boudier & Nicolas, 1995). They can be interpreted as products of in-situ incongruent melting

of orthopyroxene, which produces olivine and a SiO_2-rich melt (*e.g.*, Niu, 1997). Alternatively, they could be the result of the reaction with an upward migrating melt percolating through the harzburgite. Kelemen (1990; Kelemen *et al.*, 1992) showed that a basaltic melt becomes undersaturated in orthopyroxene when it moves to shallower levels and will thus tend to dissolve orthopyroxene crystals present in the host peridotite. Fluids may also cause incongruent dissolution of orthopyroxene. Indeed, in the coarse-grained tectonites of the footwall block there are signs for the presence of water-bearing minerals (*e.g.*, pargasitic amphibole) during deformation. However, the irregular type-I orthopyroxene crystals are not restricted to the footwall block, and in all other domains amphibole is relatively rare and always late-stage, *i.e.*, it crystallised after deformation. An origin by incongruent dissolution seems, therefore, not very likely. On the other hand, there is abundant evidence that melts played a prominent role in the formation of the Othris peridotites (chapter 4). The presence of large cross-cutting replacive dunite bodies in the footwall block and smaller transposed and cross-cutting dunites in the hanging wall block is consistent with orthopyroxene removal by a melt (Kelemen, 1990). For that reason, type-I orthopyroxene porphyroclasts are most likely the result of melting or a melt-rock reaction leading to orthopyroxene 'corrosion' (figure 5.13) due to the melt-producing reaction:

orthopyroxene + low-Si melt → olivine + high-Si melt

Type-II orthopyroxene, *i.e.*, clusters of irregular grains with the same crystallographic orientations, are probably a more advanced stage of orthopyroxene replacement due to reaction with a melt. Figure 5.13 shows some examples of possible progressive stages of orthopyroxene porphyroclast corrosion.

The orthopyroxene in the fine-grained olivine-orthopyroxene domains surrounding orthopyroxene porphyroclasts (type-III orthopyroxene) in the hanging wall tectonites may have a similar origin. The crystal orientation analysis in figure 5.10 shows that the crystal orientations of the fine-grained orthopyroxene are similar to that of the adjacent porphyroclast. It is unlikely that the fine-grained orthopyroxene is the result of dynamic recrystallisation of orthopyroxene porphyroclasts, since this process cannot explain the extensive mixing of olivine and orthopyroxene in the fine-grained domains. The melt-rock reaction invoked above to induce incongruent corrosion of orthopyroxene could explain the peculiar texture of the fine-grained domains. The irregular outlines of the porphyroclasts in the centres of the fine-grained domains suggest partial replacement and growth of olivine grains at the expense of orthopyroxene. Suhr (1993) reported similar interstitial flaser-like orthopyroxene crystals in peridotites from the transition zone between harzburgites and massive dunites in the Bay-of-Island Ophiolite, also with the [c]-axes – the main orthopyroxene slip direction - at a high angle to the lineation. Suhr argues that "a formation of orthopyroxene due to corrosion (..) would be favoured from the geological context", but adopts an interpretation in which the small orthopyroxene crystals are derived from crystallisation from a trapped melt to account for the lattice preferred orientation and the morphology of the crystals (Suhr, 1993). In Othris, the fine-grained orthopyroxenes are probably residual, with their crystal orientations being inherited from the porphyroclast from which they were derived by corrosion. Their morphologies may be the result of stress-induced migration of olivine-orthopyroxene interphase boundaries (Wheeler, 1992) during deformation of the fine-grained domains.

A residual origin is not likely for the type-IV interstitial orthopyroxene in the olivine-rich domains in the fine-grained tectonites. Their presence along subgrain or low-angle grain boundaries within recrystallising olivine aggregates suggests that they precipitated locally. As there are no orthopyroxene inclusions observed within preserved, unrecrystallised porphyroclasts, the option that such orthopyroxene crystals represent (relic) orthopyroxene inclusions

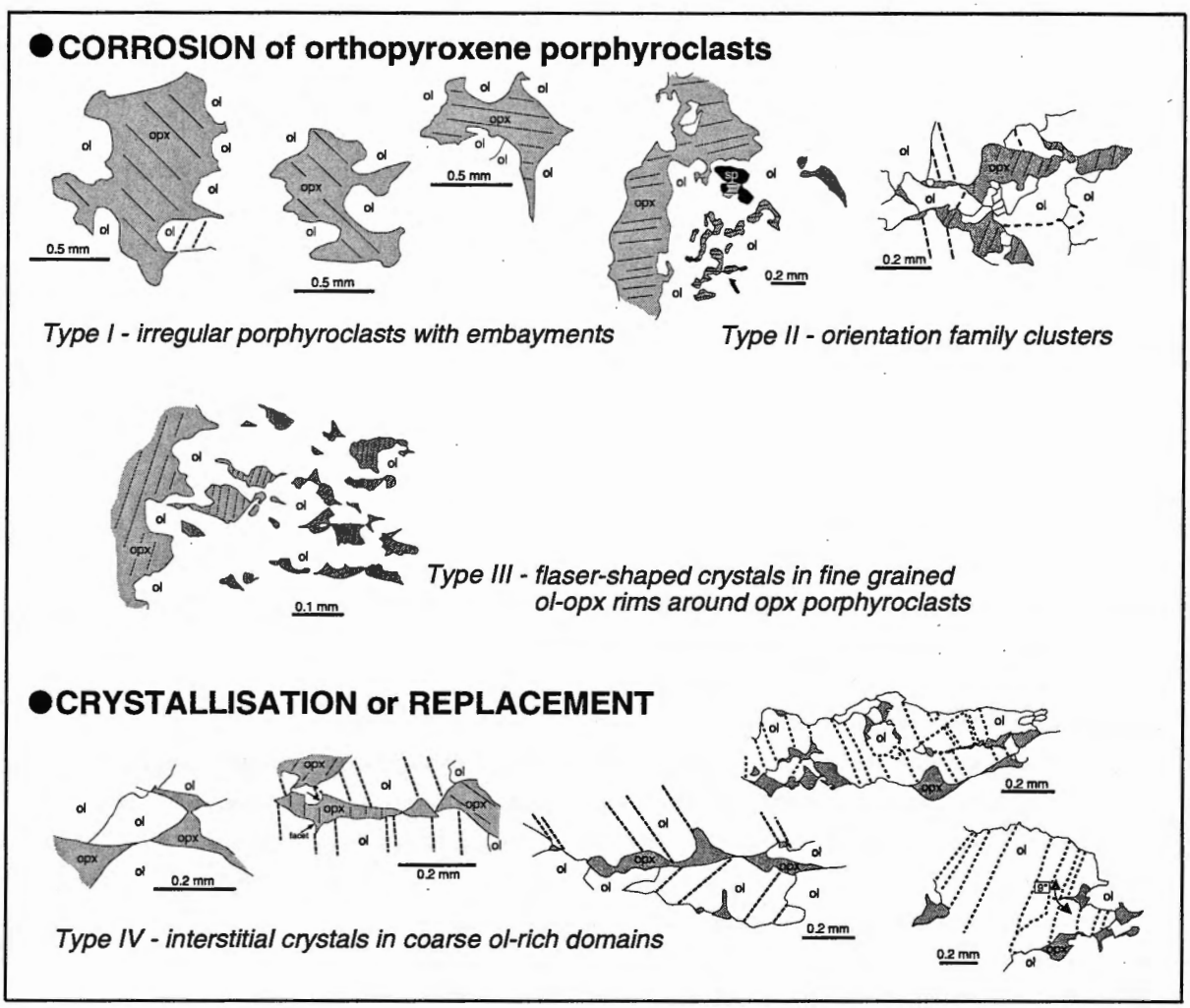

Figure 5.13: Synoptic diagram showing the different types of orthopyroxene morphologies in the Othris peridotites. Type I-III orthopyroxene grains are probably derived from corrosion of orthopyroxene porphyroclasts, whereas type IV orthopyroxene is interpreted as the product of in-situ crystallisation or of olivine replacement.

within olivine porphyroclasts which later controlled the location of subgrain boundaries developing within the olivine clast can be rejected. Instead, it is suggested that the orthopyroxene crystals originated by precipitation from a melt migrating along subgrain or low-angle grain boundaries (*cf.*, De Kloe, 2001), or by a replacement of olivine facilitated by diffusion of SiO_2 out of a melt into olivine crystals or recrystallising aggregates along such boundaries. It is difficult to envisage how a melt-absent, subsolidus reaction could have produced the precipitation of orthopyroxene along low-angle boundaries. Such a reaction would probably have required a free fluid phase present along the grain boundaries to provide the necessary fast diffusion pathways into the recrystallising olivine crystals, for which – as mentioned above - evidence is absent in the rocks involved. Clearly, a melt-rock reaction, or at least a melt-facilitated reaction is favoured to explain the observations. Together, type-III and type-IV orthopyroxene crystals point to a reaction with a melt which was probably close to orthopyroxene saturation and which was locally melt-

forming and locally melt-consuming in the same rocks:

orthopyroxene + low-Si melt ↔ olivine + high-Si melt

Interestingly, qualitative analysis suggests that orthopyroxene precipitation mainly occurred along (sub-) grain boundaries subparallel to the foliation, whereas orthopyroxene corrosion is mainly observed on grain boundaries at a high angle to the foliation, suggesting that the equilibrium of the reaction may be affected by differential stress variations.

The development of straight, facet-like crystal faces on olivine grains adjacent to type-IV orthopyroxene grains is consistent with an origin by local orthopyroxene precipitation from a melt trapped in small grain boundary melt pockets. Some of these straight faces have orientations which coincide with low-index crystal faces (figure 5.11). Low-index faces are expected to develop by crystal growth of olivine crystals next to a melt pocket (*e.g.*, Drury & Van Roermund, 1989). The preference of (111), (021), and (110) faces agrees well with theoretical morphological models of olivine, and these faces are frequently found in natural and artificial olivine crystals, whereas (121) is not uncommon ('t Hart, 1978b). The straight faces at low angles to, but not exactly coinciding with, the olivine (010) plane are more difficult to explain. They may be grain boundaries which only seem straight at light microscope resolution but which consist of a combination of stepping crystal faces at a smaller scale.

In summary, although the details of the processes leading to the orthopyroxene textures, microstructures, and crystal morphologies are not well understood, the results of these processes are evident. The footwall tectonites exhibit evidence of *dissolution* of orthopyroxene, probably by melting or by a melt-rock reaction. In contrast, type-III and type-IV orthopyroxene crystals in the hanging wall tectonites point to a more complex process of *dissolution and local precipitation* of orthopyroxene. The effect of this process in the hanging wall tectonites is that orthopyroxene is re-distributed through the harzburgites, away from porphyroclasts into the olivine domains. Such a process requires a high mobility of the enstatite components, possibly due to high diffusion rates along (melt-wetted?) grain and subgrain boundaries. The process has led to the development of well-mixed fine-grained domains surrounding orthopyroxene porphyroclasts. The preservation of the fine grain sizes in these domains shows that olivine grain growth must have been very slow or even completely arrested, probably as the result of pinning of grain boundaries by interstitial orthopyroxene grains (*cf.*, Olgaard, 1990). It is argued below that the development and stability of these fine-grained domains has been crucial in the successive development of mylonites in the Othris massif.

5.5.3. Deformation in the mylonites and the cause of localisation

Field observations show that the fine-grained domains around orthopyroxene porphyroclasts in the hanging wall tectonites become increasingly stretched when approaching the Onohonos River mylonite zone, until the fine-grained material forms continuous bands in the mylonite zone itself. The origin of the fine-grained bands in the mylonite can thus be traced back to the formation of the fine-grained rims around orthopyroxene porphyroclasts in the hanging wall tectonites, and these hanging wall tectonites can be seen as the protolith of the mylonites. This origin is also evident when the microstructures of mylonite samples are studied: orthopyroxene porphyroclasts are always found within the fine-grained bands, the fine-grained bands consist of a mixture of predominantly orthopyroxene and olivine, and the microstructures of the coarse-grained lenses strongly resemble those of the olivine bands in the hanging wall tectonites.

The fine-grained domains in the hanging-wall tectonites form isolated patches and the deformation of the tectonites was most likely controlled by the coarse-grained olivine-rich bands. In contrast, in the mylonites the deformation was probably controlled by the

continuous and interconnected fine-grained bands. Indeed, at thin section scale, coarse olivine-rich lenses are often boudinaged suggesting that they acted as relatively strong layers in the weaker fine-grained matrix which could flow around the stronger domains. This is confirmed by field observations showing that thin dunite bands are often broken-up or boudinaged. The absence of a (strong) LPO in the fine-grained bands rules out dislocation creep as the dominant deformation mechanism (Karato, 1988; Fliervoet *et al.*, 1999). The presence of numerous grain boundary alignments – which are interpreted as sliding surfaces - in the fine-grained bands suggests that some grain boundary sliding occurred. However, an additional process must have been operating adjusting the shapes of the grains to preserve the coherence of the crystal aggregate and prevent pores from opening. It is therefore most probable that the fine-grained bands deformed by a mechanism involving grain boundary sliding and diffusion creep. The apparent competency contrast between the fine-grained bands and the coarse-grained lenses and dunite layers is fully consistent with such a (grain-size sensitive) deformation mechanism.

In conclusion the following scenario for the formation of the mylonites is envisaged. The first step which was crucial to their development was the formation of fine-grained domains consisting of well-mixed olivine and orthopyroxene as the result of a reaction. The augen-shapes of the fine-grained domains in most of the tectonites show that they have been deformed to some extent during the deformation of the tectonites. The presence of an olivine LPO in the fine-grained domain in one tectonite may suggest that dislocation initially contributed to the deformation of the reaction-derived olivine. At some stage, however, the deformation mechanism in the olivine crystals in the fine-grained domains must have switched completely to grain-size sensitive creep, probably during progressive cooling. With ongoing deformation of the tectonites, the domains became increasingly stretched until some of the domains coalesced to form continuous bands. From that stage onward, deformation locally became controlled by the weak fine-grained bands. As the deformation continued, an increasing number of fine-grained domains started to connect to form continuous bands. This process reduced the bulk strength of the peridotites with progressive deformation and led to strain localisation.

The Othris peridotites thus provide a possible answer to the question, raised in the introductory section of this chapter, as to the processes that lead to a transition from dislocation creep to GSS creep. A reaction probably involving an interstitial melt led to the development of fine-grained domains. The well-mixed, polyphase character of these domains was critical, as the presence of an interstitial phase (orthopyroxene) precluded grain growth of olivine thus keeping the grain size small, thus allowing a switch to dominant GSS creep. This point will further be addressed below with the use of deformation mechanism maps.

5.5.4. Temperature constraints on the mylonitic deformation

An attempt was made to put constraints on ambient temperatures during deformation using the pyroxene geothermometers of Bertrand & Mercier (1986), Brey & Köhler (1990), and Witt-Eickschen & Seck (1991). The chemical zonation of the pyroxenes shows that they re-equilibrated during cooling. The fact that Al in orthopyroxene shows a decrease from core to rim whilst the profile for Ca is relatively flat also shows that different elemental concentrations re-equilibrated to different extents due to variations in element diffusion rates. The single-pyroxene thermometer of Brey & Köhler, for instance, yields much lower temperatures (830-900 °C) when applied to the cores of the orthopyroxene porphyroclasts in the fine tectonite of figure 5.12 than the single-pyroxene thermometer of Witt-Eickschen & Seck (1000-1060 °C). This can be attributed to the fact that the Brey & Köhler

thermometer uses the Ca concentration in orthopyroxene, whereas the Witt-Eickschen & Seck used Al. The differences in these calculated temperatures, henceforth called analytical temperatures, indicate that during cooling concentrations of Ca re-equilibrated more completely than those of Al, which is in agreement with the view that Ca diffusion is faster than Al diffusion in orthopyroxene (Witt-Eickschen & Seck, 1991). The two-pyroxene thermometers of Bertrand & Mercier (1986) and Brey & Köhler (1986), which are based on the exchange of Ca between co-existing clinopyroxene and orthopyroxene, also give low analytical temperatures in the range of 800-860°C and 725-800°C for the cores of pyroxenes, confirming the extensive re-equilibration of Ca during cooling. It is noted, however, that these two-pyroxene thermometers require that chemical equilibrium between clinopyroxene and orthopyroxene is preserved which seems unlikely in view of the re-equilibration and consequent diffusion of elements out of the pyroxenes during cooling.

The fact that fine-grained orthopyroxenes in the matrix of the studied samples are also zoned and that their Ca and Al concentrations plot on the same linear array as those of the porphyroclasts indicates that the fine-grained pyroxenes and the porphyroclasts have partly recorded the same cooling history. This means that the fine-grained orthopyroxene crystals must have formed *above* their closure temperatures for the given chemical system. The analytical temperatures obtained by geothermometry can be regarded as 'cooling temperatures' (analogous to 'cooling ages' in geochronology) and reflect the temperatures at which the grains became closed for diffusive re-equilibration. The closure temperature is dependent on, among others, the diffusion coefficient, the cooling rate, and the diffusion distance (Dodson, 1973; Spear, 1993). In geothermometry, the diffusion distance is effectively the distance to the rim of a mineral grain. Application of the Witt-Eickschen & Seck (1991) thermometer to the analyses of some of the largest orthopyroxene grains from fine-grained domains gave the highest analytical temperatures of all the fine-grained orthopyroxene analysed. This is not surprising, since the largest grains have the largest diffusion distance (15-25 μ in this case) and the Witt-Eickschen & Seck thermometer uses the relatively slowly diffusing Al. Therefore, these analyses represent the highest closure temperatures of the fine-grained orthopyroxene analysed and the analytical temperatures obtained (810-890°C) are a minimum estimate of the temperature of the formation of the fine-grained orthopyroxene.

Another temperature constraint comes from the growth of tremolite + chlorite in the spaces between broken-up orthopyroxene fragments in a plagioclase-bearing peridotite ultramylonite. The assemblage of calcic amphibole (tremolite) + chlorite is stable at temperatures below 780°C in plagioclase-peridotites (Schmädicke, 2000). Therefore, at least some of the deformation in the mylonites occurred at temperatures below 780°C. However, it is unlikely that ductile deformation of the olivine matrix continued at much lower temperatures (*i.e.*, below 600-650°C), as creep in olivine becomes very slow or is arrested altogether at low temperatures.

5.5.5. *Deformation mechanism maps*

Further information about appropriate deformation mechanisms and strain rates may be obtained by the construction of deformation mechanism maps. Such maps are principally based on experimental rheological data of minerals, in the present case of olivine polycrystals. The absence of water-bearing minerals in the mylonites, as well as in the vast majority of the fine-grained tectonites of the hanging wall block – interpreted as the protolith for the mylonites - clearly favours the use of the 'dry' olivine flow laws. Experimentally derived olivine flow laws used in this chapter are given in table 5.1b, and will be further discussed below.

First, a set of conventional two-mechanism deformation maps was constructed, using the olivine dislocation creep flow law of Chopra and Patterson (1984) and the diffusion creep flow law of Hirth and Kohlstedt (1995a). Figure 5.14a shows such a two-mechanism map for a temperature of 1100°C, which is thought relevant for the deformation of the tectonites and the formation of the fine-grained domains adjacent

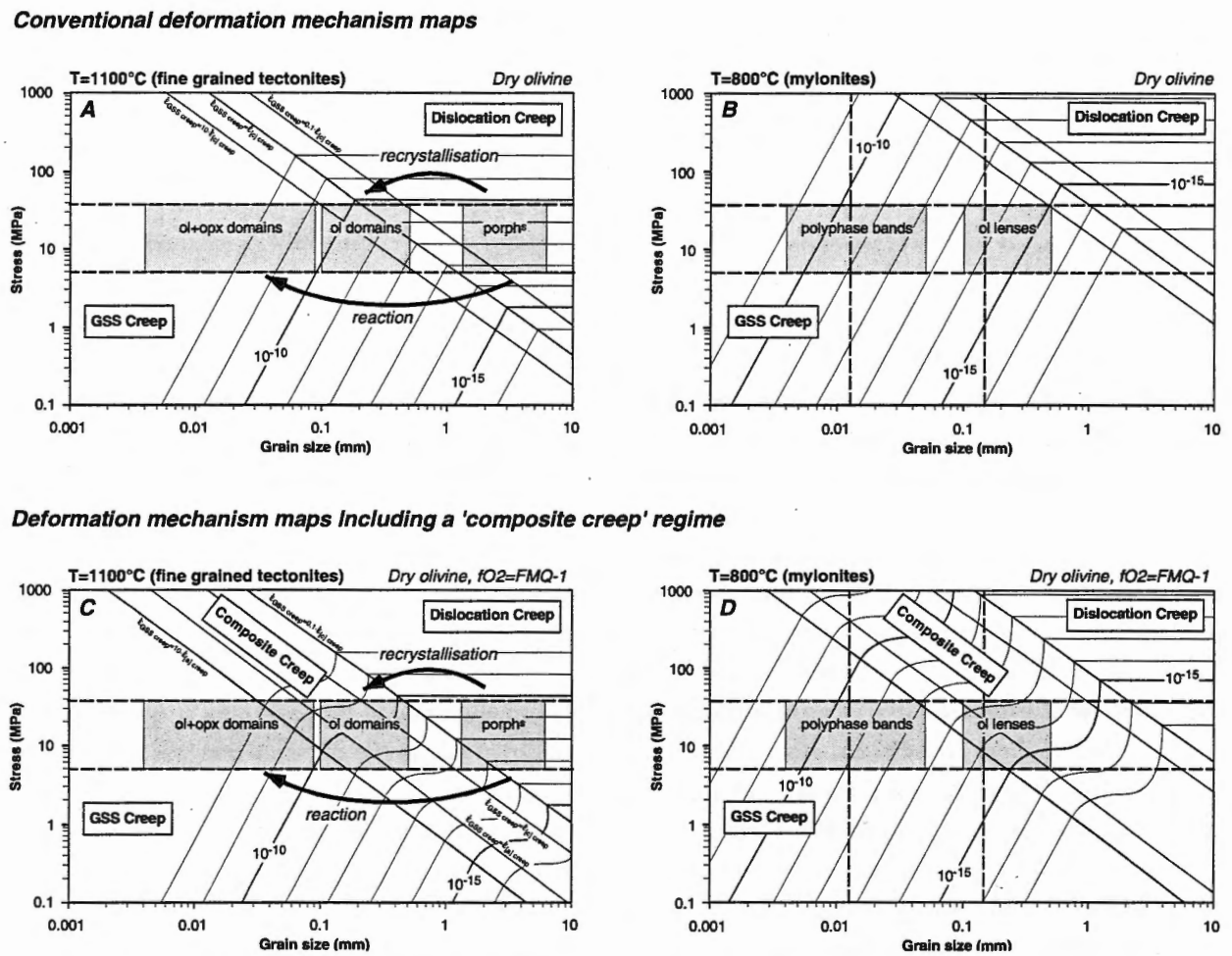

Figure 5.14: Set of deformation mechanism maps for dry olivine (maps based on olivine flow laws shown in table 5.1b). Figures A) and B) show conventional, two-mechanism maps indicating deformation conditions in the tectonites (temperature assumed as 1100°C) and during mylonitic deformation at 800°C. Thick lines running from top-left to bottom-right indicate conditions for 10%, 50%, and 90% dislocation creep (flow law of Chopra & Patterson, 1984). Figures C) and D) show deformation mechanism maps for the same conditions which include a 'composite creep' regime, in which the deformation is controlled by GSS creep in combination with [a]-slip dislocation creep. Upper boundary of composite creep regime is defined by the (arbitrary) condition that the GSS creep rate is one tenth of the dislocation creep rate by [c]-slip; lower boundary is defined by condition that GSS creep is 10 times faster than [a]-slip; other thick lines shown indicate equal contributions of GSS creep and [a]-slip, and GSS creep and [c]-slip. Flow laws for GSS creep and [a]-slip in C) and D) calculated for an oxygen buffer of FMQ-1. Thin lines are strain rate contours (in s^{-1}); horizontal dashed lines are upper and lower stress estimates for fine tectonite deformation from paleopiezometry; grey boxes indicate grain size ranges in the pertinent domains (all grain sizes plotted are multiplied by 1.2 to correct for sectioning effects); vertical dashed lines in 800°C diagrams are mean linear intercept grain sizes for olivine lenses and fine-grained polyphase bands in mylonites (table 5.1a). The melt-rock reaction discussed in the text would have produced fine-grained material largely deforming in the GSS creep regime, while dynamically crystallised domains would have deformed (partly) by dislocation creep at much lower rates.

to orthopyroxene porphyroclasts. It is assumed that the protolith of the tectonites had an olivine grain size larger than 1 mm (denoted 'porph^{s}' in figure 5.14a; note that all grain sizes have been multiplied by a factor of 1.2 to correct for sectioning effects). Dynamic recrystallisation produced grains of 0.1-0.5 mm in the mono-olivine domains ('ol domains'), and the melt-rock reaction discussed above produced grains which were even smaller, down to sizes of a few microns ('ol+opx domains'). Note that for stresses of 5-38 MPa, the grain size range found in the fine-grained domains falls entirely in the GSS creep field, which would suggest that the olivine LPO found in one such a domain could not have been produced by dislocation creep. Moreover, according to the deformation mechanism map in figure 5.14 dislocation creep would only have played a moderate role in the mono-olivine domains, which is inconsistent with the widespread evidence for dislocation creep (substructure, LPO, dynamic recrystallisation) in these domains. Cooling to a temperature of 800°C would have brought both the mono-olivine domains ('ol lenses' in the mylonites) and the fine-grained domains ('polyphase bands' in the mylonites) well into the GSS creep domain (figure 5.14b). Under these conditions, the fine-grained polyphase bands would have deformed up to 4 order of magnitude faster than the coarser olivine lenses (~10^{-9}-10^{-13} versus ~10^{-13}-10^{-16} s^{-1}), but they would not have controlled the deformation in the tectonites because of their isolated (non-connected) character.

However, recent deformation experiments have shown that under conditions close to the mechanism boundary between dislocation and GSS creep, the Von Mises criterion, which requires that the relatively strong [c]-slip system is activated during deformation of olivine polycrystals, is relaxed and that deformation is controlled by the weaker [a]-slip system under those conditions (see Hirth & Kohlstedt, 1995b and Drury & FitzGerald, 1998 for discussion). This leads to a new class of deformation mechanism maps, which include a 'composite creep' regime in which GSS creep in combination with [a]-slip control the deformation (figure 5.14c,d). Within this domain the strain rate is grain size dependent as a result of the contribution of GSS creep. A 1100°C deformation mechanism map which includes such a composite creep regime (figure 5.14c) shows that dislocation creep ([a]-slip) would have played a role in the mono-olivine domains, and possibly in the coarsest material in the reaction-derived fine-grained domains in the tectonites, which is in very good agreement with the microstructural inferences regarding the active deformation mechanisms. During cooling, the deformation mechanisms would have largely remained the same as the position of the lower boundary of the composite creep regime is only weakly temperature dependent as a result of the activation energies ($Q^{\#}$) for GSS creep and [a]-slip being very similar in magnitude (compare figure 5.14c and d). Some dynamic recrystallisation could have reduced the maximum grain size in the well-mixed, reaction-derived olivine-orthopyroxene domains slightly, moving the polyphase bands in the mylonites completely into the GSS creep regime.

The deformation mechanism maps for the deformation rate in the mylonites at 800°C shows that the strain rate in the olivine lenses was low, 10^{-13}-10^{-16} s^{-1}. Dynamic recrystallisation would therefore be slow, or arrested altogether in the deformation mechanism map in figure 5.14b in which the olivine lenses lie completely in the GSS creep regime. Following the argument of De Bresser *et al.* (1998) that grain growth is the only process affecting the grain size in the GSS field (see introductory section) in the absence of (strong) dynamic recrystallisation, one would expect that the grains in the olivine lenses would have grown towards the mechanism boundary, unhindered by other minerals (so-called secondary phases, *i.e.*, phases other than the volumetrically most important, deformation controlling phase). In that case, the small grain sizes of 0.1-0.5 mm would not have been preserved in the olivine lenses in the mylonites, unless the stresses during mylonitic deformation were much higher than

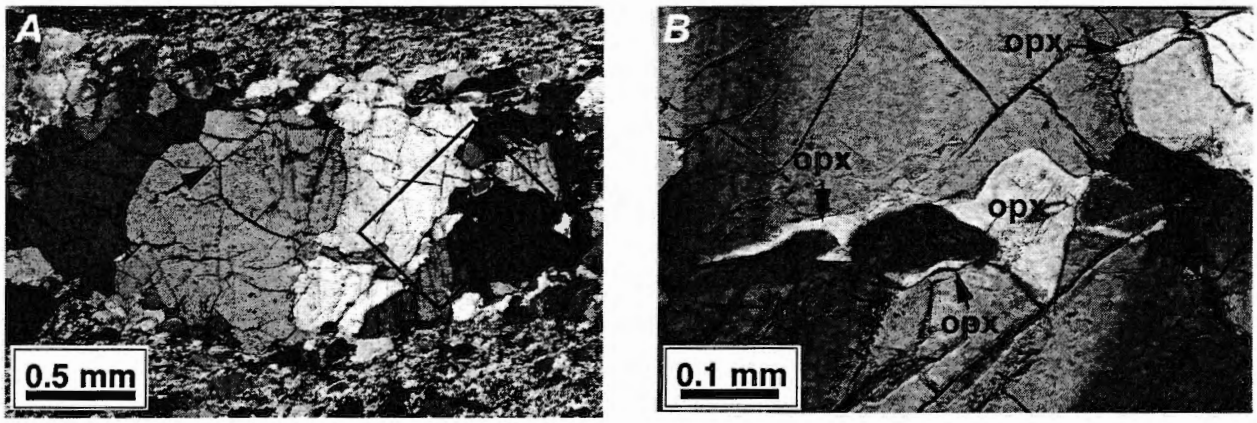

Figure 5.15: Photomicrographs (in XPL) showing evidence for local grain growth/annealing in a relatively coarse olivine lens in an ultramylonite. The granular grains in A) are much coarser than average and display near-perfect 120° triple grain junction. Area in rectangle shown in close-up in B). This area is finer-grained, possibly as the result of pinning of grain boundaries by the presence of thin interstitial orthopyroxene crystals.

during tectonite deformation. Such an increase of stress seems unlikely in the light of the high strain rates in the fine-grained polyphase bands even at low stresses; it is more likely that the stresses would have been relaxed during mylonite deformation. It is uncertain whether olivine grain growth at 780°C would be fast enough to lead to significant coarsening. Moreover, although the coarse bands consist almost entirely of olivine, the presence of secondary phases (most importantly orthopyroxene) along the grain boundaries present could also have led to pinning of grain boundaries, inhibiting grain growth and thus keeping grain sizes small. This is supported by the microstructure in figure 5.15a, which shows part of an olivine band with a granular texture with 120° triple junctions, in which the polygonal olivine grains are ~0.5-1 mm in size. The olivine grain boundaries in the coarse granular domain are free of orthopyroxene, in contrast to the grain boundaries of the adjacent irregular and much smaller olivine grains (see enlarged area in figure 5.15b). The granular domain may therefore represent an area in which olivine grain growth was not inhibited by secondary phases. This observation suggests that even very small fractions of secondary phases, often just visible at the resolution of light microscopy, are sufficient to pin grain boundaries and can inhibit grain growth. This supports a similar conclusion by Olgaard (1990) regarding the role of secondary phases.

5.6. Tectonic implications

5.6.1. Kinematic interpretation of structures

Due to the strong dismemberment of the Othris peridotite, it is difficult to unambiguously relate the present-day orientations of the structures studied to their original (intra-oceanic) geometrical framework. On the basis of the lithological and metamorphic evidence in the peridotites it was concluded in chapter 4 that the coarse tectonites west of the Onohonos zone represent relatively deep levels of the ophiolite, whereas the plagioclase-peridotites, in particular those that seem to have undergone sea-floor serpentinisation at some stage of their geological history, represent shallower levels. It was also concluded that the plagioclase-peridotites in the Othris massif represent mantle rocks which became impregnated with a melt. The plagioclase-in boundary represents the plane in P,T-space at which the interstitial melt became

saturated in plagioclase and the plagioclase-peridotites represent the low-temperature, low-pressure side of the boundary. In the present-day geometry of the massif, the plagioclase-peridotites are found at the highest levels and the plagioclase-in boundary is relatively shallowly dipping in the Katáchloron area (figure 5.2). It is therefore inferred that progressively shallower levels of the ophiolite are encountered (roughly) up- and eastward. This limits the extent to which the Othris peridotites may have undergone tectonic rotations around subhorizontal axes during or after their emplacement.

The coarse tectonites exposed west of the Onohonos mylonite zone have steep lineations. Two LPO's indicate E-up transport directions. In view of the inferences made above regarding the original geometry it is most likely that this represents a movement with a large reverse or thrust component. The lineations in the mylonites are oblique south-dipping to subhorizontal. Field evidence suggests an oblique sinistral strike-slip movement for both the N-S striking mylonites and the NW-SE striking mylonites and ultramylonites. There is some ambiguity with respect to the shear sense derived from the LPO patterns of the coarse olivine bands in the mylonites (contrasting shear senses, even within the same sample, and double [a]-axis maxima). However, the coarse olivine bands in the mylonites are interpreted above as remnants of the original tectonite structure, and their LPO was probably formed during tectonite deformation, and unrelated to the deformation in the mylonite zone (and therefore, to the mylonite reference frame, *i.e.*, foliation and lineation) which was entirely controlled by GSS creep in the fine-grained bands. Following the geometrical argument outlined above, it is most likely that the mylonites record deformation with a large sinistral strike-slip component in combination with a reverse or thrust component. Lineations in the fine-grained tectonites directly east of the Onohonos mylonite zone are generally oblique southeast- or southwest-dipping. The LPO's of several samples do not exhibit a clear asymmetry. A few asymmetric LPO's indicate sinistral plus east upward movement senses. It is, therefore, most likely that in the original framework this movement sense represents a reverse or thrust movement in combination with a possible sinistral strike slip component, perhaps with a component of flattening.

In summary, the tectonites on either side of the Onohonos mylonite zone record a reverse or thrust movement with a possible additional sinistral strike-slip component. This suggests early-stage compression or transpression in the Othris Ophiolite. The mylonites largely record strike-slip deformation in combination with a reverse or thrust movement, *i.e.*, (continued) transpression. It is important to note that in transpressional, triclinic shear zone systems it is sometimes observed that the centre of a shear zone has recorded strike-slip whereas the margins of the zone have recorded coeval reverse slip (*e.g.*, Lin *et al.*, 1998). In the case of the Othris area it is, however, clear that the deformation in the mylonites overprints the deformation in the adjacent tectonites, and that (dominant) contraction gave way to (dominant) strike-slip at a later stage.

5.6.2. Tectonic interpretation

In chapter 4 it has been concluded that the plagioclase peridotites in the Othris area record melt impregnation in a near-transform environment associated with an Mid-Atlantic-type oceanic ridge. Extensive syn- and post-tectonic dyke intrusion and melt impregnation suggest that the deformation recorded in the plagioclase-peridotites occurred close to a ridge axis, in an extensional or transtensional setting. The deformation in the mylonites and the directly adjacent and parallel striking tectonites overprints the deformation in the plagioclase-peridotites. It follows that the Othris peridotites record a tectonic history of spreading in an extensional or transtensional

environment, followed by transpression. It is most plausible that the onset of transpression marked the beginning of the emplacement of a fragment of oceanic lithosphere which eventually became the Othris Ophiolite. In this context it is noted that the synkinematic growth of tremolite in one of the studied mylonites can possibly be linked to the growth of post-kinematic tremolite in the footwall block and to the development of the - locally preserved (Spray *et al.*, 1984) – tremolite-bearing metamorphic sole thrust of the ophiolite seen at the western edge of the Othris massif.

In addition to supra-subduction zone environments, transform fault domains along mid-ocean ridges may provide another important source of ophiolites (Karson & Dewey, 1978; Suhr & Cawood, in press). Small changes in plate configurations and plate motion vectors can turn transform faults into transpressional zones in which oceanic lithosphere is thickened, or alternatively, into transtensional zones in which lower crustal or mantle rocks are exhumed (see also Kastens *et al.*, 1998). This is illustrated by the well-known occurrences along transform faults in modern oceans of 'proto-ophiolites' such as Macquarie Island in the Indian-Australian Ocean (Griffin & Varne, 1980; Goscombe & Everard, 1999) and St. Paul's Rocks in the Atlantic (Melson *et al.*, 1972; Roden *et al.*, 1984; Bonatti, 1990), and 'transverse ridges' or 'uplifts' whose emplacement may have involved reversed and normal shear zones (*e.g.*, the Vema Transverse Ridge, Mid-Atlantic Ridge, see Kastens *et al.*, 1998, or the gabbroic uplift investigated during ODP Leg 176, Hole 735B, SW Indian Ridge, Dick *et al.*, 2000). Fragments of thickened or exhumed, deeply serpentinised oceanic lithosphere arriving at convergent margins will be more buoyant, easier to detach along pre-existing weak shear zones, and are more likely to survive as ophiolites than normal oceanic lithosphere. The Othris case shows that thrusting and thickening in transpressional transform domains can be facilitated by fine-grained mantle shear zones.

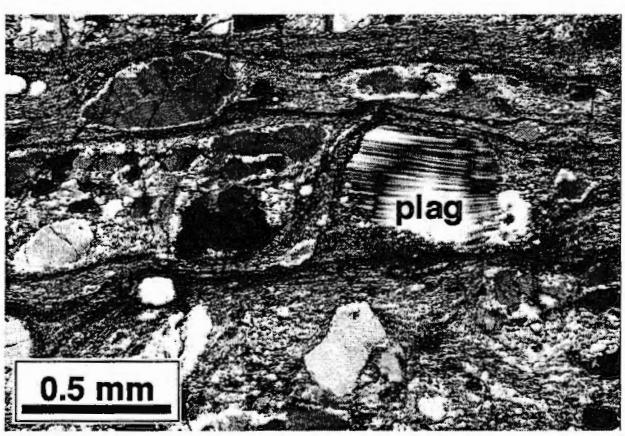

Figure 5.16: Photomicrograph (XPL) of a mylonite found within the plagioclase-peridotite domain in Othris. Note the flow of the fine-grained polyphase matrix around the plagioclase clast, suggesting that the plagioclase crystal is strong as compared to the matrix. See text for further discussion.

5.6.3. Implications for the strength of the mantle lithosphere

The case history of the Othris peridotite tectonites and mylonites illustrates how a reaction possibly involving a melt can eventually lead to strain weakening, shear localisation, and mylonite formation. This study shows that not only sub-solidus reactions (e.g., Newman *et al.*, 1999; Furusho and Kanagawa, 1999), but also melt-rock reactions can cause grain size reduction bringing olivine grains into the GSS creep field. The crucial issue is that the reaction involved not only produced small grains, but that it also led to intimate mixing of mineral phases which inhibited grain growth such as to preserve the fine grain sizes.

The ultimate effect of the process studied is extreme weakening. As discussed above, strain rates in the fine-grained, reaction-derived bands in the Othris mylonites may have been several orders of magnitude faster than the strain rate in the coarse-grained, recrystallisation-derived olivine lenses. The weakness of the Othris mylonites is further illustrated by figure 5.16,

showing a mylonite which developed in plagioclase-bearing peridotites. Plagioclase forms clasts in the fine-grained polyphase matrix, indicating that the fine-grained matrix is weaker than the plagioclase clast. Such a microstructure shows that mantle rocks transected by fine-grained mylonites deforming by GSS creep can be weaker than rocks whose rheology is controlled by dislocation creep of plagioclase (*e.g.*, lower crustal rocks). This suggests that under some conditions mantle rocks are weaker than lower crustal rocks, which is at variance with the commonly held perception that the shallow part of the mantle forms the strongest part of both the continental (*e.g.*, Kirby, 1983; Kuznir & Park, 1986; Rutter & Brodie, 1988) and oceanic (Chen & Morgan, 1990; Shaw & Lin, 1996; see also Hirth *et al.*, 1998 for discussion) lithosphere. The reduction of the bulk strength by the development of fine-grained mylonites can be of great importance to tectonic processes at ocean ridges. At magma-starved ocean ridges, as well as at slow-spreading ridges during a-magmatic stages of seafloor spreading, spreading is accomplished by stretching of the oceanic lithosphere (Lin & Parmentier, 1989; Cannat, 1993, 1996; Tucholke & Lin, 1994; Escartin *et al.*, 1997). Strength reduction due to the presence of peridotite mylonites may directly affect the rate of spreading in such settings. In addition, the structures and microstructures developed in the Othris massif show that during the onset of ophiolite emplacement, mylonite zones in the mantle may act as weak horizons along which slices of oceanic lithosphere may detach to eventually become emplaced as ophiolites.

5.7. Conclusions

Microstructural analysis of peridotite tectonites and mylonites in the Othris massif reveals a history of shear localisation which was associated with a change from dominant dislocation creep to grain-size sensitive (GSS) creep. The fine-grained olivine in the mylonite bands deforming by GSS creep was produced by a reaction involving a melt, which led to the replacement of orthopyroxene porphyroclasts by a fine-grained mixture of olivine and interstitial orthopyroxene. The well-mixed character of this fine-grained material precluded olivine grain growth, thus keeping grain sizes small. Microstructures suggest that only tiny fractions of secondary minerals are sufficient to pin grain boundaries. Ongoing deformation led to elongation and, finally, coalescence of the fine-grained domains into a continuous network of mechanically weak, fine-grained, polyphase bands controlling the deformation. The deformation in the mylonites and in the adjacent tectonites was probably associated with the onset of emplacement of the Othris Ophiolite in a transpressional environment, most likely in a near-ridge, transform-fault environment.

Chapter 6

A synthesis of tectonic and magmatic processes recorded in the Othris Peridotite Massif (Greece)

Abstract

Structural mapping and microstructural and petrological analysis of peridotites from the mantle section of the Tethyan Othris Ophiolite has revealed a multi-stage history of deformation and magmatism. The overall depleted, but clinopyroxene-bearing, compositions of the peridotites suggest that the first stage comprised partial melting and melt extraction during mantle upwelling underneath a slow-spreading ridge. Remnants of coarse, high temperature microstructures indicate that this stage was associated with low-stress deformation. Melting and low stress deformation ceased as the peridotites became part of the conductively cooled lithosphere. There is abundant petrographic evidence that interaction with melts, produced at deeper levels and percolating through the Othris harzburgites, caused melt-rock reactions followed by fractional crystallisation of mainly plagioclase, clinopyroxene, and orthopyroxene, locally producing plagioclase-peridotites. Microstructures show that melt impregnation was partly accompanied by deformation under lithospheric conditions, probably associated with extension or transtension in the mantle lithosphere in the vicinity of a transform fault. Based on analysis of fine-grained tectonite and mylonite microstructures, in combination with tentative assumptions regarding the original geometry of the ophiolite section, it is concluded that emplacement started in a sinistral transpressional setting, when the peridotites were still hot. Emplacement led to the formation of a km-wide peridotite mylonite zone. The later stages of emplacement and obduction were accommodated by serpentinite cataclasites, by a sub-ophiolitic metamorphic sole thrust, and finally by a mélange underlying the peridotites. The paleogeographic origin of the Othris Ophiolite is still a point of debate. An origin in a transform environment in either the Pindos or the Vardar Ocean is in agreement with the deformation history of the Othris peridotites deduced in the present study.

6.1. Introduction

Peridotites are regularly recovered from the ocean floor by dredging and submarine sampling (Dick *et al.*, 1984; Bonatti & Michael, 1989; Cannat *et al.*, 1995). These samples of the oceanic upper mantle provide valuable insights into the tectonic and magmatic processes taking place at depth underneath spreading centres. It has become clear that (serpentinised) mantle rocks can be found at relatively shallow levels or even exposed at the ocean floor, in particular at ridge-transform intersections at slow-spreading ridges (Karson *et al.*, 1987; Dick, 1989; Cannat *et al.*, 1992; Cannat, 1993, 1996; Auzende *et al.*, 1994). The

occurrence of mantle rocks at shallow levels can be explained by tectonic stretching of oceanic mantle lithosphere, causing exhumation of mantle rocks along detachment faults during spreading (Dick, 1989; Lin & Parmentier, 1989; Mutter & Karson, 1992; Cannat, 1993; Cannat *et al.*, 1995; Jaroslow *et al.*, 1996; Ranero & Reston, 1999). Alternatively, their exposure at the ocean floor may be due to a subordinate thickness, or even absence, of a magmatic crust as the result of limited magma production at depth or fractional crystallisation of melt within a layer of relatively cold mantle lithosphere (Cannat, 1993; Cannat, 1996; Ghose *et al.*, 1996; Sleep & Barth, 1997). The latter view is supported by the widespread evidence for magmatic impregnations in peridotite samples from the vicinity of transform faults at both slow- and fast-spreading ridges (Dick, 1989; Cannat *et al.*, 1990; Girardeau & Mercier, 1992; Bonatti *et al.*, 1992; Cannat *et al.*, 1992; Tartarotti *et al.*, 1995; Constantin, 1999).

Information about the scale and three-dimensional extent of such tectonic and magmatic processes can be obtained from structural and petrological studies of ophiolites, provided that the effects of emplacement and obduction can be recognised and distinguished from features related to spreading. Such studies have shown that a class of ophiolites exists which bear great similarity to the oceanic lithosphere at slow-spreading ridges. Ophiolites of this type (the Lherzolite Ophiolite Type, *e.g.*, Boudier & Nicolas, 1985/86; Nicolas, 1986a; Nicolas, 1989) comprise a relatively thin or absent magmatic crust, widespread evidence for deformation under lithospheric conditions in both crustal and mantle rocks, and relatively fertile residual mantle compositions.

The Othris Ophiolite of Central Greece is an example of such a lherzolite-type ophiolite which is

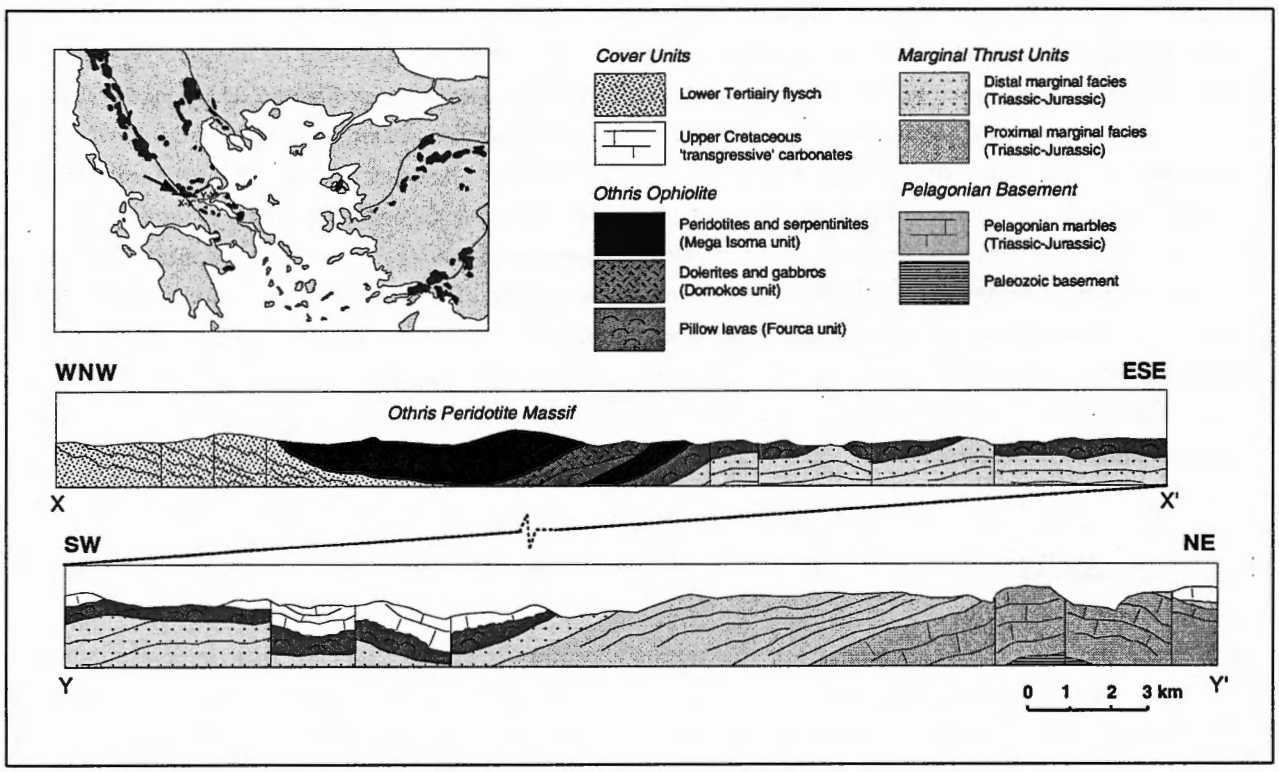

Figure 6.1: Cross-section across the Othris Mountains, redrawn from Ferrière (1985). Units after IGME (1962), Smith et al. (1975), and Ferrière (1985). Inset diagram shows location of cross-section and ophiolites in the Aegean region.

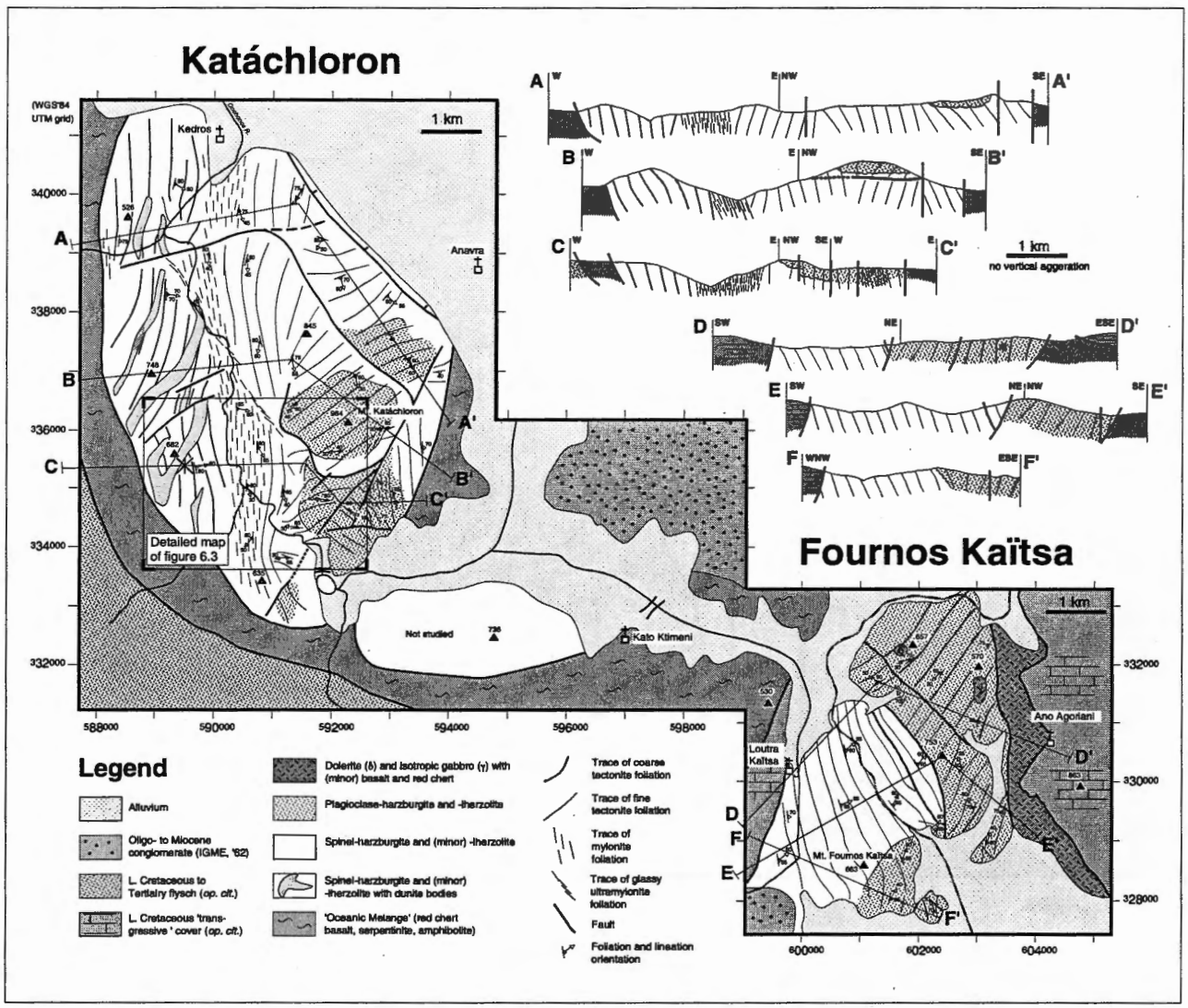

Figure 6.2: Maps and cross-sections showing peridotite structures and petrology. Outlines of large dunite bodies in western domain of the Katáchloron Massif are based on mapping and on a (photo-) geological map of Rassios (A. Rassios, personal communication, 1995). Distribution and ages of non-ophiolitic rocks based on geological map (IGME, 1962). Box outlines map area of figure 6.3.

thought to have originated in a slow-spreading environment (Menzies, 1973; Menzies & Allen, 1974; Boudier & Nicolas, 1985/86). This chapter summarises the results of a detailed structural and petrological study of the mantle section of this ophiolite. The study focuses on the interaction between the tectonic and magmatic processes which have left their imprint in the Othris peridotites. In addition, a tectonic framework for the emplacement of the ophiolite is presented.

6.2. Regional geology

The Othris Ophiolite represents a strongly dismembered fragment of oceanic lithosphere from the Mesozoic Neotethys ocean (Menzies, 1973; Menzies & Allen, 1974; Smith, 1993). The best preserved part is its mantle section, exposed in three separate bodies collectively known as the Othris Peridotite Massif. The ophiolitic rocks overly a series of thrust sheets (figure

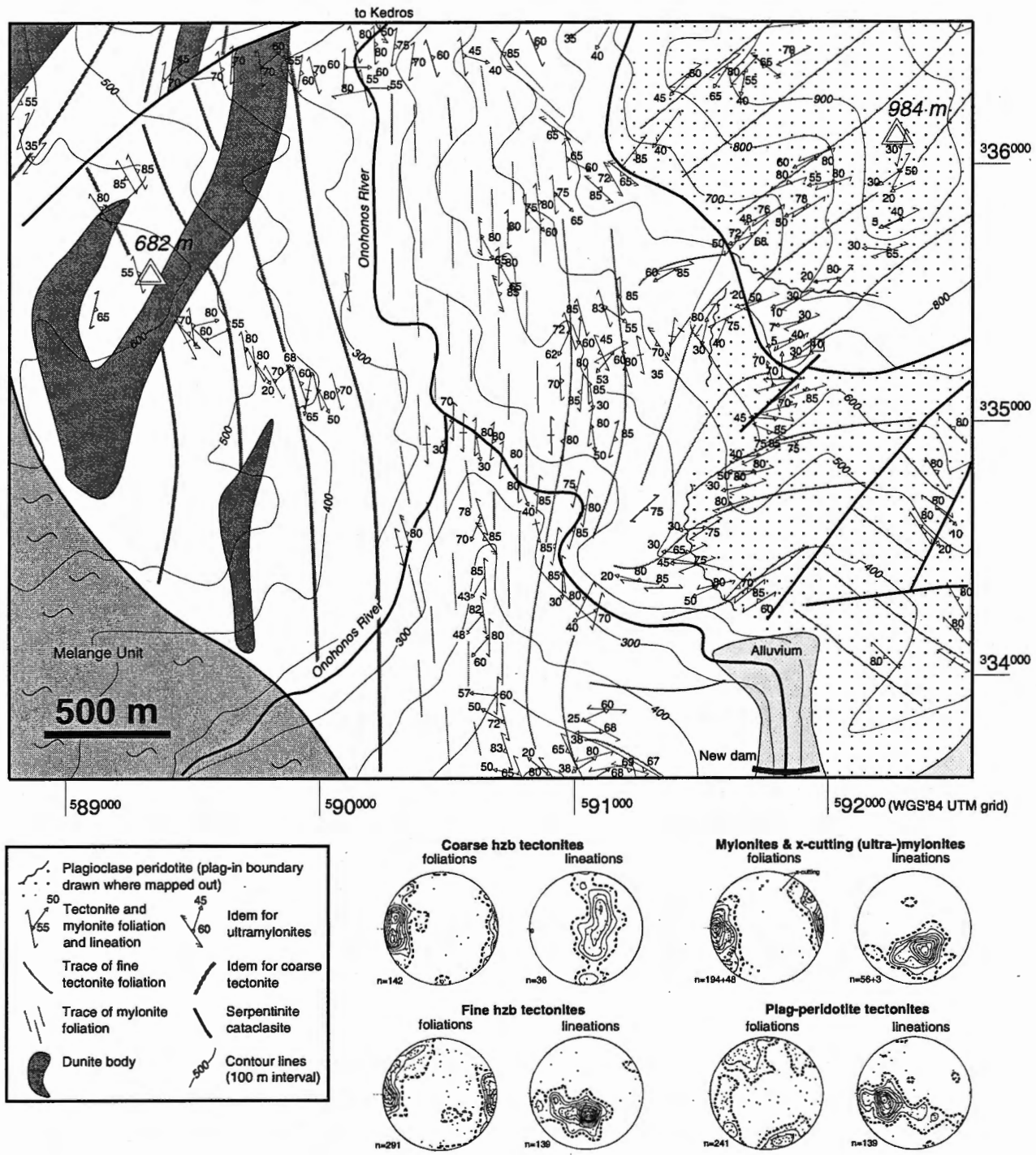

Figure 6.3: Detailed map of the southern part of the Katáchloron massif, showing mantle shear zone juxtaposing tectonite domains with different structural characteristics. Western domain consists of coarse-grained harzburgites containing large cross-cutting dunite bodies (dark grey). Eastern domain comprises fine-grained harzburgites grading up- as well as eastward into plagioclase-peridotites (stippled). Also shown are lower hemisphere, equal area projections of poles to foliations and lineations in tectonites and mylonites (contoured 1,2,3,.... times uniform).

6.1) which have the characteristics of an Upper Triassic-Jurassic passive margin sequence overlying Triassic volcanics associated with rifting; these thrust sheets were emplaced onto the Palaeozoic basement of the Pelagonian Zone in the Late Jurassic-Early Cretaceous (Hynes *et al.*, 1972; Smith *et al.*, 1975; Hynes, 1974a,b; Ferrière, 1985). Both the ophiolitic rocks and the underlying thrust sheets are unconformably overlain by an Upper Cretaceous (Cenomanian to Coniacian) transgressive cover (Hynes *et al.*, 1972; Smith *et al.*, 1975). The entire sequence has been thrust over ('Pindos') flysch of Late Cretaceous-Tertiary age (IGME, 1962; Faupl *et al.*, 1996).

At a few locations, strongly deformed and disrupted fragments of amphibolite-grade metamorphic rocks are found at the base of the peridotites (Spray & Roddick, 1980; Spray *et al.*, 1984). These rocks are thought to represent a sub-ophiolitic metamorphic sole which was formed during the onset of emplacement of the ophiolite. Their age has been established by $^{40}Ar/^{39}Ar$ dating as 169±4 Ma. This age is similar to the ages determined from the metamorphic soles of several other ophiolites along strike in Greece, Albania, and Former Yugoslavia (Spray *et al.*, 1984).

6.3. Structure and petrology of Othris peridotites

Two peridotite massifs (Katáchloron and Fournos Kaïtsa) have been mapped as part of this research project. A study of the third massif (Mega Isoma) focussing on emplacement-related structures and chromite mineralisation has been presented by Rassios & Konstantopoulou (1993).

The geometry of the Katáchloron massif is that of a km-wide N-S striking steep mantle shear zone juxtaposing two domains with different structural and petrological characteristics (figure 6.2 & 6.3), i.e., a western and an eastern domain. The western domain consists of coarse-grained harzburgites containing large, 10-100 m wide, dunite bodies cross-cutting the foliation in the harzburgites (figure 6.4a). These dunites contain cm-scale clusters of spinel, occasionally with remnants of orthopyroxene in their centres. Moreover, they enclose 1-50 m sized enclaves of foliated harzburgites. The peridotites exhibit coarse (1-3 mm) olivine microstructures with minor dynamic recrystallisation to a grain size of 0.1-0.7 mm (chapter 5). The eastern domain comprises fine-grained harzburgites, grading up- and eastward into plagioclase-bearing peridotites which form the top of Mt. Katáchloron. The harzburgites contain thin, cm- to m scale dunite bands which are generally parallel to the tectonite foliation. In two locations, small bodies were found which clearly cross-cut the foliation (figure 6.4b). In the harzburgites close to the N-S striking shear zone, dunites occur which are tightly folded with axial planes parallel to the tectonite foliation (figure 6.4g). Furthermore, 1-10 cm scale orthopyroxenites and websterites are found which are often folded, boudinaged, or both (figure 6.4h-j). The plagioclase-peridotites contain cm-thick troctolitic layers parallel to the tectonite foliation, 1-50 cm thick olivine-gabbros parallel or slightly oblique to the foliation, generally discordant 1-50 cm gabbro-norites, and thin (0.1-1 cm) concordant or discordant veins of plagioclase or plagioclase and clinopyroxene (figure 6.4c-f). Cross-cutting gabbro dykes are generally steep. Moreover, they contain numerous mm scale lenses of plagioclase ± clinopyroxene ± orthopyroxene (and sometimes amphibole) generally parallel to the tectonite foliation. Both the harzburgites and the plagioclase-peridotites have relatively fine-grained microstructures showing extensive dynamic recrystallisation of an originally coarse protolith to a grain size of 0.1-0.5 mm (chapter 4 & 5). Furthermore, they contain augen-shaped domains consisting of a mixture of fine-grained (10 μm-0.2 mm) olivine and orthopyroxene (and minor spinel and clinopyroxene) around orthopyroxene porphyroclasts (chapter 5). Where the N-S striking mantle shear zone is approached, these fine-grained augen become increasingly stretched.

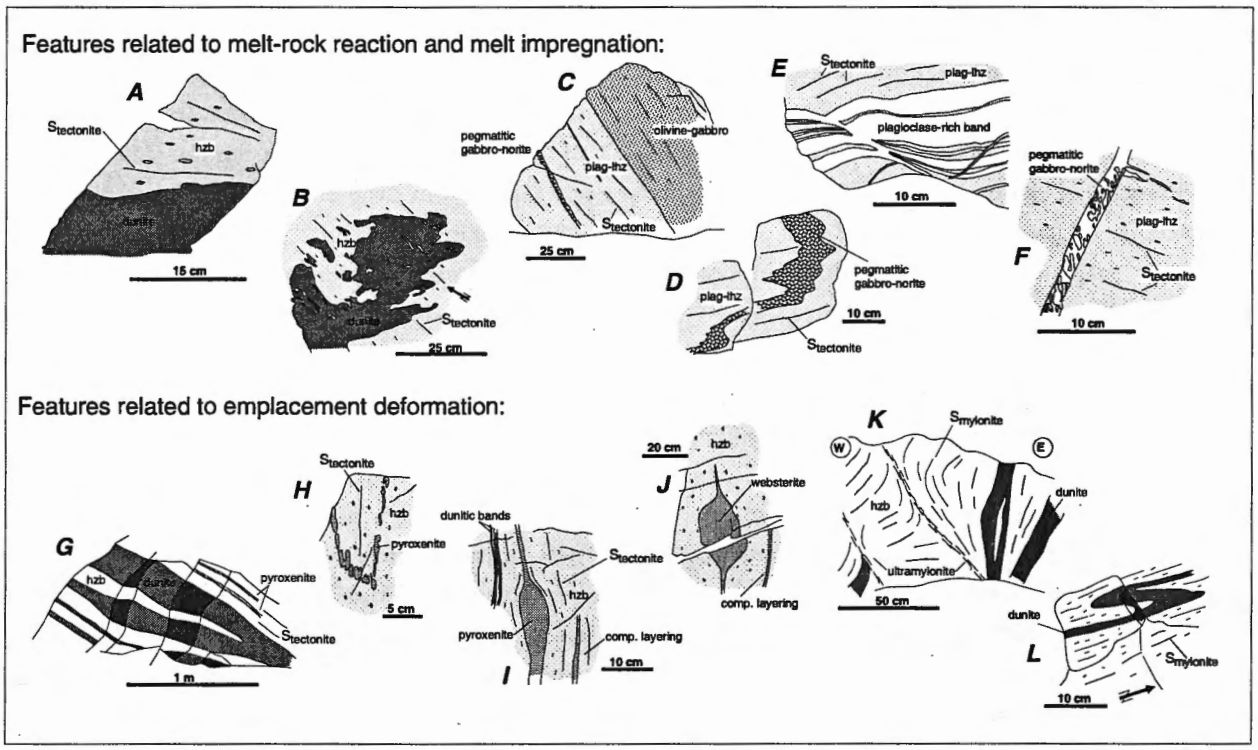

Figure 6.4: Deformation and magmatic features in Othris peridotites traced from photographs. See text for discussion.

The peridotites found in the Fournos Kaïtsa massif are broadly similar to those seen east of the mantle shear zone in the Katáchloron massif, and comprise harzburgites and plagioclase-peridotites. In the Fournos Kaïtsa massif, plagioclase-peridotites with a relatively coarse (1-2 mm) olivine microstructure occur in 1-50 m wide enclaves enclosed by finer-grained plagioclase-peridotites, as well as in a fault-bounded block in the southernmost part of the massif. In these rocks, plagioclase is found in 1-5 mm size, irregular amoeba-shaped blebs, often next to an orthopyroxene clast, rather than in small-scale lenses (as described in chapter 4). In the north-eastern part of the Fournos Kaïtsa massif, a fault-bounded block occurs of pervasively serpentinised plagioclase-peridotites in which plagioclase is completely altered to an assemblage of very fine-grained hydrogarnet and zoisite. These latter serpentinised peridotites are cross-cut by small doleritic dykes in which plagioclase is almost completely unaltered, suggesting that the serpentinisation predates dolerite intrusion and probably occurred close to the ocean floor (chapter 4).

The rocks of the N-S striking mantle shear zone in the Katáchloron massif consist of strongly foliated harzburgitic mylonites, with numerous dunite layers parallel to the mylonite foliation. Locally, the mylonites are cut by thin (1-50 cm) ultramylonites with a reverse-sinistral sense of shear (figure 6.4k). At some locations, large dunite bodies from the adjacent coarse domain to the west are seen to enter the shear zone and become strongly thinned and boudinaged. Locally, some of the dunite bands are folded, usually with an asymmetry indicating a sinistral-reverse sense of shear (figure 6.4l). Microstructurally, the mylonites are characterised by fine-grained (5-50 μm) bands mainly consisting of olivine and orthopyroxene enclosing small lenses of coarser (50 μm-0.5 mm) olivine (chapter 5). Strongly stretched and kinked orthopyroxene porphyroclasts occur within the fine-grained bands.

Finally, all of the peridotites are cut by steep NE-SW striking, and shallowly to moderately steep E-dipping, NW-SE striking serpentinite cataclasites, some of which are associated with strongly altered but clearly mylonitic peridotites.

The peridotites are underlain by a tectonic mélange consisting of basalts, red cherts, and serpentinised peridotite blocks, as well as fragments of amphibolitic meta-gabbros, which are probably remnants of the sub-ophiolitic metamorphic sole. The mélange unit is strongly deformed and in places shows a distinct foliation.

6.4. Deformation and magmatic history

Based on the structural, microstructural, and petrological characteristics of the Othris peridotites and their relative timing assessed by overprinting relationships, a deformational and magmatic history has been inferred which comprises the following stages (see also table 6.1):

(I) Melting and melt extraction. The majority of the Othris peridotites are clinopyroxene-bearing harzburgites, *i.e.*, they are residual, depleted mantle rocks which have undergone a stage of in-situ partial melting and melt extraction. The remnants found in some of the Othris peridotites of coarse olivine microstructures associated with this stage resemble so-called 'asthenospheric' microstructures (Ceuleneer *et al.*, 1988; Nicolas, 1986a, 1989; Ildefonse *et al.*, 1998a). They point to low-stress (<5 MPa) conditions during deformation, at temperatures around the peridotite solidus (>1250°C; Nicolas, 1986a, 1989).

(II) Melt-rock reaction and dunite formation. The presence of spinel clusters produced by break-down of orthopyroxene, as well as the presence of foliated harzburgitic enclaves in the large dunites in the western domain in the Katáchloron massif suggests a residual origin rather than an origin as cumulates produced by fractional crystallisation of olivine. Residual dunites are produced by reaction of an upward migrating

Table 6.1: Summary of magmatic and deformation processes in the Othris Peridotite Massif

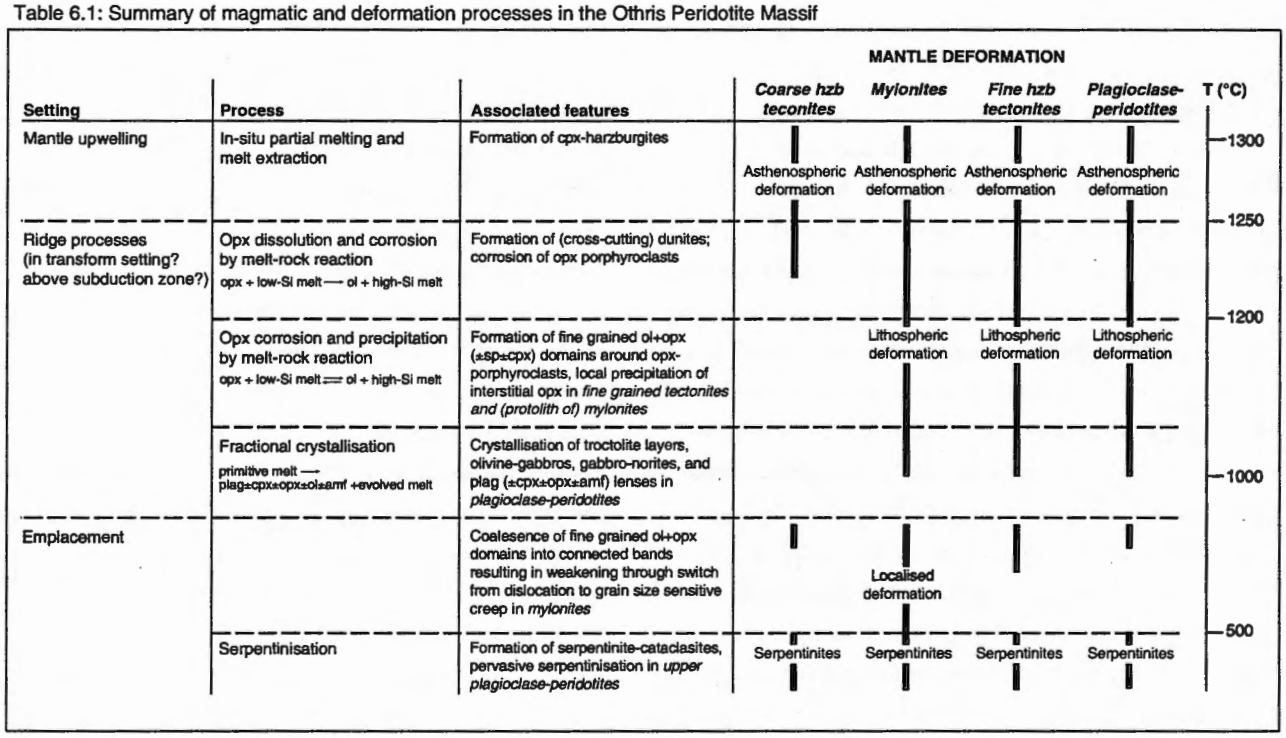

orthopyroxene-undersaturated basaltic melt with its harzburgitic host-rock (Kelemen, 1990). An origin by melt-rock reaction is further supported by the common occurrence of orthopyroxene clasts with irregular, corroded outlines and skeletal orthopyroxene crystals in the harzburgites of this domain, suggesting a *melt-producing* reaction of the form: orthopyroxene + low-Si melt → olivine + high-Si melt (chapter 5). Similar corroded orthopyroxene clasts also occur in the plagioclase-peridotites with coarse olivine microstructures found locally in the Fournos Kaïtsa massif. The dunites produced as the result of melt-rock reaction cross-cut the foliation in the harzburgite tectonites with coarse olivine microstructures in the Katáchloron massif, indicating that low-stress, high temperature deformation had ceased by the time these dunites were formed.

(III) Melt-rock reaction, melt-impregnation, and deformation in mantle lithosphere. The fine-grained harzburgites and plagioclase-peridotites occurring in the Fournos Kaïtsa massif and east of the mantle shear zone in the Katáchloron massif also bear evidence for melt-rock reaction (chapter 5). The fine-grained olivine-orthopyroxene domains around orthopyroxene porphyroclasts are thought to result from melt corrosion of orthopyroxene. Orthopyroxene found in interstices between olivine crystals and along low-angle (sub-) grain boundaries in olivine in the coarser grained olivine domains in the same rocks indicate local precipitation of orthopyroxene and/or replacement of olivine by orthopyroxene. Together, they point to a reaction of the form: orthopyroxene + low-Si melt ↔ olivine + high-Si melt. This reaction was locally *melt-producing* and locally *melt-consuming*, probably as the result of the melt being close to orthopyroxene saturation. The augen-shape of the fine-grained domains produced as a result of the reaction indicate that deformation accompanied this stage of melt-rock reaction. Furthermore, the presence along olivine low-angle (sub-) grain boundaries of orthopyroxene derived by melt-rock reaction indicates that melt-rock reaction was coeval with dynamic recrystallisation of olivine. The associated microstructures show that the deformation occurred at stresses of 5-38 MPa and at temperature between 1000-1200°C (chapter 4 & 5). These conditions correspond to those at the base of the thermal lithosphere. Coeval with, or slightly after this stage of melt-rock reaction, impregnating melts at higher levels in cooler rocks (now represented by the plagioclase-peridotites) fractionally crystallised plagioclase, clinopyroxene, orthopyroxene, possibly olivine, and minor amphibole in various types of gabbros and melt-lenses. The melt-derived plagioclase and clinopyroxene have a high anorthite content (An80-88) and high Mg# (90-93) respectively (chapter 4).The presence of discordant gabbros as well as the notion that the plagioclase in the small lenses is often only weakly or not deformed (chapter 4) both indicate that crystallisation continued after deformation ceased.

(IV) Strain localisation. The final stages of deformation under upper mantle conditions are mainly reflected in the mylonites from the shear zone in the Katáchloron massif, and in the tectonites directly adjacent to this shear zone. The folding and boudinage of most of the dunites and pyroxenites in the fine-grained harzburgite tectonites are attributed to this deformation. The onset of deformation led to increasing elongation of fine-grained olivine-orthopyroxene domains in the tectonites until these domains coalesced to form an interconnected network of fine-grained bands. This induced strain weakening, as the deformation - initially controlled by dislocation creep in the coarse-grained domains - became controlled by grain size sensitive creep in the fine-grained bands, leading to localisation of the strain into the mylonite shear zone (chapter 5). The mylonites were active at temperatures around 780°C but probably started to form at significantly higher temperatures (chapter 5).

6.5. Tectonic setting

The first stage described above comprising partial melting, melt extraction, and deformation under low-stress, high-temperature conditions probably represents decompression melting during upwelling underneath the Othris paleo-ridge. The preservation of clinopyroxene in the residue suggests moderate degrees of depletion. Clinopyroxene-bearing residual mantle rocks are commonly found at slow-spreading ridges, whereas clinopyroxene-poor harzburgites are typical for fast-spreading ridges (Michael & Bonatti, 1985; Constantin *et al.*, 1995). An origin in a slow-spreading setting is thus favoured for the Othris peridotites (chapter 4). When the Othris peridotites reached shallow levels underneath the spreading centre they likely became part of the conductively cooled lithosphere, and in-situ melting ceased. Because of the evidence that the base of the thermal lithosphere reached well into the mantle at the Othris ridge axis, it is concluded that the Othris massif originated in a particular cold part of a slow-spreading ridge system, *i.e.*, in a segment-end or transform fault environment. Melts produced at depth continued to percolate through the Othris peridotites on their way up, causing extensive melt-rock reaction. At higher levels, melt started to cool below their liquidus leading to fractional crystallisation of cumulate phases and to the formation of plagioclase-bearing peridotites (chapter 4). The high anorthite content of plagioclase and the high Mg# of clinopyroxene in the small lenses can be explained by crystallisation from a melt with a depleted or ultra-depleted composition. Such melts represent the last melt fractions of shallow-level partial melting of already depleted mantle rocks, and are occasionally found as melt inclusions in mid-ocean ridge basalts (Sobolev & Shimizu, 1993; Ross & Elthon, 1993). However, the compositions of the melt-derived plagioclase and clinopyroxene are also in agreement with an origin from a melt with boninitic composition. Boninites are produced by re-melting of hydrated harzburgites and are commonly found in supra-subduction zone environments (Crawford *et al.*, 1989).

The origin of the deformation partly accompanying melt-rock reaction and fractional crystallisation is difficult to assess. The widespread evidence for the presence of an impregnating melt suggest a tensional (spreading) environment. Tectonite foliations produced during this stage are generally steep, NE-SW striking (see stereoplots in figure 6.3 as well as in figure 4.2), but as a result of the strong dismemberment of the Othris peridotite it is difficult to unambiguously relate the present-day orientations of the structures to their original, *i.e.*, intra-oceanic, geometrical framework. However, the plagioclase-in boundary is interpreted as the plane in pressure-temperature space at which the impregnating melt became saturated in plagioclase, and the plagioclase-peridotites must represent the low-pressure, low-temperature side of that boundary (chapter 4). In the present-day geometry of the massif, the plagioclase-peridotites are found at the highest levels and the plagioclase-in boundary is relatively shallowly dipping in the Katáchloron area. This limits the extent to which the Othris peridotites may have undergone tectonic rotations around subhorizontal axes during or after their emplacement. In addition, the present-day steep orientations of cross-cutting gabbroic veins and dykes in the plagioclase-peridotites (see for instance the stereoplot in figure 4.2) also suggest limited magnitudes of rotation. Against these observations, and because least compressive stresses at ridges have subhorizontal orientations, it is likely that the present-day steep foliations, produced during deformation coeval with melt-rock reaction and melt impregnation, indeed developed as steep structures within the original intra-oceanic geometry. Steep foliations are typically found in ophiolites thought to be derived from slow-spreading ridges (Boudier & Nicolas, 1985/86; Nicolas, 1986a; Nicolas, 1989) and they may represent steep flow planes in the mantle in the vicinity of transform faults.

Shear senses (derived from crystal fabric analysis) in the N-S striking tectonites directly adjacent to the

mylonite shear zone in the Katáchloron massif indicate deformation with a large reverse component with respect to the present-day geometric framework (chapter 5). Similarly, the mylonites record deformation with a large sinistral strike-slip component in combination with a reverse component (chapter 5). In view of the inferences made above with regard to the original geometry it is most likely that the structures in these tectonites and mylonites are the result of sinistral transpressional deformation, most probably related to the early stages of emplacement of the Othris ophiolite. During later stages of emplacement and obduction, deformation became focussed in serpentinite cataclasites, in the metamorphic sole and, finally, in the rocks of the mélange units directly underneath the peridotites.

6.6. Paleogeography

The age of the ophiolite is constrained by the age derived from the emplacement-related metamorphic sole (Middle Jurassic). The high metamorphic grade of these rocks, up to garnet-amphibolite facies, indicates that during emplacement the overriding peridotites were still young and hot. This interpretation is supported by the results presented above suggesting that the initial stage of emplacement was recorded in peridotite tectonites and mylonites at relatively high temperatures (>780°C – chapter 5). It is thus likely that the Othris Ophiolite was both formed and emplaced in the Middle Jurassic.

The paleogeographic origin of the Othris Ophiolite within the Neotethys is debated (*e.g.*, Smith, 1993). One view often held is that the Othris Ophiolite formed in the Pindos Ocean, a relatively narrow oceanic basin lying west of the Pelagonian microcontinent, at a 'Mid-Pindos' ridge or above a subduction zone (as proposed for the Vourinos Ophiolite which probably originated in the same ocean, Noiret *et al.*, 1981). Formation of the Othris Ophiolites at the inception of opening of the Pindos Ocean (Menzies & Allen, 1974) is not in agreement with a 'hot emplacement' scenario. An origin in the Pindos Ocean is supported by the palinspastic reconstruction of the ophiolite and underlying thrust

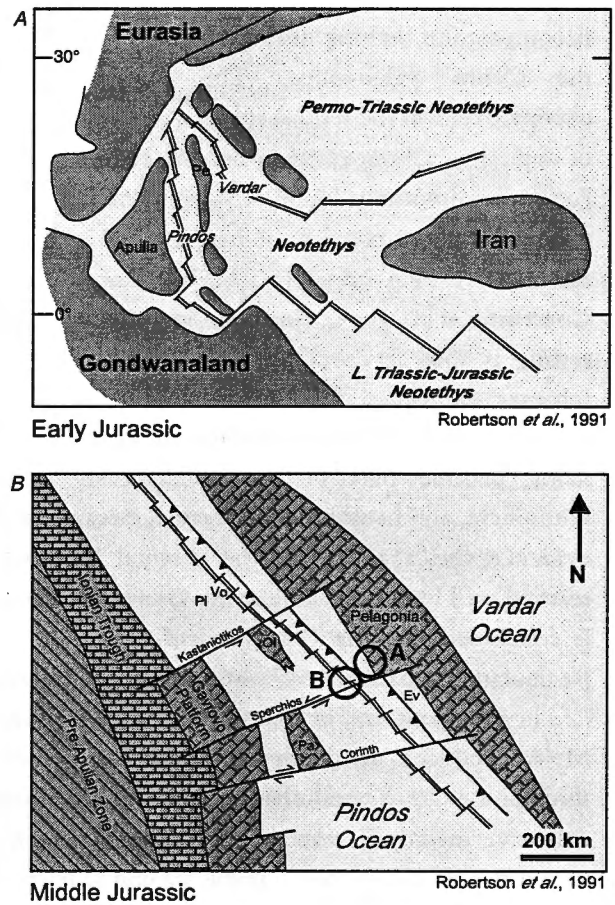

Figure 6.5: Paleogeographic reconstructions of Robertson et al. (1991) of Neotethys region. A) Narrow Pindos and Vardar oceanic basins in Early Jurassic. Reconstruction B) shows detailed map of Pindos Ocean around the time of the emplacement of the Othris Ophiolite (Middle Jurassic). Circle denoted with bold 'A' shows location of Othris according to Robertson et al. (1991) at the eastern (passive) margin of the Pindos Ocean suggesting formation of Othris at the inception of the opening of the Pindos Ocean. Such an origin is not in agreement with 'hot emplacement' scenario required to account for the high temperature of initial emplacement (see text for discussion). Therefore, a preferred origin of the Othris Ophiolite is indicated by circle 'B'. Note that the Othris Ophiolite is formed in the vicinity of a large sinistral transform fault and that emplacement of the ophiolite may have involved sinistral transpression. Proposed locations of other Greek ophiolites (Vo=Vourinos, Pi=Pindos, Ev=Evia) and of Olympos (Ol) and Parnassos (Pa) platforms are shown as well.

sheets by Smith *et al.* (1975), showing a westward facing passive margin on the western side of the Pelagonian microcontinent changing laterally into an ocean basin (represented by the Othris Ophiolite). A paleogeographic reconstruction of the Pindos Ocean by Robertson *et al.* (1991) is given in figure 6.5a-b.

An alternative view is that the Othris Ophiolite originated in the Vardar Ocean, lying east of the Pelagonian microcontinent (*e.g.*, Ferrière, 1985). The paleogeographic reconstruction of the Vardar Ocean by Stampfli *et al.* (1998) is shown in figure 6.6a-b. This particular reconstruction shows the Vardar Ocean as a supra-subduction zone ocean. As outlined above, such an origin cannot be ruled out by the results of this study because of the possibility that the melt lenses described crystallised from boninitic melts. Interestingly, both reconstructions shown provide a framework which can adequately account for the tectonic history of the Othris Ophiolite proposed in this study, involving the initial emplacement of the ophiolite in a sinistral transpressional zone which originated as an intra-oceanic transform fault (figure 6.5b and 6.6b).

6.7. Discussion and conclusions

The Othris peridotites have recorded a multi-stage history of deformation and magmatism. An early stage of upwelling and melting underneath a slow-spreading ridge was followed by melt-rock reactions and fractional crystallisation of an impregnating melt when the peridotites had become part of the conductively cooled lithosphere, probably in a (near-) transform setting. These results support hypotheses involving partial crystallisation of melt within the relatively cold lithospheric roots of transform faults at slow-spreading ridges (Cannat, 1993; Cannat, 1996; Ghose *et al.*, 1996; Sleep & Barth, 1997). Ophiolite emplacement started in a transpressional environment which led to the formation of a large, km-scale mantle shear zone. Later deformation related to emplacement and obduction was localised in serpentinite cataclasites, in the metamorphic sole of the ophiolite, and finally, in the mélange unit underlying the peridotites.

Whether the Othris Ophiolite originated at a mid-ocean ridge or at a ridge in a supra-subduction zone environment is still a point of contention. The compositions of the cumulate plagioclase and clinopyroxene can be explained by fractional crystallisation of either (ultra-) depleted melts, which are found at mid-ocean ridges, or of boninitic melts

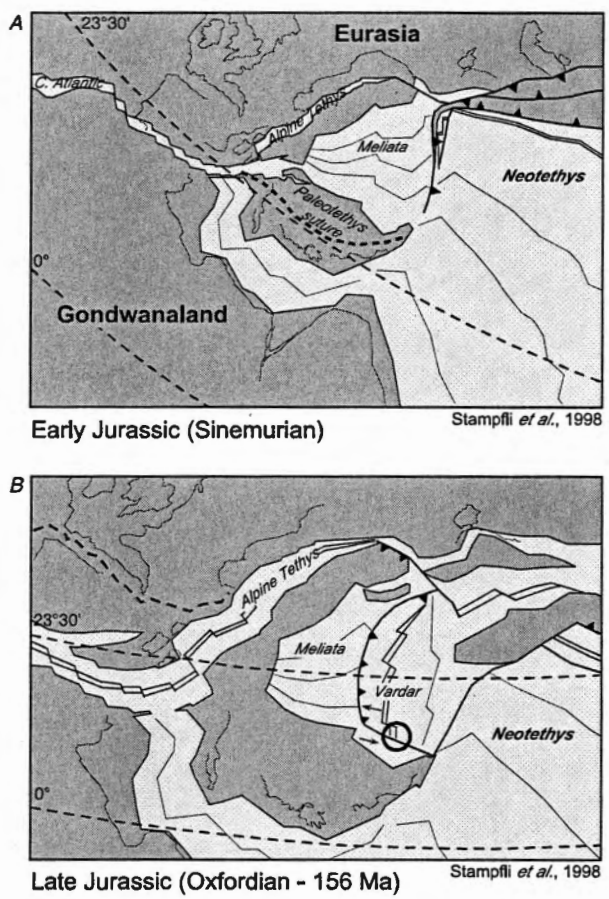

Figure 6.6: Paleogeographic reconstructions of Stampfli et al. (1998) of Neotethys region. Small arrows have been added to indicate relative plate motions. A) Early Jurassic reconstruction showing initiation of intra-oceanic subduction and opening of a supra-subduction Vardar Ocean. B) Late Jurassic reconstruction just after the time of emplacement of the Othris Ophiolite. In this reconstruction the Othris Ophiolite formed by supra-subduction zone spreading in the Vardar Ocean and is emplaced along a large sinistral transpressional transform fault.

which are typical for fore-arc environments. In this context it is noted that lavas with boninitic compositions are occasionally found in the Othris mountains (Cameron *et al.*, 1979), but their relation with the Othris peridotites is unknown.

The paleogeographic origin of the Othris Ophiolite is unresolved. It may have been part of the narrow Pindos Ocean or alternatively, it may have formed in the (supra-subduction) Vardar Ocean. Both models are in good agreement with the deformation history of the Othris peridotites.

Chapter 7

Melt weakening and the nature of the seismic crust and Moho at fast- and slow-spreading ridges: Discussion and concluding remarks

7.1. Introduction

This chapter provides a synthesis of conclusions and ideas based on the results presented in this thesis. The first two sections deal with melt weakening of peridotites, in particular with the factors that are thought to govern melt weakening in natural mantle rocks in the Hilti Massif in Oman, and in the Othris Massif in Greece, and with ideas concerning the process of indirect melt weakening. In the last section the implications of a relatively thick conductively cooled lithosphere at a slow-spreading ridge-transform intersection are explored. It is argued that such a cold structure has a profound effect on the nature of the oceanic and seismic crust, and on the strength of the lithosphere at ocean ridges.

7.2. Melt weakening

7.2.1. Melt weakening in the Hilti and Othris mantle sections

The principal scope of this project was to establish whether melt weakening of olivine rocks observed in experiments does also occur in nature. In chapter 2 and 3 it has been shown that there is indeed good evidence that melt weakening played a role in the deformation of the upper mantle peridotites just below the crust-mantle boundary in the Hilti Massif in Oman. In contrast, no clear indications have been found to demonstrate melt weakening in the mantle section of the Othris Ophiolite in Greece. The main problem in assessing possible effects of melt weakening in Othris is the fact that no particularly melt-rich domain or horizon could be identified, as *all* of the peridotites in Othris contain evidence for the presence of melts during some stage of their evolution. Melt weakening may have been operative at Othris, but it simply did not lead to obvious localisation of strain in melt-rich zones, which has been the main criterion for the recognition of melt weakening in this thesis. There are, however, a number of principal differences between Othris and Hilti with respect to the behaviour of melts that may have been important and may have precluded melt weakening in Othris. In this chapter, the factors which are thought to govern melt weakening will be evaluated for both the Hilti and Othris case.

(I) First, melt weakening in experiments has only been found to occur at deformation conditions close to the mechanism boundary between dislocation and grain size sensitive creep (Hirth and Kohlstedt, 1995a,b; Bai

et al., 1997). In Hilti, melt weakening occurred at temperatures of 1200-1250°C and stresses of 4-10 MPa (chapter 2 & 3). These conditions do indeed correspond to conditions close to the mechanism boundary (figure 7.1a). In Othris, there is evidence for the presence of melts in rocks deforming at temperatures of 1000-1200°C, at stresses of 5-38 MPa (chapter 4 & 5). These conditions also correspond to conditions close to the mechanism boundary (figure 7.2a). It follows that, based on the deformation conditions alone, there is no reason why melt weakening should not have played a role in the Othris peridotites.

(II) Secondly, for significant melt weakening to occur in olivine rocks under experimental conditions it seems that a critical melt fraction needs to be present. This critical melt fraction is approximately 4% in the olivine-basalt system (Hirth and Kohlstedt, 1995a,b; Bai *et al.*, 1997). In chapter 1 and 2 it has been discussed that such high melt fractions are not normally thought to occur in natural mantle rocks. In Hilti, however, melt probably accumulated just below the crust mantle boundary (chapter 2). Melt accumulation may have occurred in response to four different causes, *i.e.*, the presence of a permeability barrier due to fractional crystallisation of plagioclase in the lower crust and uppermost mantle which caused clogging of the porosity (Kelemen & Aharonov, 1998), a reduced vertical permeability as the result of the subhorizontal orientation of the olivine (010) planes (Daines & Kohlstedt, 1997), melt concentration into fine-grained domains (Wark & Watson, 2000), or retention of melt in a deformation zone due to piezometric pressure gradients (Rabinowicz *et al.*, 1987). In Othris, it is possible that a permeability barrier existed as the result of plagioclase (and possibly also clinopyroxene and orthopyroxene) crystallisation, causing melt accumulation in the rocks below it (the fine-grained harzburgite tectonites). Anisotropic permeabilities due to preferred alignment of olivine crystal planes did probably not cause significant melt accumulation in the Othris peridotites. In Othris, foliation planes produced by the deformation in the presence of a melt were probably steep, and so were the olivine (010) planes. Melts preferentially wetting (010) planes would therefore have been well connected in a vertical direction and, driven by their buoyancy, could have escaped easily (figure 7.2). In Othris, large grain size

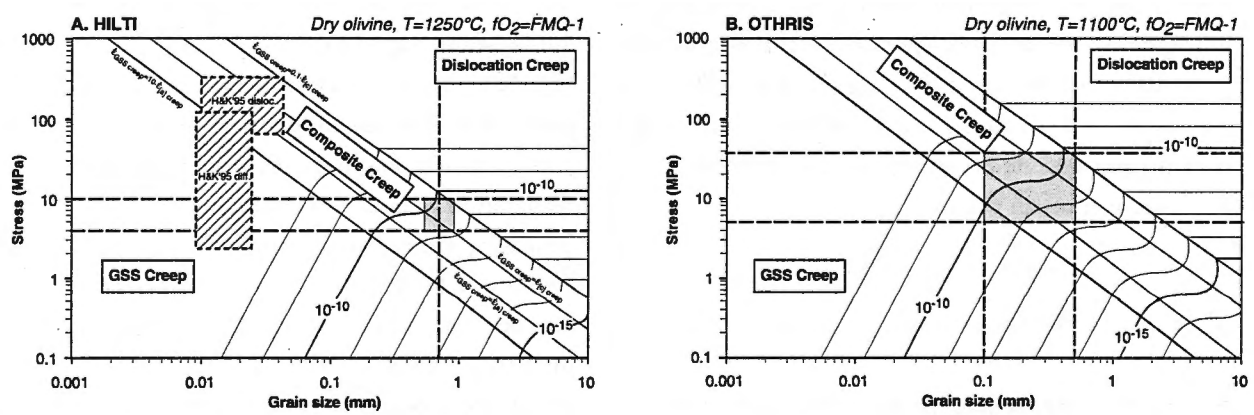

Figure 7.1: Deformation mechanism maps for (A) the peridotites just below the crust-mantle boundary in the Hilti Massif (Oman) and (B) for the fine-grained tectonites in the Othris Massif (Greece). See figure 5.14 for details about the construction of these maps. Hatched boxes indicate the deformation conditions of the deformation experiments of Hirth & Kohlstedt (1995a,b) in which melt weakening was found to occur. Both in Hilti and Othris, the deformation conditions (grey boxes) were close to the transition from dislocation to GSS creep. Grain sizes, temperatures, and stresses are based on results of chapter 2 for Hilti and chapters 4 and 5 for Othris.

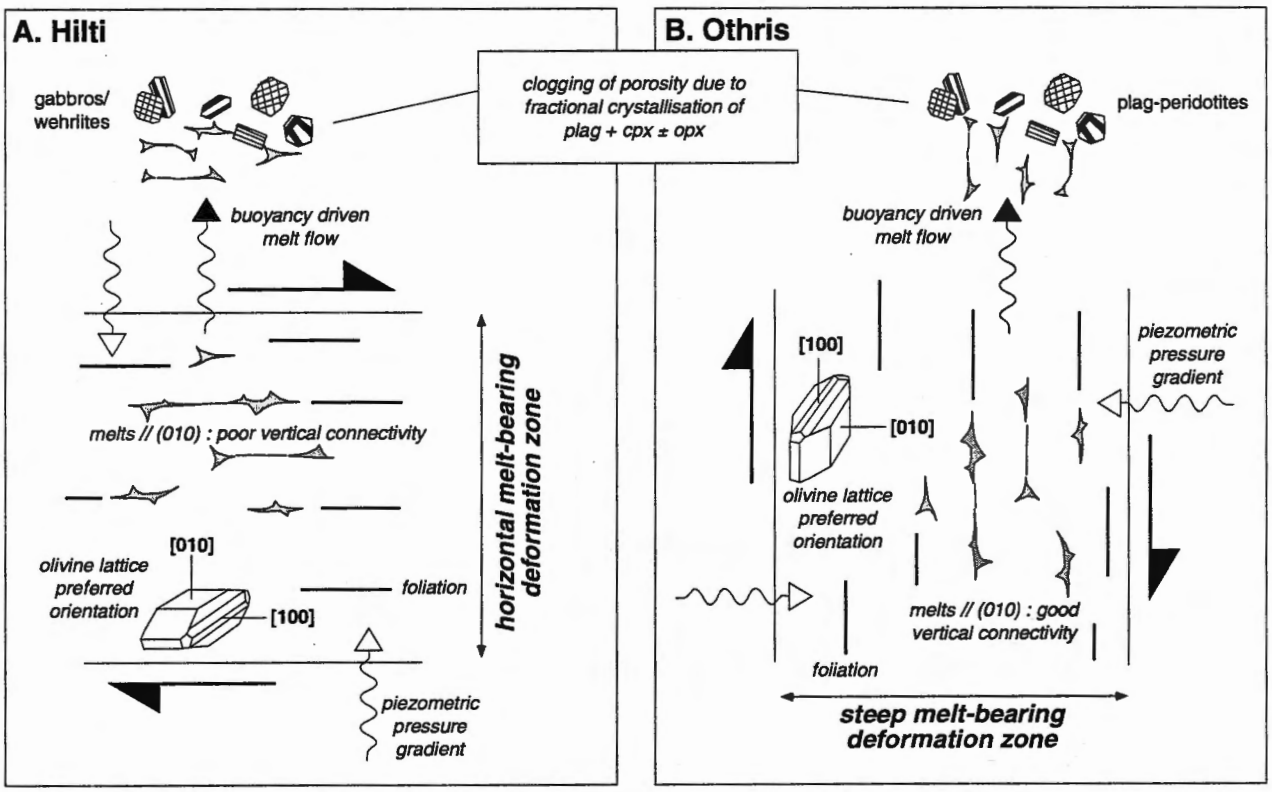

Figure 7.2: Synoptic diagram showing the processes that may have governed melt accumulation in high-strain zones in Hilti and Othris, which comprise buoyancy, permeability, anisotropy, and piezometric effects. Not shown is the effect of grain size variations: melt is predicted to be concentrated in fine-grained domains. See text for discussion.

variations exist - on a regional scale - between coarse tectonites, fine tectonites, and mylonites, as well as between coarse- fine-grained domains within tectonites, *i.e.*, down to local or sample scale. Melts preferentially residing in fine-grained rocks could easily have become concentrated as a result of these grain size variations. Finally, as the result of the steep orientations of the mantle flow planes, horizontal piezometric gradients could have existed in Othris, possibly 'sucking in' melt sideways into deformation zones. The effect of such pressure gradients would not have been as large as in Hilti where mantle flow planes were oriented horizontally causing vertical pressure gradients which act *against* melt buoyancy. However, it has been demonstrated in the Josephine Ophiolite that horizontal pressure gradients could still cause melt accumulation leading to melt weakening and strain localisation in steep shear zones (Kelemen & Dick, 1995). In short, it is possible that fractional crystallisation, grain size variations, and piezometric pressure gradients caused melts to pool in large enough amounts to lead to melt weakening in Othris. Support for the presence of relatively high melt fractions in Othris comes from the widespread evidence for reactions between the host peridotites and melts, leading to changes in the modal composition of the host rocks. Such effects are more likely to occur in rocks containing high 'instantaneous' melt fractions, whereas chromatographic effects causing changes in trace element concentrations are thought to dominate in rocks containing small melt fractions (*e.g.*, Godard *et al.*, 1995; Van der Wal & Bodinier, 1996). The question remains, however, whether melt fractions were high enough in Othris to cause significant melt weakening.

(III) Thirdly, because the most likely cause for melt weakening involves enhancement of intergranular

Table 7.1: Compilation of mantle melt compositions (and granite for comparison), melt viscosities and (relative) diffusion coefficients

	melts used in experiments			natural and theoretical melts								
	synthetic basalt *(Cooper & Kohlstedt, 1984; Hirth & Kohlstedt, 1995a)*	'MORB' *(Daines & Kohlstedt, 1993; Hirth & Kohlstedt, 1995a,b)*	natural basalt *(Waff & Faul, 1992)*	picrite (Tortuga ophiolite) *(Kelemen, 1990; Elthon & Scarfe, 1984)*	primitive MORB (Famous) *(Langmuir et al., 1977; Bender et al., 1978)*	evolved MORB (MARK) *('desired end point comp.', table 4, Grove et al., 1992)*	1% melt fraction from MORB source[#]	ultra depleted melt (MAR) *(Sobolev & Shimizu, 1993)*	high-Ca boninite (Troodos) *(Van der Laan et al., 1989)*	low-Ca boninite (Cape Vogel) *(Van der Laan et al., 1989)*	early partial melt from sp-lhz *(Raterron et al., 1997)*	granite *(Bottinga & Weill, 1972)*
oxide wt%												
SiO_2	50.71	50.02	45.33	47.25	48.60	50.37	50.72	52.90	54.93	59.34	66.0	70.18
TiO_2	0.01	1.55	2.32	0.79	0.61	2.05	1.44	0.29	0.51	0.51		0.39
Al_2O_3	14.01	15.63	11.73	13.64	16.30	15.67	21.02	15.50	13.15	10.62	24.1	14.47
Fe_2O_3					0.33			0.70				1.57
FeO	10.50[†]	9.24[†]	12.10[†]	9.77[†]	8.40	11.23[†]	6.82[†]	6.40	8.20[†]	9.27[†]	0.3[†]	1.78
MnO			0.17	0.14	0.15			0.08			0.0	0.12
MgO	8.64	9.09	12.96	17.61	10.20	7.20	9.45	10.50	11.52	12.57	0.0	0.88
CaO	13.04	11.51	10.36	9.58	12.30	10.89	5.97	12.50	10.21	5.74	4.9	1.99
Na_2O	2.96	3.12	2.31	0.89	1.90	2.76	4.58	1.12	1.17	1.37	4.6	3.48
K_2O		0.27	0.78	0.06	0.07	0.13		0.00				4.11
P_2O_5		0.21	0.33									0.19
(anhydrous) melt viscosity at 1250°C calculated using empirical model of Bottinga & Weill (1972)												
$XSiO_2$	0.55	0.55	0.49	0.50	0.55	0.57	0.58	0.59	0.59	0.62	0.74	0.79
η (Pa·s)	23.5	23.3	7.2	6.9	19.6	30.0	68.1	37.7	37.8	56.2	$1.54 \cdot 10^4$	$1.23 \cdot 10^4$
'diffusivity' at 1250°C approximated by Stokes-Einstein equation: $D=kT/6\eta r$ [!]												
$D \cdot r$ (m^3/s)[!]	$4.8 \cdot 10^{-24}$	$4.9 \cdot 10^{-24}$	$1.6 \cdot 10^{-23}$	$1.6 \cdot 10^{-23}$	$5.8 \cdot 10^{-24}$	$3.8 \cdot 10^{-24}$	$1.7 \cdot 10^{-24}$	$3.0 \cdot 10^{-24}$	$3.0 \cdot 10^{-24}$	$2.0 \cdot 10^{-24}$	$7.3 \cdot 10^{-27}$	$9.2 \cdot 10^{-27}$
relative $D \cdot r$[*]	100	101	328	341	120	78.6	34.6	62.5	62.2	41.9	0.150	0.190

[†] No distinction made between ferric and ferrous iron
[#] Calculated using bulk distribution coefficients and preferred MORB source of Niu (1997) and standard batch melting equation
[!] D=diffusion constant, k=Boltzmann's constant, η=viscosity in poise (1 poise=0.1 Pa·s), r=effective radius (r) of diffusing species
[*] Relative to 'diffusivity' in the synthetic basalt of Cooper & Kohlstedt (1984), which is set to 100.

diffusion processes (chapter 2), melt probably has to be present in pores and in melt films along grain boundaries to affect the strength of the host rock significantly. In the Hilti mantle section, this condition is probably met as cumulate clinopyroxene and plagioclase which crystallised from a melt are mainly found in grain interstices (chapter 2). In the plagioclase-peridotites in Othris, however, melt-derived plagioclase and clinopyroxene are mainly found in mm-scale lenses and veinlets (chapter 4). This leads to the suggestion that melt flow in lenses, possibly small-scale fractures, was the dominant melt transport mechanism in Othris, as opposed to porous flow in Hilti. In addition, the plagioclase-peridotites in Othris probably represent the last stages of melt infiltration, when the peridotites had cooled significantly below their solidus and deformation rates decreased (chapter 4 & 6). Under those conditions, accommodation of volume changes in the host rock associated with melt input or melt extraction (and fractional crystallisation) may have required the formation of small fractures. However, evidence for a phase of melt-rock reactions prior to fractional crystallisation of plagioclase and clinopyroxene is present throughout the plagioclase-peridotites and fine-grained harzburgites. These reactions require that melt was present in pores and melt films, as reactions between melt flowing in fractures and host peridotites are spatially limited (*e.g.*, Menzies & Hawkesworth, 1987; Bodinier *et al.*, 1990; Van der Wal & Bodinier, 1996). This shows that during the early stages of melt infiltration in the Othris peridotites, melt transport must have occurred by porous flow and that melt weakening may have played a role.

(IV) Finally, because of the role of intergranular diffusion processes, the composition of the interstitial melt could affect melt weakening. De Kloe (2001) has pointed out that melt composition, more specifically melt viscosities, could exert an important control on diffusion rates through the melt phase, and therefore on the magnitude of the melt-weakening effect. De Kloe (2001) showed that for different reported compositions of basaltic melts used in deformation and melt distribution experiments, viscosity and relative diffusion rate variations of a factor 4 would be expected. Table 7.1 shows the effect of compositions of a set of experimental, natural, and theoretical melts on melt viscosity and melt diffusivity. Viscosities are calculated using the empirical relation between melt composition (most importantly the SiO_2 content) and viscosity of Bottinga and Weill (1972) which is based on network-builder/network-modifier concept. The compilation shows that relative diffusion rates through typical basaltic melts (MORB, depleted MORB, boninite) are expected to vary by a factor 2-3. Whether the interstitial melts in Othris were of (depleted) MORB or boninite composition would therefore not have been very important for melt weakening. However, diffusion through picritic basalts, derived by high degrees of partial melting, is expected to be significantly faster, whereas diffusion through the very first fractions of partial melting of fertile mantle material (calculated 1% melt fraction and 'early partial melt') is significantly slower than MORB-like basalts. Therefore, the first melt fractions produced by in-situ partial melting of a lherzolitic source would probably not have a large weakening effect on mantle rocks, whereas the weakening effect of picritic melts could be large (as a tentative corollary, it could be concluded that the weakening effect of picritic to komatiitic melts produced at spreading ridges in Archaean times was larger than that of modern MORBs).

7.2.2. 'Indirect' melt weakening

In chapter 5 it has been shown that melts probably *did* induce melt weakening in Othris, but only in an *indirect* way. A fine-grained mixture of olivine and orthopyroxene was produced as the result of melt reacting with orthopyroxene clasts. The fine grain sizes caused a switch from dislocation creep to grain size

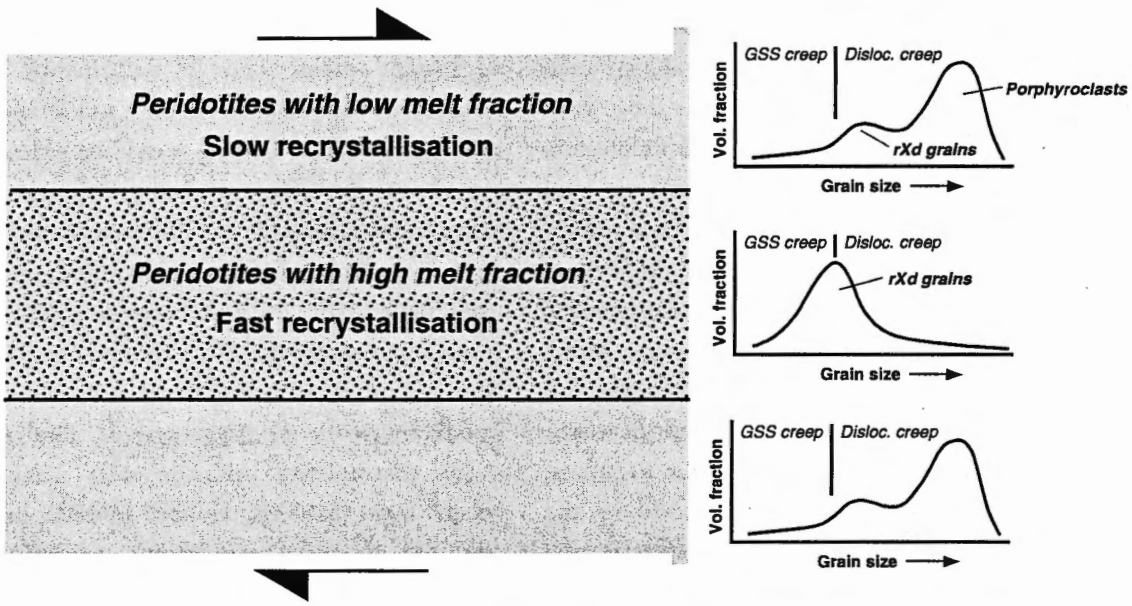

Figure 7.3: Schematic representation of indirect weakening caused by faster rates of recrystallisation and smaller recrystallised grain size in melt-rich deformation zones. Histograms represent grain size distributions in and adjacent to a melt-rich zone. See text for discussion.

sensitive creep when the fine-grained domains coalesced to form a continuous network. It is inferred that the weakening associated with this change in dominant deformation mechanism led to strain localisation in a km-wide, peridotite mylonite zone.

Similarly, there is another effect which can produce melt weakening in an indirect way. Microstructures described in chapter 5 suggest that during dynamic recrystallisation melts are able to penetrate along olivine subgrain boundaries or low-angle grain boundaries. In Othris, this process caused the crystallisation of orthopyroxene along such boundaries. Detailed microstructural analysis of experimentally deformed melt-bearing olivine-orthopyroxene aggregates show that melts can wet subgrain boundaries or form melt pockets at subgrain triple-junctions (De Kloe, 2001). It is likely that this process will effect dynamic recrystallisation. Melt present along subgrain boundaries could enhance the mobility of such boundaries, effectively turning subgrain boundaries into (low-angle) grain boundaries at small misorientations, thus possibly enhancing recrystallisation rates. It could also cause a decrease of the recrystallised grain size due to pinning of newly formed grain boundaries by melt (*e.g.*, Hirth & Kohlstedt, 1995b) or crystallisation products. If deformation conditions are close to the deformation mechanism boundary between dislocation and grain size sensitive creep, then fast recrystallisation to a relatively small grain size should, at least in theory, be able to induce weakening as a result of an increased contribution from grain size sensitive creep, leading to strain localisation in melt-rich zones (figure 7.3). Melt would then be drawn to the high-strain zone due to its small grain size and due to piezometric effects (see above), leading to a positive feedback between deformation and melt accumulation, without *direct* melt weakening as found in experiments. Note, however, that this microphysical process did *not* cause the weakening and strain localisation in the Hilti peridotites, as the contribution of grain size sensitive creep in the melt-bearing, strongly recrystallised rocks was volumetrically insignificant (chapter 2).

7.3. Nature of the seismic crust and moho at fast- and slow-spreading ridges

In chapters 4, 5 and 6, evidence is reported for the interactions of melts and residual harzburgites in the Othris Massif. Plagioclase-peridotites in Othris are interpreted as rocks from the base of the oceanic thermal lithosphere in which impregnating melts partially solidified, refertilising the peridotites by fractional crystallisation of cumulate plagioclase and clinopyroxene. Note that the thermal lithosphere is defined here as the region in which conductive heat-loss to the surface predominates over advection of heat from below (e.g., figure 1.2). It has been argued that the Othris peridotites represent mantle rocks from a slow-spreading ridge in the vicinity of a transform fault. The process of partial crystallisation of mantle melts within the thermal mantle lithosphere may, therefore, be relevant to modern-day ocean ridges.

The volume of mantle melts reaching the surface to form typical magmatic crust (gabbros, sheeted dyke complexes, and basalts) at spreading centres will be reduced due to melts partly crystallising within the thermal mantle lithosphere. It should be noted that the importance of this effect is strongly dependent on the melt transport mechanism. If melt flow is strongly channelled in melt conduits (e.g., dunites or dykes), fractional crystallisation and/or melt-wall rock reactions will be very limited. If, however, melt transport occurs by porous flow or through micro-scale cracks, significant melt mass may be lost on the way to the surface due to fractional crystallisation in a cold mantle layer. As a result, the magmatic crust is expected to be thinner than average at ridges where this process plays a role. In addition, the uppermost mantle rocks are expected to consist of a mixture of peridotites and magma-derived lenses, veins, dykes, and larger bodies with gabbroic compositions. Finally, peridotites may be partly serpentinised, as ocean water can penetrate through the thin cap of magmatic crustal rocks and penetrate into relatively cold mantle rocks occurring at shallow levels. These features are most likely to be found at spreading centres where the oceanic thermal lithosphere is thick enough to reach into the mantle, i.e., where the uppermost mantle is cooled to temperatures below ~1200°C. This is expected at slow-spreading ridges (<5 cm/yr., e.g., the Mid-Atlantic ridge) where conductive heat-loss to the surface – in combination with hydrothermal cooling - is relatively important as compared with heat input by advection, related to upwelling of hot asthenospheric material (Lin & Parmentier, 1989). A thick conductively cooled lithospheric root reaching into the mantle is especially likely to exist underneath transform faults at slow- and possibly also at fast-spreading ridges as the result of juxtaposition of young, hot mantle material against older and colder mantle lithosphere (sometimes referred to as the 'cold wall' effect, e.g., Nicolas, 1989).

There is a growing body of geological, geophysical, and geochemical evidence to support the view that the magmatic crust at slow-spreading ridges is relatively thin, and that crustal material in such ridges may be incorporated in mantle rocks, in particular in the vicinity of transform faults.

(I) *Geological evidence.* Dredging, drilling, and submarine sampling at oceanic spreading centres, in particular at ridge-transform intersections of slow-spreading ridges has revealed the frequent presence of lower crustal and upper mantle rocks at the ocean floor (figure 7.4; Karson et al., 1987; Dick, 1989; Cannat et al., 1992; Cannat, 1993, 1996; Auzende et al., 1994). Their occurrence has been explained by exhumation of deep rocks along extensional detachment faults which reach into the mantle (Dick, 1989; Lin & Parmentier, 1989; Mutter & Karson, 1992; Cannat, 1993; Cannat et al., 1995), as well as by the presence of an abnormally thin magmatic crust developed in response limited magma supply (Cannat, 1993, 1996; Ghose et al., 1996; Sleep & Barth, 1997). Many of the peridotites recovered show evidence of magmatic impregnations, such as gabbroic dykes and veins (Dick, 1989; Cannat

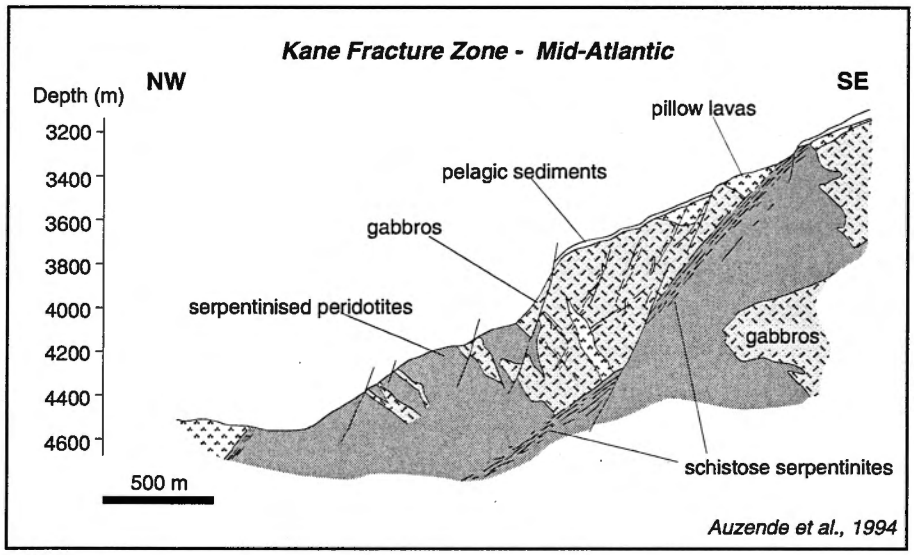

Figure 7.4
Sketch of gabbro-peridotite outcrop at the wall of the Kane Fracture Zone (Mid-Atlantic Ridge). Redrawn from Auzende *et al.* (1994).

et al., 1990; Girardeau & Mercier, 1992; Bonatti et al., 1992; Cannat et al., 1992; Girardeau & Francheteau, 1993; Tartarotti et al., 1995; Constantin, 1999).

(II) *Geophysical evidence.* Seismic studies have shown that the Moho at slow-spreading ridges is a less distinct boundary than at fast spreading centres, and that it shows more variability in structure and reflectivity (Mutter & Karson, 1992). This supports the view that crustal and mantle material in slow-spreading ridges are less well separated than in fast-spreading ones. Also, the reflectivity of the lower crust is much higher, possibly due to the presence of faults and deformation zones (Mutter & Karson, 1992) or compositional heterogeneities (Sleep & Barth, 1997). Seismic sections across very slow-spreading ridges (<2 cm/yr.) do not show the presence of a stable crustal magma lens or melt-crystal mush zone ('mush room'), and the seismic velocity gradient across the lower crust is higher than can be accounted for by pressure-related increase in gabbro velocity alone, suggesting a compositional change with depth (Sleep & Barth, 1997). Values for Poisson's Ratio for the crust at the southwest Indian Ocean (~1-2 cm/yr.) are in-between those of gabbros and partially serpentinised peridotites (Minshull & White, 1996). The same seismic characteristics exist at near-transform regions in slow-spreading oceans (Sleep & Barth, 1997). Finally, there is evidence for 'ageing' of the lower crust at slow-spreading ridges, i.e., a decrease of rock velocity with age (figure 7.5a), interpreted as the result of serpentinisation of an ultramafic component incorporated in the lower crust (White et al., 1992; Sleep & Barth, 1997).

(III) *Geochemical evidence.* Mantle melt production estimates inferred from Rare Earth Element (REE) concentrations in mid-ocean ridge lavas are significantly lower for slow-spreading ridges than for fast-spreading ridges. Importantly, at low spreading rates (<2 cm/yr.) the seismically defined crust is thicker than the thickness of the magmatic crust estimated from these REE concentrations, and the opposite is the case at high spreading rates (figure 7.5b; Bown & White, 1994). This also leads to the suggestion that the seismic crust includes a component of mantle material (Bown & White, 1994; Sleep, 1997). Although the geochemical data of Bown & White (1994) suggest that the thin magmatic crust at slow-spreading ridges is

primarily the result of lower melt production in the underlying mantle, an effect of 'melt entrapment' in mantle lithosphere cannot be excluded. A lower melt production at slow-spreading ridges is mainly attributed to mantle melting being limited to greater depth, due to the presence of thick conductively cooled lithosphere (Niu & Hékinian, 1997). It is found that at slow-spreading ridges melting stops at levels well below that of the Moho (Niu & Batiza, 1991), possibly as deep as >30 km (Zhang & Tanimoto, 1992; Niu & Hékinian, 1997). It seems most unlikely that melts can travel through a lid of sub-solidus mantle rocks without any melt-rock interaction or fractional crystallisation. This inference is supported by the geochemical study by Ghose et al. (1996) showing that crustal thickness variations along a segment of the Mid-Atlantic ridge cannot be explained by variations in mantle melt production alone, and that additional processes such as along-axis melt migration, focussed upwelling, or melt entrapment in mantle lithosphere must also have played a role.

In short, at ridges where a cold lid of mantle lithosphere can 'trap' rising mantle melts (causing fractional crystallisation) and which moves the final depth of melting to deep levels, the uppermost mantle and magmatic crust are expected to differ strongly from the typical layer-cake sequence found in some ophiolites and which has long been thought to be representative for all modern-day ocean floors (e.g., Anonymous, 1972). The seismic crust at slow-spreading ridges and at ridge-transform intersections will be more akin to the model of Hess (1962), who proposed that the ocean floor consists mainly of peridotites with a thin cap of magmatic rocks, and that the Moho coincides with the boundary from serpentinised to mainly unserpentinised peridotite (figure 7.6). Based on studies of samples recovered from the ocean floor, Cannat (1993) proposed that the seismic crust at segment ends, i.e., near-transform regions, of slow-spreading ridges consists of a mixture of gabbroic intrusions and serpentinised peridotites, and that the

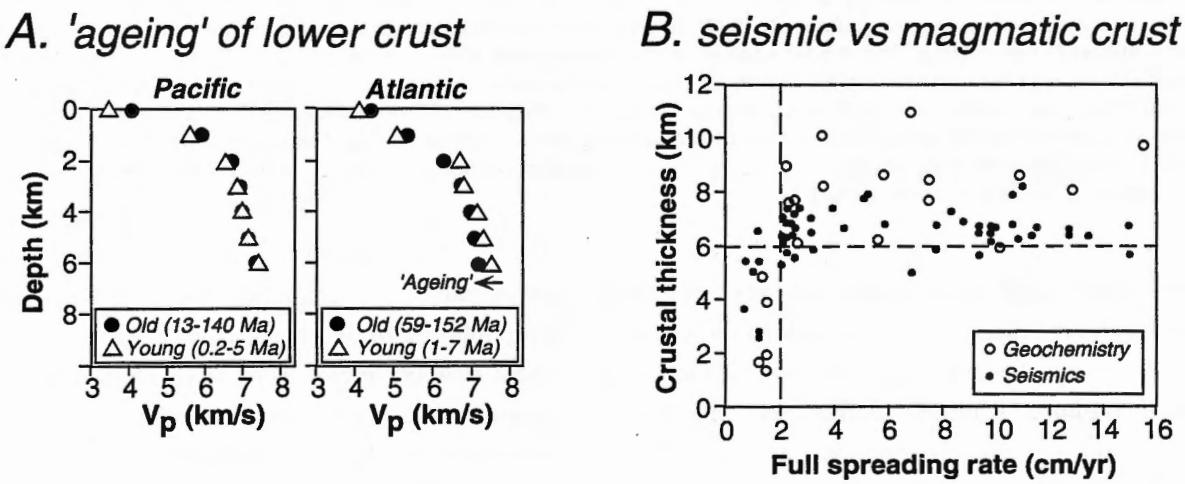

Figure 7.5: A) Seismic velocity sections through oceanic crust in the fast-spreading Pacific Ocean and the slow-spreading Atlantic Ocean (redrawn from White *et al.*, 1992). In the Atlantic, old lower crust has a lower P-wave velocity than young lower crust, possibly as a result of progressive serpentinisation of an ultramafic component in the lower crust.
B) Comparison of oceanic crustal thickness derived from seismic observations and geochemical (rare earth element) inversion of basalt compositions as a function of *full* spreading rate (redrawn from Sleep & Barth, 1997, after Bown & White, 1994). Note that for very slow spreading rates < 2cm/yr the seismically defined crust is thicker than the magmatic crust, suggesting incorporation of ultramafic material (Sleep & Barth, 1997). Also note that for slow and intermediate spreading rates, between 2 and ~8 cm/yr, the opposite is the case. This can be interpreted as evidence for loss of melt mass at depth due to fractional crystallisation in mantle lithosphere.

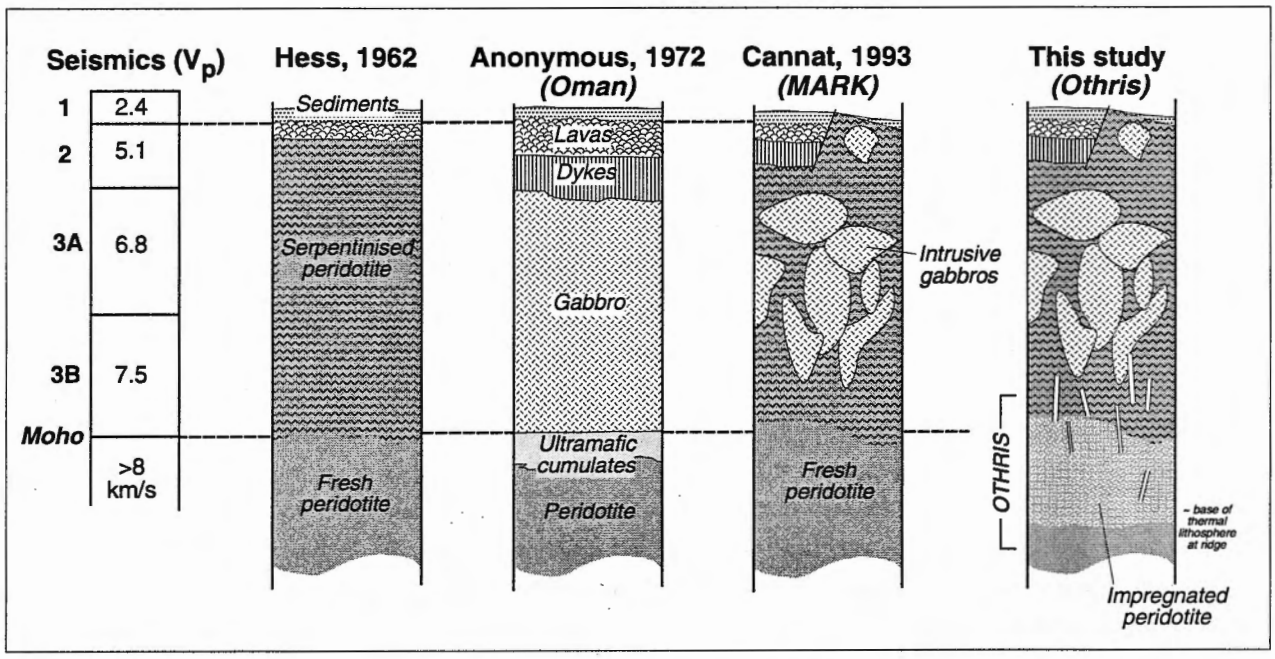

Figure 7.6: Schematic diagram showing different views on the architecture of oceanic crust and upper mantle, and the nature of the Moho. Hess (1962) proposed that the oceanic crust, defined by its low seismic velocity, consists of serpentinised peridotite with a thin cap of basalts and sediments. The recognition that ophiolites represent on-land exposures of oceanic crust and upper mantle (Anonymous, 1972) has led to the commonly held perspective that the oceanic crust consists of a typical layer-cake sequence of gabbros, sheeted dykes, pillow lavas, and pelagic sediments, which overlies residual mantle rocks (ophiolite sequence shown is taken from Nicolas, 1989, based on the Oman Ophiolite). The frequent recovery of gabbros and peridotites from the present-day Mid-Atlantic Ridge has led to the alternative model of Cannat (e.g., Cannat, 1993), in which the oceanic crust consists of a mixture of mafic intrusions and (serpentinised) peridotites. This model applies to magma-starved, slow-spreading ridge systems, in particular in the vicinity of transform faults. The present study of the Othris Ophiolite, which probably represents relatively deep levels of such a ridge system with a low magma supply, has led to a modification of the model of Cannat (1993). It is argued in this thesis that Othris represents the basal region of conductively cooled mantle lithosphere, in which melts produced at depth fractionally crystallise plagioclase, clinopyroxene, and possibly orthopyroxene, and where the transition from melt impregnation to dyke intrusion occurs.

Moho would mark the transition to lower proportions of incorporated magmatic crustal material as well as to less serpentinised peridotites. This study of the Othris Massif supports Cannat's model, but the Othris peridotites may represent deep levels, at the base of the lithosphere, which are normally not exposed at the ocean floor. In the present study it is suggested that magmatic impregnation at these levels leads to the formation of small plagioclase-bearing lenses and small gabbroic dykes as the result of fractional crystallisation, rather than to intrusion of gabbro bodies. The Othris Massif seems to show the transition from porous melt impregnation to the beginning of dyke intrusion. Interestingly, calculations by E. Rosendaal (unpublished M.Sc. thesis, Utrecht University, 1998) show that the presence of small plagioclase-bearing lenses such as in the Othris peridotites only leads to a moderate decrease in seismic (P-wave) velocity to values of 8.1 km/s as compared to 8.3 km/s for plagioclase-free peridotites. These sub-Moho velocities suggest that the Othris peridotites represent rocks from just below the Moho and that the effects of melt entrapment in oceanic mantle lithosphere are not confined to the seismically defined crust. At Othris, only the peridotites in a fault-bound block in the northeast of the Fournos Kaïtsa showing pervasive sea-

floor serpentinisation presumably close to a ridge are likely to have 'crustal' seismic velocities.

The combination of the large thickness of the lithosphere at very slow-spreading ridges and the presence, in such ridge systems and at associated segment ends, of peridotites at shallow levels also has an important mechanical effect. Ridges with a thick thermal lithosphere are about one order of magnitude stronger than ridges with a thin lithosphere (figure 7.7). The weakest part of a ridge with a thin lithosphere and a full magmatic crustal section coincides with the lower crust, and possibly with the uppermost mantle if melt accumulation and melt weakening occurs at this level (Chapter 2 & 3). In contrast, the weakest part of a ridge with a thick lithosphere and thin magmatic section coincides with the peridotites at the base of the lithosphere and, possibly, the serpentinised peridotites at shallow levels. In this context it is noted that the axial morphology, i.e., the presence of a broad axial high at fast-spreading ridges or the presence of a deep axial valley at slow-spreading ridges, has been shown to be determined primarily by the mechanical structure of the ridge (e.g., Carbotte & Macdonald, 1994; Shaw & Lin, 1996).

In summary, variations in spreading rate lead to important differences in the thermal structure, melt

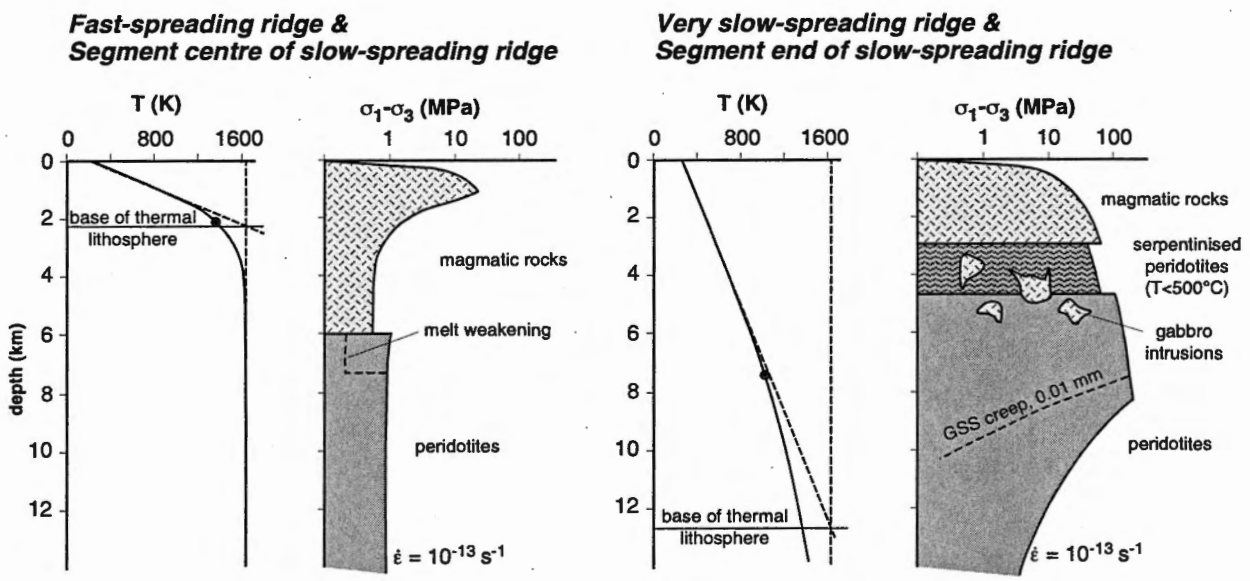

Figure 7.7: Temperature and strength profiles through A) an Oman-like ridge with 6 km thick magmatic crust and a thin (~2.2 km) thermal lithosphere, whose base lies within the crust (a fast-spreading ridge or the segment centre of a slow-spreading ridge), and B) an Othris-like ridge with a thin (3 km) magmatic crust and a thick (~13 km) thermal lithosphere which reaches well into the mantle (a very slow-spreading ridge or segment-end of a slow-spreading ridge). Temperature profiles calculated using an error-function with adiabatic temperatures (1350°C) at infinite depth; effects of along-axis temperature gradients and hydrothermal cooling are neglected. The temperature profile in A) is constrained by the 1100°C isotherm at the top of the crustal melt lens at a depth of 1.2-2.4 km underneath the East Pacific Rise (Sinton & Detrick, 1992; Chen & Morgan, 1990). The temperature profile in B) is constrained by micro-seismicity at temperatures <750°C occurring down to a depth of 6-10 km at the Mid-Atlantic Ridge (Toomey *et al.*, 1985; Chen & Morgan, 1990). Strength profiles for a tectonic strain rate of 10^{-13} s^{-1} are calculated using the diabase power-law creep flow law of Shelton & Tullis (1981; see Hirth *et al.*, 1998 for discussion) for the magmatic crust and the olivine [c]-slip flow law of Drury & Fitz Gerald (1998) based on Chopra & Patterson (1984) for peridotite, limited by a frictional relation at high stresses (following Sibson, 1977). Also shown in A) is the effect of melt-weakening of olivine just below the crust-mantle boundary (represented by the [a]-slip flow law of Drury & Fitz Gerald), and in B) the effects of peridotite serpentinisation at temperatures <500°C (according to Escartin *et al.*, 1997) and of the presence of fine-grained (10 μm) peridotite mylonite zones deforming by grain-size sensitive creep (using the dry diffusion creep flow law of Hirth & Kohlstedt, 1995a).

production at depth, magma delivery to the surface, magmatic crustal thickness, seismic structure, mechanical structure, and axial morphology at ocean ridges. These differences are also reflected in the structure and petrology of ophiolites, and have led to the recognition of different ophiolite types (Boudier & Nicolas, 1985/86; Nicolas, 1986a; Nicolas, 1989). The Oman and Othris ophiolites probably represent fragments of the two end-member types of spreading centres.

Chapter 8

Main conclusions and suggestions for further research

8.1. Main conclusions

(I) In the Hilti Massif (Oman) high temperature ('asthenospheric') mantle deformation was localised in the first 500-800 m below the crust-mantle boundary. There is also evidence that basaltic melt accumulated in this zone. It is concluded that the melt concentration in the peridotites of the crust-mantle transition zone was high enough to bring about melt weakening such as found in recent deformation experiments of mantle-like materials containing 4-10% interstitial basaltic melt.

(II) The localised deformation just below the crust-mantle boundary in the Hilti Massif was probably associated with the onset of compression close to the Oman paleo-ridge. The deformation led to the collapse of the melt-rich crust-mantle transition zone and to intrusion of a crystal-melt mush into the just consolidated oceanic crust, forming wehrlite bodies. It is less likely that the deformation was the related to forced mantle flow caused by active upwelling of mantle diapirs and small scale convection underneath the Oman paleo-ridge, as previously proposed.

(III) In the Othris Massif (Greece) there is also evidence for the presence of melt during mantle deformation. However, most of this deformation occurred under 'lithospheric' conditions, at temperatures below 1200 °C. It is therefore concluded that the Othris peridotites record a stage of melt impregnation and fractional crystallisation in the base of the thermal lithosphere underneath the Othris paleo-ridge. The Othris Ophiolite most likely originated in a near-transform fault environment at a slow-spreading ridge, where the thermal, conductively cooled lithosphere was thick enough to reach down into the mantle.

(IV) There is also petrographic evidence that reactions between peridotites and transient melts preceded and accompanied melt impregnation in Othris. These reactions led to the break-down of large orthopyroxene porphyroclasts and the formation of fine-grained domains consisting of an olivine-orthopyroxene mixture. During later deformation, probably associated with the start of emplacement of the Othris Ophiolite in a sinistral transpressional setting, the fine-grained domains coalesced to form a continuous network of fine-grained bands. Deformation in these bands became controlled by grain-size sensitive creep, which led to progressive strain weakening and strain localisation in fine-grained peridotite mylonite shear zones. The study of the Othris peridotites thus provides a case of *indirect* melt weakening.

(V) Melt weakening of peridotites such as found in the Hilti Massif and in deformation experiments is probably related to enhancement of grain boundary processes (grain boundary sliding and/or grain boundary diffusion) rather than to enhancement of intragranular processes. Grain boundary processes may be enhanced in porous melt-bearing materials by fast diffusion along melt-wetted grain boundaries, by concentration of stresses at solid-solid contacts due to a decrease in load-bearing area, and by shortening of the grain boundary diffusion distance due to the formation of short circuit pathways. These processes are most significant in fine-grained rocks. Peridotite melt-weakening is therefore

most likely to occur in rocks containing sufficient amounts of melts, deforming at conditions close to the mechanism boundary between dislocation and grain-size sensitive (diffusion) creep. Moreover, melt probably has to form a connected network, being distributed along grain boundaries and in grain interstices rather than in isolated melt lenses and veins, to cause weakening. Finally, highly siliceous, very viscous melts, such as the first melt fractions produced by partial melting of peridotites, are less likely to cause melt weakening than silica-poor melt fractions produced by high degrees of partial melting, because of slow diffusion in viscous melts.

(VI) Oman and Othris are two ophiolite end-member types. The Oman Ophiolite probably represents a fast-spreading ridge with a relatively thin thermal lithosphere and a high magma supply. In such an environment the oceanic crust reaches its full thickness of ~6 km, consisting of a sequence of gabbros, sheeted dolerite dykes, and basaltic pillow lavas; peridotites microstructures predominantly preserve evidence for deformation under 'asthenospheric' conditions. In contrast, it is concluded that the Othris Ophiolite represents a transform fault at a slow-spreading ridge, where magma supply is low, where the oceanic crust is thin or absent, and where rising melts fractionally crystallise minerals in the base of a relatively thick lithospheric layer, which is undergoing extensive internal ('lithospheric') deformation.

8.2. Suggestions for further research

(I) It is concluded in this thesis that the deformation in the melt-bearing crust-mantle transition zone in the Hilti Massif did not take place on-axis, but slightly off-axis, and that it was associated with the onset of compression at the Oman paleo-ridge. Melt accumulation in the crust-mantle transition zone may therefore be a feature of a dying, rather than an active, spreading centre. The composition of the interstitial melt in the peridotites of this zone may provide important clues about the spreading environment and may reveal whether the wehrlite intrusives in the overlying crust are genetically linked to the melts in the crust-mantle transition zone. It is therefore proposed that detailed trace element geochemistry be carried out on the cumulate minerals (clinopyroxene and plagioclase) in this zone, preferably using laser-ablation ICP-MS because of the good spatial and textural control of this technique.

(II) The two-stage, high temperature deformation history proposed for the Hilti Massif may also be valid for other ophiolitic massifs in Oman. It would be particularly interesting to test whether or not a similar deformation history can be reconstructed for areas where on-axis, diapiric flow patterns have been recognised.

(III) Detailed geochemistry on the cumulate minerals in the Othris plagioclase-peridotites using laser-ablation ICP-MS can possibly reveal whether the impregnating melt had a (depleted) MORB-like or more boninitic composition. This is important for the reconstruction of the environment of origin of the Othris Ophiolite, as the presence of boninitic melts imply an origin in a supra-subduction zone setting.

(IV) The use of calibrated stress-recrystallised grain size relationship to determine the stress during deformation and recrystallisation (piezometry) is one of the most important and useful tools for the reconstruction of deformation conditions of naturally deformed peridotites. There are now questions as to the validity of the most widely used and supposedly most accurate stress-recrystallised grain size relationship (the Van der Wal piezometer) at low stresses, since recent low-stress deformation experiments produced markedly smaller recrystallised grains than expected from the Van der Wal relation. It would be useful to set up a new series of deformation experiments encompassing a large range of stresses to test the accuracy of the Van der Wal piezometer. Moreover, it is important to determine the effects of temperature, melt content, and water fugacity

on the recrystallised grain size. Furthermore, the use of correction factors to compensate for sectioning effects should be discarded, or should at least be standardised (now, correction factors of 1.2, 1.5, and 1.75 are used). Finally, it would be useful to determine the effects of stress and strain on (recrystallised) grain size *distributions* in deformed rocks.

(V) For a better understanding of the mechanisms underlying melt weakening of peridotites, it is important to investigate the effects of peridotite grain sizes, melt distributions, and melt compositions (viscosities) on the magnitude of the strength reduction. If melt weakening is indeed caused by enhancement of grain boundary processes then these factors are expected to have a significant effect on the strength of melt-weakened peridotites.

References

Anonymous, 1972, Ophiolites, Penrose Field Conference, Geotimes, December 1972, 24-25.

Auzende, J.M., M. Cannat, P. Gente, J-P. Henriet, T. Juteau, J. Karson, Y. Lagabrielle, C. Mével, & M. Tivey, 1994. Observation of sections of oceanic crust and mantle cropping out on the southern wall of the Kane FZ (N. Atlantic), Terra Nova 6, 143-148.

Bai, Q., Z-M. Jin, & H. Green II, 1997. Experimental investigation of the rheology of partially molten peridotite at upper mantle pressures and temperatures, in: M.B. Holness (ed.), Deformation-enhanced fluid transport in the Earth's crust and mantle, Chapman & Hall, London, 40-61.

Bender, J.F., F.N. Hodges, & A.E. Bence, 1978. Petrogenesis of basalts from the project FAMOUS area: Experimental study from 0 to 15 Kbars, Earth Plan. Sci. Lett. 41, 277-302.

Benn, K., A. Nicolas, & I. Reuber, 1988. Mantle-crust transition zone and origin of wehrlitic magmas: Evidence from the Oman Ophiolite, Tectonophysics 151, 75-85.

Bertrand, Ph. & J-C.C. Mercier, 1986. The mutual solubility of coexisting ortho- and clinopyroxene: Toward an absolute geothermometer for the natural system?, Earth Plan. Sci. Lett. 76, 109-122.

Bird, R.T., D.F. Naar, R.L. Larson, R.C. Searle, & C.R. Scotese, 1998. Plate tectonic reconstructions of the Juan Fernandez microplate: Transformation from internal shear to rigid rotation, J. Geoph. Res. 103, no. B4, 7049-7067.

Bloomer, S.H., J.H. Natland, & R.L. Fischer, 1989. Mineral relationships in gabbroic rocks from fracture zones of Indian Ocean ridges: Evidence for extensive fractionation, parental diversity, and boundary-layer recrystallization, in: A.D. Saunders & M.J. Norry (eds.), Magmatism in the Ocean Basins, Geol. Soc. Spec. Publ. 42, 107-124.

Bodiner, J-L., G. Vasseur, J. Vernières, C. Dupuy, & J. Fabriès, 1990. Mechanisms of mantle metasomatism: geochemical evidence from the Lherz orogenic peridotite, J. Pet. 31, 597-628.

Bodinier, J.L., 1988. Geochemistry and petrogenesis of the Lanzo peridotite body, western Alps, Tectonophysics 149, 67-88.

Bonatti, E. & P.J. Michael, 1989. Mantle peridotites from continental rifts to ocean basins to subduction zones, Earth Plan. Sci. Lett. 91, 297-311.

Bonatti, E., A. Peyve, P. Kepezhinskas, N. Kurentsova, M. Seyler, S. Skolotnev, & G. Udintsev, 1992. Upper mantle heterogeneity below the Mid-Atlantic ridge, 0°-15°N, J. Geoph. Res. 97, 4461-4476.

Bottinga, Y. & D.F. Weill, 1972. The viscosity of magmatic silicate liquids: A model for their calculation, Am. J. Sci. 272, 438-475.

Boudier, F., 1978. Structure and petrology of the Lanzo peridotites massif (Piedmont Alps), Geol. Soc. Am. Bull. 89, 1574-1591.

Boudier, F. & A. Nicolas, 1972. Fusion partielle gabbroique dans le lherzolite de Lanzo (Alpes Piémontaises), Schweiz. Mineral. Petrogr. Mitt. 52, 39-56.

Boudier, F. & A. Nicolas, 1985. Harzburgite and lherzolite subtypes in ophiolitic and oceanic environments, Earth Plan. Sci. Lett. 76, 84-92.

Boudier, F. & A. Nicolas, 1995. Nature of the Moho Transition Zone in the Oman Ophiolite, J. Petr. 36, 777-796.

Boudier, F., G. Ceuleneer, & A. Nicolas, 1988. Shear zones, thrusts and related magmatism in the Oman ophiolite: Initiation of thrusting on an oceanic ridge, Tectonophysics 151, 275-296.

Boudier, F., E. Le Suer, & A. Nicolas, 1989. Structure of an atypical ophiolite: The Trinity Complex, eastern Klamath Mountains, California, Geol. Soc. of Am. Bull. 101, 820-833.

Boudier, F., A. Nicolas, & B. Ildefonse, 1996. Magma chambers in the Oman ophiolite: Fed from the top and the bottom, Earth Plan. Sci. Lett. 144, 239-250.

Boudier, F., A. Nicolas, & A. Meshi, 1999. A slow-spreading accretion in the ophiolites of Mirdita (Albania), European Union of Geosciences, Journal of Conference, Abstracts, volume 4, Cambridge Publications, 382.

Boudier, F., A. Nicolas, B. Ildefonse, & D. Jousselin, 1997. EPR microplates, a model for the Oman Ophiolite, Terra Nova 9, 79-82.

Boullier, A-M & Y. Gueguen, 1975. SP-mylonites: Origin of some mylonites by superplastic flow, Contrib. Mineral. Petrol. 50, 93-104.

Bown, J.W. & R.S. White, 1994. Variation with spreading rate of oceanic crustal thickness and geochemistry, Earth Plan. Sci. Lett. 121, 435-449.

Brey, G.P. & T. Köhler, 1990. Geothermobarometry in four-phase lherzolites II. New thermobarometers, and practical assessment of existing thermobarometers, J. Petrology 31, 1353-1378.

Bussod, G.Y. & J.M. Christie, 1991. Textural development and melt topology in spinel lherzolite experimentally deformed at hypersolidus conditions, J. Petr., Special Lherzolite Issue, 17-39.

Cameron, W.E., E.G. Nisbet, & V.J. Dietrich, 1979. Boninites, komatiites and ophiolitic basalts, Nature 280, 550-553.

Cann, J., 1998. News and views: Subtle minds and mid-ocean ridges, Science 393, 625-628.

Cannat, M., 1993. Emplacement of mantle rocks in the seafloor at mid-ocean ridges, J. Geoph. Res. 98, 4163-4172.

Cannat, M., 1996. How thick is the magmatic crust at slow spreading ridges?, J. Geoph. Res. 101, 2847-2857.

Cannat, M. & J.F. Casey, 1995. An ultramafic lift at the Mid-Atlantic Ridge: Successive stages of magmatism in serpentinized peridotites from the 15°N region, in: R.L.M. Vissers & A. Nicolas (eds.), Mantle and lower crust exposed in oceanic ridges and in ophiolites, Kluwer Academic Publishers, Dordrecht, The Netherlands, 5-34.

Cannat, M. & C. Lécuyer, 1991. Ephemeral magma chambers in the Trinity peridotite, northern California, Tectonophysics 186, 313-328.

Cannat, M., D. Bideau, & H. Bougault, 1992. Serpentinized peridotites and gabbros in the Mid-Atlantic Ridge axial valley at 15°37'N and 16°52'N, Earth Plan. Sci. Lett. 109, 87-106.

Cannat, M., D. Bideau, & R. Hébert, 1990. Plastic deformation and magmatic impregnation in serpentinized ultramafic rocks from the Garrett transform fault (East Pacific Rise), Earth Plan. Sci. Lett. 101, 216-232.

Cannat, M., C. Mével, M. Maia, C. Deplus, C. Durand, P. Gente, P. Agrinier, A. Belarouchi, G. Dubuisson, E. Humler, J. Reynolds, 1995. Thin crust, ultramafic exposures, and rugged faulting patterns at the Mid-Atlantic Ridge (22°-24°N), Geology 23, 49-52.

Carbotte, S.M. & K.C. Macdonald, 1994. The axial topographic high at intermediate and fast spreading ridges, Earth Plan. Sci. Lett. 128, 85-97.

Ceuleneer, G. & M. Rabinowicz, 1992. Mantle flow and melt migration beneath oceanic ridges: Models derived from observations in ophiolites, in: J.P. Morgan, D.K. Blackman, & J.M. Sinton (eds.), Mantle flow and melt generation at mid-oceanic ridges, Geoph. Monograph 71, American Geophysical Union, 123-154.

Ceuleneer, G., A. Nicolas, & F. Boudier, 1988. Mantle flow patterns at an oceanic spreading centre: The Oman peridotites record, Tectonophysics 151, 1-26.

Chen, Y. & W. Jason Morgan, 1990. A nonlinear rheology model for mid-ocean ridge axis topography, J. Geoph. Res. 95, 17583-17604.

Chopra, P.N. & M.S. Patterson, 1984. The role of water in the deformation dunite, J. Geoph. Res. 89, 7861-7876.

Coleman, R.G., 1984. The diversity of ophiolites, in: Zwart, H.J., P. Hartman & A.C. Tobi (eds.),

Ophiolites and ultramafic rocks – a tribute to Emile den Tex, Geologie en Mijnbouw 63, 141-150.

Constantin, M., 1999. Gabbroic intrusions and magmatic metasomatism in harzburgites from the Garrett transform fault: implications for the nature of mantle-crust transition at fast-spreading ridges, Contrib. Mineral. Petrol. 136, 111-130.

Constantin, M., R. Hékinian, A. Ackermand, & P. Stoffers, 1995. Mafic and ultramafic intrusions into upper mantle peridotites from fast spreading centers of the Easter microplate (South East Pacific), in: R.L.M. Vissers & A. Nicolas (eds.), Mantle and lower crust exposed in oceanic ridges and in ophiolites, Kluwer Academic Publishers, Dordrecht, The Netherlands,71-120.

Cooper, R.F. & D.L. Kohlstedt, 1984. Solution-precipitation enhanced diffusional creep of partially molten olivine basalt aggregates during hot-pressing, Tectonophysics 107, 207-233.

Coulton, A.J., G.D. Harper, & D.S. O'Hanley, 1995. Oceanic versus emplacement age serpentinization in the Josephine ophiolite: Implications for the nature of the Moho at intermediate and slow spreading ridges, J. Geoph. Res. 100, 22245-22260.

Crawford, A.J., T.J. Falloon, D.H. Green, 1989. Classification, petrogenesis and tectonic setting of boninites, in: Crawford, A.J. (ed.): Boninites, Unwin Hyman, London, United Kingdom, 1-49.

Daines, M.J. & D.L. Kohlstedt, 1993. A laboratory study of melt migration, Phil. Trans. R. Soc. Lond. A 342, 43-52.

Daines, M.J. & D.L. Kohlstedt, 1997. Influence of deformation on melt topology in peridotites, J. Geoph. Res. 102, 10257-10271.

Daines, M.J. & F.M. Richter, 1986. An experimental method for directly determining the interconnectivity of melt in partially molten systems, Geoph. Res. Lett. 15, 1459-1462.

Davies, G.F. & M.A. Richards, 1992. Mantle convection, J. Geol. 100, 151-206.

Davis, J.C. Statistics and data inversion in geology, John Wiley & Sons, New York, 1986, 646 pp.

De Bresser, J.H.P., C.J. Peach, J.P.J. Reijs, & C.J. Spiers, 1998. On dynamic recrystallization during solid state flow: Effects of stress and temperature, Geoph. Res. Lett. 25, 3457-3460.

De Kloe, R., 2001. Deformation mechanisms and melt nano-structures in experimentally deformed olivine-orthopyroxene rocks with low melt fractions – An electron microscopy study, Ph.D. thesis, Universiteit Utrecht, Geologica Ultraiectina, 201, 173 pp.

Den Tex, E. 1969. Origin of ultramafic rocks. Their tectonic setting and history. Tectonophysics 7, 457-488.

Derby, B. & M.F. Ashby, 1987. On dynamic recrystallization, Scripta Metall. 21, 879-884.

Dick, H.J.B. & T. Bullen, 1984. Chromian spinel as a petrogenetic indicator in abyssal and alpine-type peridotites and spatially associated lavas, Contrib. Mineral. Petrol. 86, 84-76.

Dick, H.J.B., 1989. Abyssal peridotites, very slow spreading ridges and ocean ridge magmatism, in: A.D. Saunders & M.J. Norry (eds.), Magmatism in the Ocean Basins, Geol. Soc. Spec. Publ. 42, 71-105.

Dick, H.J.B., Natland, J.H., and others, 2000. A long in situ section of the lower ocean crust: results of ODP Leg 176 drilling at the Southwest Indian Ridge, Earth Plan. Sci. Lett. 179, 31-51.

Dick, H.J.B., R.L. Fisher, & W.B. Bryan, 1984. Mineralogic variability of the uppermost mantle along mid-ocean ridges, Earth Plan. Sci. Lett. 69, 88-106.

Dijkstra, A.H., M.R. Drury, & R.L.M. Vissers, 2001. Structural petrology of plagioclase-peridotites in the West Othris Mountains (Greece): Melt impregnation in mantle lithosphere, J. Petrology 42, 5-24.

Dodson, M.H., 1973. Closure temperature in cooling geochronological and petrological systems, Contrib. Mineral. Petrol. 40, 259-274.

Drury, M.R. & J.D. Fitz Gerald, 1998. Mantle rheology: Insights from laboratory studies of deformation and phase transition, in: I.N.S. Jackson (ed.), The Earth's Mantle – composition, structure and evolution, Cambridge University Press, 503-559.

Drury, M.R. & J.L. Urai, 1990, Deformation-related recrystallization processes, Tectonophysics 172, 235-253.

Drury, M.R. & H.L.M. Van Roermund, 1989. Fluid assisted recrystallisation in upper mantle peridotite xenoliths from kimberlites, J. Petrology 30, 133-152.

Drury, M.R., E.H. Hoogerduijn Strating, & R.L.M. Vissers, 1990. Shear zone structures and microstructures in mantle peridotites from the Voltri Massif, Ligurian Alps, NW Italy, Geologie en Mijnbouw 69, 3-17.

Drury, M.R., F.J. Humpreys, & S.H. White, 1985. Large strain deformation studies using polycrystalline magnesium as a rock analogue. Part II. Dynamic recrystallization mechanisms at high temperatures, Phys. Earth. Planet. Inter. 40, 208-222.

Drury, M.R., R.L.M. Vissers, D. Van der Wal, & E.H. Hoogerduijn Strating, 1991. Shear localization in upper mantle peridotites, Pure and Applied Geoph. 137, 439-460.

Dunn, R.A. & D.R. Toomey, 1997. Seismological evidence for three-dimensional melt migration beneath the East Pacific Rise, Nature 388, 259-262.

Elthon, D. & C.M. Scarfe, 1984. High-pressure phase equilibria of a high-magnesia basalt and the genesis of primary oceanic basalt, Am. Mineralogist 69, 1-15.

Escartin, J., G. Hirth, & B. Evans, 1997. Effect of serpentinization on the lithospheric strength and the style of normal faulting at slow-spreading ridges, Earth Plan. Sci. Lett. 151, 181-189.

Etheridge, M.A. & J.C. Wilkie, 1979. Grainsize reduction, grain boundary sliding and the flow strength of mylonites, in: T.H. Bell & R.H. Vernon (eds.), Microstructural processes during deformation and metamorphism, Tectonophysics 58, 159-178.

Faul, U.H., 1997. Permeability of partially molten upper mantle rocks from experiments and percolation theory, J. Geoph. Res. 102, 10299-10311.

Faupl, P., A. Pavlopoulos, M. Wagreich, & G. Migiros, 1996. Pre-Tertiary blueschist terrains in the Hellenides: Evidence from detrital minerals of flysch successions, Terra Nova 9, 186-190.

Ferrière, J., 1985. Nature et developpement des ophiolites Helleniques du secteur Othrys-Pelion, Ofioliti 10, 255-278.

Fliervoet, T.F., M.R. Drury, & P. Chopra, 1999. Crystallographic preferred orientations and misorientations in some olivine rocks deformed by diffusion or dislocation creep, Tectonophysics 303, p. 1-27

Freeman, B. & C.C. Ferguson, 1986. Deformation mechanism maps and micromechanics of rocks with distributed grain sizes, J. Geoph. Res. 91, 3849-3860.

Ghent, E.D. & M.Z. Stout, 1981. Metamorphism at the base of the Semail Ophiolite, southeastern Oman Mountains, J. Geoph. Res. 86, 2557-2571.

Ghose, I., M. Cannat, & M. Seyler, 1996. Transform fault effect on mantle melting in the MARK area (Mid-Atlantic Ridge south of the Kane transform), Geology 24, 1139-1142.

Girardeau, J. & J. Francheteau, 1993. Plagioclase-wehrlites and peridotites on the East Pacific Rise (Hess Deep) and the Mid-Atlantic Ridge (DSDP Site 334): evidence for magma percolation in the oceanic upper mantle, Earth Plan. Sci. Lett. 115, 137-149.

Girardeau, J. & J-C. C. Mercier, 1992. Evidence for plagioclase-lherzolite intrusion in the Mid-Atlantic Ridge, DSDP Leg 37, in: Parson, L.M., B.J. Murton, & P. Browning (eds.), Ophiolites and their modern oceanic analogues, Geol. Soc. Spec. Publ. 60, 241-250.

Godard, M., J-L. Bodinier, & G. Vasseur, 1995. Effects of mineralogical reactions on trace element redistributions in mantle rocks during percolation processes: A chromatographic approach, Earth Plan. Sci. Lett. 133, 449-461.

Green II, H.W. & R.S. Borch, 1987. High pressure and temperature deformation experiments in a liquid confining medium, in: The brittle-ductile transition in rocks, Geoph. Monogr., Am. Geoph. Union, 56, 195-200.

Gregory, R.T., 1984. Melt percolation beneath a spreading ridge: evidence from the Semail peridotite, Oman, in: Gass, I.G., S.J. Lippard, & A.W. Shelton (eds.), Ophiolites and oceanic lithosphere, Geol. Soc. Spec. Publ. 13, 55-62.

Grove, T.L., R.J. Kinzler, & W.B. Bryan, 1992. Fractionating of Mid-Ocean Ridge basalt (MORB), in: J.P. Morgan, D.K. Blackman, J.M. Sinton (eds.), Mantle flow and melt generation at mid-oceanic ridges, Geoph. Monograph 71, American Geophysical Union, 281-310.

Hacker, B.R. & E. Gnos, 1997. The conundrum of Samail: explaining the metamorphic history, Tectonophysics 279, 215-226.

't Hart, J., 1978a. The structural morphology of olivine I. A qualitative derivation, Canadian Mineralogist 16, 175-186.

't Hart, J., 1978b. The structural morphology of olivine II. A quantitative derivation, Canadian Mineralogist 16, 547-560.

Haskell, N.A., 1937. The viscosity of the asthenosphere, Am. J. Sci. 33, 22-28.

Hess, H.H., 1962. The history of ocean basins, in: Engel, A.E.J., H.L. James, & B.F. Leonard (eds.), Petrologic Studies: A volume to honor A.F. Buddington, Geol. Soc. Am., 599-620.

Hirth, G. & D.L. Kohlstedt, 1995a. Experimental constraints on the dynamics of the partially molten upper mantle: Deformation in the diffusion creep regime, J. Geoph. Res. 100, 1981-2001.

Hirth, G. & D.L. Kohlstedt, 1995b. Experimental constraints on the dynamics of the partially molten upper mantle 2. Deformation in the dislocation creep regime, J. Geoph. Res. 100, 15441-15449.

Hirth, G. & D.L. Kohlstedt, 1996. Water in the oceanic mantle: Implications for rheology, melt extraction, and the evolution of the lithosphere, Earth Plan. Sci. Lett. 144, 93-108.

Hirth, G., J. Escartin, & J. Lin, 1998. The rheology of the lower oceanic crust: Implications for lithospheric deformation at mid-ocean ridges, in: W.R. Buck, W.R., P.T. Delaney, J.A. Karson, & Y. Lagabrielle (eds.), Faulting and magmatism at mid-ocean ridges, Geoph. Monograph 106, American Geophysical Union, 291-303.

Hobbs, B.E., H-B. Mühlhaus, & A. Ord, 1990. Instability, softening and localization of deformation, in: R.J. Knipe & E.H. Rutter (eds.), Deformation mechanisms, rheology and tectonics, Geol. Soc. London Spec. Publ. 54, 143-165.

Holland, T.J.B. & R. Powell, 1990. An enlarged and updated internally consistent thermodynamic dataset with uncertainties and correlations: the system K_2O-Na_2O-CaO-MgO-MnO-FeO-Fe_2O_3-Al_2O_3-TiO_2-SiO_2-C-H_2-O_2, J. Metam. Geol. 8, 89-124.

Hoogerduijn Strating, E.H., E. Rampone, G.B. Piccardo, M.R. Drury, & R.L.M. Vissers, 1993. Subsolidus emplacement of mantle peridotites during incipient oceanic rifting and opening of the Mesozoic Tethys (Voltri Massif, NW Italy), J. Petr. 23, 901-927.

Hoxha, M. & A-M. Boullier, 1995. The peridotites of the Kukës ophiolite (Albania): structure and kinematics, Tectonophysics 249, 217-231.

Hynes, A.J., 1974a. Notes on the petrology of some ophiolites, Othris Mountains, Greece, Contr. Mineral. Petrol. 46, 233-239.

Hynes, A.J., 1974b. Igneous activity at the birth of ocean basin in eastern Greece, Can. J. of Earth Sci. 11, 842-853.

Hynes, A.J., E.G. Nisbet, A. Gilbert Smith, M.J.P. Welland, & D.C. Rex, 1972. Spreading and emplacement ages of some ophiolites in the Othris region (eastern central Greece), Z. Deutsch. Geol. Ges. 123, 455-468.

IGME (Institute for Geology and Mineral Exploration), Geological Map of Greece, Leontarion sheet, scale 1:50,000, 1962.

Ildefonse, B., S. Billiau, & A. Nicolas, 1995. A detailed study of mantle flow away from diapirs in the Oman Ophiolite, in: R.L.M. Vissers & A. Nicolas (eds.), Mantle and lower crust exposed in oceanic ridges and in ophiolites, Kluwer Academic Publishers, The Netherlands, 163-177.

Ildefonse, B., F. Boudier, & A. Nicolas, 1998a. Asthenospheric deformation in ophiolitic peridotite, in: A.W. Snoke, J. Tullis, & V.R. Todd (eds.), Fault-related rocks – a photographic atlas, Princeton University Press, Princeton, New Jersey, 588-589.

Ildefonse, B., F. Boudier, & A. Nicolas, 1998b. Lithospheric deformation in ophiolitic peridotite, in: A.W. Snoke, J. Tullis, & V.R. Todd (eds.), Fault-related rocks – a photographic atlas, Princeton University Press, Princeton, New Jersey, 590-591.

Jackson, E.D., H.W. Green II, & E.J. Moores, 1975. The Vourinos Ophiolite, Greece: Cyclic units of lineated cumulates overlying harzburgite tectonite, Geol. Soc. Am. Bull. 86, 390-398.

Jacobsen, S.B., J.E. Quick, & G.J. Wasserburg, 1984. A Nd and Sr isotopic study of the Trinity peridotite: Implications for mantle evolution, Earth Plan. Sci. Lett. 68, 361-378.

Jaroslow, G.E., G. Hirth, & H.J.B. Dick, 1996. Abyssal peridotite mylonites: Implications for grain-size sensitive flow and strain localization in the oceanic lithosphere, Tectonophysics 256, 17-37.

Jin, D., S-I. Karato, & M. Obata, 1998. Mechanism of shear localization in the continental lithosphere: Inference from the deformation microstructures of peridotites from the Ivrea zone, northwestern Italy, J. Struct. Geol. 20, 195-209.

Jousselin, D., A. Nicolas, & F. Boudier, 1998. Detailed mapping of a mantle diapir below a paleo-spreading center in the Oman Ophiolite, J. Geoph. Res. 103, no. B8, 18153-18170.

Juteau, T., M. Ernewein, I. Reuber, H. Whitechurch, & R. Dahl, 1988. Duality of magmatism in the plutonic sequence of the Sumail Nappe, Oman, Tectonophysics 151, 107-135.

Karato, S-I., 1984. Grain-size distribution and rheology of the upper mantle, Tectonophysics 104, 155-176.

Karato, S-I, 1988. The role of recrystallization in the preferred orientation of olivine, Phys. Earth Planet. Inter. 51, 107-122.

Karato, S-I & P. Wu, 1993. Rheology of the upper mantle: A synthesis, Science 260, 771-778.

Karato, S-I., M.S. Paterson, & J.D. Fitz Gerald, 1986. Rheology of synthetic olivine aggregates: Influence of grain size and water, J. Geoph. Res. 91, 8151-8176.

Karato, S-I., M. Toriumi, & T. Fujii, 1980. Dynamic recrystallization of olivine single crystals during high-temperature creep, Geoph. Res. Lett. 7, 649-652.

Karato, S-I., M. Toriumi, & T. Fujii, 1982. Dynamic recrystallization and high-temperature rheology of olivine, in: S. Akimoto, S., M.H. Manghnani (eds.), High pressure research in geophysics, Center of Academic Publications, Japan, 171-189.

Karson, J.A., & J.F. Dewey, 1978. Coastal Complex, western Newfoundland: An early Ordovician oceanic fracture zone, Geol. Soc. Am. Bull. 89, 1037-1049.

Karson, J.A., G. Thompson, S.E. Humphries, J.M. Edmond, W.B. Bryan, J.R. Brown, A.T. Winters, R.A. Pockalny, J.F. Casey, A.C. Campbell, G. Klinkhammer, M.R. Palmer, R.J. Kinzler, & M.M. Sulanowska, 1987. Along axis variations in seafloor spreading in the MARK area, Nature 328, 681-685.

Kastens, K., E. Bonatti, D. Caress, G. Carrara, O. Dauteuil, G. Frueh-Green, M. Ligi, & P. Tartarotti, 1998. The Vema transverse ridge, Marine Geoph. Res. 20, 533-556.

Kelemen, P.B., 1990. Reaction between ultramafic rock and fractionating basaltic magma I. Phase relations, the origin of calc-alkaline magma series, and the formation of discordant dunite, J. Pet. 31, 51-98.

Kelemen, P.B. & E. Aharonov, 1998. Periodic formation of magma fractures and generation of layered gabbros in the lower crust beneath oceanic spreading ridges, in: W.R. Buck, W.R., P.T. Delaney, J.A. Karson & Y. Lagabrielle (eds.), Faulting and magmatism at mid-ocean ridges, Geoph. Monograph 106, American Geophysical Union, 267-289.

Kelemen, P.B. & H.J. Dick, 1995. Focused melt flow and localized deformation in the upper mantle: Juxtaposition of replacive dunite and ductile shear zones in the Josephine peridotite, SW Oregon, J. Geoph. Res. 100, 423-438.

Kelemen, P.B., H.J. Dick, & J.E. Quick, 1992. Formation of harzburgite by pervasive melt/rock reaction in the upper mantle, Nature 358, 635-641.

Kinzler, R.J. & T.L. Grove, 1992. Primary magmas of mid-ocean ridge basalts 2. Applications, J. Geoph. Res. 97, 6907-6926.

Kirby, S.H., 1983. Rheology of the lithosphere. Rev. Geoph. Space Phys. 21, 1458-1487.

Kohlstedt, D.L., 1992. Structure, rheology and permeability of partially molten rocks at low melt fractions, in: J.P. Morgan, D.K. Blackman, & J.M. Sinton (eds.), Mantle flow and melt generation at mid-oceanic ridges, Geoph. Monograph 71, American Geophysical Union, 103-121.

Kuznir, N.J. & R.G. Park, 1986. Continental lithosphere strength: the critical role of lower crustal deformation. In: Dawson, J.B., D.A. Carswell, J. Hall, & K.H. Wedepohl (eds.), The nature of the lower continental crust, Geol. Soc. London Spec. Publ. 24, 79-93.

Langmuir, C.H., J.F. Bender, A.E. Bence, G.N. Hanson, & S.R. Taylor, Petrogenesis of basalts from the FAMOUS area: Mid-Atlantic Ridge, Earth Plan. Sci. Lett. 36, 133-156.

Larson, R.L., R.C. Searle, M.C. Kleinrock, H. Schouten, R.T. Bird, D.F. Naar, R.I. Rusby, E.E. Hooft, & H. Lasthiotakis, 1992. Roller-bearing tectonic evolution of the Juan Fernandez microplate, Nature 356, 571-576.

Lin, J. & E.M. Parmentier, 1989. Mechanism of lithospheric extension at mid-ocean ridges, Geoph. Journal 96, 1-22.

Lin, S, D. Jiang, & P.F. Williams, 1998. Transpression (or transtension) zones of triclinic symmetry: natural example and theoretical modelling, in: R.E. Holdsworth, R.A. Strachan, & J.F. Dewey (eds.), Continental transpressional and transtensional tectonics, Geol. Soc. London Spec. Publ. 135, 41-57.

Lippard, S.J., A.W. Shelton, & I.G. Gass, 1986. The ophiolite of northern Oman, Blackwell Scientific Publications, Oxford, 178 pp.

Lloyd, G.E., A.B. Farmer, & D. Mainprice, 1997. Misorientation analysis and the formation and orientation of subgrain and grain boundaries, Tectonophysics 279, 55-78.

Macdougal, J.D., 1995. Using short-lived U and Th series isotopes to investigate volcanic processes, Annu. Rev. Earth Planet. Sci. 23, 143-167.

Mackwell, S.J., Q. Bai, & D.L. Kohlstedt, 1990. Rheology of olivine and the strength of the lithosphere, Geoph. Res. Lett. 17, 9-12.

MacLeod, C.J. & D.A. Rothery, 1992. Ridge axial segmentation in the Oman Ophiolite: Evidence from along-strike variations in the sheeted dykes complex, In: Parson, L.M., B.J. Murton, & P. Browning (eds.), Ophiolites and their modern oceanic analogues, Geol. Soc. Spec. Publ. 60, 39-63.

Mainprice, D. & A. Nicolas, 1989. Development of shape and lattice preferred orientations; application to the seismic anisotropy of the lower crust, J. Struct. Geol. 11, 175-189.

Mancktelow, N., Stereoplot v2, 1989.

McKenzie, D., 1984. The generation and compaction of partially molten rock, J. Pet. 25, 713-765.

McKenzie, D., 1985. 230Th-238U disequilibrium and the melting process beneath ridge axes. Earth Planet. Sci. Lett. 74, 81-91.

McKenzie, D., 1989. Some remarks on the movement of small melt fractions in the mantle, Earth Planet. Sci. Lett. 95, 53-72.

Mei, S. & D.L. Kohlstedt, 2000a. Influence of water on plastic deformation of olivine aggregates 1. Diffusion creep regime, J. Geoph. Res. 105, 21457-21469.

Mei, S. & D.L. Kohlstedt, 2000b. Influence of water on plastic deformation of olivine aggregates 2. Dislocation creep regime, J. Geoph. Res. 105, 21471-21481.

MELT Seismic Team, 1998. Imaging the deep seismic structure beneath a mid-ocean ridge: The MELT experiment, Science 280, 1215-1218.

Menzies, M., 1973. Mineralogy and partial melt textures within an ultramafic-mafic body, Greece, Contrib. Mineral. Petrol. 42, 273-285.

Menzies, M., 1974. Petrogenesis of the Makrirrakhi Ultramafic Complex, unpublished Ph.D. thesis, Cambridge University, 154 pp + appendices.

Menzies, M., 1975. Spinel compositional variation in the crustal and mantle lithologies of the Othris Ophiolite, Contrib. Mineral. Petrol. 51, 303-309.

Menzies, M., 1976a. Rare earth geochemistry of fused ophiolitic and alpine lherzolites – I. Othris, Lanzo and Troodos, Geochim. Cosmochim. Act. 40, 645-656.

Menzies, M., 1976b. Rifting of a Tethyan continent – rare earth evidence of an accreting plate margin, Earth Plan. Sci. Lett. 28, 427-438.

Menzies, M. & C. Allen, 1974. Plagioclase lherzolite – residual mantle relationships within two eastern Mediterranean ophiolites, Contrib. Mineral. Petrol. 45, 197-213

Menzies, M.A. & C.J. Hawkesworth, 1987. Mantle metasomatism, Academic Press, London, United Kingdom, 472 pp.

Menzies, M., D. Blanchard, J. Brannon, & R. Korotev, 1977. Rare earth geochemistry of fused ophiolitic and alpine lherzolites – II. Beni Bouchera, Ronda and Lanzo, Contrib. Mineral. Petrol. 64, 53-74.

Mercier, J-C.C. & A. Nicolas, 1975. Textures and fabrics of upper-mantle peridotites as illustrated by xenoliths from basalts, J. Petr. 16, 454-487.

Michael, P. & E. Bonatti, 1985. Peridotite compositions from the North Atlantic: Regional and tectonic variations and implications for partial melting, Earth Plan. Sci. Lett. 73, 91-104.

Michibayashi, K., L. Gerbert-Gaillard, & A. Nicolas. Shear sense inversion in the Hilti mantle section (Oman ophiolite) and active mantle uprise. Submitted to J. Marine Geology.

Ministry of Petroleum and Minerals, 1987. Geological Map; Al Wasit – sheet NG40-14E-III, scale 1:50,000.

Minshull, T.A. & R.S. White, 1996. Thin crust on the flanks of the slow-spreading Southwest Indian Ridge, Geoph. J. Int. 125, 139-148.

Mutter, J.C. & J.A. Karson, 1992. Structural processes at slow-spreading ridges, Science 257, 627-634.

Naar, D.F. & R.N. Hey, 1991. Tectonic evolution of the Easter microplate, J. Geoph. Res. 96, no. B5, 7961-7993.

National Institutes of Health, USA, 1996. NIH Image v. 1.6.1.

Natland, J.H., 1989. Partial melting of a lithologically heterogeneous mantle: Inferences from crystallization histories of magnesian abyssal tholeiites from the Siqueiros Fracture Zone, in: A.D. Saunders & M.J. Norry (eds.), Magmatism in the Ocean Basins, Geol. Soc. Spec. Publ. 42, 41-70.

Newman, J. W.M. Lamb, M.R. Drury, & R.L.M. Vissers, 1999. Deformation processes in a peridotite shear zone: Reaction-softening by an H2O-deficient, continuous net transfer reaction, Tectonophysics 303, 193-222.

Nicolas, A., 1986a. Structure and Petrology of peridotites: Clues to their geodynamic environment, Rev. Geoph. 24, 875-895.

Nicolas, A., 1986b. A melt extraction model based on structural studies in mantle peridotites, J. Petr. 27, 999-1022.

Nicolas, A. Structures of ophiolites and dynamics of oceanic lithosphere, Kluwer Academic Publishers, Dordrecht, The Netherlands, 1989, 367 pp.

Nicolas, A. & F. Boudier, 1995. Mapping oceanic segments in Oman ophiolite. J. Geoph. Res. 100, no. B4, 6179-6197.

Nicolas, A. & C. Dupuy, 1984. Origin of ophiolitic and oceanic lherzolites, Tectonophysics 110, 177-187.

Nicolas, A. & M. Jackson, 1972. Répartition en deux provinces de péridotites des chaînes alpines longeant la Méditerranée: Implications géotectoniques, Schweiz. Mineral. Petrogr. Mitt. 52, 479-495.

Nicolas, A. & J-P. Poirier. Crystalline plasticity and solid state flow in metamorphic rocks, John Wiley & Sons, London, U.K., 1976, 444 pp.

Nicolas, A. & A. Prinzhofer, 1983. Cumulative or residual origin for the transition zone in ophiolites: Structural evidence, J. Petr. 24, 188-206.

Nicolas, A. & J.F. Violette, 1982. Mantle flow beneath oceanic ridges: models derived from ophiolites. Tectonophysics 81, 319-339.

Nicolas, A., F. Boudier, & B. Ildefonse, 1994. Evidence from the Oman ophiolite for active mantle upwelling beneath a fast-spreading ridge, Nature 370, 51-53.

Nicolas, A., F. Boudier, & B. Ildefonse, 1996. Variable crustal thickness in the Oman Ophiolite: Implications for oceanic crust, J. Geoph. Res. 101, no. B8, 17941-17950.

Nicolas, A., F. Boudier, & A. Meshi, 1999. Slow spreading accretion and mantle denudation in the Mirdita ophiolite (Albania), J. Geoph. Res. 104, 15155-15167.

Nicolas, A., I. Reuber, & K. Benn, 1988b. A new magma chamber model based on structural studies in the Oman Ophiolite, Tectonophysics 151, 87-105.

Nicolas, A., G. Ceuleneer, F. Boudier, & M. Misseri, 1988. Structural mapping in the Oman ophiolites: Mantle diapirism along an oceanic ridge, Tectonophysics 151, 27-56.

Niu, Y., 1997. Mantle melting and melt extraction processes beneath ocean ridges: Evidence from abyssal peridotites, J. Petr. 38, no. 8, 1047-1074.

Niu, Y. & R. Batiza, 1991. An empirical method for calculating melt compositions produced beneath mid-ocean ridges; for axis and off-axis (seamounts) melting application, J. Geoph. Res. 96, 21753-21777.

Niu, Y. & R. Hékinian, 1997. Spreading-rate dependence of the extent of mantle melting beneath ocean ridges, Nature 385, 326-329.

Olgaard, D.L., 1990. The role of second phase in localizing deformation, in: R.J. Knipe & E.H. Rutter (eds.), Deformation mechanisms, rheology and tectonics, Geol. Soc. London Spec. Publ. 54, 175-181.

Pallister, J.S. & C.A. Hopson, 1981. Samail ophiolite plutonic suite: Field relations, phase variation and layering and a model of a spreading ridge magma chamber, J. Geoph. Res. 86, 2593-2644.

Pamic', J., 1983. Considerations on the boundary between lherzolite and harzburgite subprovinces in the Dinarides and northern Hellenides, Ophioliti 8, 153-164.

Parker, R.L. & D.W. Oldenburg, 1973. Thermal model of ocean ridges, Nature 242, 137-139.

Pearce, J.A., T. Alabaster, A.W. Shelton, & M.P. Searle, 1981. The Oman Ophiolite as a Cretaceous arc-basin complex: Evidence and implication, Phil. Trans. R. Soc. Lond. A 300, 299-317.

Peltier, W.R., 1996. Mantle viscosity and ice-age ice sheet topography, Science 273, 1359-1364.

Phipps Morgan, J. & Y.J. Chen, 1993. The genesis of oceanic crust: Magma injection, hydrothermal circulation and crustal flow, J. Geoph. Res. 98, 6283-6297.

Phipps Morgan, J., W.J. Morgan, Y-S. Zhang, & W.H.F. Smith, 1995. Observational hints for a plume-fed, suboceanic asthenosphere and its role in mantle convection, J. Geoph. Res. 100, 12753-12767.

Pognante, U., U. Rösli, & L. Toscani, 1985. Petrology of ultramafic and mafic rocks from the Lanzo peridotite body (Western Alps), Lithos 18, 201-214.

Poirier, J.P., 1980. Shear localization and shear instability in materials in the ductile field, J. Struct. Geol. 2, 135-142.

Powell, R. & T.J.B. Holland, 1988. An internally consistent dataset with uncertainties and correlations: 3. Applications to geobarometry, worked examples and a computer program, J. Metam. Geol. 6, 173-204.

Prinzhofer, A. & A. Nicolas, 1980. The Bogota Peninsula, New Caledonia: A possible oceanic transform fault, J. Geol. 88, 387-398.

Prior, D.J., 1999. Problems in determining the misorientations axes for small angular misorientations using electron backscatter diffraction in SEM, J. Microsc. 195, 217-225.

Prior, D.J., P.W. Trimby, U.D. Weber, & D.J. Dingley, 1996. Orientation contrast imaging of microstructures in rocks using forescatter detectors in the scanning electron microscope, Mineral. Mag. 60, 859-869.

Quick, J.A., 1981a. Petrology and petrogenesis of the Trinity peridotite, an upper mantle diapir in the eastern Klamath Mountains, northern California, Contrib. Mineral. Petr. 86, 11837-11863.

Quick, J.A., 1981b. The origin and significance of large, tabular dunite bodies in the Trinity Peridotite, northern California, Contrib. Mineral. Petrol. 78, 413-422.

Quick, J.E. & R.P. Denlinger, 1993. Ductile deformation and the origin of layered gabbros in ophiolites, J. Geoph. Res. 98, 14015-14027.

Rabinowicz, M., G. Ceuleneer, & A. Nicolas, 1987. Melt segregation and flow in mantle diapirs below spreading centers: Evidence from the Oman Ophiolite, J. Geoph. Res. 92, 3475-3486.

Rabinowicz, M., A. Nicolas, & J.L. Vigneresse, 1984. A rolling mill effect in asthenosphere beneath oceanic spreading centers, Earth Plan. Sci. Lett. 67, 97-108.

Rampone, E., G.B. Piccardo, R. Vanucci, & P. Bottazzi, 1997. Chemistry and origin of trapped melts in ophiolitic peridotites, Geochim. Cosmochim. Act. 61, 4557-4560.

Ranalli, G., 1991. The microphysical approach to mantle rheology, in: Sabadini, R., K. Lambeck, & E. Boschi (eds.), Glacial isostasy, sea-level and mantle rheology, Kluwer Academic Publishers, Dordrecht, The Netherlands, 343-378.

Randle, V. Microtexture determination and its applications, Institute of Materials, London, 1992, 174 pp.

Ranero, C.R. & T.J. Reston, 1999. Detachment faulting at ocean core complexes, Geology 27, 983-986.

Rassios, A. & G. Konstantopoulou, 1993. Emplacement tectonism and the position of chrome ores in the Mega Isoma peridotites, SW Othris, Greece, Bull. Geol. Soc. Greece XXVIII/2, 463-474.

Raterron, P., G.Y. Bussod, N. Doukhan, & J-C. Doukhan, 1997. Early partial melting in the upper mantle: an A.E.M. study of a lherzolite experimentally annealed at hypersolidus conditions, Tectonophysics 279, 79-91.

Reuber, I., 1988. Complexity of the crustal sequence in the northern Oman ophiolite (Fizh and southern Aswad blocks): The effect of early slicing?, Tectonophysics 151, 137-165.

Reuber, I., 1991. Geometry and flow pattern of the plutonic sequence of the Salahi Massif (Northern Oman Ophiolite) – A key to decipher successive magmatic events, in: Peters, Tj., A. Nicolas, & R.G. Coleman (eds), Ophiolite genesis and evolution of the oceanic lithosphere, Proceedings

of the ophiolite conference held in Muscat, Oman, 7-18 January 1990, Kluwer Academic Publishers, Dordrecht, The Netherlands, 83-103.

Ribe, N.M., 1987. Theory of melt segregation – a review, J. of Volc. And Geoth. Res. 33, 241-253.

Robertson, A.H.F., P.D. Clift, P.J. Degnan, & G. Jones, 1991. Palaeogeographic and palaeotectonic evolution of the Eastern Mediterranean Neotethys, Palaeogeography, Palaeoclimatology, Palaeoecology 87, 289-343.

Rosendaal, E.A., The effect of peridotite composition on elastic seismic velocities in the upper mantle, unpublished doctoral thesis, Utrecht, The Netherlands, 1998, 57 pp.

Ross, J.V., H.G. Ave Lallemant, & N. Carter, 1980. Stress dependence of recrystallized-grain and subgrain size in olivine, Tectonophysics 70, 39-61.

Ross, J.V., J-C.C. Mercier, H.G. Ave Lallemant, N.L. Carter, & J. Zimmerman, 1980. The Vourinos Ophiolite Complex, Greece: The tectonite suite, Tectonophysics 70, 63-83.

Ross, K. & D. Elthon, 1993. Cumulates from strongly depleted mid-ocean-ridge basalt, nature 365, 826-829.

Rusby, R.I. & R.C. Searle, 1993. Intraplate thrusting near the Easter microplate, Geology 21, 311-314.

Rutter, E.H., 1999. On the relationship between the formation of shear zones and the form of the flow law for rocks undergoing dynamic recrystallization, Tectonophysics 303, 147-158.

Rutter, E.H. & K. Brodie, 1988. The role of tectonic grain size reduction in the rheological stratification of the lithosphere, Geologische Rundschau 77, 295-308.

Salters, V.J.M. & J. Longhi, 1999. Trace element partitioning during the initial stages of melting beneath mid-ocean ridges, Earth Plan. Sci. Lett. 166, 15-30.

Schmädicke, E., 2000. Phase relations in peridotitic and pyroxenitic rocks in the model systems CMASH and NCMASH, J. Petrology 41, 69-86.

Schubert, G., C. Froidevaux, & D.A. Yuen, 1976. Oceanic lithosphere and asthenosphere: Thermal and mechanical structure, J. Geoph. Res. 81, 3525-3540.

Scott, D.R. & D.J. Stevenson, 1989. A self-consistent model of magma melting, magma migration and buoyancy-driven circulation beneath mid-ocean ridges, J. Geoph. Res. 94, 2973-2988.

Searle, M. & J. Cox, 1999. Tectonic setting, origin, and obduction of the Oman Ophiolite. GSA Bulletin 111, no. 1, 104-122.

Searle, M. & J. Malpas, 1982. Petrochemistry and origin of sub-ophiolitic metamorphic and related rocks in the Oman Mountains. Geol. Soc. of London J. 139, 235-248.

Shaw, W.J. & J. Lin, 1996. Models of ocean ridge lithospheric deformation: Dependence on crustal thickness, spreading rate, and segmentation. J. Geoph. Res. 101, 17977-17993.

Shelton, G. & J.A. Tullis, 1981. Experimental flow laws for crustal rocks, Trans. Amer. Geoph. Union 62, 396.

Sibson, R.H., 1977. Fault rocks and fault mechanisms, J. Geol. Soc. London 133, 191-213.

Sinton, R.S. & Detrick, J.M., 1992. Mid-ocean ridge magma chambers, J. Geoph. Res. 97, 197-216.

Sleep, N.H. & G.A. Barth, 1997. The nature of oceanic lower crust and shallow mantle emplaced at low spreading rates, Tectonophysics 279, 181-191.

Smewing, J.D., N.I. Christensen, I.D. Bartholomew, & P. Browning, 1984. The structure of the oceanic upper mantle and lower crust as deduced from the northern section of the Oman Ophiolite, in: S.J. Gass, S.J. Lippard, & A.W. Shelton (eds.), Ophiolites and oceanic lithosphere, Spec. Publ. Geol. Soc. London 13, 41-54.

Smith, A.G., 1993. Tectonic significance of the Hellenic-Dinaric ophiolites, in: H.M. Prichard, T. Alabaster, N.B.W. Harris & C.R. Neary (eds.) Magmatic processes and plate tectonics, Geol. Soc. Spec. Publ. 76, 213-243.

Smith, A.G. & J.G. Spray, 1984. A half-ridge transform model for the Hellenic-Dinaric ophiolites. in: J.E. Dixon & A.H.F. Robertson (eds.), Geological evolution of the eastern Mediterranean, Geol. Soc. Spec. Publ. 17, 629-644.

Smith, A.G., A.J. Hynes, M. Menzies, E.G. Nisbet, I. Pryce, M.J. Welland, & J. Ferrière, 1975. The stratigraphy of the Othris Mountains, eastern central Greece: A deformed Mesozoic continental margin sequence, Eclogae Geol. Helv. 68, 463-481.

Sobolev, A.V. & N. Shimizu, 1993. Ultra-depleted primary melt included in an olivine from the Mid-Atlantic Ridge, Nature 363, 151-154.

Spear, F.S., 1993. Metamorphic phase equilibria and pressure-temperature-time paths, Mineralogical Society of America Monograph, 79 pp.

Spiegelman & M., T. Elliott, 1993. Consequences of melt transport for uranium series disequilibrium in young lavas, Earth Plan. Sci. Lett. 118, 1-20.

Spiegelman, M. & D. McKenzie, 1987. Simple 2-D models for melt extraction at mid-ocean ridges and island arcs, Earth Plan. Sci. Lett. 83, 137-152.

Spray, J.G. & J.C. Roddick, 1980. Petrology and 40Ar/39Ar geochronology of some Hellenic sub-ophiolite metamorphic rocks, Contrib. Mineral. Petrol. 72, 43-55.

Spray, J.G., J. Bébien, D.C. Rex, & J.C. Roddick, 1984. Age constraints on igneous and metamorphic evolution of the Hellenic-Dinaric ophiolites, in: J.E. Dixon & A.H.F. Robertson (eds.), Geological evolution of the eastern Mediterranean, Geol. Soc. Spec. Publ. 17, 619-627.

Stampfli, G.M., J. Mosar, A. De Bono, & I. Vavasi, 1998. Late Paleozoic, early Mesozoic plate tectonics of the Western Tethys, Bull. Geol. Soc. Greece, XXXII/1, 113-120.

Suhr, G., 1992. Upper mantle peridotites in the Bay of Islands Ophiolite, Newfoundland: Formation during the final stages of a spreading centre?, Tectonophysics 206, 31-53.

Suhr, G., 1993. Evaluation of upper mantle microstructures in the Table Mountain massif (Bay of Islands ophiolite), J. Struct. Geol. 151, 1273-1292.

Suhr, G. & P.A. Cawood, in press, The southeastern Lewis Hills (Bay of Islands Ophiolite): geology of a deeply eroded, inside-corner, ridge-transform intersection, Geological Society of America Bulletin.

Suhr, G. & P.T. Robinson, 1994. Origin of mineral chemical stratification in the mantle section of the Table Mountain massif (Bay of Islands Ophiolite, Newfoundland, Canada), Lithos 31, 81-102.

Tartarotti, P., M. Cannat, & C. Mével, 1995. Gabbroic dikelets in serpentinized peridotites from the Mid-Atlantic ridge at 23°20'N, in: R.L.M. Vissers & A. Nicolas (eds.), Mantle and lower crust exposed in oceanic ridges and in ophiolites, Kluwer Academic Publishers, Dordrecht, The Netherlands,35-69.

Ter Heege, J.H., J.H.P. De Bresser, & C.J. Spiers, 1999. The role of microstructure in determining rheology, in: European Geophysical Society (EGS) Symposium Proceedings, p. 69.

Toomey, D.R., S.C. Solomon, G.M. Purdy, & M.H. Murray, 1985. Microearthquakes beneath the median valley of the Mid-Atlantic Ridge near 23°N: Hypocentres and focal mechanisms, J. Geoph. Res. 90, 5443-5458.

Trimby, P.W., M.R. Drury, & C.J. Spiers, 2000. Recognising the crystallographic signature of recrystallisation processes in deformed rocks: a study of experimentally deformed rocksalt, J. Struct. Geol. 22, 1609-1620.

Trimby, P.W., D.J. Prior, & J. Wheeler, 1998. Grain boundary hierarchy development in a quartz mylonite, J. Struct. Geol. 20, 917-935.

Tucholke, B.E. & J. Lin, 1989. A geological model for the structure of ridge-segments in slow-spreading ocean crust, J. Geoph. Res. 99, 11937-11958.

Twiss, R.J. 1977. Theory and applicability of a recrystallised grain size paleopiezometer. Pure and Applied Geoph. 115, 227-244.

Urai, J.L., W.D. Means, & G.S. Lister, 1986. Dynamical recrystallisation of minerals, in: B.E. Hobbs, H.C. Head (eds.), Mineral and rock deformation: Laboratory studies - The Paterson Volume, Geophys. Monogr. 36, American Geophysical Union, 161-199.

Van der Laan, S.R., M.F.J. Flower, & A.F. Koster van Groos, 1989. Experimental evidence for the origin of boninites: near-liquidus phase relations to 7.5 kbar, in: A.J. Crawford (ed.), Boninites, Unwin Hyman Ltd, London, 112-134.

Van der Wal, D. & J-L. Bodinier, 1996. Origin of the recrystallisation front in the Ronda peridotite by km-scale pervasive porous melt flow, Contrib. Mineral. Petrol. 122, 387-405.

Van der Wal, D., P. Chopra, M.R. Drury, & J.D. Fitz Gerald, 1993. Relationship between dynamically recrystallised grain size and deformation conditions in experimentally deformed olivine rocks, Geoph. Res. Lett. 20, 1479-1482.

Van der Wal, D., R.L.M. Vissers, M.R. Drury, E.H. Hoogerduijn Strating, 1992. Oblique fabrics in porphyroclastic Alpine-type peridotites: A shear sense indicator for upper mantle flow, J. Struct. Geol. 14, 839-846.

Vissers, R.L.M., M.R. Drury, E.H. Hoogerduijn Strating, & D. van der Wal, 1991. Shear zones in the upper mantle: A case study in an Alpine lherzolite massif, Geology 19, 990-993.

Vissers, R.L.M., M.R. Drury, J. Newman, & T.F. Fliervoet, 1997. Mylonitic deformation in upper mantle peridotites of the North Pyrenean Zone (France): implications for strength and strain localization in the lithosphere, Tectonophysics 279, 303-325.

Vissers, R.L.M., M.R. Drury, E.H. Hoogerduijn Strating, C.J. Spiers, & D. Van der Wal, 1995. Mantle shear zones and their effect on lithosphere strength during continental break-up, Tectonophysics 249, 155-171.

Von Bargen, N. & H.S. Waff, 1986. Permeabilities, interfacial areas, and curvatures of partially molten systems: Results of numerical computations of equilibrium microstructures, J. Geoph. Res. 91, 9261-9276.

Waff, H.S. & U.H. Faul, 1992. Effects of crystalline anisotropy on fluid distribution in ultramafic partial melts, J. Geoph. Res. 97, 9003-9014.

Wang, X.J., J.R. Cochran, & G.A. Barth, 1996. Gravity anomalies, crustal thickness, and the pattern of mantle flow at the fast-spreading East Pacific Rise, 9°-10°N: Evidence for three-dimensional upwelling. J. Geoph. Res. 101, 17927-17940.

Wark, D.A. & E.B. Watson, 2000. Effect of grain size on the distribution and transport of deep-seated fluids and melts, Geoph. Res. Lett. 27, p. 2029-2032.

Wheeler, J., 1992. Importance of pressure solution and Coble creep in the deformation of polymineralic rocks, J. Geoph. Res. 94, 145-159.

White, R.S., D. McKenzie, & R.K. O'Nions, 1992. Oceanic crustal thickness from seismic measurements and rare earth element inversions, J. Geoph. Res. 97, 19683-19715.

White, S.H. & R.J. Knipe, 1978. Transformation- and reaction-enhanced ductility in rocks, J. Geol. Soc. London 135, 513-516.

White, S.H., S.E. Burrows, J. Carreras, N.D. Shaw, & F.J. Humphreys, 1980. On mylonites in ductile shear zones, J. Struct. Geol. 2, 175-187.

Witt-Eickschen, G. & H.A. Seck, 1991. Solubility of Ca and Al in orthopyroxene from spinel-peridotite: An improved version of an empirical geothermometer, Contrib. Mineral. Petrol. 106, 431-439.

Wogelius, R.A. & F.C. Bishop, 1989. Subsolidus emplacement history of the Lanzo massif, northern Italy, Geology 17, 995-999.

Wood, B.J. & S. Banno, 1973. Garnet-orthopyroxene and orthopyroxene-clinopyroxene relationships in simple and complex systems, Contrib. Mineral. Petrol. 42, 109-124.

Zhang, S. & S-I. Karato, 1995. Lattice preferred orientation of olivine aggregates deformed in simple shear, Nature 375, 774-777.

Zhang, S., S-I. Karato, J. Fitz Gerald, U.H. Faul, & Y. Zhou, 2000. Simple shear deformation of olivine aggregates, Tectonophysics 316, 133-152.

Zhang, Y-S. & T. Tanimoto, 1992. Ridges, hotspots and their interaction as observed in seismic velocity maps, Nature 355, 45-49.

Dankwoord/Acknowledgments

Ofschoon een promotieonderzoek een taak die je grotendeels in je eentje moet volbrengen, is het duidelijk dat een succesvolle afronding ondoenlijk is zonder de steun van een groot aantal mensen. Een proefschrift is dan ook niet compleet zonder dankwoord, dat immers vaak het meest gelezen onderdeel is. Omdat het vrijwel onmogelijk is om geen mensen te vergeten die gedurende de afgelopen jaren direct of indirect hebben bijgedragen aan mijn promotie, wil ik alvast beginnen met al mijn familie, vrienden, kenissen, collega's en stafleden aan de faculteit Aardwetenschappen in Utrecht van harte te bedanken voor hun bijdrage aan een fijne en geslaagde tijd, waarop ik met veel plezier zal terugkijken. De volgende mensen wil ik echter met naam een toenaam noemen:

Laat ik beginnen met Martyn Drury en Reinoud Vissers. Ik vind dat ik erg heb geboft om jullie als begeleiders te mogen hebben. Natuurlijk heb ik jullie wel eens vervloekt, vanwege het onderzoek waar mee jullie me hadden opgezadeld wanneer ik even geen uitweg uit een probleem zag, of vanwege jullie goedbedoelde en meestal vruchteloze pogingen om me achter de broek te zitten om voor de verandering eens te proberen een deadline te halen. Gelukkig kwamen die momenten zelden voor en duurden ze nooit lang. Integendeel, bijna altijd overheerste de gedachte dat ik het fantastisch getroffen had met het onderzoek, waarin veel ruimte was voor veldwerk in Griekenland en Oman, dat me naar plekken als IJsland, het Spaanse Ronda Massief, de Californische Coast Ranges, de Italiaanse Liguriden, en het Engelse Lizard schiereiland bracht, dat altijd uitdagend was, en dat ruimschoots gelegenheid bood om onverwacht opdoemende zijwegen te bewandelen. Daarnaast was jullie nimmer aflatende enthousiasme voor alle aspecten van de geologie bijzonder aanstekelijk en heb ik bijzonder veel van jullie geleerd op het gebied van geologie van mantel stenen, het doen van onderzoek en het presenteren van resultaten. In het bijzonder wil ik jullie bedanken voor de vrije hand die jullie mij hebben gegeven in mijn onderzoek, zodat ik zelf kon beslissen in welke openstaande problemen 'mijn tanden te zetten'. Deze vorm van begeleiden op gepaste afstand, al dan niet gedwongen door jullie drukke bestuurs en onderwijs verantwoordelijkheden, heb ik als bijzonder prettig ervaren. Ik heb nooit het gevoel gehad aan mijn lot te worden overgelaten, omdat jullie wel altijd beschikbaar waren op momenten dat jullie inbreng noodzakelijk was. Dat geldt vooral voor Martyn, wiens deur altijd openstond voor waardevolle suggesties and adviezen, maar ook voor Reinoud die mij tijdens de relatief zeldzame besprekeningen gedurende zijn drukke periode als onderwijsdirecteur toch altijd op het goede spoor wist te zetten, en die in de laatste maanden van mijn onderzoek er nog even 'de beuk erin zette' om snel en nauwgezet mijn teksten te corrigeren. Martyn en Reinoud, bedankt voor alles! Stan wil ik bedanken voor zijn rol als promotor, voor het lezen van mijn proefschrift, en in het algemeen voor het leiden van een ontzettend leuke groep stafleden, postdocs, promovendi en studenten.

Mijn collega's in de structurele geologie/HPT groep (met een regelmatig inbreng uit de petrologie hoek) hebben een belangrijke rol gespeeld in het creëren van een hele gezellige tijd in Utrecht, onder andere door de vele koffiepauzes, lange lunches, talloze vrijdagmiddagpraatjes en -borrels (inclusief zinloze spelletjes), etentjes and cocktailfeestjes. Dus Andor, René, Marga, Armelle, Fraukje, Rachel, Tanja, Kike, Bernard B., Marije, Geert, Julie, Will, Martyn, Jill, Herman, Reinoud, Hugo, Coen, Timon, Magda, Stan, Fernando, Salvador, Pat, Paul, Jason, Bart, Jan, Rob, Siese, Rian, Chris, Hans, Colin en Bernard de J., hartelijk bedankt voor de leuke sfeer in 'ons' hoekje van het IVA! Ik denk dat er vooral een hele hechte band binnen de groep van structurele geologie promovendi bestond. Helaas, maar onvermijdelijk, valt de groep nu uiteen omdat ieder nu zijns weegs gaat. Het ga jullie allemaal goed, en ik hoop nog lang contact

met jullie te houden! Marga, Jan, Kike en Marije, veel succes met jullie (laatste) loodjes! Uiteraard verdient mijn lagere en middelbare school klasgenoot, geologie jaargenoot en collega-promovendus c.q. kamergenoot Andor hier een speciale vermelding. Ik ben uit Utrecht vertrokken net voordat we ons vierde lustrum konden vieren..... Bedankt voor de vele mokken koffie en het eindeloze, soms oeverloze, maar nooit storende, gezellige gezwets in onze kamer (die toch wel enigszins bekend stond als 'de zoete inval') maar ook voor de inhoudelijke discussies en adviezen!

Van de vele docenten die mij geologie hebben bijgebracht tijdens mijn studie in Utrecht wil ik in het bijzonder diegenen bedanken die mij tijdens colleges, practica en veldwerken hebben warm gemaakt voor structurele geologie en tektoniek, een fantastisch vakgebied waarin ik voorlopig nog lange tijd hoop te kunnen werken. Dus met name Reinoud, Martyn, Stan, Hans, Chris, Hugo, Cees van den E., Cees P., Colin en Leo, bedankt voor jullie inspirerende onderwijs. Laat ik toch ook Tony's enthousiaste pogingen om petrologie net zo leuk te laten lijken als structurele geologie niet onvernoemd laten.

Verder wil ik Magda en Marnella bedanken voor de secretariële ondersteuning. Magda, zonder jou zou je structurele geologie groep niet kunnen draaien! Bedankt ook Inge en Otto voor de vele slijpplaten, Boudewijn voor het regelen van vluchten en huurauto's, Paul in het algemeen voor de audiovisuele ondersteuning, Paul en Jaco voor de mooie opmaak van het proefschrift, Birgit voor het maken van vele mooie dia's, en de dames van de kantine, met name Margret en Berna voor de goede lunches. Lidy, Agathe, Marcel, Jan, Wim en Frans van de bibliotheek wil ik ook niet vergeten: de IVA bieb is ongetwijfeld een van de beste en meest plezierige ter wereld, mede door jullie behulpzaamheid en vriendelijkheid. Dat realiseer ik me vooral pas sinds ik te maken heb met een heel ander soort bibliotheek hier in Leicester.

Verder wil ik de studenten René, Eveliene, Douwe en Daan bedanken voor hun nuttige werk op stenen uit Othris of Oman.

Of the many graduate students I met during conferences and summer schools in Iceland and Oman, I would especially like to mention Mélanie, Eric, Jorg, and Astri; I hope to meet you again in the future some time. I also would like to thank Martin Menzies, Adolphe Nicolas, Françoise Boudier, Benoit Ildefonse, Peter Kelemen, Günther Suhr, George Ceuleneer, Chris MacLeod, Thierry Juteau, Elisabetta Rampone, and Giovanni Piccardo for instructive fieldtrips and useful feedback at conferences. Martin Menzies is also acknowledged for suggesting the Othris Massif as an interesting place to work. I didn't always agree with that, especially not during hot summer days when I had to climb Mt. Katáchloron, but in retrospect I must admit that it is a fascinating place, which I have missed dearly during the last few years. I further wish to express my thanks to Anna Rassios for an introduction to the Othris and Vourinos Ophiolites and for fieldwork support. Adolphe Nicolas, Françoise Boudier, and Benoit Ildefonse are thanked for their support during the fieldwork in Oman.

I also would like to thank the people of the villages of Makrirrahi, Loutra Kaïtsa, Loutra Smokovou, and Smokovou for their hospitality. Special thanks are due to Kostas Moschos for being my English-speaking interpreter, γιαγια Sophia, γιαγια Evangelina, and the villagers of Smokovou for providing accommodation, and Giorgos and his wife and son for making his tavern in Makrirahi my home-away-from-home (and whom I, coincidentally, honour by defending my thesis on St. George's day!).

Julie and Will, thank you very much for your hospitality during my stay in College Station, Texas. Julie, you were also a great person to work with during our short fieldtrip in Othris! I also wish to thank Ray Guillemette for his assistance with the microprobe analyses at Texas A&M University.

Thanks are also due to the members of my dissertation committee, Gareth Davies, Greg Hirth, Will Lamb, Martin Menzies, and Adolphe Nicolas for reviewing the thesis.

I also would like to acknowledge my colleagues at Leicester University, especially Dickson Cunningham, for letting me finish my thesis while I was supposed to be working on the Mongolian rocks; thanks for your patience!

Terug naar Utrecht, of liever gezegd, naar Zeist.....Ik wil het niet nalaten mijn huisgenoten die

tijdens mijn promotietijd op Warande 201 hebben gewoond te noemen: Linda, Urs, Truus, Marten, Geert, Amindo, Cora, Wanda, Sietske, Miranda en Edwin. Jullie hebben allemaal bijgedragen aan de gezellige sfeer in huis, en indirect heeft dat natuurlijk meegewerkt in de afronding van mijn promotie. Ik zal proberen contact te houden. Truus, Geert en Marten ook heel veel succes bij (het afronden) van jullie promoties!

Verder wil ik hier ook mijn studiegenoten, later vrienden, en nu ook paranimfen Arnaud en Gerard noemen. Arnaud was mijn veldmaat in Castel de Cabra, de Pyreneeën, Karya, en later in de Ukraïne. Volgens mij zijn we altijd een erg goed team geweest! Gerard, jij ook bedankt voor de gezellige veldwerken in Castel, Karya en de Oekraïne, en voor de samenwerking tijdens onze studie. Maar bovenal wil ik jullie beiden (en ook Anne!) bedanken voor jullie vriendschap, die we door onze verschillende bezigheden en woonplaatsen niet meer zo heel erg actief kunnen onderhouden, maar waarvan we de draad altijd weer snel blijken te kunnen oppakken gedurende lange wandelingen, etentjes, en borrelavonden.....

De familie Hulscher wil ik bedanken voor het gebruik van jullie huis als werkplek tijdens de laatste paar weken van de schrijffase van mijn proefschrift, maar vooral voor de gezellige dagen in Groningen de afgelopen paar jaar sinds ik bij jullie over de vloer kom.

Rob, ik waardeer de liefde die je mijn moeder geeft bijzonder, en ik hoop dat jullie nog lang samen mogen zijn. Lieve Mischa, lieve mamma, jullie rol in mijn leven is natuurlijk van onnoemelijke betekenis. Wat betreft mijn promotie is jullie altijd aanwezige interesse en steun van groot belang geweest. Mamma, de jaren voorafgaand aan en tijdens mijn promotie zijn in velerlei opzichten enorm moeilijk geweest, maar gelukkig ziet alles er nu weer veel rooskleuriger uit. Mischa, succes ook met jouw promotie in Kopenhagen, maar ik twijfel er niet aan dat je mede door je mateloze en aanstekelijke enthousiasme voor biologie, in het bijzonder voor het sociale gedrag van mieren, je er met veel succes doorheen zult slaan!

Lieve Bregje, mijn vriendin en 'reisgenoot op weg naar Ithaka', bedankt voor je steun tijdens de laatste jaren van mijn promotie, voor de discussies op het vlak van de geologie, maar vooral voor je liefde en simpelweg voor het 'er zijn' (ook al zit je op dit moment aan het andere einde van de wereld!). Ik hoop dat we nog lang samen onderweg mogen zijn.....

Pappa, aan jou draag ik dit proefschrift op. Jouw en mamma's liefdevolle opvoeding, jullie enthousiasme en onvoorwaardelijke steun bij alles wat ik deed, en in het bijzonder uitstapjes de we met z'n tweeën maakten op jacht naar mooie mineralen, nu bijzonder dierbare herinneringen, hebben de basis gevormd voor mijn liefde voor de aardwetenschappen. Zonder jouw aanmoedigingen was ik nooit geologie gaan studeren. Ik heb vaak gedacht aan je ideeën dat we ernaar moeten streven om iets 'blijvends' na te laten op deze wereld, hoe klein ook, en ze hebben een belangrijke rol gespeeld in de keuze voor wetenschappelijk onderzoek. Met andere woorden, zonder jou was dit proefschrift er uiteindelijk nooit gekomen.....

Leicester, 21 februari 2001

Curriculum Vitae

2000-heden	*Marie Curie* Postdoctoral Research Fellow University of Leicester, United Kingdom
1995-2000	Onderzoeker-in-Opleiding Projectgroep Structurele Geologie en Tektoniek Universiteit Utrecht
1989-1995	Studie Geologie, specialisatie Structurele Geologie Faculteit Aardwetenschappen Universiteit Utrecht
1986-1989	Ongedeeld Voorbereidend Wetenschappelijk Onderwijs Stedelijk Lyceum, Zutphen
1983-1986	Gymnasium Stedelijk Gymnasium, Breda
1977-1983	Lagere School Openbare Basisschool "de Klokkebei", Ulvenhout
1975-1977	Kleuterschool "de Kleine Wereld", Breda
1971	Geboren 7 maart te Rotterdam